MONASH University

Particle astrophysics aspects of supersymmetric models

Giancarlo Pozzo
MSc, BSc

A thesis submitted for the degree of Doctor of Philosophy at
Monash University in 2019

Copyright notice

Abstract

Supersymmetry offers possible solutions to several problems that require physics beyond the Standard Model (SM). Two of the biggest among these problems are the dark matter (DM) and the origin of the baryonic matter. We explore these two problems using the Minimal Supersymmetric Standard Model (MSSM) and the Next-to-MSSM (NMSSM).

Firstly, we assume the lightest neutralino $\tilde{\chi}_1^0$ of the R-parity conserving MSSM is the lightest supersymmetric particle. We consider the resonant annihilation of $\tilde{\chi}_1^0$ via a Z or a light Higgs boson. A resonant annihilation of $\tilde{\chi}_1^0$ produces signals that can be probed with both astrophysical and collider experiments. In particular, we combine the current constraints from experiments on DM direct detection, Z and Higgs invisible decay, direct searches for electroweakinos and sleptons at the Large Hadron Collider (LHC) and the muon anomalous magnetic moment. We implement these constrains in scans over the parameter spaces of a simplified model and the phenomenological MSSM. We find that the allowed parameter spaces are very constrained and will be almost fully explored by ongoing and future experiments, such as LUX-ZEPLIN and high luminosity LHC.

Secondly, we study the cosmological phase transitions in electroweak baryogenesis. We use the one-loop temperature-dependent effective potential of the two Higgs doublet model plus a singlet (THDMS) that is an effective field theory of the NMSSM. As the Universe evolves and the temperature decreases, we trace the path of minima of the potential and find possible phase transitions between these minima. We scan the THDMS parameter space looking for points such that: the deepest minimum of the potential at zero temperature lies at the observed vacuum expectation value of the electroweak symmetry breaking (246 GeV), the Universe experiences a strong first-order phase transition (SFOPT) and the Large Electron-Positron Collider and LHC constraints are satisfied. We discover and classify different patterns of the phase structure. We find that the SM-like Higgs is almost always the next to lightest Higgs and for some of the parameters in the model, we identify the most favourable values for a SFOPT.

Thesis including published works declaration

I hereby declare that this thesis contains no material which has been accepted for the award of any other degree or diploma at any university or equivalent institution and that, to the best of my knowledge and belief, this thesis contains no material previously published or written by another person, except where due reference is made in the text of the thesis.

This thesis includes two original papers published in peer reviewed journals. The core theme of the thesis is the study of dark matter and baryogenesis in supersymmetric models. The ideas, development and writing up of all the papers in the thesis were the principal responsibility of myself, the student, working within the School of Physics and Astronomy under the supervision of Csaba Balázs.

The inclusion of co-authors reflects the fact that the work came from active collaboration between researchers and acknowledges input into team-based research.

In the case of chapters 5 and 6 my contribution to the work involved the following:

Thesis Chapter	Publication Title	Status	Nature and % of student contribution	Co-author name(s) Nature and % of Co-author's contribution	Co-author(s), Monash student Y/N
5	Constraining resonant dark matter with combined LHC electroweakino searches	Published	Run scan, analysing data and writing part of the article. 50%	Yang Zhang. Setup and run scan, analysing data and writing article. 50%	N
6	Strong first-order phase transitions in the NMSSM – a comprehensive survey	Published	Setup and run scan, analysing data, writing first draft and part of the final version of the article. 50%	P. Athron 10% C. Balazs 10% A. Fowlie 10% G. White 10% Y. Zhang 10% Setup scan, analysing data, writing part of the article.	N to all

I have not renumbered sections of published papers.

Student name: Giancarlo Pozzo

Student signature: Date:

The undersigned hereby certify that the above declaration correctly reflects the nature and extent of the student's and co-authors' contributions to this work. In instances where I am not the responsible author I have consulted with the responsible author to agree on the respective contributions of the authors.

Main Supervisor name: Csaba Balázs

Main Supervisor signature: Date:

Acknowledgements

It has been a long time from when I arrived in Australia, this country so far away from the old Italy. And yet, I still remember the moment when the aeroplane landed in Melbourne, when I found myself "on the other side" of the world, without knowing anyone. However, in Australia, I soon found people like Csaba, Peter, Andrew, Graham, Haitao, Nadine, Sujeet, Jean and many others that now I can call friends and made me feel like at home. I want to thank all these people for making my PhD and my life here in Australia an enjoyable experience. In particular, I want to thank my supervisors, Csaba and Peter. With Csaba I had to face a tough problem: try to be serious after he makes jokes and I just want to laugh for the following ten minutes... Well, jokes apart, I really appreciate and admire his ability to always have a overall view of a problem and his talent for explaining complex concepts in an astounding simple but precise way. I'd like one day I can be close to his brilliance. After Peter. I can say that about 80% of all I learnt and done is thanks to him. The remaining 20%, well, I just couldn't understand his Scottish accent... Again, jokes apart, I thank him for his patience and perseverance to explain concepts, again and again, spending hours to understand my problems and help me to fix them. Without him and Csaba, my PhD wouldn't have been possible.

I also want to thank all the other people I worked with: Yang, Tomas, Sujeet, Graham and Andrew: I learnt a lot from all of you! Sometimes I learnt from our discussion and meetings, sometimes I learnt "secretly", trying to imitate and acquire your skills. Thanks for all the time and help you devoted to me.

Even though I spent much time at the University, I want to thank all the friends with whom I spent time outside the University. Our trips, dinners, discussions and cultural exchanges are unique and very precious in my life. You let me open my mind although, I know, it was not always easy. But thanks to you, I feel I am a better person with a better understanding of the world. You showed me the beauty of the humans' variety, I'll always thank you for that.

Finally, there is a person that deserve a special thanks for her support, her tenacity and her Love. I'm sorry for all the bad thing I did (and, yes, I know I still do). You gave me the opportunity to look inside me, understand better myself and improve. I simply cannot say how much grateful I am for all this, thanks for all the moments you gave to me.

Moreover, I thank all the people who enabled me to be here. I start with people that supported me through the Monash Graduate Scholarship (MGS) and the Monash Postgraduate Research Scholarship (MIPRS). Thank you for giving me this fantastic opportunity.

And now I have to thank the people who made possible me to arrive until the first bus that brought me to Australia. All these people continued and will continue to support me in Australia or wherever I will be, and since they are more confident with the Italian language, let me the freedom to switch to my mother tongue.

Non so se leggerete mai questi ringraziamenti, ad ogni modo sono ringraziamenti che porto dentro di me e che voi stessi sapete essere dentro di me. Scriverli non cambia molto, ma è Natale, e mi fa piacere dedicare qualche riga e qualche minuto per attribuirvi un po' della gratitudine che meritate su un documento, la mia tesi di dottorato, che, lo so, vi rende orgogliosi.

Innanzitutto ringrazio tutti i miei amici che mi hanno accompagnato negli anni. Siamo cresciuti e cambiati ma ci vogliamo ancora bene. E questo è semplicemente bello. Nonostante io stia in questa terra lontanissima da tutto, ogni volta che torno mi fate sempre sentire di nuovo a casa. Grazie!

Infine, il più grande ringraziamento va alla mia famiglia, senza la quale io non sarei quello che sono. Se siete orgogliosi di me, se vedete del buono in me, dovete prima di tutto essere orgogliosi di voi perché il buono che è in me ce l'avete messo voi. E anche se sono in Australia o in altre parti del mondo, voi rappresentate e rappresenterete sempre la mia casa. GRAZIE!

Contents

Abstract iii

Thesis including published works declaration v

Acknowledgements vii

1 Introduction 1

2 Standard Model 9
- 2.1 SM particle content . . . 11
  - 2.1.1 Fermions . . . 11
  - 2.1.2 Bosons . . . 15
- 2.2 Symmetries and interactions . . . 16
  - 2.2.1 Abelian interaction . . . 17
  - 2.2.2 Non-Abelian interaction . . . 19
  - 2.2.3 Gauge terms . . . 21
- 2.3 Electroweak symmetry breaking . . . 25
  - 2.3.1 Gauge bosons masses . . . 28
  - 2.3.2 Fermion masses . . . 29
  - 2.3.3 CKM matrix . . . 30
- 2.4 Gauge fixing . . . 32
  - 2.4.1 Coulomb Gauge . . . 33
  - 2.4.2 Lorenz Gauge . . . 34
  - 2.4.3 R_ξ gauges . . . 34
- 2.5 Beyond SM . . . 35

3 Supersymmetry 39
- 3.1 Motivations . . . 39
- 3.2 Notation . . . 41
- 3.3 Chiral SUSY Lagrangian . . . 45
  - 3.3.1 Free Lagrangian . . . 45

3.3.2 Auxiliary Lagrangian . . . 45
3.3.3 Interaction Lagrangian . . . 48
3.3.4 Elimination of auxiliary fields . . . 53
3.4 Abelian gauge SUSY Lagrangian . . . 54
3.4.1 Free Lagrangian . . . 54
3.4.2 Auxiliary Lagrangian . . . 55
3.4.3 Interaction Lagrangian . . . 55
3.4.4 Elimination of auxiliary fields . . . 57
3.5 Non-Abelian gauge SUSY Lagrangian . . . 58
3.5.1 Free and Auxiliary Lagrangian . . . 58
3.5.2 Interactions and elimination of auxiliary fields . . . 59
3.6 SUSY breaking . . . 62
3.6.1 $\mathcal{F}$-terms . . . 63
3.6.2 $\mathcal{D}$-terms . . . 63
3.6.3 Soft terms . . . 65
3.7 MSSM . . . 65
3.7.1 Spectrum . . . 66
3.7.2 Superpotential . . . 67
3.7.3 Matter parity and R-parity . . . 67
3.7.4 Soft breaking . . . 68
3.7.5 Problems . . . 69
3.8 NMSSM . . . 70
3.8.1 Superpotential . . . 71
3.8.2 Higgs sector . . . 72

4 Matter-Antimatter asymmetry problem 75
4.1 Sakharov conditions . . . 77
4.2 Electroweak baryogenesis outline . . . 79
4.3 Phase transitions . . . 80
4.3.1 Second order phase transitions . . . 82
4.3.2 First order phase transitions . . . 82
4.4 Arising of CP asymmetry . . . 83
4.5 Sphaleron transitions . . . 85
4.5.1 Outside the bubble . . . 85
4.5.2 Inside the bubble . . . 87
4.6 Freezing out the B asymmetry . . . 88
4.7 Phase transition strength . . . 89
4.7.1 Order parameter . . . 89
4.7.2 Strength of the transition . . . 90
4.8 Effective potential . . . 91

5 Dark matter constraint from combined experiments **97**
5.1 Published material 98

6 Electroweak phase transition in the NMSSM **109**
6.1 Published material 109

7 Outlook and conclusions **151**

A SARAH files **153**
A.1 THDMS.m 153
A.2 parameters.m 156
A.3 particles.m 158
A.4 SPheno.m 161

Bibliography **163**

Chapter 1

Introduction

The Standard Model (SM) of particle physics describes elementary particles and their interactions. It encapsulates decades of theoretical researches and experimental findings. It explains almost all the particle physics phenomena we observe today providing predictions with astounding precision. Indeed, it is so successful that it deservedly gained the adjective "standard".

Nevertheless, the Standard Model has some problems a few of which are listed here.

Gravity The SM does not include gravity. Because of the very small value of the coupling constant of gravity compared to other coupling constant values, this does not affect the predictions of the model. A quantum theory of gravity is however really indispensable to understand phenomena where the strength of gravity becomes comparable to other interactions, for example at the beginning of the Universe or in black holes or at the Plank scale. In these cases, the SM cannot make a reliable prediction.

Dark matter and dark energy The SM only accommodates particles that are experimentally observed. However, from astrophysical data [1] we infer that the SM particles constitute only 5% of the matter in the Universe, while about 26% of the energy density of the Universe is made of some unknown kind of matter and the remaining 69% is made of the so-called dark energy responsible for the acceleration of the Universe. Even though there are many searches in this direction and some of them require to modify the theory of gravity [2], dark matter and dark energy remain a mystery in the SM.

Baryon asymmetry From astrophysical data, we know that the Universe contains matter and there are no regions in the observable Universe that contain substantial amount of antimatter [3]. The SM, on the

other hand, cannot quantitatively explain how such a prominent matter-antimatter asymmetry is created. In particular, even though the C symmetry, the charge conjugation that transforms matter to antimatter, is violated in the SM, the amount of asymmetry that we observe cannot be explained within the SM.

Hierarchy problem The free parameters of the SM must be related in a precise but unexplained way to account for some experimental results. In particular, performing the calculation of the Higgs mass in an effective filed theory containing the SM and so utilising its parameters that are experimentally measured, we would expect a Higgs mass much bigger than observed. The actual measured value of $m_H \simeq 125\,\text{GeV}$ can still be inferred from the above calculation, but it requires very precise cancellations of terms in the m_H expression. This requirement is known as fine-tuning and represents an indication that some mechanism that can explain such accurate cancellation is still hidden beyond the SM. Such a mechanism can be originated from a symmetry and is indeed implemented in supersymmetric theories.

Anomalies Some calculations performed in the SM have a significant discrepancy with the corresponding experimental result. This, for example, happens with precision experiments. An example is the value of the magnetic dipole moment of the muon that is measured with a precision of about half a part per million [4]. This allows a very precisely check against the SM prediction. The predicted and measured values deviate at 3-4 sigma level [5–8].

Free parameters The SM does not provide any mechanism that justifies the presence and the values of 19 free parameters in the theory.[1] A deeper comprehension of the physics could relate and derive some of these parameters, reducing the number of free parameters.

Possible solutions to these problems constitute the very active research area of the physics beyond the SM (BSM). One of the main of these research areas is Supersymmetry (SUSY). SUSY is a theory that postulates a symmetry, not present in the SM, that relates bosons with fermions. This simple idea has profound consequences. It gives a solution to many of the problems mentioned above of the SM.

[1] Here we assume that the neutrinos are massless. Considering the neutrinos masses increase the number of free parameters.

Hierarchy problem Thanks to the new symmetry, fermion and boson loop corrections to the Higgs mass cancel exactly, solving the hierarchy problem.

Gravity Promoting the supersymmetry to a local symmetry, gravity emerges as a gauge theory.

Dark Matter Assuming the lightest SUSY particle is stable, it is a DM candidate.

Baryon asymmetry Electroweak baryogenesis can quantitatively explain the observed matter-antimatter asymmetry.

We have to mention that besides all these the new solutions, SUSY also offers some challenging questions. The most pressing one is the spectrum of SUSY particles, the supersymmetric partners of the SM particles. The Large Hadron Collider has not found evidences of SUSY particles and puts lower bounds on their possible masses. If, with new experiments, these bounds keep on growing the hierarchy problem comes back with the necessity to explain why there is such a big hierarchy between SM and SUSY masses.

In the thesis, we contribute to the research in this field in two directions corresponding to two of the problems mentioned above of the SM for which SUSY offers a solution: the dark matter and the baryon asymmetry of the Universe.

In particular, we structure the thesis in the following way.

Chapter 2 We review the SM introducing concepts that are used to develops the next chapters. Specifically, we present the SM particle content that coincides with the particles we experimentally observe and their mathematical description. After, we introduce the interaction among these particles that are studied with symmetries and the group theory. With this background, we can present the electroweak symmetry breaking (EWSB): a process that leads to the mass generation. In this context, we also present the CKM matrix, a matrix that shows that the CP violation is allowed in the SM.

These two subjects are the foundation of the following chapters since the CP violation in the CKM matrix is not enough to account for the amount of matter-antimatter asymmetry that we observe in the Universe. Consequently, to explain the observed matter-antimatter asymmetry, we will study the electroweak baryogenesis in the BSM context that can explain the observed excess of matter over antimatter.

Finally, we exemplify the topic of gauge fixing showing different gauge choices and how a good choice can simplify some calculation. Again, this sub-

ject will be useful in the electroweak baryogenesis study where an appropriate choice of the gauge simplifies the expressions and reduces the execution time of a computational scan that we perform in the published material.

Chapter 3 We introduce the SUSY theory presenting some findings relevant to the dark matter and baryogenesis studies. In particular, we start introducing the notation used in the Lagrangian formalism and the SUSY algebra. Specifically, the SUSY algebra defines the operator that turns a fermionic state into a bosonic state and vice-versa and is at the root of SUSY. In fact, Noether's theorem associates this operator with the SUSY transformations of the fields.

Using a Lagrangian $\mathcal{L}$ with scalar and fermion fields, we show these transformations that leave $\mathcal{L}$ invariant up to total derivatives, satisfying Hamilton's principle. Considering interaction terms in $\mathcal{L}$ we derive the superpotential, a function that holds information about the interactions.

Next, we introduce gauge theory, starting with the Abelian case. We add Abelian vector supermultiplets together with their interactions and show the new SUSY transformations. We finish building the Lagrangian analysing the non-Abelian case. We include non-abelian vector supermultiplets together with their interactions and show the general form of the Lagrangian and the SUSY transformations. After this, motivated by experimental evidence, we present the topic of SUSY breaking, illustrating a different possible way to break the symmetry.

On these grounds, we introduce the Minimal Supersymmetric Standard Model (MSSM) that is the simplest SUSY model. We present its spectrum and superpotential. We discuss the SUSY breaking in this specific model showing the Lagrangian breaking terms. We conclude by listing some problems that this model shows, in particular, its inability to explain the observed matter-antimatter asymmetry.

Motivated by these problems, we study the Next-to-Minimal Supersymmetric Standard Model (NMSSM). Again, we show the spectrum, the superpotential and the SUSY breaking terms. Also, we examine the Higgs sector that we will use in the work on baryogenesis. We conclude the chapter studying the Two Higgs Doublet Model plus a Singlet (THDMS). The THDMS is an effective field theory model of the NMSSM and is utilised in our study on baryogenesis.

Chapter 4 We introduce the matter-antimatter problem and describe the electroweak baryogenesis. Specifically, we introduce the asymmetry parameter that quantifies the difference between the amount of matter and antimatter

in the Universe. A mechanism that can produce this matter-antimatter asymmetry is called baryogenesis. The asymmetry parameter represents the final goal of any baryogenesis theory. In contrast, the Sakharov conditions constitute the initial requirements. We illustrate the Sakharov conditions, the three requirements that any baryogenesis theory has to satisfy.

We present the Electroweak Baryogenesis (EWBG), a mechanism that satisfies the Sakharov condition and that can give the observed value of the asymmetry parameter. EWBG takes place during a first-order phase transition at the beginning of the Universe in a very hot plasma in which two different phases are mixed together. This is a complex scenario in which non-perturbative processes and non-equilibrium thermodynamics play a fundamental role. We outline the different steps of the Universe's evolution that lead to the matter-antimatter asymmetry. These steps start after the Big Bang when the SU(2)$\otimes$U(1) gauge symmetry is still unbroken, and the temperature-dependent Higgs potential has a parabolic-like shape. During the cooling of the Universe, the breaking of the SU(2)$\otimes$U(1) gauge symmetry can lead to a first-order phase transition. This phase transition happens through the nucleation and expansion of bubbles. We illustrate how the combination of these expanding bubbles and non-perturbative processes generates a mechanism that produces matter-antimatter asymmetry. We introduce concepts such as the phase transition strength that can quantify the rate at which matter is created and the effective potential that describe the potential at variable high temperature. These concepts will be used in the study of phase transitions in the NMSSM.

Chapter 5 We present a published work in which we investigate if the lightest neutralino of the R-parity conserving MSSM is consistent with the current DM and collider experiments constraints.

Before the article, we describe the motivation of this study. In particular, we wanted to investigate if the MSSM, one of the simplest SUSY model, can still provide a candidate for dark matter. This is an important question because the presence of dark matter is one of the SM problems where SUSY gives a BSM solution. Be briefly review the DM problem introducing experimental evidences of DM. We mention some proposed solution to the problem noting, however, that there is still no consensus about what DM is made of.

Finally, we present our work on DM resonant annihilation in the context of the MSSM. Here we firstly use a simplified model where all apart from three MSSM parameters are fixed. The fixed parameters have a value such that the SUSY particles are decoupled and we can satisfy collider experiments.

With this setting, we perform a scan over the remaining three parameters.

For each point in the scan, we calculate the relic DM density and check it against DM observations. In this way, DM experiments place limits on the allowed parameter space.

After that, we consider constraints from collider experiments so that the parameter space is further constrained. We present the allowed parameter space and show the future projected limit given by the High Luminosity Large Hadron Collider experiment and LUX-ZEPLIN experiment.

Finally, we examine the parameter space in the phenomenological MSSM, repeating the same analysis with more experimental constraints.

Chapter 6 We present a published work in which we study EWBG in the context of the NMSSM. Here, starting from the information presented in Chapter 4, we first introduce the NMSSM. To perform precise calculations using a one-loop NMSSM potential, we introduce the THDMS that represent an effective field theory of the NMSSM. The precise calculations in the THDMS are possible because the NMSSM heavy SUSY particles are integrated out so that we avoid large logarithms in the Coleman-Weinberg correction of the tree level NMSSM potential. To connect the NMSSM and the THDMS potentials, we match their parameters. We complete the THDMS potential adding to it temperature corrections that are essential to describe the early Universe conditions.

Using this effective potential at finite temperature, we study the possible phase transitions during EWBG. To do so, we scan the NMSSM parameter space limiting the parameter ranges according to experimental constraints. We adopt a different approach from previous articles in the literature. Previous works mainly focused on calculating baryogenesis parameters such as the critical temperature or the nucleation temperature. Our work is the first one that studies the rich underlying phenomenology of the possible cosmological phase transitions. In particular, we show that there are different possible phases of the potential. We call a cosmological history the transition from the early Universe's phase to the today Universe's phase. A cosmological history can happen directly or through one or more other phases. In general, different NMSSM points lead to different cosmological histories. We classify the collected NMSSM points according to their corresponding cosmological histories. We identify four classes and show the different characteristics of each class studying:

- the masses of the non-SM-like Higgs bosons,
- the values of the vacua at the critical temperature,

- the values and the relationships between baryogenesis parameters and NMSSM parameters.

Appendix A The scan performed in the EWBG study described in the previous paragraph and Chapter 6 required to set the NMSSM parameters at an energy scale appropriate for the early Universe conditions. These parameters are matched to the THDMS and evolved with the renormalisation group equations to be used in the zero-temperature potential. The matching and running procedure is implemented by `FlexibleSUSY` and `SARAH` using the files displayed in this Appendix.

Chapter 2

Standard Model

The Standard Model (SM) is a model in particle physics that include all known elementary particles and describe their dynamics and their interactions. The SM explains all the known fundamental interactions, except the gravitational one that is not included in the theory. Nevertheless, since current experiments are not sensitive to quantum gravity effects, the absence of gravity does not influence the agreement between SM predictions and high energy physics experiments. In fact, at energies currently probed by experiments, the gravitational coupling constant α_G, which expresses the "strength" of gravity, is many order of magnitude smaller than the coupling constant of the weak, electromagnetic and strong force. Looking at the variety of phenomena the SM can explain and the level of agreement between predictions and experiments, the SM is often called one of the most successful physics theory ever.

The SM is based on the theoretical framework of quantum field theory (QFT). In QFT elementary particles are described as excited states of a field, and interactions between particles are described by the exchange of other additional elementary particles called mediators or force carriers. QFT uses the Lagrangian formalism in which an operator valued function, the Lagrangian density called Lagrangian for simplicity, includes all the information to quantitatively describe the dynamics and interactions of fields. Given a system of fields and given the symmetries under which the system is invariant, the Lagrangian is typically constructed to be the most general renormalizable function of the fields which respects the given symmetries. The SM Lagrangian is a function of the fields describing all elementary particles and respect the Poincaré symmetry and the $\mathrm{SU(3)_C} \otimes \mathrm{SU(2)_L} \otimes \mathrm{U(1)_Y}$ gauge.

		Elementary Particles											
		Fermions Half-integer spin							Bosons Integer spin				
		Quarks SU(3) triplet				Leptons SU(3) singlet			Gauge bosons Spin 1			Scalar boson Spin 0	
	$\left(\substack{\text{SU(3), SU(2)}\\\text{rep. U(1) ch.}}\right)$	Left $(\mathbf{3},\mathbf{2},{}^{1}/_{6})$		Right $(\bar{\mathbf{3}},\mathbf{1},{}^{2}/_{3})$	Right $(\bar{\mathbf{3}},\mathbf{1},{}^{-1}/_{3})$	Left $(\bar{\mathbf{1}},\mathbf{2},{}^{-1}/_{2})$		Right $(\bar{\mathbf{1}},\mathbf{1},-1)$	$(\mathbf{8},\mathbf{1},0)$	$(\mathbf{1},\mathbf{3},0)$	$(\mathbf{1},\mathbf{1},0)$	$(\mathbf{1},\mathbf{2},0)$	
	(Y_W, T_3)	$({}^{1}/_{3}, {}^{1}/_{2})$	$({}^{1}/_{3}, {}^{-1}/_{2})$	$({}^{4}/_{3}, 0)$	$({}^{-2}/_{3}, 0)$	$(-1, {}^{1}/_{2})$	$(-1, {}^{-1}/_{2})$	$(-2, 0)$	$(0,0)$	$\left(0, \substack{+1\\-1\\0}\right)$	$(0,0)$	$({}^{1}/_{2}, {}^{-1}/_{2})$	$({}^{1}/_{2}, {}^{1}/_{2})$
Unbroken symmetry	gen. 1	$(u_{\mathrm{L}}$	$d_{\mathrm{L}})$	u_{R}	d_{R}	$(\nu_{e\mathrm{L}}$	$e_{\mathrm{L}})$	e_{R}	$g^{(1)\ldots(8)}$	$W^{\pm}_{0}$	B^0	$(H^0$	$H^+)$
	gen. 2	$(c_{\mathrm{L}}$	$s_{\mathrm{L}})$	c_{R}	s_{R}	$(\nu_{\mu\mathrm{L}}$	$\mu_{\mathrm{L}})$	μ_{R}					
	gen. 3	$(t_{\mathrm{L}}$	$b_{\mathrm{L}})$	t_{R}	b_{R}	$(\nu_{\tau\mathrm{L}}$	$\tau_{\mathrm{L}})$	τ_{R}					
Broken symmetry		Sing.	m(MeV)	Sing.	m(MeV)	Sing.	Sing.	m(MeV)	Sing.	Sing.	m(GeV)	Sing.	m(GeV)
	gen. 1	u	2	d	5	ν_e	e	0.5	$g^{(1)\ldots(8)}$	$W^{\pm}$	80.4	H^0	125
	gen. 2	c	1.3×10^3	s	100	ν_μ	μ	106		Z^0	91.2		
	gen. 3	t	173×10^3	b	4.2×10^3	ν_τ	τ	1780		γ	0		

Table 2.1: Elementary particles of the standard model. For each of this particles exists a corresponding antiparticle with same mass but opposite charges. Particles such as γ, Z and H are their own antiparticle since they have zero charges. All these particles are experimentally observed. So far, there are no experimental evidence of other elementary particles. In this table we emphasize the SU(2) structure; we do not report that each quark can carry different colour charges, as described by quantum chromodynamics. The weak isospin T_3 and weak hypercharge Y_w are related to the electric charge Q by the formula $Q = T_3 + \frac{1}{2}Y_W$. Before the symmetry breaking all the particle are massless. Note that only fermions are grouped in generations, bosons are not. Here we consider neutrino as massless particles. Regarding the masses, digits with errors are omitted and numbers with more than tree significant digits are rounded, see [9] for state of the art values.

2.1 SM particle content

The SM spectrum consists of all the known elementary particles that are particles that, at the present understanding, are not composed of other particles. Each elementary particle is uniquely identified by its quantum numbers. According to the spin quantum number, or spin, all the elementary particles in the SM are divided into two groups, see Table 2.1:

Fermions The members of this group have the distinctive characteristic of having a half-integer spin and, according to the spin-statistic theorem [10], they obey the Fermi-Dirac statistics.

Bosons The members of this group are all the force carriers and the Higgs particle; they have the distinctive characteristic of having an integer spin. According to the spin-statistic theorem, bosons obey to the Bose-Einstein statistics.

2.1.1 Fermions

In addition to their half-integer spin, fermions can carry different kind of charges. Fermions that carry a charge of colour, for example, are called quarks while fermions with no colour charge are called leptons. The charge influences the interactions between particles: if a particle carries a given charge it will interact under the corresponding force. Quarks, for example, interact via the strong force while leptons do not.

Having fixed the spin and charge, quarks and leptons are further divided into generations or families. In the first generation of quarks, there are the up quark, or u, with an electric charge of $+\frac{2}{3}e$ and down quark, or d, with an electric charge of $-\frac{1}{3}e$, where e is the positron electric charge. In the second generation, the quark charm, or c, has the same spin and electrical charge of u but has a higher mass. In the same second generation, the strange quark, or s, has the same spin and electric charge of d but has a higher mass. In the third generation the quarks top, or t, and bottom, or b, have the same spin and electric charge of u and d respectively, but mass higher than all the other quarks [11].

In the same way, in the first generation of leptons, there is the electron, e, and the electron neutrino ν_e, while in the second generation the muon μ and the muon neutrino ν_μ, finally in the third generation the tau and the tau neutrino ν_τ. The e, μ and τ all have the same electric charge, while their masses are such that $m_e < m_\mu < m_\tau$; as stated by the lepton universality, μ and τ can be considered as a heavier copy of the electron. All the neutrinos have a zero electric charge; in the standard model, they only interact via

the weak interaction. Regarding the neutrino masses, it is still a very active field of research: experimentally it has been found that neutrinos have mass and an upper limit for these masses is around a fraction of few electronvolts (see [12]).

There is no evidence for further generations of quarks or leptons. In particular the possibility of a fourth type of light neutrino, that is a neutrino whose mass is less than half the Z-boson mass, is excluded by all collider experiments [13]. Also a possible fourth-generation quark t' with mass $m_{t'} < 1160\,\mathrm{GeV}$ is excluded at 95 % CL, and a similar limit holds for b' quarks [14, 15].

Left- and right-handed free fermions

All fermions are divided in left-handed and right-handed according to whether they are excitations of a left-handed or right-handed chiral field. These fields appear in the kinematic description of free fermions.

Free fermions are described by the Dirac Lagrangian:

$$\mathcal{L}_{\mathrm{Dirac}} = \bar{\psi}\big(\mathrm{i}\gamma^\mu\partial_\mu - m\,\mathbb{1}_{4\times4}\big)\psi \tag{2.1}$$

where m is the mass of the fermion, $\mathbb{1}_{4\times4}$ is the 4 by 4 identity matrix, ψ is the fermion field represented as a 4-component spinor, $\bar{\psi} \equiv \psi^\dagger\gamma^0$ is the adjoint spinor of ψ and γ^0 is one of the four Dirac matrices γ^μ, where μ runs from 0 to 3, that can be expressed in the Weyl representation as:

$$\gamma^0 = \begin{pmatrix} \mathbb{0} & \mathbb{1} \\ \mathbb{1} & \mathbb{0} \end{pmatrix} \qquad \gamma^i = \begin{pmatrix} \mathbb{0} & \sigma^i \\ -\sigma^i & \mathbb{0} \end{pmatrix} \tag{2.2}$$

where i runs from 1 to 3. The entries of the γ^μ are the zero $\mathbb{0}$, the identity $\mathbb{1}$ and the Pauli σ^i 2 by 2 matrices defined as

$$\mathbb{0} = \begin{pmatrix} 0 & 0 \\ 0 & 0 \end{pmatrix} \qquad \mathbb{1} = \begin{pmatrix} 1 & 0 \\ 0 & 1 \end{pmatrix} \tag{2.3}$$

$$\sigma^1 = \begin{pmatrix} 0 & 1 \\ 1 & 0 \end{pmatrix} \qquad \sigma^2 = \begin{pmatrix} 0 & -\mathrm{i} \\ \mathrm{i} & 0 \end{pmatrix} \qquad \sigma^3 = \begin{pmatrix} 1 & 0 \\ 0 & -1 \end{pmatrix} \tag{2.4}$$

where the Pauli matrices obey the commutation relations

$$\left[\sigma^a, \sigma^b\right] = 2\mathrm{i}\epsilon^{abc}\sigma^c \tag{2.5}$$

with ϵ^{abc} being the three dimensional Levi-Civita symbol. Defining the 4-elements $\boldsymbol{\sigma}$ and $\bar{\boldsymbol{\sigma}}$ whose elements are 2 by 2 matrices

$$\boldsymbol{\sigma}^{\mu} = \left(\mathbb{1}, \sigma^1, \sigma^2, \sigma^3\right) \qquad \bar{\boldsymbol{\sigma}}^{\mu} = \left(\mathbb{1}, -\sigma^1, -\sigma^2, -\sigma^3\right) \tag{2.6}$$

the Dirac Lagrangian can be written as

$$\mathcal{L}_{\text{Dirac}} = \left({\psi^{\dagger}}_{\text{R}}, {\psi^{\dagger}}_{\text{L}}\right) \begin{pmatrix} -m\mathbb{1} & \mathrm{i}\boldsymbol{\sigma}^{\mu}\partial_{\mu} \\ \mathrm{i}\bar{\boldsymbol{\sigma}}^{\mu}\partial_{\mu} & -m\mathbb{1} \end{pmatrix} \begin{pmatrix} \psi_{\text{L}} \\ \psi_{\text{R}} \end{pmatrix}. \tag{2.7}$$

The fields ψ_{L} and ψ_{R} are respectively left-handed and right-handed chiral fields and excitations of these fields are the left-handed and right-handed fermions.

A special case is when the mass parameter is zero $m = 0$; in the SM, this is the case of neutrinos. The Dirac Lagrangian corresponds to two decoupled Euler-Lagrange equations, one for ψ_{L} and ${\psi^{\dagger}}_{\text{L}}$ and another one for ψ_{R} and ${\psi^{\dagger}}_{\text{R}}$. While experiments confirm the existence of left-handed neutrinos, there is no evidence for right-handed neutrino [12].

Left- and right-handed interacting fermions

Interactions arise from symmetry groups that are associated, via the Noether's theorem, with a conserved charge. Thus, particles that have a charge associated with a symmetry are subjected to the interaction arising from that symmetry. Left- and right-handed fermions together with their properties under the groups that give rise to the forces, are summarised in Table 2.1. This table shows that fermions belong to various representations of $\text{SU}_{\text{C}}(3)$, $\text{SU}_{\text{L}}(2)$ and $\text{U}_{\text{Y}}(1)$ carrying different charges under these gauge groups. Particles labelled by **1** under a group are singlet under that group, that is they are unchanged under the group transformation and do not interact via the force described by the corresponding symmetry. Particles corresponding to a representation different from **1** transform under the corresponding symmetry non-trivially and have a charge that allows interaction via the corresponding force.

From the Table 2.1 we can see that only left-handed fermions interact via the weak force that is described by the SU(2) symmetry group. They form SU(2) doublets

$$L_1 = \begin{pmatrix} \nu_{e\text{L}} \\ e_{\text{L}} \end{pmatrix} \quad L_2 = \begin{pmatrix} \nu_{\mu\text{L}} \\ \mu_{\text{L}} \end{pmatrix} \quad L_3 = \begin{pmatrix} \nu_{\tau\text{L}} \\ \tau_{\text{L}} \end{pmatrix} \quad Q_1 = \begin{pmatrix} u_{\text{L}} \\ d_{\text{L}} \end{pmatrix} \quad Q_2 = \begin{pmatrix} c_{\text{L}} \\ s_{\text{L}} \end{pmatrix} \quad Q_3 = \begin{pmatrix} t_{\text{L}} \\ b_{\text{L}} \end{pmatrix} \tag{2.8}$$

and these doublets transform under SU(2) as left-handed Weyl spinors. On the other hand, right-handed fermions do not interact via the weak force and transform as singlets under a SU(2) transformation

$$\begin{array}{lll} e_{1\mathrm{R}} = e_{\mathrm{R}} \quad e_{2\mathrm{R}} = \mu_{\mathrm{R}} \quad e_{3\mathrm{R}} = \tau_{\mathrm{R}} & u_{1\mathrm{R}} = u_{\mathrm{R}} \quad u_{2\mathrm{R}} = c_{\mathrm{R}} \quad u_{3\mathrm{R}} = t_{\mathrm{R}} \\ & d_{1\mathrm{R}} = d_{\mathrm{R}} \quad d_{2\mathrm{R}} = s_{\mathrm{R}} \quad d_{3\mathrm{R}} = b_{\mathrm{R}} \,. \end{array} \tag{2.9}$$

Looking at the property under the SU(3) symmetry, Table 2.1 shows that only quarks and gluons interact via the strong force described by the SU(3) symmetry.

A particular property of interactions between quantised fields is that the strength of the interaction depends on the energy scale. At low energy, for example, the strong interaction is very strong compared to the weak and electromagnetic interactions, while at high energy it becomes less and less strong and eventually its strength becomes comparable to the strength of the other interactions. At low energies (order of MeV) the strong interaction leads to the phenomenon of colour confinement: particles with a colour charge, the charge associated with the SU(3) symmetry, cannot be isolated and directly observed. We can only detect particles with a net colour charge of zero, called colourless particles. So, if we start with a colourless particle composed of a bound state of coloured subparticles and we try to separate these subparticles adding more and more energy to the bound system, at some point the creation of a colourless quark-antiquark couple becomes energetically possible. This couple combines with the bound state resulting in the appearance of colourless particles that can be separated and observed. This means that at low energies, coloured particles, such as quarks and gluons, are always found in bound states. These states are called hadrons. The only two experimentally observed hadron states are mesons, composed of a valence quark and a valence antiquark, and baryons, composed of three valence quarks [11]. All mesons and bound states of mesons are unstable and decay to other particles. Among the baryons, the proton is a stable state of uud valence quarks and the neutron is an unstable state of udd valence quarks, with a mean life of about 880 s [16]. In the Standard Model, protons must be stable because the baryon quantum number B, defined as

$$B = \frac{1}{3}\left(n_q - n_{\bar{q}}\right) \tag{2.10}$$

where n_q is the number of quarks and $n_{\bar{q}}$ is the number of antiquarks, is conserved and protons are the lightest baryons. This is experimentally confirmed: the proton mean life is $\tau \gtrsim 10^{29}$ years [16] (the age of the Universe, in comparison, is $\sim 10^{10}$ years).

From astronomical observation, we know that the Universe is composed only of matter, while antimatter is almost absent: about 73 % of the observed

matter is hydrogen and 25 % is helium. Since nearly all the mass of an atom is made of its nucleus, and since atomic nuclei are made of baryons (protons and neutrons), the bulk of the observed matter in the Universe is baryonic matter.

2.1.2 Bosons

In the SM there are thirteen bosons: twelve gauge bosons with spin 1 and the Higgs boson with spin 0. Eight of the gauge bosons mediate the strong force and they form an octet under the SU(3) group, the group that describes strong interactions, and have colour charges. The remaining four mediate the electroweak force and are singlet under the SU(3) group thus they do not have a colour charge, see Table 2.1.

In the SM, gauge bosons are the particles that mediate the interactions; interactions, on the other hand, are described by symmetries, so that gauge bosons are related to these symmetries. The SM gauge symmetries are described by the SU(3) SU(2) and U(1) groups.

The Higgs boson is associated with a mechanism, the Higgs mechanism, that spontaneously breaks the SM electroweak gauge symmetry $SU(3)_C \otimes SU(2)_L \otimes U(1)_Y$ to the electromagnetic gauge symmetry $SU(3)_C \otimes U(1)_{QED}$.

Massive gauge bosons interact with the Higgs boson field. Without this interaction, all the gauge bosons were massless. A force mediated by a massless particle is a long-range force, as the electromagnetic field. But the weak force is a short-range force and the gauge bosons that mediate this force have a mass different from zero. Gauge bosons receive mass via the electroweak symmetry breaking (EWSB) mechanism. This mechanism, at currently probed energies, leads to three massive bosons in the electroweak sector. After symmetry breaking, we can thus identify the $W^{\pm}$ and Z^0 boson as mediators of the weak force. The photon γ is the fourth gauge boson in the electroweak sector. It is massless and is identified as the mediator of the electromagnetic field.

In the strong sector, there are eight gauge bosons that correspond to eight linear independent types of gluons. Even though gluons are massless, the strong interaction is a short-range interaction. This is due to the colour confinement mechanism that prevents strong charged particles from being separated without producing new strong charged particles. This means that, at currently probed energies, it is not possible to isolate free quarks or gluons.

2.2 Symmetries and interactions

The Lagrangian contains all the physical information of the system. To describe laws of physics that do not depend on a particular choice of the frame of an observer, the Lagrangian must be invariant under translation, rotation and boost transformations. These are described by the translation and Lorentz groups which together form the Poincaré group. Thus the Lagrangian must be invariant under the Poincaré group.

In addition, the SM describes how particles interact. The description is provided by specific terms in the Lagrangian each of which is associated with a symmetry. The Lagrangian is typically found by studying the quantities that are conserved in a physical system. Implementing the corresponding symmetries in the Lagrangian ensures that the Lagrangian leads to the observed conservations.

The strength of an interaction is given by a dimensionless parameter g that appears in Lagrangian terms that describe the considered interaction. Since g is dimensionless for the known fundamental interactions, it provides a way to compare strengths of different interactions. For example, the weak interaction is weak since its coupling constant g_2 is small compared to 1. On the other hand, the strong interaction is strong because its coupling constant g_s is order 1.

In spite of the name "constant", the value of the coupling constants varies with the energy scale. This means that different measurements may give different values of the same coupling constant depending on the energy scale at which the coupling constant is observed. This phenomenon is called running of the coupling constants and is described by the renormalization group.

The running of the coupling constants has profound implications: if an interaction is weak, as the weak interaction, the theory can be well approximated using perturbative techniques. In a perturbative theory it is possible to develop calculations using expansions in power of the coupling constant g, since successive terms in an expansion, depending on bigger and bigger power of g that has a value $g \ll 1$, are smaller and smaller. On the other hand, if an interaction is strong, such as the strong interaction, a perturbation theory is meaningless because successive terms in an expansion become greater and greater. In this case, other techniques have to be developed. Nevertheless, since the coupling constants depend on the energy, the same interaction can be treated perturbatively in some energy regimes and non-perturbatively in others. For example, the coupling constant of the strong interaction decreases when the energy increase. In this way, the strong interaction becomes weaker at high energy and we can apply perturbative techniques to study it. At lower energies the coupling constant of the strong interaction is too big to use

a perturbative theory: new features, such as the colour confinement, become predominant and cannot be explained with perturbative techniques.

Another implication of the running of the coupling constants is the theorized unification of the strong and electroweak interaction. Since the strength of the interactions varies with energy, it is possible that at very high energies these interactions have the same strength ad can be described as a unified interaction with a single coupling constant. Such theories are called Grand Unified Theories (GUT) and the energy scale at which the electromagnetic and strong interactions can be described as a single interaction is called the GUT scale.

2.2.1 Abelian interaction

Matrices together with matrix multiplication form a group. Generally, matrix multiplication is not commutative, that is, given two matrices A and B on which matrix multiplication is defined, $AB \neq BA$. The non-commutative property implies that the group of matrices together with matrix multiplication is a non-commutative group also called a non-Abelian group.

A particular case is represented by the 1×1 matrices: they correspond to a number so that the multiplication is commutative, $AB = BA$. In this case the 1×1 matrices together with the numeric multiplication form an Abelian group.

An interaction that corresponds to an Abelian group is called Abelian interaction. An example of Abelian interaction is the electromagnetic force, the fermionic sector of which is described by the Lagrangian given in (2.7). This Lagrangian is symmetric under the U(1) group that is composed of all the 1×1 complex unitary matrices, that is 1×1 matrices U such that $UU^\dagger = U^\dagger U = \mathbb{1}$. These matrices are represented by the complex numbers $\mathrm{e}^{\mathrm{i}\alpha}$ and embody rotations, by the angle of rotation α, about the origin in the complex plane.

The U(1) invariance of the Dirac Lagrangian means that the Lagrangian (2.7) and the Lagrangian obtained by the substitution

$$\psi \to \mathrm{e}^{\mathrm{i}q\alpha}\psi \tag{2.11}$$

(where the factor q is introduced for a subsequent use) are the same:

$$\mathcal{L}_{\text{Dirac}} \xrightarrow{\psi \to \mathrm{e}^{\mathrm{i}q\alpha}\psi} \mathrm{e}^{-\mathrm{i}q\alpha}\bar{\psi}\big(\mathrm{i}\gamma^\mu\partial_\mu - m\big)\mathrm{e}^{\mathrm{i}q\alpha}\psi = \mathcal{L}_{\text{Dirac}}\,. \tag{2.12}$$

The transformation (2.11) is a global transformation, that is the angle α does not depend on the spacetime coordinate. The free Lagrangian (2.7)

is only invariant under the global symmetry (2.11) and not under the local symmetry

$$\psi \to \mathrm{e}^{\mathrm{i}q\alpha(x)}\psi \tag{2.13}$$

where x represent spacetime coordinates. In fact, applying the local transformation (2.13) to (2.1) we obtain

$$\mathcal{L}_{\text{Dirac}} \xrightarrow{\psi\to\mathrm{e}^{\mathrm{i}q\alpha(x)}\psi} \mathcal{L}_{\text{Dirac}} - q\bar{\psi}\big(\gamma^\mu\partial_\mu\alpha(x)\big)\psi\ . \tag{2.14}$$

Following the principle of local gauge invariance, we require the symmetry to be local that implies that the left hand side and the right hand side of (2.14) can differ only by a total derivative. To achieve this, we are obligated to modify the Dirac Lagrangian introducing an interaction. The right form for this interaction comes from classical electromagnetism where interactions are described using the four-potential $F_{\mu\nu}$ defined from the electromagnetic potential A_μ:

$$A_\mu \equiv (V, \boldsymbol{A}) \tag{2.15}$$

$$F_{\mu\nu} \equiv \partial_\nu A_\mu - \partial_\mu A_\nu \tag{2.16}$$

where V and $\boldsymbol{A}$ are the electric and magnetic potential. Since the potentials V and $\boldsymbol{A}$ are not uniquely defined we can apply the following gauge transformation

$$A_\mu \to A_\mu - \partial_\mu\alpha(x) \qquad \forall \text{ scalar function } \alpha \tag{2.17}$$

and the four-potential $F_{\mu\nu}$ remains unchanged:

$$F_{\mu\nu} \equiv \partial_\nu A_\mu - \partial_\mu A_\nu \ \to\ \big(\partial_\nu A_\mu - \partial_\nu\partial_\mu\alpha\big) - \big(\partial_\mu A_\nu - \partial_\mu\partial_\nu\alpha\big) = F_{\mu\nu}\ . \tag{2.18}$$

This invariance under a transformation such as (2.17) is called gauge invariance.

With this background, we can finally modify the Dirac Lagrangian adding to it an interaction term. This addition is performed by substituting, in the Dirac Lagrangian, the normal derivative ∂_μ with a covariant derivative D_μ:

$$\partial_\mu \to D_\mu = \partial_\mu + \mathrm{i}qA_\mu \tag{2.19}$$

so that the Dirac Lagrangian (2.1) becomes

$$\begin{aligned}\mathcal{L}_{\text{Dirac int}} &= \bar{\psi}\big(\mathrm{i}\gamma^\mu D_\mu - m\big)\psi = \bar{\psi}\big(\mathrm{i}\gamma^\mu\partial_\mu - m\big)\psi - q\bar{\psi}\gamma^\mu A_\mu\psi \\ &= \mathcal{L}_{\text{Dirac}} - q\bar{\psi}\gamma^\mu A_\mu\psi\,.\end{aligned} \tag{2.20}$$

The covariant derivative is thus responsible for a term $-q\bar{\psi}\gamma^\mu A_\mu\psi$ that, thanks to the gauge transformation (2.17) gives a term $q\bar{\psi}\big(\gamma^\mu\partial_\mu\alpha\big)\psi$ that cancels the term $-q\bar{\psi}\big(\gamma^\mu\partial_\mu\alpha\big)\psi$ in (2.14) and makes the Dirac Lagrangian invariant under the U(1) symmetry. In other words, the Lagrangian $\mathcal{L}_{\text{Dirac int}}$ in (2.20) is invariant when both the transformations

$$\begin{aligned} &\text{local U(1) symmetry:} && \psi \to \mathrm{e}^{\mathrm{i}q\alpha(x)}\psi \\ &\text{gauge transformation:} && A_\mu \to A_\mu - \partial_\mu\alpha(x) \end{aligned} \tag{2.21}$$

are performed together. In fact, starting from the previous Dirac Lagrangian (2.20), applying the local U(1) symmetry $\psi \to \mathrm{e}^{\mathrm{i}q\alpha(x)}\psi$ we obtain

$$\mathcal{L}_{\text{Dirac int}} \xrightarrow{\psi\to\mathrm{e}^{\mathrm{i}q\alpha(x)}\psi} \mathcal{L}^{\text{U(1)}}_{\text{Dirac int}} = \bar{\psi}\big(\mathrm{i}\gamma^\mu\mathrm{i}q\partial_\mu\alpha + \mathrm{i}\gamma^\mu\partial_\mu - m\big)\psi - q\bar{\psi}\gamma^\mu A_\mu\psi \tag{2.22}$$

where α is intended to have a spacetime dependence x even though it is not explicitly written. After, applying the gauge transformation $A_\mu \to A_\mu - \partial_\mu\alpha(x)$ to the previous expression (2.22), we obtain

$$\begin{aligned} \mathcal{L}^{\text{U(1)}}_{\text{Dirac int}} &\xrightarrow{A_\mu\to A_\mu+\partial_\mu\alpha} \bar{\psi}\big(-q\gamma^\mu\partial_\mu\alpha + \mathrm{i}\gamma^\mu\partial_\mu - m\big)\psi - q\bar{\psi}\gamma^\mu A_\mu\psi + q\bar{\psi}\gamma^\mu\big(\partial_\mu\alpha\big)\psi \\ &= \mathcal{L}_{\text{Dirac int}} \end{aligned} \tag{2.23}$$

thus we find again the Dirac Lagrangian in (2.20), that is $\mathcal{L}_{\text{Dirac int}}$ is invariant under the two transformations (2.21).

In summary, modifying the Lagrangian to be invariant under the local U(1) symmetry leads to the addition of a new term that describes interactions via the electromagnetic potential.

2.2.2 Non-Abelian interaction

Besides the U(1) group, the SM Lagrangian is also invariant under the SU(2) and SU(3) group. These are special unitary groups of degree 2 and 3 respectively. The word "unitary" refers to the property, already seen in U(1), that $UU^\dagger = U^\dagger U = \mathbb{1}$ satisfied by all matrices U in the unitary group. The word "special" refers to the property that $\det U = 1$ for all matrices U in the special group. So the SU(2) and SU(3) group are fundamentally represented by 2×2 matrices and 3×3 matrices respectively that respect both the properties mentioned above.

Since the multiplication between 2×2 matrices, as well as the multiplication between 3×3 matrices, is not commutative, SU(2) and SU(3) are non-commutative, or non-Abelian, groups. An interaction that corresponds to a non-Abelian group is called a non-Abelian interaction.

Following a similar procedure to the Abelian case, we substitute the normal derivative ∂_μ with a covariant derivative D_μ. In this way, we introduce new interaction terms and make the Lagrangian invariant under the new SU(2) and SU(3) symmetries.

In particular, the electroweak sector is described by a Lagrangian invariant under the $\mathrm{SU(2)_L}\otimes\mathrm{U(1)_Y}$ symmetry that gives rise to the covariant derivative

$$D_\mu = \partial_\mu + \mathrm{i}\frac{g_1}{2} Y B_\mu + \mathrm{i}\frac{g_2}{2}\tau W_\mu \,. \tag{2.24}$$

Here g_1 and g_2 are the coupling constants associated, respectively, with the $\mathrm{U(1)_Y}$ gauge field B_μ and with the tree $\mathrm{SU(2)_L}$ gauge fields $W_\mu = (W_\mu^1, W_\mu^2, W_\mu^3)$, Y is the weak hypercharge and $\tau = (\sigma^1, \sigma^2, \sigma^3)$ is written in terms of the Pauli matrices (2.4).

In the SM, leptons only have electroweak interactions. So in the Lagrangian, the left-handed lepton dynamical terms are written via the covariant derivative (2.24):

$$\mathcal{L}_{\text{Lepton, left}} = \bar{L}_i \mathrm{i}\bar{\boldsymbol{\sigma}}^\mu D_\mu L_i + \text{h.c.} \tag{2.25}$$

where the index i runs over the three generations, as specified in equation (2.8). Right-handed leptons do not interact with the gauge fields W_μ; in other words the coupling constant g_2 is null for right-handed fermions so that the covariant derivative is defined as

$$D_\mu = \partial_\mu + \mathrm{i}\frac{g_1}{2} Y B_\mu \,. \tag{2.26}$$

With this covariant derivative, the right-handed dynamical term is

$$\mathcal{L}_{\text{Lepton, right}} = \bar{e}_{i\mathrm{R}} \mathrm{i}\boldsymbol{\sigma}^\mu D_\mu e_{i\mathrm{R}} + \text{h.c.} \tag{2.27}$$

where, again, the index i represent the generation as in equation (2.9).

Fermions that also interact via the strong interaction are called quarks (see table 2.1). The symmetry that characterizes the strong interaction is the SU(3) symmetry.

Quarks interact through all the SM interaction so that the complete relevant symmetry is $\mathrm{SU(3)_C}\otimes\mathrm{SU(2)_L}\otimes\mathrm{U(1)_Y}$. The corresponding covariant derivative is

$$D_\mu = \partial_\mu + \mathrm{i}\frac{g_1}{2} Y B_\mu + \mathrm{i}\frac{g_2}{2}\tau W_\mu + \mathrm{i}\frac{g_s}{2}\lambda G_\mu \tag{2.28}$$

where g_s is the strong coupling constant, G_μ are the eight gluon gauge fields and $\lambda = (\lambda_1, \ldots, \lambda_8)$ are the Gell-Mann matrices [10].

As for the right-handed leptons, we could use this covariant derivative for all the fermions, specifying that g_s is null for leptons, that is leptons do not interact via the strong force.

Using this covariant derivative, the left-handed Lagrangian quark dynamical term is

$$\mathcal{L}_{\text{Quark, left}} = \bar{Q}_i \mathrm{i}\bar{\boldsymbol{\sigma}}^\mu D_\mu Q_i + \text{h.c.} \tag{2.29}$$

Like right-handed leptons, right-handed quarks do not interact with the W_μ gauge fields so that their covariant derivative is

$$D_\mu = \partial_\mu + \mathrm{i}\frac{g_1}{2} Y B_\mu + \mathrm{i}\frac{g_s}{2}\lambda G_\mu \tag{2.30}$$

and the right-handed dynamical terms are

$$\mathcal{L}_{\text{Quark, right}} = \bar{u}_{i\text{R}} \mathrm{i}\boldsymbol{\sigma}^\mu D_\mu u_{i\text{R}} + \bar{d}_{i\text{R}} \mathrm{i}\boldsymbol{\sigma}^\mu D_\mu d_{i\text{R}} + \text{h.c.} \tag{2.31}$$

2.2.3 Gauge terms

In the covariant derivative (2.28) we introduce the gauge fields B_μ, W_μ and G_μ. To find their kinetic terms, we start with the group theory of the symmetry groups SU(3), SU(2) and U(1). Each element U of these groups, and in general of SU(N), can be written as [10, 17]:

$$\text{SU}(N): \qquad U = \exp\left(\mathrm{i}gT^a\theta^a\right) \quad \text{with} \quad a = 1, \ldots, N^2 - 1 \tag{2.32}$$

where T^a are the generators of the group, which in in the fundamental representation can be represented by Hermitian traceless matrices of dimension $N \times N$, while θ^a are the transformation parameters. g is a common numerical factor that can be fixed normalizing the generators. It plays a fundamental role in physics: g is the coupling constant of the interaction described by the related symmetry group. The generators T^a satisfy the commutation relations

$$\left[T^a, T^b\right] = \mathrm{i}f^{abc}T^c \tag{2.33}$$

where the numbers f are the structure constants. The relations (2.33) define the algebra of the group. The normalization of the generators is arbitrary. To normalise the generators we can impose the structure constants f to satisfy

$$\sum_{c,d} f^{acd} f^{bcd} = N\delta^{ab} \tag{2.34}$$

so that the generators for SU(N) satisfy

$$\text{Tr}\left(T^a T^b\right) = \frac{1}{2}\delta^{ab}\,. \tag{2.35}$$

From the structure constants f we can define the quantity

$$\left(T^a_{\text{adj}}\right)^{bc} = -\mathrm{i}f^{abc}\,. \tag{2.36}$$

Since T^a_{adj} satisfy Eq. (2.33), as can be verified using (2.34), T^a_{adj} is a valid representation of the group and is called adjoint representation.

As we have seen in the previous sections, we start with a Lagrangian that is invariant under a global SU(3)⊗SU(2)⊗U(1) transformation, that means the Lagrangian is invariant if we apply the SU(3), SU(2) and U(1) transfromation (2.32) to the field ψ, where θ does not depend on the spacetime coordinates x. Now we can apply the gauge principle, that is require the Lagrangian to be invariant under the local transformation

$$\psi \to \psi' = U(x)\psi \qquad \text{with} \quad U(x) = \exp\left(\mathrm{i}gT^a\theta^a(x)\right) . \tag{2.37}$$

To satisfy this requirement of invariance, we have to introduce the covariant derivative

$$D_\mu = \partial_\mu + \mathrm{i}gA^a_\mu T^a . \tag{2.38}$$

In the SM for the SU(2) case, the above coupling constant g correspond to g_2, the fields A^a_μ correspond to the three gauge fields W^i_μ and the T^a matrices correspond to the $\frac{1}{2}\sigma^a$ matrices where σ^a are the Pauli matrices:

$$\text{SU(2):} \quad \begin{cases} g \to g_2 \\ A^a_\mu \to W^i_\mu \\ T^a \to \dfrac{1}{2}\sigma^a \end{cases} . \tag{2.39}$$

In this case we get the covariant derivatives (2.24) and (2.26) acting on the left- and right-handed electroweak particles.

In the SU(3) case, the coupling constant g correspond to g_s, the fields A^a_μ correspond to the eight gluon gauge fields G^a_μ and the T^a matrices correspond to the $\frac{1}{2}\lambda^a$ matrices where λ^a are the Gell-Mann matrices:

$$\text{SU(3):} \quad \begin{cases} g \to g_s \\ A^a_\mu \to G^a_\mu \\ T^a \to \dfrac{1}{2}\lambda^a \end{cases} . \tag{2.40}$$

In this case we get the covariant derivatives (2.28) and (2.30) acting on the left- and right-handed strongly interacting particles.

In the covariant derivatives each gauge field is related to each generator of the corresponding group. From the covariant derivative expressions, the following generator-field associations hold:

- the U(1) generator Y and the single gauge field B_μ;

- the three SU(2) generators $\tau = (\sigma^1, \sigma^2, \sigma^3)$ and the three gauge fields W^i_μ;
- the eight SU(3) generators, the Gell-Mann matrices $\lambda = (\lambda_1, \ldots, \lambda_8)$ and the eight gauge matrix valued fields G^a_μ.

Since these gauge fields propagate in spacetime we can describe them with a gauge invariant kinetic Lagrangian. To do so, we define the gauge field A_μ

$$A_\mu \equiv A^a_\mu T^a \tag{2.41}$$

where A^a_μ was introduced in Eq. (2.38), (2.39) and (2.40). The corresponding field strength tensor is defined as

$$F_{\mu\nu} = \partial_\mu A_\nu - \partial_\nu A_\mu - \mathrm{i}g\big[A_\mu, A_\nu\big] \tag{2.42}$$

and can be expanded over the generators T^a

$$F_{\mu\nu} = F^a_{\mu\nu} T^a = \partial_\mu A^a_\nu - \partial_\nu A^a_\mu + g f^{abc} A_{b\mu} A_{c\nu} \,. \tag{2.43}$$

In the expansion we used Eq. (2.33), f are the structure constants defined in (2.33) and (2.34) and g is the coupling constant defined in (2.32). Finally, from the field strength tensor of the gauge field, using the normalization of the generators (2.35), we derive the kinetic Lagrangian for the gauge fields as

$$\mathcal{L}_{\text{gauge}} = -\frac{1}{2} \operatorname{Tr} F_{\mu\nu} F^{\mu\nu} = -\frac{1}{2} F^a_{\mu\nu} F^{\mu\nu b} \operatorname{Tr} T^a T^b = -\frac{1}{4} F^a_{\mu\nu} F^{\mu\nu a} \tag{2.44}$$

that is invariant under the gauge transformation

$$F_{\mu\nu} \to F'_{\mu\nu} = U F_{\mu\nu} U^\dagger \,. \tag{2.45}$$

From this expression we can infer the transformation of the components $F^a_{\mu\nu}$

$$F^a_{\mu\nu} \to (F^a_{\mu\nu})' = F^a_{\mu\nu} + f^{bac} \theta^b F^c_{\mu\nu} = F^a_{\mu\nu} + \mathrm{i}(T^b_{\text{adj}})^{ac} \theta^b F^c_{\mu\nu} \tag{2.46}$$

where we have used the asymmetry of the structure constants and the definition (2.36). This expression is the infinitesimal form of

$$F_{\mu\nu} = \exp\left(\mathrm{i} T^b_{\text{adj}} \theta^b\right) F_{\mu\nu} \tag{2.47}$$

that shows that the field strength tensor $F_{\mu\nu}$ transforms in the adjoint representation.

For example, in case of the $\mathrm{U}(1)_\mathrm{Y}$ symmetry, from the gauge field B_μ, we define the field strength tensor $B_{\mu\nu}$

$$B_{\mu\nu} = \partial_\mu B_\nu - \partial_\nu B_\mu \tag{2.48}$$

that correspond to the 4-potential (2.16). This particular field strength tensor does not have the structure constants f because the U(1) group is composed of complex numbers together with the normal number multiplication and the structure constants, that define the multiplication, all vanish. Indeed, from the definition (2.33)

$$\mathrm{i} f^{abc} T_c = \Big[T^a, T^b\Big] = T^a T^b - T^b T^a \quad \xrightarrow[group]{commutative} \quad T^a T^b - T^a T^b = 0 \tag{2.49}$$

For a commutative group, such as U(1), all the generators commute with each other.

Having defined the field strength tensor $B_{\mu\nu}$, from (2.44) the U(1) gauge field kinetic term is

$$\mathcal{L}_{\mathrm{U}(1)} = -\frac{1}{4} B_{\mu\nu} B^{\mu\nu} \ . \tag{2.50}$$

In the SU(2) and SU(3) cases the structure constants are not zero. In fact, while U(1) elements can be represented by complex numbers that commute, SU(2) and SU(3) elements are the matrices (2.32) where the generators do not commute.

In the particular case of SU(2), the generators are the Pauli matrices (2.4) conventionally normalized as:

$$T^a = \frac{\sigma^a}{2} \tag{2.51}$$

whose commutation relations are, from (2.5),

$$\Big[T^a, T^b\Big] = \mathrm{i}\epsilon^{abc} T^c \ . \tag{2.52}$$

The structure constants are represented by the Levi-Civita symbol ϵ^{abc}. The SU(2) strength tensor $W^a_{\mu\nu}$ is thus defined as

$$W^a_{\mu\nu} = \partial_\mu W^a_\nu - \partial_\nu W^a_\mu + g\epsilon^{abc} W_{b\mu} W_{c\nu} \tag{2.53}$$

where W^a_μ are the SU(2) gauge fields. The kinetic Lagrangian of W_μ is

$$\mathcal{L}_{\mathrm{SU}(2)} = -\frac{1}{2} \mathrm{Tr}\left(W_{\mu\nu} W^{\mu\nu}\right) = -\frac{1}{4} W^a_{\mu\nu} W^{\mu\nu}_a \ . \tag{2.54}$$

In a similar way, we can find the generators of SU(3) that are eight 3 by 3 matrices, known as Gell-Mann matrices [10] and denoted by λ_i. They respect the commutations relations

$$\left[\frac{\lambda_i}{2}, \frac{\lambda_j}{2}\right] = \mathrm{i} f^{ijk} \frac{\lambda_k}{2} \tag{2.55}$$

where the structure constants f^{ijk} are completely antisymmetric in the three indices and have values $f^{123} = 1$, $f^{147} = f^{165} = f^{246} = f^{257} = f^{345} = f^{376} = \frac{1}{2}$ and $f^{458} = f^{678} = \frac{\sqrt{3}}{2}$. The SU(3) gauge fields are denoted by G^a_μ and are called gluon fields. From the gluon fields and the structure constants, we can define the field strength tensor $G^a_{\mu\nu}$

$$G^a_{\mu\nu} = \partial_\mu G^a_\nu - \partial_\nu G^a_\mu - g_s f^{abc} G^b_\mu G^c_\nu \tag{2.56}$$

and with $G^a_{\mu\nu}$ we can write the kinetic Lagrangian of the SU(3) gauge field:

$$\mathcal{L}_{\mathrm{SU(3)}} = -\frac{1}{2} \mathrm{Tr}\left(G_{\mu\nu} G^{\mu\nu}\right) = -\frac{1}{4} G^a_{\mu\nu} G^{\mu\nu}_a \quad . \tag{2.57}$$

2.3 Electroweak symmetry breaking

Experimentally, all fermions and the gauge bosons mediators of the weak interactions, the $W^\pm$ and Z^0 particles, are massive particles. This fact must be reflected in the Lagrangian where we expect some terms, called mass terms, to be included for fermions, $W^\pm$ and Z^0. In the Dirac Lagrangian (2.1) fermion mass terms take the form $-m\bar{\psi}\psi = -m\Big(\bar{\psi}_\mathrm{L}\psi_\mathrm{R} + \bar{\psi}_\mathrm{R}\psi_\mathrm{L}\Big)$ and such terms imply that fermion could flip chirality. Doing so, the total hypercharge, that is different for left and right-handed fermions, would not be conserved. For the $W^\pm$ and Z^0 bosons, a mass term of the form $mA^\mu A_\mu$ would spoil the gauge principle because a non-vanishing m breaks the local gauge invariance of the Lagrangian. So, to generate masses, on the one hand, we need to break the gauge symmetry, and on the other hand, we need a fully symmetric Lagrangian.

The Higgs mechanism solves both these problems introducing a new complex scalar field ϕ that give mass to fermions, via Yukawa interactions between fermions and Higgs fields, and to the gauge bosons $W^\pm$ and Z^0, via the spontaneous symmetry breaking (SSB) mechanism. To explain this mechanism consider a field ϕ, called Higgs field that is a $\mathrm{SU(2)_L}$ doublet

$$\phi(x) = \begin{pmatrix} \phi^+(x) \\ \phi^0(x) \end{pmatrix} \tag{2.58}$$

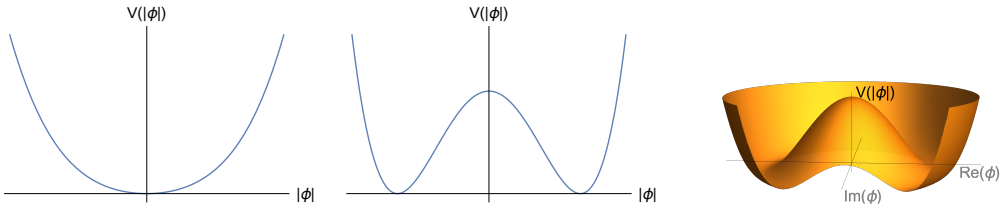

(a) *Parabolic-like potential* **(b)** *Mexican hat potential* **(c)** *3D Mexican hat*

Figure 2.1: The parabolic-like potential is characterised by $\mu^2 \geq 0$ while the Mexican hat potential has $\mu^2 < 0$; the two dimensional Mexican hat potential has a continuous set of degenerate minima.

and start with the Lagrangian

$$\mathcal{L} = \left(\partial_\mu \phi\right)^\dagger \partial^\mu \phi - V(\phi) \qquad V(\phi) = \mu^2 \phi^\dagger \phi + \lambda \left(\phi^\dagger \phi\right)^2 . \tag{2.59}$$

This Lagrangian is invariant under the U(1) global symmetry $\phi(x) \to \mathrm{e}^{\mathrm{i}\alpha}\phi(x)$ where α does not depend on the spacetime coordinate x.

To make this Lagrangian invariant under the local $SU(2)_\mathrm{L} \otimes U(1)_\mathrm{Y}$ we substitute the derivative with the covariant derivative (2.24) so that the Lagrangian becomes

$$\mathcal{L} = \left(D_\mu \phi\right)^\dagger D^\mu \phi - \mu^2 \phi^\dagger \phi - \lambda \left(\phi^\dagger \phi\right)^2 . \tag{2.60}$$

In the potential $V(\phi)$, Eq. (2.59), the parameter λ is chosen to be positive, $\lambda > 0$, in order that the potential is bounded from below. Regarding μ^2 there are two possible choices, $\mu^2 \geq 0$ and $\mu < 0$. For $\mu^2 \geq 0$ the potential, depicted in Fig. 2.1a, has a parabolic-like shape and it is not useful for the Higgs mechanism. The interesting case $\mu^2 < 0$ leads instead to the so-called Mexican hat potential, see Fig. 2.1b and 2.1c. With this choice, the potential exhibits a local maximum at the origin so that the system is unstable at the origin. Away from the origin there are minima where the system is stable. The Higgs mechanism requires $\mu^2 < 0$ so we will focus on this case.

To develop a perturbative quantum field theory we need to consider excitations around a minimum of the potential that correspond to the ground state of the system. These field configurations can be found requiring $\frac{\partial V(|\phi|^2)}{\partial |\phi^2|} = 0$ and are such that:

$$|\phi|^2 = \frac{-\mu^2}{2\lambda} \equiv \frac{1}{2} v^2 \tag{2.61}$$

where we have defined $v \equiv \sqrt{\frac{-\mu^2}{\lambda}}$.

In two dimensions, fig. 2.1b, there are only two solutions of (2.61): $\phi = \pm\frac{v}{\sqrt{2}}$, while in three dimensions, fig. 2.1c, there is a continuous set of degenerate minima, that can be parametrised with a phase θ: $\phi(x) = \frac{v}{\sqrt{2}}\mathrm{e}^{\mathrm{i}\theta}$. Since these are minima of the potential, the system spontaneously tends to settle into these configurations.

Now we consider excitations of the ground state expressing the Higgs field $\phi(x)$ as the sum of its vacuum expectation value (VEV), $\langle\phi\rangle$, given by a solution of (2.61) that is a numerical constant, and a function $H(x)$: $\phi(x) = \langle\phi\rangle + H(x)$. Plugging this expression into the Lagrangian (2.59) and expanding it, we can identify the mass m_H of the Higgs boson, the particle associated with the excitation of the Higgs field:

$$m_H = \sqrt{-2\mu^2} = \sqrt{2\lambda}\, v \,. \tag{2.62}$$

Once the system is in the ground state configuration, a particular minimum of the potential $V(\phi)$, Eq. (2.59), have been chosen among all the degenerate minima. This choice breaks the symmetry of the system. In one dimension it corresponds to choosing one out of the two possible solutions of Eq. (2.61), so that the VEV of the Higgs field ϕ can be plus or minus $\frac{v}{\sqrt{2}}$; for simplicity it is usual to choose the positive sign so that the VEV is $\langle\phi\rangle = \frac{v}{\sqrt{2}}$. In two dimensions breaking the symmetry corresponds to choose a specific phase θ among the all the possible values in $[0, 2\pi[$ that is a direction in the complex plane, see fig. 2.1c. Again for simplicity, we choose the value $\theta = 0$ so that the real and imaginary part of the VEV are $\mathrm{Re}\,\langle\phi\rangle = \frac{v}{\sqrt{2}}$, $\mathrm{Im}\,\langle\phi\rangle = 0$ that is we choose the direction of the positive real axis.

In the standard model the Higgs field is made of four real fields: $\phi = \begin{pmatrix} {\phi^+}_\mathrm{R} + \mathrm{i}{\phi^+}_\mathrm{I} \\ {\phi^0}_\mathrm{R} + \mathrm{i}{\phi^0}_\mathrm{I} \end{pmatrix}$ where the R and I subscripts indicate the real and imaginary part of the elements of the $\mathrm{SU(2)_L}$ doublet (2.58). Now we can parametrise $\phi(x)$ in terms of three angles $\theta^{i=1,2,3}(x)$ and a function $H(x)$ in the following general form:

$$\phi(x) = \frac{1}{\sqrt{2}} \exp\left[\mathrm{i}\frac{\sigma_i}{2}\theta^i(x)\right] \begin{pmatrix} 0 \\ v + H(x) \end{pmatrix} \tag{2.63}$$

where σ_i are the generators of $\mathrm{SU(2)_L}$, Eq. (2.4), and the θ^i are the Nambu-Goldstone bosons each of which correspond, according to the Goldstone theorem, to a generator of a broken symmetry.

Now we can take advance of the $\mathrm{SU(2)_L}$ gauge invariance and fix the three $\theta^i = 0$ so that the Higgs field simplifies to

$$\phi(x) = \frac{1}{\sqrt{2}} \begin{pmatrix} 0 \\ v + H(x) \end{pmatrix} . \tag{2.64}$$

The gauge in which the Higgs field has the expression (2.64) is called unitary gauge. This Higgs field interacts and gives mass to fermions and gauge bosons, as shown in the following sections.

2.3.1 Gauge bosons masses

The gauge bosons masses come from the kinetic term $\left(D_\mu\phi\right)^\dagger D^\mu\phi$ in (2.60). To calculate this we use the covariant derivative (2.24) and the Higgs field in unitary gauge (2.64):

$$D_\mu\phi = \frac{1}{\sqrt{2}}\left[\partial_\mu\begin{pmatrix}0\\ v+H(x)\end{pmatrix} + \mathrm{i}\frac{g_1}{2}YB_\mu\begin{pmatrix}0\\ v+H(x)\end{pmatrix} + \mathrm{i}\frac{g_2}{2}\begin{pmatrix}W_\mu^3 & W_\mu^1-\mathrm{i}W_\mu^2\\ W_\mu^1+\mathrm{i}W_\mu^2 & -W_\mu^3\end{pmatrix}\begin{pmatrix}0\\ v+H(x)\end{pmatrix}\right]. \tag{2.65}$$

Now we can introduce the physical fields

$$W_\mu^+ = \frac{1}{\sqrt{2}}\left(W_\mu^1-\mathrm{i}W_\mu^2\right) \qquad W_\mu^- = \frac{1}{\sqrt{2}}\left(W_\mu^1+\mathrm{i}W_\mu^2\right) \tag{2.66}$$

so that the kinetic term is

$$\left(D_\mu\phi\right)^\dagger D^\mu\phi = \frac{1}{2}\left[\left|\mathrm{i}\frac{g_2}{2}(v+H)W_\mu^+\right|^2 + \left|\partial_\mu H + \mathrm{i}\frac{g_1}{2}YB_\mu(v+H) - \mathrm{i}\frac{g_2}{2}(v+H)W_\mu^3\right|^2\right]. \tag{2.67}$$

To diagonalise masses, we rotate the B_μ and W_μ^3 fields by an angle θ_W, called Weinberg angle or weak mixing angle, and define the new fields as A_μ and Z_μ:

$$\begin{pmatrix}A_\mu\\ Z_\mu\end{pmatrix} \equiv R(\theta_W)\begin{pmatrix}B_\mu\\ W_\mu^3\end{pmatrix} = \begin{pmatrix}\cos\theta_W B_\mu + \sin\theta_W W_\mu^3\\ -\sin\theta_W B_\mu + \cos\theta_W W_\mu^3\end{pmatrix} \tag{2.68}$$

$$\implies \begin{pmatrix}B_\mu\\ W_\mu^3\end{pmatrix} = \begin{pmatrix}\cos\theta_W A_\mu - \sin\theta_W Z_\mu\\ \sin\theta_W A_\mu + \cos\theta_W Z_\mu\end{pmatrix}. \tag{2.69}$$

Plugging these expressions into the kinetic term (2.67), expanding it and noting that $\left(W_\mu^+\right)^\dagger = W_\mu^-$, we find the following mass terms [10]

$$0A_\mu A^\mu + \frac{1}{4}\left(g_1^2+g_2^2\right)v^2 Z_\mu Z^\mu + \frac{1}{4}g_2^2v^2W_\mu^+W^{\mu+} \tag{2.70}$$

so that the photon, the Z boson and the $W^{\pm}$ bosons, that are the particles associated with the A_μ, Z_μ and $W^{\pm}_\mu$ fields, have masses

$$m_\gamma = 0 \qquad m_Z = \frac{1}{2}v\sqrt{g_1^2 + g_2^2} \qquad m_{W^\pm} = \frac{1}{2}vg_2 \,. \tag{2.71}$$

2.3.2 Fermion masses

The Higgs field couples to the fermion fields. We can describe this coupling in the Lagrangian with a $\mathrm{SU(3)_C}\otimes\mathrm{SU(2)_L}\otimes\mathrm{U(1)_Y}$ gauge invariant terms known as Yukawa terms:

$$\mathcal{L}_\mathrm{Y} = -Y^e_{ij}\bar{L}^i\phi e^j{}_\mathrm{R} - Y^d_{ij}\bar{Q}^i\phi d^j{}_\mathrm{R} - Y^u_{ij}\bar{Q}^i\tilde{\phi}u^j{}_\mathrm{R} + \mathrm{h.c.} \tag{2.72}$$

Here Y^e_{ij}, Y^d_{ij} and Y^u_{ij} are the Yukawa matrices with indices i, j running over the three generations, ϕ is the Higgs field and $\tilde{\phi} \equiv \mathrm{i}\sigma^2\phi^\dagger$, and the other fields are defined in Eq. (2.8) and (2.9). The elements of the Yukawa matrices are dimensionless constant that represents the strength of the interaction between the fermion and the Higgs fields and thus depend on the fermion field taken into consideration.

Using the unitary gauge where the Higgs field is expressed by (2.64) and expanding the $\mathrm{SU(2)_L}$ doublets fermion fields, the Yukawa term is

$$\begin{aligned}\mathcal{L}_\mathrm{Y} = -\frac{1}{\sqrt{2}}\Bigg[&Y^e_{ij}(\bar{\nu}_{e\mathrm{L}}, \bar{e}_\mathrm{L})^i \begin{pmatrix} 0 \\ v + H(x) \end{pmatrix} e^j{}_\mathrm{R} \\ &+ Y^d_{ij}\begin{pmatrix}\bar{u}_\mathrm{L}, \bar{d}_\mathrm{L}\end{pmatrix}^i \begin{pmatrix} 0 \\ v + H(x) \end{pmatrix} d^j{}_\mathrm{R} + Y^u_{ij}\begin{pmatrix}\bar{u}_\mathrm{L}, \bar{d}_\mathrm{L}\end{pmatrix}^i \begin{pmatrix} v + H^\dagger(x) \\ 0 \end{pmatrix} u^j{}_\mathrm{R}\Bigg] + \mathrm{h.c.}\end{aligned} \tag{2.73}$$

To find the masses we consider only terms with two fields that are

$$\mathcal{L}_m = -\frac{v}{\sqrt{2}}\Big(Y^e_{ij}\bar{e}^i{}_\mathrm{L}e^j{}_\mathrm{R} + Y^d_{ij}\bar{d}^i{}_\mathrm{L}d^j{}_\mathrm{R} + Y^u_{ij}\bar{u}^i{}_\mathrm{L}u^j{}_\mathrm{R}\Big) + \mathrm{h.c.} \tag{2.74}$$

To diagonalise the masses, we can write the Yukawa matrices as

$$Y^e = U^e M^e K^{e\dagger} \qquad Y^d = U^d M^d K^{d\dagger} \qquad Y^u = U^u M^e K^{u\dagger} \tag{2.75}$$

where M^e, M^d and M^u are diagonal matrices and U^e, U^d, U^u, K^e, K^d and K^u are unitary matrices. Now we can transform the fields as

$$e_\mathrm{L} \to U^e e'_\mathrm{L} \qquad d_\mathrm{L} \to U^d d'_\mathrm{L} \qquad u_\mathrm{L} \to U^u u'_\mathrm{L} \tag{2.76}$$

$$e_\mathrm{R} \to K^e e'_\mathrm{R} \qquad d_\mathrm{R} \to K^d d'_\mathrm{R} \qquad u_\mathrm{R} \to K^u u'_\mathrm{R} \tag{2.77}$$

where the fields on the left hand side are expressed in the flavour basis, while the prime symbol on the fields on the right hand side means the fields are expressed in the mass basis. Plugging expressions (2.75), (2.76) and (2.77) into the Lagrangian (2.74) removes the U and K unitary matrices leaving only the diagonal M matrices; thus we can write the Lagrangian (2.74) as

$$\mathcal{L}_m = -\frac{v}{\sqrt{2}} M^e_{ii} \bar{e'}^i{}_{\mathrm{L}} e'^i{}_{\mathrm{R}} - \frac{v}{\sqrt{2}} M^d_{ii} \bar{d'}^i{}_{\mathrm{L}} d'^i{}_{\mathrm{R}} - \frac{v}{\sqrt{2}} M^u_{ii} \bar{u'}^i{}_{\mathrm{L}} u'^i{}_{\mathrm{R}} + \text{h.c.} \tag{2.78}$$

and we can identify the fermion masses

$$m_{e'^i} = \frac{v}{\sqrt{2}} M^e_{ii} \qquad m_{d'^i} = \frac{v}{\sqrt{2}} M^d_{ii} \qquad m_{u'^i} = \frac{v}{\sqrt{2}} M^u_{ii} \,. \tag{2.79}$$

2.3.3 CKM matrix

Equations (2.76) and (2.77) represent the transformation from the so called flavour basis to the mass basis. Since the U and K matrices are unitary, in the Lagrangian all the terms $\bar{f} f$ are equal to $\bar{f}' f'$, where f is one of the left- or right-handed fermion fields $e_{\mathrm{L}}, d_{\mathrm{L}}, l_{\mathrm{L}}, e_{\mathrm{R}}, d_{\mathrm{R}}, l_{\mathrm{R}}$ in the flavour basis and f' is the corresponding field in the mass basis. Thus going from the flavour basis to the mass basis does not change these terms.

On the other hand, Lagrangian terms that mix u and d type quarks are modified since in general $U^{u\dagger} U^d \neq \mathbb{1}$. Thus, the u and d type quarks mixing generates a new unitary matrix V:

$$\bar{u}_{\mathrm{L}} d_{\mathrm{L}} = \left(U^u u'_{\mathrm{L}}\right)^\dagger \left(U^d d'_{\mathrm{L}}\right) = \bar{u}'_{\mathrm{L}} U^{u\dagger} U^d d'_{\mathrm{L}} = \bar{u}'_{\mathrm{L}} V d'_{\mathrm{L}} \tag{2.80}$$

where V is the Cabibbo-Kobayashi-Maskawa matrix, also called CKM matrix

$$V \equiv U^{u\dagger} U^d = \begin{pmatrix} V_{ud} & V_{us} & V_{ub} \\ V_{cd} & V_{cs} & V_{cb} \\ V_{td} & V_{ts} & V_{tb} \end{pmatrix} . \tag{2.81}$$

The elements of V couple all possible u and d type quarks and their square indicate the transition probability from a u type quark to a d type quark.

The CKM matrix is a complex 3 by 3 matrix, but since by construction it is a unitary matrix it can be expressed by 6 phases and 3 angles. Now Lagrangian terms that mix u and d type quarks are of the form $(u, c, t) V \begin{pmatrix} d \\ s \\ b \end{pmatrix} = uV_{ud}d + uV_{us}s + uV_{ub}b + cV_{cd}d + cV_{cs}s + cV_{cb}b + tV_{td}d + tV_{ts}s + tV_{tb}b$ so we can absorb 5 phases of the V elements in the quark fields using the U(1) symmetry, that is redefining, for example, $u \to \mathrm{e}^{i\phi_u} u$, $s \to \mathrm{e}^{i\phi_s} s$, $b \to \mathrm{e}^{i\phi_b} b$, $c \to \mathrm{e}^{i\phi_c} c$,

$t \to \mathrm{e}^{i\phi_t} t$. After this redefinition we have 1 phase and 3 angles, so 4 real parameters define the CKM matrix. Choosing different angles and phase leads to different expression of the CKM matrix. The standard parametrization uses angles θ_{23}, θ_{13} and θ_{12}, that correspond to rotation in the flavour planes and a phase attached to the θ_{13} rotation:

$$V = \begin{pmatrix} 1 & 0 & 0 \\ 0 & \cos\theta_{23} & \sin\theta_{23} \\ 0 & -\sin\theta_{23} & \cos\theta_{23} \end{pmatrix} \tag{2.82}$$
$$\times \begin{pmatrix} \cos\theta_{13} & 0 & \mathrm{e}^{-\mathrm{i}\delta}\sin\theta_{13} \\ 0 & 1 & 0 \\ -\mathrm{e}^{\mathrm{i}\delta}\sin\theta_{13} & 0 & \cos\theta_{13} \end{pmatrix} \begin{pmatrix} \cos\theta_{12} & \sin\theta_{12} & 0 \\ -\sin\theta_{12} & \cos\theta_{12} & 0 \\ 0 & 0 & 1 \end{pmatrix}$$
$$= \begin{pmatrix} c_{12}c_{13} & c_{13}s_{12} & s_{13}\mathrm{e}^{-\mathrm{i}\delta} \\ -c_{23}s_{12} - c_{12}s_{13}s_{23}\mathrm{e}^{\mathrm{i}\delta} & c_{12}c_{23} - s_{12}s_{13}s_{23}\mathrm{e}^{\mathrm{i}\delta} & c_{13}s_{23} \\ s_{12}s_{23} - c_{12}c_{23}s_{13}\mathrm{e}^{\mathrm{i}\delta} & -c_{23}s_{12}s_{13} - c_{12}s_{23}\mathrm{e}^{\mathrm{i}\delta} & c_{13}c_{23} \end{pmatrix} \tag{2.83}$$

where $c_{ij} \equiv \cos\theta_{ij}$ and $s_{ij} \equiv \sin\theta_{ij}$. The experimental values, taking into account theoretical constraints such as the unitarity of the three generations [18], are

$$V_{\mathrm{exp}} = \begin{pmatrix} 0.97446 \pm 0.00010 & 0.22452 \pm 0.00044 & 0.00365 \pm 0.00012 \\ 0.22438 \pm 0.00044 & 0.97359^{+0.00010}_{-0.00011} & 0.04214 \pm 0.00076 \\ 0.00896^{+0.00024}_{-0.00023} & 0.04133 \pm 0.00074 & 0.999105 \pm 0.000032 \end{pmatrix}. \tag{2.84}$$

where each element is the measure of the absolute value of the corresponding element in (2.83), for example, $|s_{13}\mathrm{e}^{-\mathrm{i}\delta}| = \sin\theta_{13} = 0.00365 \pm 0.00012$. From the expressions (2.83) and the values (2.84) we can infer the angles θ_{ij}

$$\theta_{12} = \arctan\frac{V_{12}}{V_{11}} = 12.975^\circ \pm 0.025^\circ \qquad \theta_{13} = \arcsin V_{13} = 0.209^\circ \pm 0.007^\circ$$
$$\theta_{23} = \arctan\frac{V_{23}}{V_{33}} = 2.42^\circ \pm 0.04^\circ\,. \tag{2.85}$$

Since the CKM matrix is almost a diagonal matrix, the most likely charged-current transitions are between quarks belonging to the same generation. In terms of the mixing between different generations, the angle θ_{12}, that is the angle between the first two generations, is the predominant one.

The phase δ can be easily found in the Wolfenstein parametrization of the CKM matrix. This parametrization relates the standard parameters θ_{ij} and

the phase δ to the parameters A, λ, ρ and η in this way, [19–21]:

$$\sin\theta_{12} = \lambda = \frac{|V_{12}|}{\sqrt{|V_{11}|^2 + |V_{12}|^2}} \qquad \sin\theta_{23} = A\lambda^2 = \lambda\frac{|V_{23}|}{|V_{12}|} \tag{2.86}$$

$$\sin\theta_{13}\mathrm{e}^{\mathrm{i}\delta} = V_{13}^* = \frac{A\lambda^3(\rho+\mathrm{i}\eta)\sqrt{1-A^2\lambda^4}}{\sqrt{1-\lambda^2}\left[1-A^2\lambda^4(\rho+\mathrm{i}\eta)\right]} \tag{2.87}$$

and the experimental values, given by the CKMfitter Group, are [21, 22]

$$\begin{aligned} A &= 0.8403^{+0.0056}_{-0.0201} & \lambda &= 0.224747^{+0.000254}_{-0.000059} \\ \rho &= 0.1577^{+0.0096}_{-0.0074} & \eta &= 0.3493^{+0.0095}_{-0.0071} \end{aligned} \quad . \tag{2.88}$$

Dividing the imaginary part by the real part of both sides of equation (2.87) we can find the expression of $\tan\delta$:

$$\tan\delta = \frac{\eta}{\rho - A^2\lambda^4\left(\eta^2+\rho^2\right)} \implies \delta = 65.7^{\circ\,+1.4^\circ}_{\;-1.1^\circ} \tag{2.89}$$

where the numerical value of δ is given by the experimental values (2.88).

CP violation

In the CKM matrix, the phase δ represents a crucial parameter: it implies a complex coefficient in the SM Lagrangian. Now, since the T operator is anti-unitary, that is $T\mathrm{i} = -\mathrm{i}T$, the imaginary part of a complex term violates T and so, to be TCP invariant, this imaginary term must violate CP too. In this way, the phase δ is a source of CP violation in the SM.

An important and active field of research where the CP violation is fundamental is the study of the baryonic asymmetry of the Universe (BAU). Astrophysical observation suggests that all the content of our Universe, for example galaxies, stars, planets, gas clouds and atoms, is made of matter while no antimatter is detected with similar abundance. The CP violation is a necessary element to explain the origin of this asymmetry. However, the CP violation originated from the phase δ in the CKM matrix cannot explain the abundance of matter over antimatter we observe in the Universe. Indeed, the inability of the SM to explain the BAU is one of the theoretical problems that require the development of physics beyond the SM.

2.4 Gauge fixing

Gauge theories describe physical systems in terms of fields that present more degrees of freedom than the ones the physical system has. A clear example is

given by the gauge electromagnetic theory described with the electromagnetic potential A_μ: as seen in Equation (2.17) the scalar function $\alpha(x)$ introduce a new degree of freedom that does not modify the physical electric E and magnetic B fields. The freedom given by the free choice of $\alpha(x)$ allows us to impose a constraint on the gauge fields A_μ; this constraint represents a gauge fixing.

Choosing a gauge influence deeply the calculations, so that a good gauge choice is represented by a gauge that simplifies the calculations.

There is lots of freedom in choosing a gauge. Here we describe some standard gauges that will be useful later.

2.4.1 Coulomb Gauge

The Coulomb gauge is fixed by the condition that the four-potential A has no divergence:

$$\partial^i A_i = 0 \tag{2.90}$$

where i runs from 1 to 3.

This gauge is useful, for example, in electromagnetism see [10]. In this case, the four-potential A_μ describes the photon field that, in free space, can be written as:

$$A_\mu(x) = \int \frac{\mathrm{d}^4 p}{(2\pi)^4}\, \mathrm{e}^{-\mathrm{i}p^\nu x_\nu} \epsilon_\mu(p) \tag{2.91}$$

where $\epsilon_\mu(p)$ is the polarization vector that depend only on the four-momentum p and not on the spacetime position x_μ.

Fixing the Coulomb gauge (2.90),

$$\partial^i A_i = \int \frac{\mathrm{d}^4 p}{(2\pi)^4}\, \partial^i \left[\mathrm{e}^{-\mathrm{i}p^\nu x_\nu} \epsilon_i(p)\right] = \int \frac{\mathrm{d}^4 p}{(2\pi)^4} \left[-\mathrm{i}\mathrm{e}^{-\mathrm{i}p^\nu x_\nu} p^i \epsilon_i(p)\right] = 0 \tag{2.92}$$

and considering that the exponential can always be different from zero for an appropriate choice of x_ν, leads immediately to the condition:

$$p^i \epsilon_i = 0 \tag{2.93}$$

that means the photon field A_μ has a transverse polarization.

Choosing the frame in which $p_\mu = (E, 0, 0, E)$ and imposing a second gauge condition $\epsilon_0 = 0$, that avoid the unphysical timelike polarization $\epsilon_0 = (1, 0, 0, 0)$, we can write a solution of (2.93) as

$$\epsilon^1_\mu = (0, 1, 0, 0) \qquad \epsilon^2_\mu = (0, 0, 1, 0) \tag{2.94}$$

corresponding to linearly polarized light, or as

$$\epsilon_\mu^{\mathrm{R}} = \frac{1}{\sqrt{2}}(0,1,\mathrm{i},0) \qquad \epsilon_\mu^{\mathrm{L}} = \frac{1}{\sqrt{2}}(0,1,-\mathrm{i},0) \tag{2.95}$$

corresponding to circularly polarized light.

The transverse nature of the photon polarizations, valid regardless of the particular gauge choice, is trivially found in the Coulomb gauge.

2.4.2 Lorenz Gauge

Even though the Coulomb gauge simplifies some calculations, it sacrifices a manifest Lorenz invariance so that the field quanta in Coulomb gauge are described in a way that is not manifestly Lorentz-covariant. A gauge that is manifestly Lorentz invariant is the Lorenz gauge.

The Lorenz gauge is defined by

$$\partial^\mu A_\mu = 0 \tag{2.96}$$

that is a Lorentz-covariant constraint.

In this gauge, for example, the free field equations have a very simple form, see [23]. In fact, starting from the Lagrangian (2.44), $-\frac{1}{4}F_{\mu\nu}F^{\mu\nu}$, the Euler-Lagrangian equation of motion are

$$\partial^\nu F_{\mu\nu} = 0\,. \tag{2.97}$$

Simply, plugging into this equation the definition (2.16), $F_{\mu\nu} \equiv \partial_\nu A_\mu - \partial_\mu A_\nu$, we obtain a very simple equation of motion in terms of the potential A_μ :

$$\partial^\nu F_{\mu\nu} = \partial^\nu \partial_\nu A_\mu - \partial^\nu \partial_\mu A_\nu = 0 \implies \partial^\nu \partial_\nu A_\mu = 0 \tag{2.98}$$

where the negative term is null because of the particular choice of the Lorenz gauge.

2.4.3 R_ξ gauges

The R_ξ gauges emerge in the context of quantum electrodynamic (QED), see [24–27].

The idea is to fix the additional degrees of freedom given by the gauge adding to the Lagrangian, that is a function of the gauge fields, the amount

$$\Delta\mathcal{L} = -\frac{1}{2\xi}\left(\partial^\mu A_\mu\right)^2 \tag{2.99}$$

that depends on ξ, a parameter that fixes the gauge.

A gauge that depends on the Lagrangian in this way is called a R_ξ gauge and depend on the number ξ that can have different values.

Since the Lagrangian is defined up to a total derivative, a different definition for R_ξ gauges is

$$\delta\mathcal{L} = B\partial_\mu A^\mu + \frac{\xi}{2}B^2 \tag{2.100}$$

where we have introduced an auxiliary field B.

Since the parameter ξ can vary, the R_ξ gauges represent a class of gauges. This class includes, for example, the Lorenz gauge (2.96) that is obtained with $\xi \to 0$, the Feynman–'t Hooft gauge obtained with $\xi = 1$ and the Yennie gauge obtained with $\xi = 3$, see [27]. In particular, the $\xi = 1$ gauge is useful to work with the photon propagator that, in this gauge, has the simple expression $D(k)_{\mu\nu} = -\frac{g_{\mu\nu}}{k^2}$, see, e.g. [25].

2.5 Beyond SM

Even though the SM is a very successful model, describing the electromagnetic, weak and strong force together with all the known elementary particles, it exhibits both theoretical and experimental problems.

Theoretical problems

The SM cannot explain or can explain in a no fully satisfactory way, important physical phenomena. Some examples are:

Hierarchy problem In the SM, there is no satisfactory way to explain why the ratio between the Higgs mass m_H and the Plank mass m_P is very small: $\frac{m_H}{m_P} \ll 1$. In fact, quantum corrections to the Higgs boson mass m_H arise from every particle that couples with the Higgs field, see [28] and references therein. These corrections lead to quadratic divergences in m_H. If new physics at the Planck scale cuts off these divergences we see a quadratic sensitivity to that scale. Thus it is difficult to explain how all these contributions to m_H can cancel each other without assuming a very delicate fine-tuning of the SM parameters (for an attempt to solve this problem in the SM see, for example, [29]).

Gravity Despite many efforts, the SM cannot explain the physics of strong gravitational effects that, for example, has to describe black holes or the very early Universe [30]. Attempt to investigate this area of physics with QFT

on curved background has led to problems such as the information paradox [31, 32] that show how we still have to understand the gravity force at the quantum level.

Free parameters In the SM, excluding the neutrino masses, there are 19 parameters that are completely free and cannot be explained in the model. Since there are relationships that relate free parameters with other parameters in the theory, the choice of what are the free parameters is not univocal. A possible list is

- 3 lepton masses m_e, m_μ and m_τ;
- 6 quark masses m_u, m_d, m_c, m_s, m_t and m_b;
- 3 CKM angles $\theta_{12}, \theta_{13}, \theta_{23}$, see Eq. (2.85);
- 1 CKM phase δ, see Eq. (2.89);
- 1 U(1) gauge coupling g';
- 1 SU(2) gauge coupling g;
- 1 SU(3) gauge coupling g_s;
- 1 QCD vacuum angle θ_{QCD};
- 1 Higgs vacuum expectation value v;
- 1 Higgs mass m_{H}.

It is believed that a more fundamental theory can derive these parameters from a smaller set of parameters.

On top of these problems, there are other appealing characteristics that are not realized in the SM and that different models beyond the standard model (BSM) exhibit. An example is the unification of the coupling constant, see Fig. 3.1 and Sec. 3.1: in the SM the values of the coupling constant of the strong, electromagnetic and weak interactions become similar but not equal. In theory such as the supersymmetry, these values unify in a single value.

Experimental problems

Even though the SM can very precisely explain an impressive amount of experimental data, there are measurements that do not fit into the current SM framework.

Dark matter and dark energy One of the most evident problems is the presence, in the Universe, of a considerable amount of dark matter and dark energy. As the Plank collaboration reports [1], only 5% of the total energy density in the Universe is in the form of baryonic matter, that is matter described by the SM. About 26% of the total energy density is called dark matter (DM) and is responsible for the structure formation in the Universe. This DM is not composed of SM particles, and there is still no consensus about its composition. The remaining 69% of the total energy density in the Universe is the so-called dark energy (DE) and is responsible for the expansion of the Universe. Again there is no a standard accepted theory that can describe the observed rate of acceleration of our Universe.

Baryon asymmetry Another important problem is the baryon asymmetry of the Universe (BAU). While astronomical data suggest there is no antimatter in the observable Universe, it is not quantitatively clear how the observed excess of matter over antimatter can be originated. Provided that a mechanism for the production of matter exists, Sakharov showed that such a mechanism [33] has to produce C and CP violation together with an out-of-thermal-equilibrium process. In the SM, there is not enough CP violation to account for the observed BAU and going out of thermal equilibrium requires the Higgs boson to have a mass of about 75 GeV [34, 35].

Muon anomaly The anomalous magnetic dipole moment of the muon $a_\mu = \frac{g-2}{2}$ also is generally recognized as a hint of new physics beyond the SM. The value of a_μ was measured at the E821 experiment at Brookhaven National Laboratory with a precision of about half a part per million [4]. Using the SM, theoretical calculations give a value that deviate at 3-4 sigma level [5–8]. A new experiment at Fermilab [36] aims to improve about four times the relative precision of the E821 experiment with a confidence level exceeding a discovery threshold and to have the statistical sensitivity necessary to either refute or confirm the discrepancy with the SM predictions.

Chapter 3

Supersymmetry

Supersymmetry (SUSY) is a beyond SM theory that combines space-time symmetries and internal symmetries extending the Poincaré group. Space-time symmetries imply the invariance of the law of physics under translations, rotations and boosts and are described by the Poincaré group. Internal symmetries are symmetries of the Lagrangian that imply that gauge transformations leave the Lagrangian invariant up to total derivatives.

The Coleman–Mandula theorem [37] proves that under quite general physical assumptions spacetime symmetries and internal symmetries can be combined only in a trivial way. The Coleman–Mandula theorem is based on the algebra given by the commutators of the generators of spacetime symmetries and internal symmetries. The Haag-Lopuszański-Sohnius theorem [38] weakens the assumptions of the Coleman–Mandula theorem by considering *graded Lie algebras* defined using anticommutation operations, as well as the commutation operations of Lie algebras. With this more general assumption, the Haag-Lopuszański-Sohnius theorem proves that supersymmetry represents the only non-trivial extension of the Poincaré group. This allows one to extend the Poincaré algebra to include supersymmetry generators that change the spin of a state. As a result supersymmetry turns out to be a symmetry between fermions and bosons. In this chapter, we introduce supersymmetric theories following S. Martin's primer [28].

3.1 Motivations

Supersymmetry solves a number of SM problems. For example, the hierarchy problem is solved by SUSY, which implies a symmetry between bosons and fermions. As a result new BSM particles, called sparticles, are introduced. For each standard model particle there is a sparticle with the same quantum

numbers, but different spin. Considering both particles and sparticles leads to a cancellation of quadratic divergences between fermionic and bosonic loops. Specifically, quadratic corrections to the Higgs mass, are generated by loops corrections involving SM fermions and bosons and these quadratic divergences are cancelled exactly by the loop corrections from the corresponding sparticles due to the different spin. This makes it possible to have a Higgs mass which is much lighter than the Planck scale without requiring fine-tuning between the quadratic divergences and the bare Higgs mass.

Regarding gravity, in the framework of supersymmetry, it is possible to develop a theory, called supergravity, which introduces gravitational interactions. This is done promoting supersymmetry to a local symmetry, which is applying the same principle of local gauge invariance described in Sec. 2.2. Although local supergravity is a non-renormalizable theory, the natural emergence of the gravitational interaction is an appealing feature of SUSY, and supergravity may be an effective theory of a correct theory of gravity.

Moreover, in the minimal realisation of SUSY (and many other supersymmetric extensions), the coupling constants of the strong, electromagnetic and weak interactions can evolve to a common value at the grand unification theory (GUT) scale. Compared to the SM, a similar calculation shows that the coupling constants evolve to different values, see fig. 3.1 taken from [28]. Successful unification in SUSY models is dependent on the SUSY breaking scale and the particular particle content, which plays a role in the renormalization group equations (RGEs) used to calculate the running of coupling constants. This is a hint that at GUT scale the physics can be described by a symmetry group that breaks to the SM gauge group, $SU(3)_C \otimes SU(2)_L \otimes U(1)_Y$, which describes the gauge interactions at lower scales.

Supersymmetry can also provide a particle explanation for dark matter. The discrete $\mathbb{Z}_2$ symmetry, that leads to baryon and lepton number conservation, is normally imposed, see sec. 3.7.3. The $\mathbb{Z}_2$ symmetry also implies that the lightest supersymmetric particle (LSP), is stable. If the LSP is one of the neutral, weakly interacting SUSY particles, it can be a promising candidate for the cold dark matter.

Finally, supersymmetric models, such as the Next to Minimal Supersymmetric Model (NMSSM) can quantitatively account for the observed baryon asymmetry of the Universe. The excess of matter over antimatter in the Universe requires a specific mechanism to explain the origin of this excess. One of such mechanisms is the electroweak baryogenesis, see sec. 4.2. The electroweak baryogenesis in the SM cannot account for the measured quantity of matter and absence of antimatter in the Universe [35, 39]. In contrast, SUSY models such as the NMSSM, provide an ideal framework in which the observed matter-antimatter asymmetry can be generated in the early

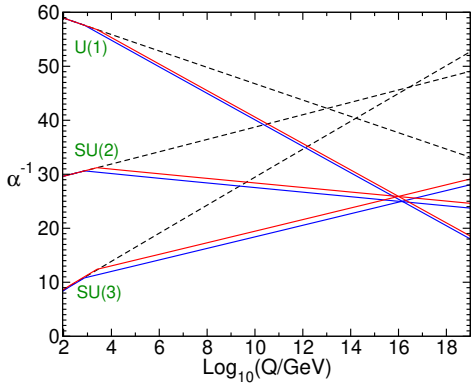

Figure 3.1: The x-axis shows the energy Q on logarithmic scale, while the y-axis shows the values $\alpha^{-1}_{\mathrm{SU(3),\,SU(2),\,U(1)}}(Q)$, calculated at two-loop, of the inverse of the $\mathrm{SU(3)_C}$, $\mathrm{SU(2)_L}$ and $\mathrm{U(1)_Y}$ coupling constants for the SM (dashed lines) and the MSSM (solid lines) [figure taken from [28]].

Universe, see the published article in chapter 6 and references within it.

3.2 Notation

A Dirac spinor Ψ has four complex components that can be transformed under Lorentz transformations

$$\Psi = \begin{pmatrix} \xi_1 \\ \xi_2 \\ \chi^{\mathrm{i}\dagger} \\ \chi^{\dot{2}\dagger} \end{pmatrix} = \begin{pmatrix} \psi_{\mathrm{L}} \\ \psi_{\mathrm{R}} \end{pmatrix} . \tag{3.1}$$

A fermion field is described by a single left-handed two-component Weyl fermion. The first couple of components, $\begin{pmatrix} \xi_1 \\ \xi_2 \end{pmatrix}$, transforms as a left-chiral spinor, while the second couple of components, $\begin{pmatrix} \chi^{\mathrm{i}\dagger} \\ \chi^{\dot{2}\dagger} \end{pmatrix}$, transforms as a right-chiral spinor. We differentiate the first and second couple using normal indices for the first couple and dotted indices for the second couple.

Dotted and undotted indexes are raised and lowered thanks to the symbol ε that can be defined from the Pauli matrices σ^2 in Eq. (2.4):

$$\begin{aligned} \varepsilon^{ab} &= (\mathrm{i}\sigma^2)^{ab} & \qquad \varepsilon_{ab} &= (-\mathrm{i}\sigma^2)_{ab} \\ \varepsilon^{\dot{a}\dot{b}} &= (\mathrm{i}\sigma^2)^{\dot{a}\dot{b}} & \qquad \varepsilon_{\dot{a}\dot{b}} &= (-\mathrm{i}\sigma^2)_{\dot{a}\dot{b}} \end{aligned} . \tag{3.2}$$

Note that while dotted indices are used for the components of ψ_{L} and undotted indices are used for the components of ψ_{R}, dotted and undotted indices are interchangeable when they indicate the matrix elements, that is $\sigma_{\dot{a}\dot{b}} \equiv \sigma_{ab}$.

A supersymmetry transformation turns a fermion state into a boson state and vice-versa thanks to an operator Q that satisfy the algebra

$$\left\{Q_a, Q^\dagger_{\dot{a}}\right\} = -2\sigma^\mu_{a\dot{a}} P_\mu \qquad \left\{Q_a, Q_b\right\} = \left\{Q^\dagger_{\dot{a}}, Q^\dagger_{\dot{b}}\right\} = 0 \tag{3.3a}$$

$$\left[Q_a, P^\mu\right] = \left[Q^\dagger_{\dot{a}}, P^\mu\right] = 0 \qquad \left[Q_a, M^{\mu\nu}\right] = (\sigma^{\mu\nu})^b_a Q_b \tag{3.3b}$$

where P^μ is the generator of the four-momentum spacetime translations, $M^{\mu\nu}$ is the generator of Lorentz transformations and $\sigma^{\mu\nu}$ is the antisymmetric product of the Pauli matrices σ:

$$(\sigma^{\mu\nu})^b_a = \frac{\mathrm{i}}{4}(\sigma^\mu \bar{\sigma}^\nu - \sigma^\nu \bar{\sigma}^\mu)^b_a \,. \tag{3.4}$$

This algebra represents a particular case of a graded algebra. A graded algebra generalise the anticommutators (3.3a) introducing new operators Q^A with $A = 1 \ldots \mathcal{N}$, with the following anticommutator rules

$$\left\{Q^A_a, Q^\dagger_{\dot{a}B}\right\} = -2\sigma^\mu_{a\dot{a}} P_\mu \delta^A_B \qquad \left\{Q^A_a, Q^B_b\right\} = \epsilon_{ab} Z^{AB} \tag{3.5}$$

where δ^A_B is the Kronecker delta, ϵ_{ab} is defined in Eq. (3.2) and Z^{AB} is called central charge and satisfy

$$Z^{AB} = -Z^{BA}$$

$$\left[Z^{AB}, P^\mu\right] = \left[Z^{AB}, M^{\mu\nu}\right] = \left[Z^{AB}, Q^A_a\right] = \left[Z^{AB}, Z^{CD}\right] = \left[Z^{AB}, T_a\right] = 0 \tag{3.6}$$

where T_a are the generators of the SU(N), see Eq. (2.32) and Eq. (2.33). We can see that the algebra Eq. (3.3) represents the special case in which $A = B = 1$. This special case is the algebra of the so-called simple or $\mathcal{N} = 1$ supersymmetry.

Now we want to define supermultiplets in the $\mathcal{N} = 1$ supersymmetry. Here, for simplicity, we consider the case when all the particles are massless, that is before the spontaneous symmetry breaking. After the symmetry breaking, when multiplet become massive, it is the spin (rather than the helicity, h, we discuss here) that distinguishes the elements of the supermultiplet, see [40]. In the massless case, we can choose a reference frame in which

$$P_\mu = (E, 0, 0, E) \tag{3.7}$$

where E is the energy. We can introduce the creation and annihilation operators

$$a = \frac{-\mathrm{i}}{2\sqrt{E}} Q_1 \qquad a^\dagger = \frac{-\mathrm{i}}{2\sqrt{E}} Q_{\dot{1}}^\dagger \tag{3.8}$$

that satisfy the anticommutation rules

$$\left\{a, a^\dagger\right\} = 1 \qquad \left\{a, a\right\} = \left\{a^\dagger, a^\dagger\right\} = 0 \,. \tag{3.9}$$

The operators a and $a^\dagger$ modify the helicity of a quantum state. To see their action on a state, consider the commutators $[a, J^3]$ and $[a^\dagger, J_3]$, where J_i are the generators of rotations. These commutators can be easily calculated considering the Pauli-Lubanski vector W_μ

$$W_\mu = \frac{1}{2} \epsilon_{\mu\nu\rho\sigma} P^\nu M^{\rho\sigma} \tag{3.10}$$

where $\epsilon_{\mu\nu\rho\sigma}$ is the four-dimensional totally antisymmetric Levi-Civita symbol. In component W_μ is

$$W_0 = \boldsymbol{P} \cdot \boldsymbol{J} \qquad \boldsymbol{W} = P_0 \boldsymbol{J} - \boldsymbol{P} \times \boldsymbol{K} \tag{3.11}$$

where $\boldsymbol{K}$ is the generator of the Lorentz boosts. Using Eq. (3.7) into the last expression we derive

$$W_0 = E J_3 \,. \tag{3.12}$$

Also, the commutator $\left[Q_a, W_\mu\right]$ can be calculated from the definition of W_μ in Eq. (3.10) and the commutator $[Q_a, M^{\mu\nu}]$ given in Eq. (3.3):

$$\left[Q_a, W_\mu\right] = \mathrm{i} P_\nu (\sigma^{\mu\nu})_a^b Q_b \tag{3.13}$$

Using Eq. (3.12), the commutator $\left[a, J^3\right]$ becomes

$$\left[a, J^3\right] = \frac{1}{E}[a, W_0] = \frac{1}{E} \frac{-\mathrm{i}}{2\sqrt{E}} [Q_1, W_0] = \frac{1}{E} \frac{-\mathrm{i}}{2\sqrt{E}} \mathrm{i} P_\nu (\sigma^{0\nu})_{\dot{1}}^b Q_b \tag{3.14}$$

where we have used the definition of a in Eq. (3.8) and the previous expression (3.13). Considering again Eq. (3.7) and suming over ν we have

$$\left[a, J^3\right] = \frac{1}{E} \frac{1}{2\sqrt{E}} E \Big((\sigma^{00})_{\dot{1}}^b Q_b + (\sigma^{03})_{\dot{1}}^b Q_b \Big) = \frac{1}{2\sqrt{E}} \left(\frac{\mathrm{i}}{2} (-\sigma^3)_{\dot{1}}^b Q_b \right) \tag{3.15}$$

where we have used the definitions of $\sigma^{\mu\nu}$ in Eq. (3.4). Finally, expanding the sum over b and using the definition of σ^3 in Eq. (2.4) we obtain

$$\left[a, J^3\right] = \frac{-\mathrm{i}}{2\sqrt{E}} \left(\frac{1}{2} Q_1 \right) = \frac{1}{2} a \tag{3.16}$$

where we have used the definition (3.8) of a. Now we can consider a state with four-momentum p^μ and helicity h: $|p^\mu, h\rangle$. Applying J_3 to the state $a\,|p^\mu, h\rangle$ and using the result (3.16) we obtain:

$$\begin{aligned} J_3\big(a\,|p^\mu, h\rangle\big) &= \big(aJ_3 - [a, J_3]\big)\,|p^\mu, h\rangle = \left(aJ_3 - \frac{1}{2}a\right)|p^\mu, h\rangle \\ &= \left(h - \frac{1}{2}\right)\big(a\,|p^\mu, h\rangle\big) \end{aligned} \tag{3.17}$$

that is the helicity of $a\,|p^\mu, h\rangle$ is $h - \frac{1}{2}$. With the same steps, we can show that $[a^\dagger, J_3] = -\frac{1}{2}a^\dagger$ and

$$J_3\Big(a^\dagger\,|p^\mu, h\rangle\Big) = \left(h + \frac{1}{2}\right)\Big(a^\dagger\,|p^\mu, h\rangle\Big) \tag{3.18}$$

that is $a^\dagger\,|p^\mu, h\rangle$ has helicity $h + \frac{1}{2}$. Now, calling $|p^\mu, h_{\min}\rangle$ a vacuum state with minimum helicity $h_{\min}$, applications of a on $|p^\mu, h_{\min}\rangle$ must be null otherwise $a\,|p^\mu, h_{\min}\rangle$ would have helicity $h_{\min} - \frac{1}{2} < h_{\min}$ contradicting the assumption that $|p^\mu, h_{\min}\rangle$ has minimum helicity. Also, indicating with $\left|p^\mu, h_{\min} + \frac{1}{2}\right\rangle$ the state $a^\dagger\,|p^\mu, h_{\min}\rangle$, further applications of $a^\dagger$ on $\left|p^\mu, h_{\min} + \frac{1}{2}\right\rangle$ are null since $a^\dagger a^\dagger = 0$ from the anticummutation rules (3.9). Therefore an irreducible representation of the supersymmetry is given by the two elements,

$$\left\{\ |p^\mu, h_{\min}\rangle\,, \quad \left|p^\mu, h_{\min} + \tfrac{1}{2}\right\rangle\ \right\}\,. \tag{3.19}$$

The CPT conjugate of the states in the supermultiplet (3.19) are

$$\left\{\ |p^\mu, -h_{\min}\rangle\,, \quad \left|p^\mu, -h_{\min} - \tfrac{1}{2}\right\rangle\ \right\}\,. \tag{3.20}$$

Merging together the states in Eq. (3.19) and Eq. (3.20) we define a supermultiplet that is composed of four states

$$\left\{\ \left|p^\mu, -h - \tfrac{1}{2}\right\rangle\,, \quad |p^\mu, -h\rangle\,, \quad |p^\mu, h\rangle\,, \quad \left|p^\mu, h + \tfrac{1}{2}\right\rangle\ \right\}\,. \tag{3.21}$$

Note that, as it will be discuss in the SUSY transformations of the fields, see sec. 3.3.2, another non-propagating field will also be included in the supermultiplet to account for off-shell degrees of freedom.

All the SM fermions are members of a chiral supermultiplet while all the SM gauge bosons are members of a vector supermultiplet. The Higgs boson belongs to a chiral supermultiplet.

3.3 Chiral SUSY Lagrangian

A chiral SUSY Lagrangian $\mathcal{L}^{\mathrm{c}}_{\mathrm{SUSY}}$ can be divided into kinetic terms for scalars $\mathcal{L}^{\mathrm{c}}_{\mathrm{s}}$, kinetic terms for fermions $\mathcal{L}^{\mathrm{c}}_{\mathrm{f}}$, an interaction term $\mathcal{L}^{\mathrm{c}}_{\mathrm{int}}$ and an extra auxiliary term $\mathcal{L}^{\mathrm{c}}_{\mathrm{aux}}$:

$$\mathcal{L}^{\mathrm{c}}_{\mathrm{SUSY}} = \mathcal{L}^{\mathrm{c}}_{\mathrm{s}} + \mathcal{L}^{\mathrm{c}}_{\mathrm{f}} + \mathcal{L}^{\mathrm{c}}_{\mathrm{aux}} + \mathcal{L}^{\mathrm{c}}_{\mathrm{int}} \ . \tag{3.22}$$

We describe these terms in the following sections.

3.3.1 Free Lagrangian

A free Lagrangian describes fields that do not interact. Considering fermions and scalars fields, it can be written as

$$\mathcal{L}^{\mathrm{c}}_{\mathrm{free}} = \mathcal{L}^{\mathrm{c}}_{\mathrm{s}} + \mathcal{L}^{\mathrm{c}}_{\mathrm{f}} = -\partial^{\mu}\phi^{\dagger}\partial_{\mu}\phi + \mathrm{i}\psi^{\dagger}_{\dot{a}}\bar{\sigma}^{\mu\dot{a}b}\partial_{\mu}\psi_{b} \tag{3.23}$$

where ϕ is a scalar field and ψ a fermion field.

Hamilton's principle requires the variation of the action S to be zero, or, equivalently, the variation of the Lagrangian to be the total derivative of a function f: $\delta S = 0 \Leftrightarrow \delta\mathcal{L} = \partial_{\mu} f$. Calling ϵ an infinitesimal anti-commuting constant Weyl spinor, the supersymmetry transformations of the fields that leave the Lagrangian invariant up to total derivatives are

$$\begin{aligned} \delta\phi &= \epsilon^{a}\psi_{a} & \delta\psi_{a} &= -\mathrm{i}\sigma^{\mu}_{a\dot{b}}\epsilon^{\dagger\dot{b}}\partial_{\mu}\phi \\ \delta\phi^{\dagger} &= \epsilon^{\dagger}_{\dot{a}}\psi^{\dagger\dot{a}} & \delta\psi^{\dagger}_{\dot{a}} &= \mathrm{i}\epsilon^{b}\sigma^{\mu}_{b\dot{a}}\partial_{\mu}\phi^{\dagger} \end{aligned} \qquad \Longrightarrow \qquad \delta S = 0 \tag{3.24}$$

as can be explicitly verified by plugging these variations into the variation $\delta\mathcal{L}^{\mathrm{c}}_{\mathrm{free}}$ from Eq. (3.23). These transformations encode the idea that bosonic and fermion fields are transformed one into the other.

3.3.2 Auxiliary Lagrangian

According to Noether's theorem, a continuous symmetry transformation that leaves the action invariant, such as the (3.24), corresponds to a conserved current, in SUSY called supercurrent. This supercurrent and its hermitian conjugate are associated with conserved charges $Q_a, Q^{\dagger}_{\dot{a}}$, called supercharges, which are the generators of supersymmetry transformations. These supercharges, once promoted to quantum operators, have to satisfy the SUSY algebra (3.3). To explicitly find the algebra of the supercharges, we need to consider the commutator of two transformations with generic infinitesimal

parameter ϵ_1 and ϵ_2. Considering the scalar field ϕ, this commutator can be expressed as,

$$\big[\delta_{\epsilon_2},\delta_{\epsilon_1}\big]\phi = \delta_{\epsilon_2}(\epsilon_1^a\psi_a) - \delta_{\epsilon_1}(\epsilon_2^a\psi_a) = \Big(-\mathrm{i}\epsilon_1^a\sigma^\mu_{a\dot{b}}\epsilon_2^{\dagger\dot{b}} + \mathrm{i}\epsilon_2^a\sigma^\mu_{a\dot{b}}\epsilon_1^{\dagger\dot{b}}\Big)\partial_\mu\phi \tag{3.25}$$

where we have used the SUSY transformations (3.24). The operator $-\mathrm{i}\partial_\mu$ is the generator of the spacetime translations P_μ that appears in the algebra of the charges (3.3). Unfortunately, if instead of the scalar field ϕ we consider the spinor field ψ we get a different algebra for the charges Q and $Q^\dagger$. In fact, the commutator $\big[\delta_{\epsilon_2},\delta_{\epsilon_1}\big]\psi$, using again the transformations (3.24), can be expressed as

$$\big[\delta_{\epsilon_2},\delta_{\epsilon_1}\big]\psi_a = -\mathrm{i}\sigma^\mu_{a\dot{b}}\epsilon_1^{\dagger\dot{b}}\big(\epsilon_2^c\partial_\mu\psi_c\big) + \mathrm{i}\sigma^\mu_{a\dot{b}}\epsilon_2^{\dagger\dot{b}}\big(\epsilon_1^c\partial_\mu\psi_c\big) \tag{3.26}$$

to make the last expression more similar to Eq. (3.25) we can use the Fierz rearrangement identity

$$\chi_a(\xi^b\eta_b) + \xi_a(\eta^b\chi_b) + \eta_a(\chi^b\xi_b) = 0 \tag{3.27}$$

where we need to raise and lower the index of χ, ξ and η using the ε symbol defined in equation (3.2). With this identity we can move the two derivatives of the fermion field $\partial_\mu\psi$ from inside the spinor products to outside them:

$$\begin{aligned}\big[\delta_{\epsilon_2},\delta_{\epsilon_1}\big]\psi_a = \mathrm{i}\Big\{(\varepsilon_{ad}\epsilon_2^d)\big[(\varepsilon^{cd}\partial_\mu\psi_d)(\sigma^\mu_{c\dot{b}}\epsilon_1^{\dagger\dot{b}})\big] + (\partial_\mu\psi_a)\big[(\varepsilon^{cd}\sigma^\mu_{d\dot{b}}\epsilon_1^{\dagger\dot{b}})(\varepsilon_{cd}\epsilon_2^d)\big]\Big\}\\ -\mathrm{i}\Big\{(\varepsilon_{ad}\epsilon_1^d)\big[(\varepsilon^{cd}\partial_\mu\psi_d)(\sigma^\mu_{c\dot{b}}\epsilon_2^{\dagger\dot{b}})\big] + (\partial_\mu\psi_a)\big[(\varepsilon^{cd}\sigma^\mu_{d\dot{b}}\epsilon_2^{\dagger\dot{b}})(\varepsilon_{cd}\epsilon_1^d)\big]\Big\}\,.\end{aligned} \tag{3.28}$$

Now summing on both lines $\varepsilon^{cd}\varepsilon_{cd}\epsilon^d = \epsilon^d$ and using the identity

$$\chi^a\sigma^\mu_{a\dot{b}}\xi^{\dagger\dot{b}} = -\xi^\dagger_{\dot{a}}\bar{\sigma}^{\mu\dot{a}b}\chi_b \tag{3.29}$$

we can rearrange the previous terms in the expression

$$\begin{aligned}\big[\delta_{\epsilon_2},\delta_{\epsilon_1}\big]\psi_a = -\mathrm{i}\epsilon_{2a}\Big(\epsilon^\dagger_{1\dot{b}}\bar{\sigma}^{\mu\dot{b}c}\partial_\mu\psi_c\Big) + \mathrm{i}\epsilon_{1a}\Big(\epsilon^\dagger_{2\dot{b}}\bar{\sigma}^{\mu\dot{b}c}\partial_\mu\psi_c\Big)\\ + \mathrm{i}\Big(\epsilon_2^d\sigma^\mu_{d\dot{b}}\epsilon_1^{\dagger\dot{b}} - \epsilon_1^d\sigma^\mu_{d\dot{b}}\epsilon_2^{\dagger\dot{b}}\Big)\partial_\mu\psi_a\,.\end{aligned} \tag{3.30}$$

The second line of the last commutator (3.30) is what we got from the commutator for the scalar field (3.25). Unfortunately, since the first line of Eq. (3.30) is in general different from zero, the algebra originated by the transformations of the scalar field is different from the algebra originated by

the transformations of the spinor field. However, if the spinor field satisfy the equation of motion the first line of Eq. (3.30) is null. In fact, from (3.23) the Euler-Lagrangian equations are

$$\partial_\mu \frac{\partial \mathcal{L}^{\mathrm{c}}_{\mathrm{free}}}{\partial(\partial_\mu \psi^\dagger_{\dot{a}})} - \frac{\partial \mathcal{L}^{\mathrm{c}}_{\mathrm{free}}}{\partial \psi^\dagger_{\dot{a}}} = 0 \quad \Longrightarrow \quad -\mathrm{i}\bar{\sigma}^{\mu\dot{a}b}\partial_\mu \psi_b = 0 \tag{3.31}$$

that implies that the first two terms in (3.30) are zero. This is true only when ψ satisfies the equations of motion thus Eq. (3.25) and (3.30) imply the same algebra only on-shell. Off-shell the algebra does not close, that is the algebra obtained by the transformations of the spinor field is different from the algebra obtained by the transformations of the scalar field. This is problematic because if the algebra does not close off-shell, then the supersymmetry does not hold at the quantum mechanic level.

A solution to this problem comes analysing the degrees of freedom: a two-component Weyl spinor contains two complex variables, so it has four degrees of freedom if it is off-shell. These four degrees of freedom do not match the two bosonic degrees of freedom of the complex scalar field. This is a problem only off-shell because on-shell the equations of motions reduce by two the fermionic degrees of freedom which then match the two bosonic degrees of freedom. The trick is thus to introduce a bosonic field $\mathcal{F}$ that has two off-shell degrees of freedom and zero on-shell degrees of freedom. A field with this property is called auxiliary field and is indicated with a calligraphic character. In this way, the bosonic and fermion degrees of freedom are the same both on- and off-shell. In order not to have an on-shell degree of freedom, we require the auxiliary field $\mathcal{F}$ to appear in the Lagrangian as $\mathcal{F}\mathcal{F}^\dagger$:

$$\mathcal{L}^{\mathrm{c}}_{\mathrm{free+aux}} = \mathcal{L}^{\mathrm{c}}_{\mathrm{free}} + \mathcal{F}\mathcal{F}^\dagger \tag{3.32}$$

since there are no kinetic terms for $\mathcal{F}$, the equation of motion for this auxiliary field is $\mathcal{F} = \mathcal{F}^\dagger = 0$ and $\mathcal{F}$ has no on-shell degree of freedom.

Having introduced the new field $\mathcal{F}$ in the Lagrangian, we need to require again that

- the variation of the bosonic, fermionic and auxiliary fields annul the variation of the action S;
- the algebra closes on the ϕ and ψ fields as well as on the new auxiliary field $\mathcal{F}$.

It can be explicitly verified that the variations that satisfy these require-

ments are

$$\begin{aligned}
&\delta(\phi)_i = \epsilon^a(\psi_a)_i \\
&\delta(\phi^\dagger)^i = \epsilon^\dagger_{\dot a}(\psi^{\dagger \dot a})^i \\
&\delta(\psi_a)_i = -\mathrm{i}\sigma^\mu_{a\dot b}\epsilon^{\dagger \dot b}\partial_\mu(\phi)_i + \epsilon_a(\mathcal{F})_i \\
&\delta(\psi^\dagger_{\dot a})^i = \mathrm{i}\epsilon^b\sigma^\mu_{b\dot a}\partial_\mu(\phi^\dagger)^i + \epsilon^\dagger_{\dot a}(\mathcal{F}^\dagger)^i \\
&\delta(\mathcal{F})_i = -\mathrm{i}\epsilon^\dagger_{\dot a}\bar\sigma^{\mu \dot a b}\partial_\mu(\psi_b)_i \\
&\delta(\mathcal{F}^\dagger)^i = \mathrm{i}\partial_\mu(\psi^\dagger_{\dot a})^i\bar\sigma^{\mu \dot a b}\epsilon_b
\end{aligned} \qquad \Longrightarrow \qquad \begin{aligned}
&\delta S = 0 \\
&\text{Closure of the algebra} \\
&\text{on } \phi_i,\ \psi_i \text{ and } \mathcal{F}_i \text{ fields:} \\
&\left[\delta_{\epsilon_2}, \delta_{\epsilon_1}\right] X = f(\epsilon_1, \epsilon_2)\mathrm{i}\partial_\mu X \\
&X = \left\{\phi_i, \phi_i^\dagger, \psi_i, \psi_i^\dagger, \mathcal{F}_i, \mathcal{F}_i^\dagger\right\}
\end{aligned} \tag{3.33}$$

where $f(\epsilon_1, \epsilon_2)$ is a function of the transformation parameters ϵ_1 and ϵ_2 showed in the first line of Eq. (3.30) and we have introduced an index i to describe more than one field. We use the convention that the i index is a lower index for ϕ, ψ and $\mathcal{F}$ fields while it is a raised index for $\phi^\dagger$, $\psi^\dagger$ and $\mathcal{F}^\dagger$ fields. Even though this index is not a spacetime index, this conventions helps in case of summed index.

Finally, the free Lagrangian that describes scalar, spinor and auxiliary fields is:

$$\mathcal{L}^{\mathrm{c}}_{\mathrm{free+aux}} = \mathcal{L}^{\mathrm{c}}_{\mathrm{s}} + \mathcal{L}^{\mathrm{c}}_{\mathrm{f}} + \mathcal{L}^{\mathrm{c}}_{\mathrm{aux}} = -\partial^\mu(\phi^\dagger)^i\partial_\mu(\phi)_i + \mathrm{i}(\psi^\dagger_{\dot a})^i\bar\sigma^{\mu \dot a b}\partial_\mu(\psi_b)_i + (\mathcal{F}^\dagger)^i(\mathcal{F})_i\ . \tag{3.34}$$

3.3.3 Interaction Lagrangian

In order for the theory to be renormalizable each Lagrangian term has to have a field content with mass dimension that is less than or equal to 4, where $[\phi] = [\phi^\dagger] = [\mathrm{mass}]^1$, $[\psi] = [\psi^\dagger] = [\mathrm{mass}]^{\frac{3}{2}}$ and $[\mathcal{F}] = [\mathcal{F}^\dagger] = [\mathrm{mass}]^2$. The interaction is given by writing all the possible Lorentz-invariant terms that respect this requirement:

$$\mathcal{L}^{\mathrm{c}}_{\mathrm{int}} = U(\phi_k, \phi^{\dagger k}) + x^{ij}(\phi_k, \phi^{\dagger k})\mathcal{F}_i\mathcal{F}_j + W^i(\phi_k, \phi^{\dagger k})\mathcal{F}_i - \frac{1}{2}W^{ij}(\phi_k, \phi^{\dagger k})\psi^a_i\psi_{ja} + \mathrm{h.c.} \tag{3.35}$$

where the indices of ϕ and ψ label different supermultiplets and W^i, W^{ij}, U and x^{ij} are generic function of the scalar fields ϕ_k and $\phi^{\dagger k}$. The factor $\frac{1}{2}$ is included to simplify later results. Note that the term $\mathcal{F}^{\dagger i}\mathcal{F}_i$ is already included in Eq. (3.34).

Since we require the variation of the total Lagrangian $\mathcal{L}^{\mathrm{c}}_{\mathrm{tot}} = \mathcal{L}^{\mathrm{c}}_{\mathrm{free}} + \mathcal{L}^{\mathrm{c}}_{\mathrm{int}}$ to be invariant under the SUSY transformations (3.33) and since $\delta\mathcal{L}^{\mathrm{c}}_{\mathrm{free}}$ is already invariant, we need to require $\delta\mathcal{L}^{\mathrm{c}}_{\mathrm{int}}$ to be invariant, that is to be equal

to the total derivative of a function f:

$$\delta\mathcal{L}^{\rm c}_{\rm int} = \delta U + \delta(x^{ij}\mathcal{F}_i\mathcal{F}_j) + \delta(W^i\mathcal{F}_i) - \delta\left(\frac{1}{2}W^{ij}\psi^a_i\psi_{ja}\right) + \text{h.c.} = \partial_\mu f \ . \quad (3.36)$$

Now, using the transformations (3.33), δU is

$$\delta U(\phi_i,\phi^{\dagger i}) = \frac{\partial U}{\partial\phi_i}\delta\phi_i + \frac{\partial U}{\partial\phi^{\dagger i}}\delta\phi^{\dagger i} = \frac{\partial U}{\partial\phi_i}\epsilon^a\psi_{ai} + \frac{\partial U}{\partial\phi^{\dagger i}}\epsilon^\dagger_{\dot a}\psi^{\dagger\dot a i} \ . \quad (3.37)$$

Since the terms in δU cannot be cancelled by terms in the variations $\delta(x^{ij}\mathcal{F}_i\mathcal{F}_j)$, $\delta(W^i\mathcal{F}_i)$ and $\delta(W^{ij}\psi^a_i\psi_{ja})$ (see Eq. (3.39), (3.42) and (3.43)), the only way in which $\delta\mathcal{L}^{\rm c}_{\rm int}$ can be a total derivative is that U is a constant that can always be set equal to zero:

$$U = 0 \ . \quad (3.38)$$

Applying the same argument, the variation $\delta(x^{lm}\mathcal{F}_l\mathcal{F}_m)$ is

$$\delta\Big[x^{lm}(\phi_i,\phi^{\dagger i})\mathcal{F}_l\mathcal{F}_m\Big] = \frac{\partial x^{lm}}{\partial\phi_i}\epsilon^a\psi_{ai}\mathcal{F}_l\mathcal{F}_m + \frac{\partial x^{lm}}{\partial\phi^{\dagger i}}\epsilon^\dagger_{\dot a}\psi^{\dagger\dot a i}\mathcal{F}_l\mathcal{F}_m + x^{lm}\delta(\mathcal{F}_l\mathcal{F}_m) \quad (3.39)$$

and again there are no other terms that can cancel the $\epsilon^a\psi_{ai}\mathcal{F}_l\mathcal{F}_m$ and $\epsilon^\dagger_{\dot a}\psi^{\dagger\dot a i}\mathcal{F}_l\mathcal{F}_m$ terms. Thus, as done for U, we set the function x^{ij} to zero:

$$x^{ij} = 0 \ . \quad (3.40)$$

In this way, that the variation of the interacting Lagrangian does not depend on U or x^{ij}: $\delta\mathcal{L}^{\rm c}_{\rm int} = \delta(W^i\mathcal{F}_i) - \delta(\frac{1}{2}W^{ij}\psi^a_i\psi_{ja})$.

The variation $\delta(W^i\mathcal{F}_i)$ is

$$\delta(W^i\mathcal{F}_i) = \left(\frac{\partial W^i}{\partial\phi_k}\delta\phi_k\right)\mathcal{F}_i + \left(\frac{\partial W^i}{\partial\phi^{\dagger k}}\delta\phi^{\dagger k}\right)\mathcal{F}_i + W^i\delta\mathcal{F}_i \quad (3.41)$$

and using the SUSY transformations (3.33)

$$\delta(W^i\mathcal{F}_i) = \frac{\partial W^i}{\partial\phi_k}\epsilon^a\psi_{ak}\mathcal{F}_i + \frac{\partial W^i}{\partial\phi^{\dagger k}}\epsilon^\dagger_{\dot a}\psi^{\dagger\dot a k}\mathcal{F}_i + W^i(-\mathrm{i})\epsilon^\dagger_{\dot a}\bar\sigma^{\mu\dot a b}\partial_\mu\psi_{bi} \ . \quad (3.42)$$

The last variation in (3.36) is $\delta(-\frac{1}{2}W^{ij}\psi^a_i\psi_{ja})$:

$$\delta\left(-\frac{1}{2}W^{ij}\psi^a_i\psi_{ja}\right) = -\frac{1}{2}\frac{\partial W^{ij}}{\partial\phi_k}\epsilon^a\psi_{ak}\psi^b_i\psi_{bj} - \frac{1}{2}\frac{\partial W^{ij}}{\partial\phi^{\dagger k}}\epsilon^\dagger_{\dot a}\psi^{\dagger\dot a k}\psi^b_i\psi_{bj} - \frac{1}{2}W^{ij}\delta(\psi^a_i\psi_{aj}). \quad (3.43)$$

The first term $-\frac{1}{2}\frac{\partial W^{ij}}{\partial\phi_k}\epsilon^a\psi_{ak}\psi^b_i\psi_{bj}$ cannot be cancelled with the other terms in $\delta\mathcal{L}^{\rm c}_{\rm int}$ since its field content is different from all other terms. In order to

have $\mathcal{L}^{\mathrm{c}}_{\mathrm{int}}$ invariant we need this term to be a constant. We require $\frac{\partial W^{ij}}{\partial \phi_k}$ to be totally symmetric under the interchange of i, j and k so that, summing over i and j and using the Fierz identity (3.27), the first term is zero:

$$\frac{\partial W^{ij}}{\partial \phi_k} \text{ symmetric } \implies \frac{\partial W^{ij}}{\partial \phi_k} \epsilon^a \psi_{ak} \psi_i^b \psi_{bj} = 0 \,. \tag{3.44}$$

The second term in Eq. (3.43), $-\frac{1}{2}\frac{\partial W^{ij}}{\partial \phi^{\dagger k}} \epsilon^{\dagger}_{\dot{a}} \psi^{\dagger \dot{a} k} \psi_i^b \psi_{bj}$, again has a field content that prevents it from cancelling with other terms in $\delta \mathcal{L}^{\mathrm{c}}_{\mathrm{int}}$. Since here we cannot apply the Fierz identity, we have to impose its coefficient to be zero:

$$\frac{\partial W^{ij}(\phi_k, \phi_k^\dagger)}{\partial \phi^{\dagger k}} = 0 \tag{3.45}$$

that is W^{ij} is a holomorphic function of ϕ_k.

From the interaction Lagrangian (3.35), since for the spinor fields $[\psi_i^a] = [\psi_{ja}] = [\text{mass}]^{\frac{3}{2}}$, we can see that W^{ij} has the dimension of a mass. Since $W^{ij}(\phi_k)$ depends only on ϕ_k and not on $\phi_k^\dagger$, we can in general express $W^{ij}(\phi_k)$ as

$$W^{ij}(\phi_k) = M^{ij} + y^{ijk}\phi_k \tag{3.46}$$

where y^{ijk} has to be totally symmetric under the interchange of i, j and k as we required $\frac{\partial W^{ij}}{\partial \phi_k}$ to be totally symmetric and we can always choose M^{ij} to be symmetric. In this way, W^{ij} is symmetric under the exchange of i and j. In general, we can express $W^{ij}(\phi_k)$ in terms of another function W in this way:

$$W^{ij} = \frac{\partial^2 W}{\partial \phi_i \partial \phi_j} \tag{3.47}$$

with

$$W = f(\phi_i^\dagger) + c^i \phi_i + c^{ij} \phi_i^\dagger \phi_j + \frac{1}{2} M^{ij} \phi_i \phi_j + \frac{1}{6} y^{ijk} \phi_i \phi_j \phi_k \tag{3.48}$$

where W is the most generic function of ϕ_i and $\phi_i^\dagger$ such that W^{ij} is symmetric under the exchange of i and j and has a form as in (3.46). The function W is called superpotential.

The last term in Eq. (3.43) is

$$-\frac{1}{2} W^{ij} \delta(\psi_i^a \psi_{aj}) = -\frac{1}{2} W^{ij} 2 \psi_i^a \delta \psi_{aj} = -W^{ij} \psi_i^a \Big[(-\mathrm{i}) \sigma^\mu_{a\dot{b}} \epsilon^{\dagger \dot{b}} \partial_\mu \phi_j + \epsilon_a \mathcal{F}_j \Big] \tag{3.49}$$

where we have considered that W^{ij} is symmetric under the exchange of i, j and the SUSY transformations (3.33). To sum this term with the last term in Eq. (3.42), we can use again the identity (3.29):

$$\begin{aligned} -\frac{1}{2}W^{ij}\delta(\psi_i^a\psi_{aj}) &= \mathrm{i}W^{ij}(\psi_i^a\sigma^\mu_{a\dot{b}}\epsilon^{\dagger\dot{b}})\partial_\mu\phi_j - W^{ij}\psi_i^a\epsilon_a\mathcal{F}_j \\ &= -\mathrm{i}W^{ij}(\epsilon^\dagger_{\dot{a}}\bar{\sigma}^{\mu\dot{a}b}\psi_{bi})\partial_\mu\phi_j - W^{ij}\psi_i^a\epsilon_a\mathcal{F}_j\ . \end{aligned} \tag{3.50}$$

Now, we can plug Eq. (3.38), (3.40), (3.42) and (3.43) into Eq. (3.36), and take into account Eq. (3.44), (3.45) and (3.50):

$$\begin{aligned} \delta\mathcal{L}^{\mathrm{c}}_{\mathrm{int}} = \frac{\partial W^i}{\partial\phi_k}\epsilon^a\psi_{ak}\mathcal{F}_i + \frac{\partial W^i}{\partial\phi^{\dagger k}}\epsilon^\dagger_{\dot{a}}\psi^{\dagger\dot{a}k}\mathcal{F}_i - \mathrm{i}W^i\epsilon^\dagger_{\dot{a}}\bar{\sigma}^{\mu\dot{a}b}\partial_\mu\psi_{bi} \\ - \mathrm{i}W^{ij}\epsilon^\dagger_{\dot{a}}\bar{\sigma}^{\mu\dot{a}b}\psi_{bi}\partial_\mu\phi_j - W^{ij}\psi_i^a\epsilon_a\mathcal{F}_j + \mathrm{h.c.} \end{aligned} \tag{3.51}$$

The two terms with $\bar{\sigma}^{\mu\dot{a}b}$ can be summed to get a total derivative. To show this, first we need to note that, using Eq. (3.47) and considering Eq. (3.45) that is the superpotential W is a holomorphic function of ϕ_i, we have

$$W^{ij}\partial_\mu\phi_j = \frac{\partial^2 W}{\partial\phi_i\partial\phi_j}\partial_\mu\phi_j = \partial_\mu\left(\frac{\partial W}{\partial\phi_i}\right)\ . \tag{3.52}$$

Now, the sum of two terms with $\bar{\sigma}^{\mu\dot{a}b}$ in Eq. (3.51) become:

$$-\mathrm{i}W^i\epsilon^\dagger_{\dot{a}}\bar{\sigma}^{\mu\dot{a}b}\partial_\mu\psi_{bi} - \mathrm{i}\partial_\mu\left(\frac{\partial W}{\partial\phi_i}\right)\epsilon^\dagger_{\dot{a}}\bar{\sigma}^{\mu\dot{a}b}\psi_{bi} \tag{3.53}$$

and we can finally see that setting

$$W^i = \frac{\partial W}{\partial\phi_i} \tag{3.54}$$

the sum of the two terms is a total derivative:

$$-\mathrm{i}W^i\epsilon^\dagger_{\dot{a}}\bar{\sigma}^{\mu\dot{a}b}\partial_\mu\psi_{bi} - \mathrm{i}\partial_\mu W^i\epsilon^\dagger_{\dot{a}}\bar{\sigma}^{\mu\dot{a}b}\psi_{bi} = -\mathrm{i}\partial_\mu\left(W^i\epsilon^\dagger_{\dot{a}}\bar{\sigma}^{\mu\dot{a}b}\psi_{bi}\right) \tag{3.55}$$

so that these two terms can be ignored in the variation of the interaction Lagrangian (3.51) that becomes

$$\delta\mathcal{L}^{\mathrm{c}}_{\mathrm{int}} = \frac{\partial W^i}{\partial\phi_k}\epsilon^a\psi_{ak}\mathcal{F}_i + \frac{\partial W^i}{\partial\phi^{\dagger k}}\epsilon^\dagger_{\dot{a}}\psi^{\dagger\dot{a}k}\mathcal{F}_i - W^{ij}\psi_i^a\epsilon_a\mathcal{F}_j + \mathrm{h.c.} \tag{3.56}$$

Considering Eq. (3.47) and (3.54) we have

$$W^{ij} = \frac{\partial}{\partial\phi_i}\frac{\partial W}{\partial\phi_j} = \frac{\partial W^i}{\partial\phi_j} \tag{3.57}$$

so that, with the indices substitution $i \to j$ and $k \to i$, the first term in Eq. (3.56) becomes

$$\frac{\partial W^j}{\partial\phi_i}\epsilon^a\psi_{ai}\mathcal{F}_j = W^{ji}\epsilon^a\psi_{ai}\mathcal{F}_j = W^{ij}\epsilon^a\psi_{ai}\mathcal{F}_j \tag{3.58}$$

where we have taken into account the symmetry of W^{ij} given by Eq. (3.47). The last expression is opposite to the third term in (3.56), that is the sum of the first and third term in (3.56) is zero and the variation of the interaction Lagrangian is:

$$\delta\mathcal{L}^{\mathrm{c}}_{\mathrm{int}} = \frac{\partial W^i}{\partial\phi^{\dagger k}}\epsilon^\dagger_{\dot a}\psi^{\dagger\dot a k}\mathcal{F}_i + \mathrm{h.c.} \tag{3.59}$$

Finally, since we require the variation of the interaction Lagrangian to be zero, we impose $\frac{\partial W^i}{\partial\phi^\dagger_k} = 0$. This, in turn, from Eq. (3.54), implies that the coefficient c^{ij} in the superpotential (3.48) is zero:

$$\frac{\partial W^i}{\partial\phi^\dagger_i} = 0 \implies \frac{\partial W}{\partial\phi^\dagger_i\partial\phi_j} = c^{ij} = 0\,. \tag{3.60}$$

The function $f(\phi^\dagger_i)$ can also be set to zero because, considering the definitions (3.47) and (3.54), the Lagrangian only includes derivatives respect to ϕ_i:

$$f(\phi^\dagger_i) = 0\,. \tag{3.61}$$

With these considerations, the superpotential (3.48) become

$$W = c^i\phi_i + \frac{1}{2}M^{ij}\phi_i\phi_j + \frac{1}{6}y^{ijk}\phi_i\phi_j\phi_k \tag{3.62}$$

from which we can derive the expression for the functions W^{ij} and W^i:

$$W^i = \frac{\partial W}{\partial\phi_i} = c^i + M^{ij}\phi_j + \frac{1}{2}y^{ijk}\phi_j\phi_k \tag{3.63}$$

$$W^{ij} = \frac{\partial^2 W}{\partial\phi_i\partial\phi_j} = \frac{\partial W^i}{\partial\phi_j} = M^{ij} + y^{ijk}\phi_k\,. \tag{3.64}$$

Gathering Eq. (3.34) and (3.35) and considering that $U = 0$ and $x^{ij} = 0$ as in Eq. (3.38) and (3.40), the total Lagrangian is

$$\begin{aligned}\mathcal{L}^{\mathrm{c}}_{\mathrm{SUSY}} &= \mathcal{L}^{\mathrm{c}}_{\mathrm{s}} + \mathcal{L}^{\mathrm{c}}_{\mathrm{f}} + \mathcal{L}^{\mathrm{c}}_{\mathrm{aux}} + \mathcal{L}^{\mathrm{c}}_{\mathrm{int}} \\ &= -\partial^\mu\phi^{\dagger i}\partial_\mu\phi_i + \mathrm{i}\psi^{\dagger i}_{\dot a}\bar\sigma^{\mu\dot a b}\partial_\mu\psi_{bi} + \mathcal{F}^{\dagger i}\mathcal{F}_i + \left(W^i\mathcal{F}_i - \frac{1}{2}W^{ij}\psi^a_i\psi_{ja} + \mathrm{h.c.}\right).\end{aligned} \tag{3.65}$$

3.3.4 Elimination of auxiliary fields

The auxiliary fields $\mathcal{F}_i$ and $\mathcal{F}^{\dagger i}$ can be eliminated using the equations of motion:

$$\begin{aligned} \partial_\mu \frac{\partial \mathcal{L}^{\mathrm{c}}_{\mathrm{SUSY}}}{\partial(\partial_\mu \mathcal{F}_i)} - \frac{\partial \mathcal{L}^{\mathrm{c}}_{\mathrm{SUSY}}}{\partial \mathcal{F}_i} = 0 \quad &\Longrightarrow \quad \mathcal{F}^{\dagger i} = -W^i = -\frac{\partial W}{\partial \phi_i} \\ \partial_\mu \frac{\partial \mathcal{L}^{\mathrm{c}}_{\mathrm{SUSY}}}{\partial(\partial_\mu \mathcal{F}^{\dagger i})} - \frac{\partial \mathcal{L}^{\mathrm{c}}_{\mathrm{SUSY}}}{\partial \mathcal{F}^{\dagger i}} = 0 \quad &\Longrightarrow \quad \mathcal{F}_i = -W^\dagger_i = -\left(\frac{\partial W}{\partial \phi_i}\right)^\dagger \end{aligned} \tag{3.66}$$

so that the interaction Lagrangian become

$$\mathcal{L}^{\mathrm{c}}_{\mathrm{int}} = -W^i W^*_i - \frac{1}{2} W^{ij} \psi^a_i \psi_{ja} + \mathrm{h.c.} \tag{3.67}$$

summing this and the $\mathcal{F}^{\dagger i}\mathcal{F}_i$ term that appears in Eq. (3.65) gives

$$\begin{aligned} \mathcal{L}^{\mathrm{c}}_{\mathrm{int}} + \mathcal{F}^{\dagger i}\mathcal{F}_i &= -W^i W^\dagger_i - W^\dagger_i W^i - \left(\frac{1}{2} W^{ij} \psi^a_i \psi_{ja} + \mathrm{h.c.}\right) + W^i W^\dagger_i \\ &= -\left|\frac{\partial W}{\partial \phi_i}\right|^2 - \left(\frac{1}{2}\frac{\partial^2 W}{\partial \phi_i \partial \phi_j} \psi^a_i \psi_{ja} + \mathrm{h.c.}\right) \end{aligned} \tag{3.68}$$

where the term $W^\dagger_i \mathcal{F}^{i\dagger}$ comes from the hermitian conjugate part and we have used Eq. (3.64). Plugging this expression into the total Lagrangian (3.65) we obtain:

$$\mathcal{L}^{\mathrm{c}}_{\mathrm{SUSY}} = -\partial^\mu \phi^{\dagger i} \partial_\mu \phi_i + \mathrm{i}\psi^{\dagger i}_{\dot{a}} \bar{\sigma}^{\mu \dot{a} b} \partial_\mu \psi_{bi} - \left|\frac{\partial W}{\partial \phi_i}\right|^2 - \left(\frac{1}{2}\frac{\partial^2 W}{\partial \phi_i \partial \phi_j} \psi^a_i \psi_{aj} + \mathrm{h.c.}\right) \tag{3.69}$$

where W is the superpotential (3.62) whose derivatives can be expanded as in Eq. (3.63) and (3.64):

$$\begin{aligned} \mathcal{L}^{\mathrm{c}}_{\mathrm{SUSY}} &= -\partial^\mu \phi^{\dagger i} \partial_\mu \phi_i + \mathrm{i}\psi^{\dagger i}_{\dot{a}} \bar{\sigma}^{\mu \dot{a} b} \partial_\mu \psi_{bi} \\ &\quad - \left|c^i + M^{ij}\phi_j + \frac{1}{2} y^{ijk} \phi_j \phi_k\right|^2 - \left(\frac{1}{2} M^{ij} \psi^a_i \psi_{ja} + \frac{1}{2} y^{ijk} \phi_k \psi^a_i \psi_{ja} + \mathrm{h.c.}\right) . \end{aligned} \tag{3.70}$$

The Lagrangian (3.70) implies that the tree level masses of a particle and its superpartner are the same. In fact, from the equations of motion for the scalar field $\phi^{\dagger i}$ we obtain

$$\partial^\mu \partial_\mu \phi_k = M^{ij} M_{ik} \phi_j \, . \tag{3.71}$$

On the other hand, the equations of motion for the fields $\psi^{\dagger i}$ and ψ_i are

$$\mathrm{i}\bar{\sigma}^{\mu\dot{a}b}\partial_\mu\psi_{bi} + M^\dagger_{ij}\psi^{\dagger\dot{a}j} = 0 \tag{3.72}$$

$$-\mathrm{i}\sigma^\mu_{a\dot{b}}\partial_\mu\psi^{\dagger\dot{b}i} + M^{ij}\psi_{ja} = 0 \tag{3.73}$$

where in the second equation we have used Eq. (3.29). The equations of motion for the scalar and spinor field employ the same mass matrix M^{ij} implying that all the particle and sparticles in a supermultiplet have to have the same mass.

3.4 Abelian gauge SUSY Lagrangian

We can divide the gauge theory in Abelian and non-Abelian gauge theory. Here we study an Abelian U(1) gauge theory whose spectrum includes one bosonic gauge field and its supersymmetric partner, a gaugino.

We follow the procedure of the previous 3.3.1, 3.3.2, 3.3.3 and 3.3.4 sections that is

- start with a free Lagrangian;
- add auxiliary fields to close the algebra;
- introduce interactions;
- eliminate the auxiliary fields.

3.4.1 Free Lagrangian

Consider a vector supermultiplet in which there is a bosonic gauge field A_μ and its supersymmetric partner denoted by λ. As in Eq. (3.23) and using the field strength tensor of the gauge field A_μ as in Eq. (2.44), we can write the Lagrangian kinetic terms:

$$\mathcal{L}^{\mathrm{Av}}_{\mathrm{free}} = -\frac{1}{4}F_{\mu\nu}F^{\mu\nu} + \mathrm{i}\lambda^\dagger\bar{\sigma}^\mu\partial_\mu\lambda \tag{3.74}$$

where the superscript Av stands for Abelian vector supermultiplet and $F_{\mu\nu}$ is defined in Eq. (2.16) for the U(1) Abelian case.

Now we can introduce the SUSY transformations of the gauge field A_μ and the spinor field λ

$$\delta A_\mu = -\frac{1}{\sqrt{2}}\left(\epsilon^\dagger\bar{\sigma}_\mu\lambda + \lambda^\dagger\bar{\sigma}_\mu\epsilon\right) \qquad \delta\lambda_\alpha = \frac{\mathrm{i}}{2\sqrt{2}}(\sigma^\mu\bar{\sigma}^\nu\epsilon)_\alpha F_{\mu\nu}\ . \tag{3.75}$$

It can be explicitly verified that with these transformations (3.75) the variation of the free Lagrangian (3.74) is a total derivative and so the action is invariant. However, as in the previous section 3.3.2, the algebra does not close off-shell on the A_μ and λ fields.

3.4.2 Auxiliary Lagrangian

Following sec. 3.3.2, we introduce an auxiliary field $\mathcal{D}$ with one off-shell bosonic degree of freedom and zero on-shell degree of freedom. This compensates the two on-shell, three off-shell degree of freedom of the vector field A_μ and the two on-shell, four off-shell degree of freedom of the spinor field λ. The real scalar field $\mathcal{D}$ together with its variation $\delta\mathcal{D}$ can allow the closure of the algebra on the A_μ, λ and $\mathcal{D}$ fields. Thus, we add the auxiliary term

$$\mathcal{L}^{\text{Av}}_{\text{aux}} = \frac{1}{2}\mathcal{D}^2 \tag{3.76}$$

to the free Lagrangian (3.74). The total Lagrangian $\mathcal{L}^{\text{Av}}_{\text{free}}+\mathcal{L}^{\text{Av}}_{\text{aux}}$ is not invariant under the SUSY transformation (3.75), so we modify these transformations in order to have both Lagrangians invariant up to total derivatives and the closure of the algebra on the A_μ, λ and $\mathcal{D}$ fields. As can be verified, the variations

$$\begin{gathered}\delta A_\mu = -\frac{1}{\sqrt{2}}\big(\epsilon^\dagger\bar\sigma_\mu\lambda + \lambda^\dagger\bar\sigma_\mu\epsilon\big) \qquad \delta\lambda_a = \frac{\mathrm{i}}{2\sqrt{2}}(\sigma^\mu\bar\sigma^\nu\epsilon)_a F_{\mu\nu} + \frac{1}{\sqrt{2}}\mathcal{D}\epsilon_a \\ \delta\mathcal{D} = \frac{1}{\sqrt{2}}\big(-\epsilon^\dagger\bar\sigma^\mu\partial_\mu\lambda + \partial_\mu\lambda^\dagger\bar\sigma^\mu\epsilon\big)\end{gathered} \tag{3.77}$$

make the Lagrangian

$$\mathcal{L}^{\text{Av}}_{\text{free}} + \mathcal{L}^{\text{Av}}_{\text{aux}} = -\frac{1}{4}F_{\mu\nu}F^{\mu\nu} + \mathrm{i}\lambda^\dagger\bar\sigma^\mu\partial_\mu\lambda + \frac{1}{2}\mathcal{D}^2 \tag{3.78}$$

invariant and allow the closure of the algebra.

3.4.3 Interaction Lagrangian

In order to combine the Abelian vector supermultiplet $\{\, A_\mu, \lambda, \mathcal{D}\,\}$ and the chiral supermultiplet $\{\,\phi, \psi, \mathcal{F}\,\}$ a first attempt would be to sum the Lagrangian $\mathcal{L}^{\text{c}}_{\text{free+aux}}$ in Eq. (3.34) and the above gauge Lagrangian (3.78). However, such a sum is not gauge-invariant. Following the methodology of sec. 2.2.1, we

can write the gauge invariant Lagrangian

$$\begin{aligned}\mathcal{L}^{\text{c+Av}}_{\text{fr+au+int}} &= \mathcal{L}^{\text{c}}_{\text{free}} + \mathcal{L}^{\text{c}}_{\text{aux}} + \mathcal{L}^{\text{Av}}_{\text{free}} + \mathcal{L}^{\text{Av}}_{\text{aux}}\Big|_{\partial_\mu \to D_\mu = \partial_\mu + \mathrm{i}qA_\mu} \\ &= (D_\mu\phi)^\dagger (D^\mu\phi) + \mathrm{i}\psi^\dagger\bar{\sigma}^\mu D_\mu\psi + \mathcal{F}^\dagger\mathcal{F} - \frac{1}{4}F_{\mu\nu}F^{\mu\nu} + \mathrm{i}\lambda^\dagger\bar{\sigma}^\mu\partial_\mu\lambda + \frac{1}{2}\mathcal{D}^2\end{aligned} \tag{3.79}$$

where the chiral supermultiplet transform according Eq. (2.13) and we have used the covariant derivative in place of the normal derivative, according to Eq. (2.19), to make the Lagrangian gauge invariant. The strength field $F_{\mu\nu}$ and the corresponding gauge field A_μ of an Abelian supermultiplet are gauge invariant. Thus, since all members of a supermultiplet have to have the same gauge transformation, also λ is gauge invariant and the covariant derivative D_μ reduces to the normal derivative ∂_μ that appears in the $\mathrm{i}\lambda^\dagger\bar{\sigma}^\mu\partial_\mu\lambda$ term in the above Eq. (3.79).

As in sec. 2.2.1, the introduction of the covariant derivative couples the boson field A_μ with the scalar and fermion fields, ϕ and ψ respectively. Indeed, expanding $D_\mu = \partial_\mu + \mathrm{i}qA_\mu$ in Eq. (3.79), we find the interaction terms:

$$\mathcal{L}^{\text{c+Av}}_{\text{int, covariant}} = \partial_\mu\phi^\dagger \mathrm{i}qA^\mu\phi - \mathrm{i}qA_\mu\phi^\dagger\partial^\mu\phi + \mathrm{i}\psi^\dagger\bar{\sigma}^\mu\mathrm{i}qA_\mu\psi\ . \tag{3.80}$$

Apart from the previous interaction terms, there are also the other possible gauge invariant interaction terms

$$\mathcal{L}^{\text{c+Av}}_{\text{int,residual}} = c_1\phi^\dagger\phi\mathcal{D} + c_2\Big(\phi^\dagger\psi\lambda + \text{h.c.}\Big) \tag{3.81}$$

where c_1 and c_2 are dimensionless coefficient. Conversely to $\mathcal{L}^{\text{c+Av}}_{\text{int, covariant}}$ in Eq. (3.80), these interaction terms are not already included in the Lagrangian (3.79) so we need to add them to Eq. (3.79). Any other term that combines fields from the Abelian vector supermultiplet, with dimensions $[A_\mu] = [\text{mass}], [\lambda] = [\text{mass}]^{\frac{3}{2}}, [\mathcal{D}] = [\text{mass}]^2$, and the chiral supermultiplet, with dimensions $[\phi] = [\text{mass}]^1, [\psi] = [\text{mass}]^{\frac{3}{2}}, [\mathcal{F}] = [\text{mass}]^2$, is excluded because it has a dimension bigger than 4 or it do not respect Lorentz invariance.

As always, we require the total Lagrangian

$$\mathcal{L}^{\text{c+Av}} = \mathcal{L}^{\text{c+Av}}_{\text{fr+au+int}} + \mathcal{L}^{\text{c+Av}}_{\text{int,residual}} \tag{3.82}$$

sum of Eq. (3.79) and Eq. (3.81), to be invariant up to total derivatives under some SUSY transformations to be determined. Previously, the free and auxiliary Lagrangian $\mathcal{L}^{\text{c}}_{\text{free+aux}}$ (3.34) was invariant under the SUSY transformations (3.33). However, the variations $\delta\psi$ and $\delta\mathcal{F}$ are now modified by the

introduction of the covariant derivative. Thus the variation $\delta(\mathcal{L}^{\mathrm{c}}_{\mathrm{free+aux}}|_{\partial_\mu \to D_\mu})$ presents new terms that have to be taken into account when we require $\delta S = 0$. It can be verified that the variation of the total Lagrangian is null up to total derivatives if the coefficients c_1 and c_2 in Eq. (3.81) are

$$c_1 = -q \qquad c_2 = -\sqrt{2}q \tag{3.83}$$

and if the fields satisfy the SUSY transformations

$$\begin{aligned}
\delta\phi_i &= \epsilon\psi_i & \delta\psi_{ia} &= -\mathrm{i}(\sigma^\mu\epsilon^\dagger)_a D_\mu\phi_i + \epsilon_a\mathcal{F}_i \\
\delta A_\mu &= -\frac{1}{\sqrt{2}}\big(\epsilon^\dagger\bar\sigma_\mu\lambda + \lambda^\dagger\bar\sigma_\mu\epsilon\big) & \delta\lambda_a &= \frac{\mathrm{i}}{2\sqrt{2}}(\sigma^\mu\bar\sigma^\nu\epsilon)_a F_{\mu\nu} + \frac{1}{\sqrt{2}}\mathcal{D}\epsilon_a \\
\delta\mathcal{D} &= \frac{1}{\sqrt{2}}\big(-\epsilon^\dagger\bar\sigma^\mu D_\mu\lambda + D_\mu\lambda^\dagger\bar\sigma^\mu\epsilon\big) & \delta\mathcal{F}_i &= -\mathrm{i}\epsilon^\dagger\bar\sigma^\mu D_\mu\psi_i + \sqrt{2}q_i\phi_i\lambda^\dagger\epsilon^\dagger
\end{aligned} \tag{3.84}$$

where q_i is the coupling constant charge that appears in the covariant derivative (2.19) and we have introduced an index i to consider more than one chiral superfield.

3.4.4 Elimination of auxiliary fields

As we have done at the end of sec. 3.3.3, we can eliminate the auxiliary field $\mathcal{D}$ looking at the equations of motion of this field. Plugging Eq. (3.79), (3.81) and (3.83) into Eq. (3.82) we obtain the Lagrangian that combine chiral and vector supermultiplets:

$$\begin{aligned}
\mathcal{L}^{\mathrm{c+Av}} &= \mathcal{L}^{\mathrm{c}}_{\mathrm{free}} + \mathcal{L}^{\mathrm{c}}_{\mathrm{aux}} + \mathcal{L}^{\mathrm{Av}}_{\mathrm{free}} + \mathcal{L}^{\mathrm{Av}}_{\mathrm{aux}}\Big|_{\partial_\mu\to D_\mu} + \mathcal{L}^{\mathrm{c+Av}}_{\mathrm{int,residual}} \\
&= (D_\mu\phi^i)^\dagger(D^\mu\phi_i) + \mathrm{i}\psi^{\dagger i}\bar\sigma^\mu D_\mu\psi_i + \mathcal{F}^{\dagger i}\mathcal{F}_i - \frac{1}{4}F_{\mu\nu}F^{\mu\nu} + \mathrm{i}\lambda^\dagger\bar\sigma^\mu\partial_\mu\lambda + \frac{1}{2}\mathcal{D}^2 \\
&\qquad - q\phi^{\dagger i}\phi_i\mathcal{D} - \sqrt{2}q\Big(\phi^{\dagger i}\psi_i\lambda + \mathrm{h.c.}\Big)
\end{aligned} \tag{3.85}$$

where the index i is used to label more than one field. The equation of motion for $\mathcal{D}$ is

$$\mathcal{D} - q\phi^{\dagger i}\phi_i = 0 \tag{3.86}$$

that can be used to replace the auxiliary field $\mathcal{D}$ with the scalar field ϕ.

The Lagrangian (3.85) combine chiral and vector supermultiplets but does not include the interaction among members of the chiral supermultiplet. To obtain the full Lagrangian we finally have to add to Eq. (3.85) the interaction

Lagrangian (3.67) for chiral supermultiplet:

$$\begin{aligned}\mathcal{L} &= \mathcal{L}^{\text{c}}_{\text{free}} + \mathcal{L}^{\text{c}}_{\text{aux}} + \mathcal{L}^{\text{Av}}_{\text{free}} + \mathcal{L}^{\text{Av}}_{\text{aux}}\Big|_{\partial_\mu \to D_\mu} + \mathcal{L}^{\text{c+Av}}_{\text{int,residual}} + \mathcal{L}^{\text{c}}_{\text{int}} \\ &= (D_\mu \phi^i)^\dagger (D^\mu \phi_i) + \mathrm{i}\psi^{\dagger i}\bar{\sigma}^\mu D_\mu \psi_i - \frac{1}{4}F_{\mu\nu}F^{\mu\nu} + \mathrm{i}\lambda^\dagger \bar{\sigma}^\mu \partial_\mu \lambda - \frac{1}{2}\Big(q\phi^{\dagger i}\phi_i\Big)^2 \\ &\quad - \sqrt{2}q\Big(\phi^{\dagger i}\psi_i\lambda + \text{h.c.}\Big) - \left|\frac{\partial W}{\partial \phi_i}\right|^2 - \left(\frac{1}{2}\frac{\partial^2 W}{\partial\phi_i \partial\phi_j}\psi^a_i \psi_{ja} + \text{h.c.}\right)\end{aligned} \tag{3.87}$$

where we have eliminated both the auxiliary field $\mathcal{D}$ using Eq. (3.86) and the auxiliary fields $\mathcal{F}_i$ summing $\mathcal{L}^{\text{c}}_{\text{int}}$ and $\mathcal{F}^{\dagger i}\mathcal{F}_i$ as done in Eq. (3.68). From this Lagrangian $\mathcal{L}$ we can see that the scalar field potential $V(\phi, \phi^\dagger)$ is

$$V(\phi, \phi^\dagger) = \left|\frac{\partial W}{\partial \phi_i}\right|^2 + \frac{1}{2}\Big(q\phi^{\dagger i}\phi_i\Big)^2 \equiv V_{\mathcal{F}} + V_{\mathcal{D}} \tag{3.88}$$

where W is the superpotential (3.62) and we have introduced the $\mathcal{F}$-term and $\mathcal{D}$-term

$$V_{\mathcal{F}} \equiv \left|\frac{\partial W}{\partial \phi_i}\right|^2 = \mathcal{F}^{\dagger i}\mathcal{F}_i \qquad V_{\mathcal{D}} \equiv \frac{1}{2}\Big(q\phi^{\dagger i}\phi_i\Big)^2 = \frac{1}{2}\mathcal{D}^2 \tag{3.89}$$

that will be further studied in sec 3.6.1 and 3.6.2.

3.5 Non-Abelian gauge SUSY Lagrangian

In this section, we consider the SU(2) and SU(3) non-Abelian gauge theory. As discussed in sec. 2.2.3, the SU(N) groups have $N^2 - 1$ generators, see Eq. (2.32), that correspond to $N^2 - 1$ gauge fields. We indicate the gauge fields with A^a, the gaugino fields with λ^a and the auxiliary fields with $\mathcal{D}^a$, where a run from 1 to 3 in the SU(2) case and from 1 to 8 in the SU(3) case.

3.5.1 Free and Auxiliary Lagrangian

Using the result found in sec. 2.2.3, we generalise the free and auxiliary Lagrangian in Eq. (3.74) and (3.76)

$$\mathcal{L}^{\text{NAv}}_{\text{free+aux}} = -\frac{1}{4}F^a_{\mu\nu}F^{\mu\nu a} + \mathrm{i}\lambda^{\dagger a}\bar{\sigma}^\mu D_\mu \lambda^a + \frac{1}{2}\mathcal{D}^a\mathcal{D}^a \tag{3.90}$$

where $F^a_{\mu\nu}$ is defined in Eq. (2.43), λ^a are the gaugino fields and $\mathcal{D}^a$ are the auxiliary fields necessary to close the algebra. The gaugino fields are called winos and gluinos respectively in the SU(2) and SU(3) case.

Eq. (3.90) is a generalization of Eq. (3.78) and the covariant derivative D_μ takes the place of the normal derivative ∂_μ. To see the form of the covariant derivative D_μ, we note that the gaugino fields transforms as in Eq. (3.84) for the Abelian case, that is

$$\delta\lambda_b^a = \frac{\mathrm{i}}{2\sqrt{2}}(\sigma^\mu\bar{\sigma}^\nu\epsilon)_b F_{\mu\nu}^a + \frac{1}{\sqrt{2}}\mathcal{D}^a\epsilon_b \tag{3.91}$$

where the superscript a index is the gauge index while the subscript b index is the spinor index. This shows that the gauginos λ^a, the auxiliary fields $\mathcal{D}^a$ and the strength tensor $F_{\mu\nu}$ and so the corresponding the gauge field A_μ have to transform in the same way under the gauge symmetry. As shown in Eq. (2.47), in the non-Abelian case $F_{\mu\nu}$ transforms in the adjoint representation thus also λ^a and $\mathcal{D}^a$ transform in the adjoint representation under the gauge symmetry. Now, generalising the transformation (3.84) for the auxiliary field $\mathcal{D}^a$ in the non-Abelian case,

$$\delta\mathcal{D}^a = \frac{1}{\sqrt{2}}\big(-\epsilon^\dagger\bar{\sigma}^\mu D_\mu\lambda^a + D_\mu\lambda^{\dagger a}\bar{\sigma}^\mu\epsilon\big) \tag{3.92}$$

and requiring that $\mathcal{D}^a$ transforms in the adjoint representation imply a redefinition of the covariant derivative D_μ. In fact, as λ^a transforms in the adjoint representation, the covariant derivative acting on λ^a, to ensure gauge invariance, has to be defined in the adjoint representation, that is with generators defined in Eq. (2.36). Thus, instead of the definition (2.38), in the Lagrangian (3.90) we define the covariant derivative as

$$D_\mu\lambda^a \equiv D_\mu^{\mathrm{adj}}\lambda^a = \partial_\mu\lambda^a + \mathrm{i}g(T_{\mathrm{adj}}^a)^{bc}A_\mu^b\lambda^c = \partial_\mu\lambda^a + gf^{abc}A_\mu^b\lambda^c \tag{3.93}$$

where $(T_{\mathrm{adj}}^a)^{bc}$ is defined in Eq. (2.36) and all the other symbols are defined in sec. 2.2.3.

With this conventions and the transformation

$$\delta A_\mu^a = -\frac{1}{\sqrt{2}}\big(\epsilon^\dagger\bar{\sigma}_\mu\lambda^a + \lambda^{\dagger a}\bar{\sigma}_\mu\epsilon\big) \tag{3.94}$$

it can be verified that the variation of the Lagrangian (3.90) is null up to total derivatives.

3.5.2 Interactions and elimination of auxiliary fields

Following sec. 3.4.3, we start with a Lagrangian that describes the interaction between the non-Abelian vector supermultiplet $\left\{ A_\mu^a, \lambda^a, \mathcal{D}^a \right\}$ and the chiral

supermultiplet $\left\{ \phi^b, \psi^b, \mathcal{F}^b \right\}$:

$$\mathcal{L}^{\text{c+NAv}}_{\text{fr+au+int}} = (D_{\mu bc}\phi^b)^\dagger (D^\mu_{bc}\phi^b) + \mathrm{i}\psi^{\dagger b}\bar{\sigma}^\mu D_{\mu bb'}\psi^{b'} + \mathcal{F}^{\dagger b}\mathcal{F}^b - \frac{1}{4}F^a_{\mu\nu}F^{\mu\nu a} + \mathrm{i}\lambda^{\dagger a}\bar{\sigma}^\mu D^{\text{adj}}_\mu \lambda^a + \frac{1}{2}\mathcal{D}^a\mathcal{D}^a \quad (3.95)$$

where the index a labels the N^2-1 fields $\{(A^1_\mu, \ldots, A^{N^2-1}_\mu), (\lambda^1, \ldots, \lambda^{N^2-1}), (\mathcal{D}^1, \ldots, \mathcal{D}^{N^2-1})\}$ that correspond to the N^2-1 generators of the SU(N) gauge theory. These fields belong to the vector supermultiplet and transform in the adjoint representation. The index b labels the N fields $\{(\phi^1, \ldots, \phi^N), (\psi^1, \ldots, \psi^N), (\mathcal{F}^1, \ldots, \mathcal{F}^N)\}$ belonging to the chiral supermultiplet and transforming in the fundamental representation. Finally, we specify indices of the covariant derivative $(D_\mu)_{ij} = \delta_{ij}\partial_\mu + \mathrm{i}gA^a_\mu T^a_{ij}$ where A^a_μ correspond to the gauge fields and T^a_{ij} are the generators of the group.

The covariant derivatives and adjoint covariant derivatives couple both the chiral with vector fields and the vector fields with itself. Setting the superpotential to zero, $W=0$ and expanding the covariant derivative (2.38), $D_\mu = \partial_\mu + \mathrm{i}gA^a_\mu T^a$, and the adjoint covariant derivative (3.93), $D^{\text{adj}}_\mu = \partial_\mu + \mathrm{i}gA^a_\mu T^a_{\text{adj}}$, in Eq. (3.95), we get the interaction Lagrangian

$$\mathcal{L}^{\text{c+NAv}}_{\text{int, covariant}} = [\mathrm{i}gTA_\mu\phi]^\dagger\partial_\mu\phi + \partial_\mu\phi^\dagger \mathrm{i}gTA_\mu\phi - g_s^2 TA_\mu TA_\mu\phi\phi + \mathrm{i}\psi^\dagger\bar{\sigma}^\mu \mathrm{i}gTA_\mu\psi + \mathrm{i}\lambda^\dagger\bar{\sigma}^\mu \mathrm{i}g_s T_{\text{adj}}A_\mu\lambda \quad (3.96)$$

where, for simplicity, we dropped the indices.

Continuing to follow sec. 3.4.3 and mimicking the same reasoning through which we obtained Eq. (3.81), we can again get other gauge invariant interaction terms

$$\mathcal{L}^{\text{c+NAv}}_{\text{int,residual}} = c_1\phi^{b\dagger}\mathcal{D}^a(T^a)^{bc}\phi^c + c_2\Big[\phi^{b\dagger}\lambda^a(T^a)^{bc}\psi^c + \text{h.c.}\Big]\,. \quad (3.97)$$

Again, we require the total Lagrangian

$$\mathcal{L}^{\text{c+NAv}} = \mathcal{L}^{\text{c+NAv}}_{\text{fr+au+int}} + \mathcal{L}^{\text{c+NAv}}_{\text{int,residual}} \quad (3.98)$$

to be invariant, up total derivative, under the SUSY transformation

$$\begin{aligned}
\delta\phi_i &= \epsilon\psi_i & \delta\lambda^a_b &= \frac{\mathrm{i}}{2\sqrt{2}}(\sigma^\mu\bar{\sigma}^\nu\epsilon)_b F^a_{\mu\nu} + \frac{1}{\sqrt{2}}\mathcal{D}^a\epsilon_b \\
\delta\psi_{ib} &= -\mathrm{i}(\sigma^\mu\epsilon^\dagger)_b D_\mu\phi_i + \epsilon_b F_i & \delta A^a_\mu &= -\frac{1}{\sqrt{2}}\big(\epsilon^\dagger\bar{\sigma}_\mu\lambda^a + \lambda^{\dagger a}\bar{\sigma}_\mu\epsilon\big) \\
\delta\mathcal{F}_i &= -\mathrm{i}\epsilon^\dagger\bar{\sigma}^\mu D_\mu\psi_i + \sqrt{2}q\phi\lambda^\dagger\epsilon^\dagger & \delta\mathcal{D}^a &= \frac{1}{\sqrt{2}}\big(-\epsilon^\dagger\bar{\sigma}^\mu D_\mu\lambda^a + D_\mu\lambda^{\dagger a}\bar{\sigma}^\mu\epsilon\big)
\end{aligned} \quad (3.99)$$

that are the non-Abelian generalization of (3.84), as we have found in Eq. (3.91), (3.92) and (3.94). The supersymmetry invariance requirement constrains the coefficient c_1 and c_2 in the same way found in Eq. (3.83):

$$c_1 = -g \qquad c_2 = -\sqrt{2}g \; . \tag{3.100}$$

Plugging Eq. (3.95), (3.97) and (3.100) into the total Lagrangian (3.98), we get

$$\begin{aligned}\mathcal{L}^{\text{c+NAv}} = (D_{\mu bc}\phi^b)^\dagger (D^\mu_{bc}\phi^b) + \mathrm{i}\psi^{\dagger b}\bar\sigma^\mu D_{\mu bb'}\psi^{b'} + \mathcal{F}^{\dagger b}\mathcal{F}^b - \frac{1}{4}F^a_{\mu\nu}F^{\mu\nu a} + \mathrm{i}\lambda^{\dagger a}\bar\sigma^\mu D^{\text{adj}}_\mu \lambda^a \\ + \frac{1}{2}\mathcal{D}^a\mathcal{D}^a - g\phi^{b\dagger}\mathcal{D}^a(T^a)^{bc}\phi^c - \sqrt{2}g\Big[\phi^{b\dagger}\lambda^a(T^a)^{bc}\psi^c + \text{h.c.}\Big] \; .\end{aligned} \tag{3.101}$$

From the equation of motion for the auxiliary fields $\mathcal{D}^a$

$$\mathcal{D}^a - g\big[\phi^{b\dagger}(T^a)^{bc}\phi^c\big] = 0 \tag{3.102}$$

we can express $\mathcal{D}^a$ in terms of the scalar fields ϕ in Eq. (3.101). Adding to Eq. (3.101) the Lagrangian $\mathcal{L}^{\text{c}}_{\text{int}}$, Eq. (3.67) that describe the interactions among fields in the chiral supermultiplet, and eliminating the $\mathcal{F}^b$ auxiliary fields summing $\mathcal{L}^{\text{c}}_{\text{int}} + \mathcal{F}^{\dagger b}\mathcal{F}^b$ as done in Eq. (3.68), we obtain the full Lagrangian

$$\begin{aligned}\mathcal{L} &= \mathcal{L}^{\text{c+NAv}}_{\text{fr+au+int}} + \mathcal{L}^{\text{c+NAv}}_{\text{int,residual}} + \mathcal{L}^{\text{c}}_{\text{int}} \\ &= (D_{\mu bc}\phi^b)^\dagger (D^\mu_{bc}\phi^b) + \mathrm{i}\psi^{\dagger b}\bar\sigma^\mu D_{\mu bb'}\psi^{b'} - \frac{1}{4}F^a_{\mu\nu}F^{\mu\nu a} + \mathrm{i}\lambda^{\dagger a}\bar\sigma^\mu D^{\text{adj}}_\mu\lambda^a \\ &\quad - \frac{1}{2}g^2\big[\phi^{b\dagger}(T^a)^{bc}\phi^c\big]^2 - \sqrt{2}g\Big[\phi^{b\dagger}\lambda^a(T^a)^{bc}\psi^c + \text{h.c.}\Big] \\ &\quad - \left|\frac{\partial W}{\partial\phi}\right|^2 - \left(\frac{1}{2}\frac{\partial^2 W}{\partial\phi_i\partial\phi_j}\psi^a_i\psi_{ja} + \text{h.c.}\right)\end{aligned} \tag{3.103}$$

where the superpotential W can be expanded as in Eq. (3.62). From this total Lagrangian we can read that the scalar potential is given by

$$V(\phi_i,\phi_i^\dagger) = \left|\frac{\partial W}{\partial\phi}\right|^2 + \frac{1}{2}g^2\big[\phi_i^{b\dagger}(T^a)^{bc}\phi_i^c\big]^2 \equiv V_{\mathcal{F}} + V_{\mathcal{D}} \tag{3.104}$$

where, as in the Abelian case in sec. 3.4.4, we have introduced the $\mathcal{F}$-term and $\mathcal{D}$-term

$$V_{\mathcal{F}} \equiv \left|\frac{\partial W}{\partial\phi_i}\right|^2 = \mathcal{F}^{\dagger i}\mathcal{F}_i \qquad V_{\mathcal{D}} \equiv \frac{1}{2}g^2\big[\phi_i^{b\dagger}(T^a)^{bc}\phi_i^c\big]^2 = \frac{1}{2}\mathcal{D}^2 \tag{3.105}$$

that will be studied in next sec. 3.6.1 and 3.6.2.

3.6 SUSY breaking

As we have seen at the end of sec. 3.3.4, without a symmetry-breaking mechanism, every sparticle would have a mass equal to the mass of its particle superpartner. For example, charged particles such as the selectron would have a mass of about a half of MeV, and the gluino would be massless. These light charged sparticles would have been very easy to detect. Since we do not observe such particles, we need a mechanism that splits sparticle and particle masses. Such a mechanism has to break SUSY, because SUSY leads to the degenerate masses of each particle with its superpartner.

It would be desirable to break SUSY by introducing a spontaneous symmetry breaking mechanism, as done in sec. 2.3, where the Lagrangian is symmetric, but the ground state and thus the spectrum is not symmetric. In this case, the charges Q_a and $Q^\dagger_{\dot{a}}$ that generate the symmetry do not annihilate the vacuum state $|0\rangle$:

$$Q_a \,|0\rangle \neq 0 \qquad Q^\dagger_{\dot{a}} \,|0\rangle \neq 0 \tag{3.106}$$

that is the vacuum is not invariant under SUSY transformations. Now the algebra (3.3) constrains the Hamiltonian H, that is the operator P^0:

$$\left\{Q_a, Q^\dagger_{\dot{a}}\right\} = -2\sigma^\mu_{a\dot{a}} P_\mu = 2\,\mathbb{1}_{a\dot{a}} P^0 - 2\sigma^i_{a\dot{a}} P^i \,. \tag{3.107}$$

Since the sigma matrices are traceless, taking the traces of Eq. (3.107) isolates the Hamiltonian $H = P^0$:

$$Q_1 Q_1^\dagger + Q_1^\dagger Q_1 + Q_2 Q_2^\dagger + Q_2^\dagger Q_2 = H \tag{3.108}$$

and calculating the vacuum expectation value (VEV) we obtain the relationship

$$\langle 0 \,|\, H \,|\, 0\rangle = \left\| Q_1^\dagger \,|0\rangle \right\|^2 + \left\| Q_1 \,|0\rangle \right\|^2 + \left\| Q_2^\dagger \,|0\rangle \right\|^2 + \left\| Q_2 \,|0\rangle \right\|^2 > 0 \tag{3.109}$$

where the strict inequality holds because of Eq. (3.106), that is when the symmetry is broken. Considering the vacuum expectation value of the Hamiltonian kinetic terms null in the vacuum, the above inequality implies

$$\left\langle 0 \,\middle|\, V(\phi_i, \phi_i^\dagger) \,\middle|\, 0 \right\rangle > 0 \tag{3.110}$$

where the scalar potential $V(\phi_i, \phi_i^\dagger)$ is given in Eq. (3.104). Since V is the sum of two squares, to fulfil the above inequality that is to break the symmetry, one or both terms in Eq. (3.104) have to be non zero. This happens if the $\mathcal{F}$ field or the $\mathcal{D}$ field get a VEV and we speak about $\mathcal{F}$-terms or $\mathcal{D}$-terms, respectively.

3.6.1 $\mathcal{F}$-terms

In Eq. (3.104) the term $\left|\frac{\partial W}{\partial \phi}\right|^2$ comes from $\mathcal{F}^\dagger\mathcal{F}$ where $\mathcal{F}$ is the auxiliary field in the chiral supermultiplet. Symmetry breaking terms originates from the $\mathcal{F}$ field are called $\mathcal{F}$-terms. In the same way, the term $\frac{1}{2}g^2\left[\phi_i^{b\dagger}(T^a)^{bc}\phi_i^c\right]^2$ comes from the auxiliary field $\mathcal{D}$ in the vector supermultiplet and the corresponding symmetry breaking terms are called $\mathcal{D}$-terms.

When the symmetry is broken via $\mathcal{F}$-terms, the first term in Eq. (3.104) is non zero, that is the superpotential W and the scalar fields ϕ_i are such that the system of equations

$$\mathcal{F}^{\dagger i} = \frac{\partial W}{\partial \phi_i} = 0 \tag{3.111}$$

has no solution.

However, breaking the symmetry in this way leads to problems. Indeed, consider the supertrace Str defined as the following sum over all particles with mass m and spin s

$$\mathrm{STr}(m^2) \equiv \sum_s (-1)^{2s}(2s+1)\,\mathrm{Tr}(m_s^2)\,. \tag{3.112}$$

For models such as the MSSM, assuming the traces of the U(1) charges over the chiral superfields are null, the supertrace satisfy the sum rule [28]

$$\mathrm{STr}(m^2) = 0\,. \tag{3.113}$$

Since the supertrace depends on all the particle masses in the theory, this sum rule imposes a condition on sparticle masses. For example the selectrons, ignoring the possibility of flavour mixing that is ignoring the mixing with other scalars, have to satisfy the condition

$$m_{\tilde{e}_1}^2 + m_{\tilde{e}_2}^2 = 2m_e^2 \tag{3.114}$$

where $m_{\tilde{e}_1}$ is the lightest selectron mass eigenstate, $m_{\tilde{e}_2}$ is the heaviest selectron mass eigenstate and m_e is the electron mass eigenstate. This equality implies that the lightest selectron should have a mass $m_{\tilde{e}_1} < m_e \simeq 0.51\,\mathrm{MeV}$. Moreover, the selectron has to be charged because it belongs to the same supermultiplet of the electron and so it has to have the same gauge structure. However, such a light charged scalar particle is not experimentally observed.

3.6.2 $\mathcal{D}$-terms

To break the symmetry via $\mathcal{D}$-terms we can modify the total Abelian Lagrangian in Eq. (3.85). We add to this Lagrangian a linear term in $\mathcal{D}$:

$$\mathcal{L}_{\mathrm{FI}} = -\kappa\mathcal{D} \tag{3.115}$$

called Fayet-Iliopoulos term. Such a term can be introduced only in the Abelian gauge theory because the SUSY transformation (3.84) of $\mathcal{D}$ is a total derivative and $\mathcal{D}$ is gauge invariant. In the non-Abelian gauge theory, the auxiliary fields $\mathcal{D}^a$ are not gauge invariant and we cannot add a linear $\mathcal{D}^a$ term to the Lagrangian.

The Fayet-Iliopoulos term modifies the equations of motion for the field $\mathcal{D}$ so that Eq. (3.86) becomes

$$\mathcal{D} = \kappa - g \sum_i q_i |\phi_i| \tag{3.116}$$

and the potential contains the $\mathcal{D}$-term

$$V_{\mathcal{D}} \equiv \frac{1}{2}\mathcal{D}^2 = \frac{1}{2}\Big(\kappa - g \sum_i q_i |\phi_i|\Big)^2 . \tag{3.117}$$

Now, if κ and g have opposite sign Eq. (3.117) is always positive and the symmetry is broken. If κ and g have the opposite sign, Eq. (3.117) has a zero for $|\phi_i| = \sqrt{\frac{\kappa}{g q_i}}$. This means that, similarly to what we have seen in sec. 2.3, the gauge field has a non zero VEV and become massive, so even though SUSY is not broken, the gauge symmetry is spontaneously broken.

However, like the $\mathcal{F}$-terms, using $\mathcal{D}$-terms to break SUSY models that directly couple with the SM leads to problems. In fact, apart from the sum mass rule, a Fayet-Iliopoulos term implies a scalar potential with form

$$V = V_{\mathcal{F}} + V_{\mathcal{D}} = \sum_i |m_i|^2 |\phi_i|^2 + \frac{1}{2}\Big(\kappa - g \sum_i q_i |\phi_i|^2\Big)^2 . \tag{3.118}$$

Now, for example, from the MSSM superpotential, Eq. (3.122), and NMSSM superpotential, Eq. (3.129), only the Higgs doublets H_u and H_d and the scalar singlet S have a mass term. In particular, squarks and sleptons do not have mass terms. For these sparticles, setting $m_i = 0$, the condition

$$\frac{\partial V}{\partial |\phi_i|} = 0 \quad \Longrightarrow \quad \Big(\sum_i q_i |\phi_i|\Big)\Big(g^2 \sum_i q_i |\phi_i|^2 - \kappa g\Big) = 0 \tag{3.119}$$

implies a Mexican hat potential for the squark and slepton fields, see fig. 2.1 and sec. 2.3. In this way, squarks and sleptons obtain a non-zero VEVs that break $\mathrm{SU(3)_C}$ and $\mathrm{U(1)_{EM}}$ symmetries. Since this breaking is not experimentally observed, this mechanism cannot be a source, or at least cannot be the main source, of SUSY breaking.

3.6.3 Soft terms

Since the spontaneous SUSY breaking via $\mathcal{F}$-terms or $\mathcal{D}$-terms shows problems, we can parametrise the breaking mechanism without being explicit about its actual origin. This idea is framed assuming the existence of a so-called hidden sector, which does not have any renormalisable tree-level interactions with the visible sector we can observe at high energy physics experiments. We can assume that in the hidden sector SUSY is broken spontaneously via a mechanism that is still not clear. The hidden sector can only interact with the standard model sector through non-renormalisable or loop-induced couplings. When SUSY is broken in the hidden sector it is then transmitted to the the visible sector through these interactions. So according to this idea, the SUSY breaking mechanism originates in the hidden sector and is transmitted from the hidden sectror to the visible sector, leading to a set of soft SUSY breaking terms in the visible sector. In this way no mass sum rules are implied for the visible sector, so we evade this problem.

One can then build a model of SUSY breaking in the hidden sector, as discussed in sec. 3.6.1 and 3.6.2. However for phenomenology we do not need the details of how the hidden sector is constructed and how SUSY is broken there and transmitted to the visible sector. Instead we can parametrise our ignorance of how SUSY is broken, by writing down all possible soft SUSY breaking terms and treating them as independent parameters.

To do so we can introduce by hand terms in the Lagrangian that are not SUSY invariant. Among all terms that break SUSY, we select terms, called soft SUSY breaking terms, that do not to spoil the SUSY cancellations of quadratic divergences (see [41]):

$$\mathcal{L}^{\text{soft}} = \left(-\frac{1}{2}M_a\lambda^a\lambda^a + \frac{1}{6}a^{ijk}\phi_i\phi_j\phi_k - \frac{1}{2}b^{ij}\phi_i\phi_j + t^i\phi_i + \text{h.c.}\right) - \left(m^2\right)^i_{\ j}\phi^{j\dagger}\phi_i \tag{3.120}$$

where ϕ represent a scalar field and λ a gaugino field. The total Lagrangian becomes

$$\mathcal{L} = \mathcal{L}_{\text{SUSY}} + \mathcal{L}^{\text{soft}} \tag{3.121}$$

and SUSY is said to be softly broken. As shown in [41], $\mathcal{L}^{\text{soft}}$ does not introduce quadratic divergences and the total Lagrangian $\mathcal{L}_{\text{SUSY}} + \mathcal{L}^{\text{soft}}$ exhibits at high-energy the same well behaviour of $\mathcal{L}_{\text{SUSY}}$.

3.7 MSSM

The Minimal Supersymmetric Standard Model (MSSM) is a SUSY model that extends the SM, adding to it the minimum workable number of new

	multiplet	spin 0	spin $\frac{1}{2}$	spin 1	$SU(3)$	$SU(2)$	$U(1)$
Chiral	$\widehat{Q}_i$	$\widetilde{Q} = (\widetilde{u}_{\mathrm{L}}, \widetilde{d}_{\mathrm{L}})_i$	$Q = (u_{\mathrm{L}}, d_{\mathrm{L}})_i$		$\mathbf{3}$	$\mathbf{2}$	$+\frac{1}{6}$
	$\widehat{u}_i$	$\widetilde{u}^*_{\mathrm{R}i}$	$u^\dagger_{\mathrm{R}i}$		$\bar{\mathbf{3}}$	$\mathbf{1}$	$-\frac{2}{3}$
	$\widehat{d}_i$	$\widetilde{d}^*_{\mathrm{R}i}$	$d^\dagger_{\mathrm{R}i}$		$\bar{\mathbf{3}}$	$\mathbf{1}$	$+\frac{1}{3}$
	$\widehat{L}_i$	$\widetilde{L} = (\widetilde{\nu}, \widetilde{e}_{\mathrm{L}})_i$	$L = (\nu, e_{\mathrm{L}})_i$		$\mathbf{1}$	$\mathbf{2}$	$-\frac{1}{2}$
	$\widehat{e}_i$	$\widetilde{e}^*_{\mathrm{R}i}$	$e^\dagger_{\mathrm{R}i}$		$\mathbf{1}$	$\mathbf{1}$	$+1$
	$\widehat{H}_u$	$H_u = (H_u^+, H_u^0)$	$\widetilde{H}_u = (\widetilde{H}_u^+, \widetilde{H}_u^0)$		$\mathbf{1}$	$\mathbf{2}$	$+\frac{1}{2}$
	$\widehat{H}_d$	$H_d = (H_d^0, H_d^-)$	$\widetilde{H}_d = (\widetilde{H}_d^0, \widetilde{H}_d^-)$		$\mathbf{1}$	$\mathbf{2}$	$-\frac{1}{2}$
Vector	$\widehat{G}$		$\widetilde{g}$	g	$\mathbf{8}$	$\mathbf{1}$	0
	$\widehat{W}$		$\widetilde{W}^\pm$, $\widetilde{W}^0$	$W^\pm$, W^0	$\mathbf{1}$	$\mathbf{3}$	0
	$\widehat{B}$		$\widetilde{B}^0$	B^0	$\mathbf{1}$	$\mathbf{1}$	0

Table 3.1: Vector and chiral supermultiplets together with their bosonic and fermionic particle content and their gauge structure. All the SM particles have a supersymmetric partner indicated with a tilde over the field symbol. Compared to the SM, there are two Higgs doublet. Particles in the same supermultiplet have the same SU(3) and SU(2) representation and the same U(1) charge. An index $i \in \{ 1, 2, 3 \}$ is used to represent the three generations for quarks and lepton. For the chiral supermultiplets, in spin 0 and spin $\frac{1}{2}$ columns, we also write states in terms of their SU(2) components.

particles.

3.7.1 Spectrum

The MSSM spectrum includes all the SM particles, as depicted in table 2.1, and their supersymmetric partners. In contrast to the SM, there are two Higgs SU(2) doublets. From the theoretical point of view, in the SM, down and up quark masses are generated with Yukawa terms containing H and $H^\dagger$ fields, see Eq. (2.72) and (2.73). On the other hand, in the MSSM the superpotential is a holomorphic function of the chiral fields, see, eg., Eq. (3.62), so that it cannot depend on $H^\dagger$. Thus, in place of the $H^\dagger$ fields, we introduce another Higgs doublet that can generate the up quark mass. All the MSSM particles are depicted in table 3.1.

3.7.2 Superpotential

The MSSM superpotential is invariant under SU(3)⊗SU(2)⊗U(1) and is a function of the chiral supermultiplet:

$$W_{\text{MSSM}} = \widehat{e}_i\, Y_e^{ij} \widehat{H}_d \cdot \widehat{L}_j + \widehat{d}_i\, Y_d^{ij} \widehat{H}_d \cdot \widehat{Q}_j + \widehat{u}_i\, Y_u^{ij} \widehat{Q}_j \cdot \widehat{H}_u + \mu \widehat{H}_u \cdot \widehat{H}_d \quad (3.122)$$

where we have labelled the 3 generations with i and j indices, the supermultiplet are reported in tab. 3.1 and all the elements in a supermultiplet have the same SU(3) and SU(2) representation and U(1) charge; moreover the SU(2) dot product between the $\widehat{Q}$, $\widehat{L}$, $\widehat{H}_u$ and $\widehat{H}_d$ doublets is defined as

$$\begin{pmatrix} a \\ b \end{pmatrix} \cdot \begin{pmatrix} c \\ d \end{pmatrix} = ad - cb\,. \quad (3.123)$$

We can see that the two Higgs doublet have a different role after symmetry breaking: in fact only the H_u scalar doublet, with $+\frac{1}{2}$ U(1) charge, can give give mass to the u_i quarks and only the H_d scalar doublet, with $-\frac{1}{2}$ U(1) charge, can give give mass to the d_i quarks and e_i leptons.

3.7.3 Matter parity and R-parity

Other supermultiplet combinations, apart from the one in Eq. (3.122), lead to lepton or baryon number violation. For example, substituting the $\widehat{H}_d$ superfield in the superpotential (3.122) with $\widehat{L}$ superfield, which has the same gauge structure of $\widehat{H}_d$, we have the terms

$$\widehat{e}_i\, A^{ijk} \widehat{L}_j \cdot \widehat{L}_k \qquad \widehat{d}_i\, B^{ijk} \widehat{L}_j \cdot \widehat{Q}_k \qquad C^i \widehat{H}_u \cdot \widehat{L}_i \quad (3.124)$$

where A, B and C are coefficients. Since $\widehat{L}$ has a $+1$ lepton number and $\widehat{e}$ has a -1 lepton number, while all other particles have a 0 lepton number, these terms imply a lepton number violation. In a similar way, calling with D a coefficient, the term

$$\widehat{u}_i D^{ijk} \widehat{d}_j \widehat{d}_k \quad (3.125)$$

violates the baryon number since $\widehat{u}$ and $\widehat{d}$ have a $-\frac{1}{3}$ baryon number.

No baryon or lepton number violating processes have been observed, and there and various limits have been set on the couplings. The most pressing constraint comes proton decay, which can be induced when there is both B and L number violation. We can remove these dangerous operators by introducing a discrete $\mathbb{Z}_2$ symmetry called matter parity. The matter parity is described by the quantum number

$$P_M = (-1)^{3(B-L)} \quad (3.126)$$

where B is the baryon number and L is the lepton number. A valid term is composed by fields, each one with a specific matter parity $P_M(\text{field}_i)$, such that $\prod_i P_M(\text{field}_i) = +1$.

From the matter parity, we can introduce another important quantum number, called R-parity and defined as

$$P_R = P_M(-1)^{2s} = (-1)^{3(B-L)+2s} \tag{3.127}$$

where s is the spin. It follows from the conservation of the angular momentum that R-parity conservation and matter parity conservation are equivalent. We assume that the matter and R-parity are exactly conserved in the MSSM.

All the SM particles have $R = 1$. Since SM particles and their superpartners have a spin difference of $\frac{1}{2}$, all sparticles have $R = -1$. An important implication of the opposite R-parity of particle and sparticle is that, if the R-parity is exactly conserved in all the processes, the lightest supersymmetric particle (LSP) cannot decay into SM particles, that is the LSP must be stable. The nature of the LSP depend on the particular SUSY model. If the LSP is neutral weakly interacting scalar or fermion, it is a good candidate to be a dark matter constituent.

3.7.4 Soft breaking

As we have seen in Eq. (3.71) and (3.72), the scalar and spinor tree level masses are equal and given by the M^{ij} matrix. This implies that each superparticle has to have the same mass of the corresponding superpartner. Phenomenologically, light superparticles are not observed. To explain the experimental absence of mass degeneracy, the supersymmetry has to be broken as described in sec 3.6. According to sec. 3.6.3, we can write the soft breaking terms of the MSSM:

$$\begin{aligned}\mathcal{L}^{\text{soft}}_{\text{MSSM}} = &-\frac{1}{2}\Big(M_1\widetilde{B}^0\widetilde{B}^0 + M_2\widetilde{W}\widetilde{W} + M_3\widetilde{g}\widetilde{g} + \text{h.c.}\Big) \\ &- \Big(-a_e\widetilde{\bar{e}}\widetilde{L}H_d - a_d\widetilde{\bar{d}}\widetilde{Q}H_d + a_u\widetilde{\bar{u}}\widetilde{Q}H_u + \text{h.c.}\Big) \\ &- (m^2_{\widetilde{L}})^i_j\widetilde{L}^{j\dagger}\widetilde{L}_i - (m^2_{\widetilde{\bar{e}}})^i_j\widetilde{\bar{e}}^j\widetilde{\bar{e}}^\dagger_i - (m^2_{\widetilde{Q}})^i_j\widetilde{Q}^{\dagger j}\widetilde{Q}_i - (m^2_{\widetilde{\bar{d}}})^i_j\widetilde{\bar{d}}^j\widetilde{\bar{d}}^\dagger_i - (m^2_{\widetilde{\bar{u}}})^i_j\widetilde{\bar{u}}^j\widetilde{\bar{u}}^\dagger_i \\ &- m^2_{H_d}H^\dagger_d H_d - m^2_{H_u}H^\dagger_u H_u - (bH_uH_d + \text{h.c.})\end{aligned} \tag{3.128}$$

where M_1, M_2 and M_3 are the masses related to the three gauginos that, following Eq. (3.120), come from the $M_a\lambda^a\lambda^a$ term and are called, respectively, bino, wino and gluino, the a_e, a_d and a_u are trilinear couplings from the

$a^{ijk}\phi_i\phi_j\phi_k$ term, with the lower letter m we indicate mass terms that come from $(m^2)^i_j\phi^{j\dagger}\phi_i$ and finally the b parameter comes from the $b^{ij}\phi_i\phi_j$ term.

The soft breaking terms introduce many new parameters in the MSSM. In the absence of a satisfactory explanation to them, whose origin should be looked for in the hidden sector, there are theoretical arguments and experimental constraints that reduce the freedom in the soft MSSM Lagrangian, see for example flavour changing neutral currents, CP-violation and lepton flavour violation [42–47]. Other examples to reduce the number of soft breaking parameters come considering particular models of SUSY breaking. For example, consider the minimal super gravity, a $\mathcal{N} = 1$ supersymmetric theory which introduces gravitational interactions that are the mediators of SUSY breaking. In this model a set of constraints relate all the soft masses to only four parameters [28] with a drastic reduction of the number of free parameters. These constraints are normally applied at the grand unification scale that is the scale where the three[1] fundamental interactions, ie the electromagnetic, weak and strong interactions, are unified and can be described by a single gauge group. From the grand unification scale the renormalisation group equations give the set of soft SUSY breaking terms at the electroweak or SUSY breaking scale.

3.7.5 Problems

Apart from the number of parameters, the MSSM presents also other features that are not completely convincing and so constitute a theoretical problem.

The most important of these is the μ problem: there is no explanation for the order of magnitude of the mass μ that appears in the superpotential (3.122). Since μ is a superpotential parameter its origin is not related to SUSY breaking or electroweak symmetry breaking. Nothing suggests that μ should be related to these scales and therefore we can expect μ to be of the order of the Planck scale where it should be generated from a more fundamental theory incorporating quantum gravity. However, to obtain an electroweak scale VEV μ must be of the same order of magnitude as the SUSY breaking scale, M_{SUSY} and to avoid fine tuning, both μ and M_{SUSY} need to be close to the EW scale. This resembles the hierarchy problem that affects the SM, where there is no explanation to why the Higgs boson has such a light mass compared to the Plank mass. While supersymmetry protects the Higgs boson mass from quadratic divergences, supersymmetry cannot protect the μ parameter from being set to the Plank scale. Indeed the only symmetry solution would be to forbids the μ-term setting $\mu = 0$. However, this setting would imply massless

[1] Not counting gravitational interactions.

charged Higgsinos, that are not experimentally observed, unless we can also generate a replacement with the right order of magnitude. This represents one of the major theoretical problems of the MSSM because it brings back the issue of fine-tuning and naturalness of the model that the MSSM was supposed to solve, see [48–50].

Another theoretical problem of the MSSM is that it does not provide a natural framework to explain the origin of the baryon asymmetry of the Universe, one of the most pressing problems of contemporary physics. The question, of which mechanism in the early Universe could have produced the observed amount of matter removing all the antimatter, does not have a satisfactory answer. Indeed, any mechanism that explains such asymmetry has to generate enough C and CP violation and enough departure from thermal equilibrium to explain the observed amount of matter, as will be discussed in sec. 4. Compared to the SM, the MSSM provides more CP violation thanks to the μ term and a departure from thermal equilibrium that is consistent with a Higgs mass of $\sim 125\,\text{GeV}$. However, in the MSSM the CP violation cannot be enough since it is constrained by the electric dipole moment, see [51, 52]. Moreover, the departure from thermal equilibrium implies a scalar stop quark mass $m_{\tilde{t}} \lesssim 120\,\text{GeV}$ [53], that, even though it may not be entirely ruled out by the LHC experiment [54], substantially diminishes the MSSM's appeal as a candidate for explaining the baryon asymmetry of the universe.

3.8 NMSSM

The next-to-minimal supersymmetric standard model (NMSSM) is a SUSY model that extends the MSSM, adding to it a new chiral supermultiplet $\widehat{S}$. This means that the particle content of the NMSSM is given by the particle content of the MSSM, see table 3.1, plus the row representing the singlet supermultiplet in table 3.2. The new supermultiplet $\widehat{S}$ is a singlet under the SU(3)⊗SU(2)⊗U(1) gauge symmetry and even under the matter parity symmetry (3.126). More explicitly, the new supermultiplet is composed by a real scalar field and a real pseudo-scalar field that form a complex scalar field with positive R-parity (3.127) and by its fermionic superpartner with negative R-parity.

The NMSSM is particularly attractive because it solves the μ problem of the MSSM, see the previous sec. 3.7.5. In particular, the μ mass can be generated by the Yukawa term $\lambda\widehat{S}\widehat{H}_u\cdot\widehat{H}_d$ that couples the H_d, H_u and S fields: once the singlet field get a VEV $\langle S\rangle$, the term $\lambda\langle S\rangle\,\widehat{H}_u\cdot\widehat{H}_d \equiv \mu_{\text{eff}}\widehat{H}_u\cdot\widehat{H}_d$ reproduce a μ term. The value of this μ_{eff} terms comes naturally from the soft SUSY breaking terms. Since μ_{eff} is set by the singlet VEV it is naturally

	multiplet	spin 0	spin $\frac{1}{2}$	spin 1	$SU(3)$	$SU(2)$	$U(1)$
Chiral	$\widehat{Q}_i$	$\widetilde{Q} = (\widetilde{u}_{\mathrm{L}}, \widetilde{d}_{\mathrm{L}})_i$	$Q = (u_{\mathrm{L}}, d_{\mathrm{L}})_i$		$\mathbf{3}$	$\mathbf{2}$	$+\frac{1}{6}$
	$\widehat{u}_i$	$\widetilde{u}^*_{\mathrm{R}i}$	$u^\dagger_{\mathrm{R}i}$		$\bar{\mathbf{3}}$	$\mathbf{1}$	$-\frac{2}{3}$
	$\widehat{d}_i$	$\widetilde{d}^*_{\mathrm{R}i}$	$d^\dagger_{\mathrm{R}i}$		$\bar{\mathbf{3}}$	$\mathbf{1}$	$+\frac{1}{3}$
	$\widehat{L}_i$	$\widetilde{L} = (\widetilde{\nu}, \widetilde{e}_{\mathrm{L}})_i$	$L = (\nu, e_{\mathrm{L}})_i$		$\mathbf{1}$	$\mathbf{2}$	$-\frac{1}{2}$
	$\widehat{e}_i$	$\widetilde{e}^*_{\mathrm{R}i}$	$e^\dagger_{\mathrm{R}i}$		$\mathbf{1}$	$\mathbf{1}$	$+1$
	$\widehat{H}_u$	$H_u = (H_u^+, H_u^0)$	$\widetilde{H}_u = (\widetilde{H}_u^+, \widetilde{H}_u^0)$		$\mathbf{1}$	$\mathbf{2}$	$+\frac{1}{2}$
	$\widehat{H}_d$	$H_d = (H_d^0, H_d^-)$	$\widetilde{H}_d = (\widetilde{H}_d^0, \widetilde{H}_d^-)$		$\mathbf{1}$	$\mathbf{2}$	$-\frac{1}{2}$
	$\widehat{S}$	S	$\widetilde{S}$		$\mathbf{1}$	$\mathbf{1}$	0
Vector	$\widehat{G}$		$\widetilde{g}$	g	$\mathbf{8}$	$\mathbf{1}$	0
	$\widehat{W}$		$\widetilde{W}^\pm$, $\widetilde{W}^0$	$W^\pm$, W^0	$\mathbf{1}$	$\mathbf{3}$	0
	$\widehat{B}$		$\widetilde{B}^0$	B^0	$\mathbf{1}$	$\mathbf{1}$	0

Table 3.2: The particle content of the NMSSM. Compared to table 3.2, that represents the particle content of the MSSM, there is an extra chiral supermultiplets $\widehat{S}$ together with its singlet bosonic and singlino fermionic particle content and gauge structure.

of the same order as the EW scale or SUSY breaking scale.

3.8.1 Superpotential

Given the particle content of the NMSSM, the general NMSSM superpotential W_{NMSSM} consist of the W_{MSSM} superpotential (3.122) and other 4 terms that include the singlet:

$$W^{\mathrm{general}}_{\mathrm{NMSSM}} = W_{\mathrm{MSSM}} + \xi \widehat{S} + \frac{1}{2}\mu_S \widehat{S}^2 + \frac{\kappa}{3}\widehat{S}^3 + \lambda \widehat{S}\widehat{H}_u \cdot \widehat{H}_d \tag{3.129}$$

where the SU(2) product is defined in Eq. (3.123) and ξ, μ_S, κ and λ are parameters with mass dimension, respectively, of 2, 1, 0 and 0.

A common and simple scenario is when $\xi = \mu_S = 0$ and the μ parameter in the W_{MSSM} part, Eq. (3.122), also vanishes: $\mu = 0$. This scenario is called $\mathbb{Z}_3$-invariant NMSSM because all terms in the superpotential are invariant under the $\mathbb{Z}_3$ discrete symmetry defined by the transformation

$$\Phi \to \mathrm{e}^{\mathrm{i}\frac{2\pi}{3}}\Phi \tag{3.130}$$

applied to every field in the chiral supermultiplets.

From $W^{\text{general}}_{\text{NMSSM}}$, Eq. (3.129), we can write the $\mathbb{Z}_3$-invariant NMSSM superpotential:

$$W^{\mathbb{Z}_3\text{-invariant}}_{\text{NMSSM}} \equiv W_{\text{NMSSM}} = \widehat{e}\, Y_e \widehat{H}_d \cdot \widehat{L} + \widehat{d} Y_d \widehat{H}_d \cdot \widehat{Q} + \widehat{u}\, Y_u \widehat{Q} \cdot \widehat{H}_u + \frac{\kappa}{3}\widehat{S}^3 + \lambda \widehat{S} \widehat{H}_u \cdot \widehat{H}_d \ . \tag{3.131}$$

In the literature, the NMSSM mainly refers to the $\mathbb{Z}_3$-invariant NMSSM rather than the general NMSSM and from here we follow this convention.

One of the differences between the general NMSSM and the $\mathbb{Z}_3$-invariant NMSSM is that the former has a larger parameter space so that, in particular, the singlet can be lighter in the general NMSSM. These different parameter spaces lead to different scenarios, for example, in the dark matter studies, see [55].

Following Eq. (3.120), we assume that the symmetry breaking is driven by the soft Lagrangian term

$$\begin{aligned} \mathcal{L}^{\text{soft}}_{\text{NMSSM}} = & -m_L^2 |L|^2 - m_e^2 |e|^2 - m_Q^2 |Q|^2 - m_u^2 |u|^2 - m_d^2 |d|^2 \\ & - m_{H_d}^2 |H_d|^2 - m_{H_u}^2 |H_u|^2 - m_S^2 |S|^2 \\ & - \Big(Y_e A_e H_d \cdot L e + Y_d A_d H_d \cdot Q d + Y_u A_u Q \cdot H_u u \\ & + \frac{1}{3}\kappa A_\kappa S^3 + \lambda A_\lambda H_u \cdot H_d S + \text{h.c.} \Big) \end{aligned} \tag{3.132}$$

where, for simplicity, we have suppressed gauge and generation indices.

As we can see, in this case all the operators in the superpotential have a mass dimension of 3, thus all the coefficients are dimensionless. This is particularly interesting because it solves the μ problem present in the MSSM. In fact, since $\mu = 0$, in the superpotential we do not have the $\mu \widehat{H}_u \cdot \widehat{H}_d$ term that caused the μ problem, but an effective μ_{eff} term that emerges when, due to the SB, the singlet acquire a VEV $\langle S \rangle$:

$$\lambda \widehat{H}_u \cdot \widehat{H}_d \widehat{S} \xrightarrow{\text{SB}} \mu_{\text{eff}} \widehat{H}_u \cdot \widehat{H}_d \qquad \text{with} \qquad \mu_{\text{eff}} = \lambda \langle S \rangle \ . \tag{3.133}$$

As a result, the value of μ_{eff} depends on the symmetry breaking mechanism.

3.8.2 Higgs sector

The Higgs potential $V^{\text{H}}_{\text{NMSSM}}$ in the $\mathbb{Z}_3$ symmetric NMSSM can be built from two parts: the first, $V_{\mathcal{F}} + V_{\mathcal{D}}$ contains the $\mathcal{F}$- and $\mathcal{D}$-terms introduced in sec. 3.6.1 and 3.6.2; the second part, called V_{soft}, contains soft terms that originate in Eq. (3.132). Thus, we can write:

$$V^{\text{H}}_{\text{NMSSM}} = V_{\mathcal{F}} + V_{\mathcal{D}} + V_{\text{soft}} \ . \tag{3.134}$$

The part of the scalar potential that comes from the chiral supermultiplet terms, following what we have found in a general SUSY model, sec. 3.3, 3.4 and 3.5 is given by Eq. (3.104) in which the $\mathcal{F}$- and $\mathcal{D}$-terms appear. Applying Eq. (3.104) to the NMSSM case, the fields ϕ to take into considerations are H_u, H_d and S:

$$\begin{aligned} V_{\mathcal{F}} + V_{\mathcal{D}} &= \sum_{\phi_i,\phi_j=\{H_u,H_d,S\}} \left\{ \left| \frac{\partial W}{\partial \phi_i} \right|^2 + \frac{1}{2} g_a^2 \left[\phi_i^{b\dagger} (T^a)^{bc} \phi_i^c\right] \left[\phi_j^{b\dagger} (T^a)^{bc} \phi_j^c\right] \right\} \\ &= |\lambda|^2 |S|^2 \left(H_u^\dagger H_u + H_d^\dagger H_d \right) + \left| \lambda (H_u \cdot H_d) + \kappa S^2 \right|^2 \\ &\quad + \frac{1}{2} g_2^2 |H_u^\dagger H_d|^2 + \frac{g_1^2 + g_2^2}{8} \left(H_u^\dagger H_u - H_d^\dagger H_d \right)^2 \end{aligned} \tag{3.135}$$

where the second to last line is given by the sum over $\left|\frac{\partial W}{\partial \phi_i}\right|^2$ and the terms within it are called $\mathcal{F}$-terms of the Higgs potential, while the last line is given by the second term in the top line and the terms within it are called $\mathcal{D}$-terms of the Higgs potential.

We see that only the $\mathcal{F}$-terms of the Higgs potential contain the singlet while the $\mathcal{D}$-terms are not affected by the singlet and have the same expressions as in the MSSM. This is because $\widehat{S}$ is a gauge singlet and, as such, does not interact through gauge couplings g_a.

The part of the scalar potential that comes from soft terms can be found looking at Eq. (3.132):

$$V_{\text{soft}} = m_{H_d}^2 |H_d|^2 + m_{H_u}^2 |H_u|^2 + m_S^2 |S|^2 + \left(\frac{\kappa}{3} A_\kappa S^3 + \lambda A_\lambda H_u \cdot H_d S + \text{h.c.} \right). \tag{3.136}$$

Finally, summing Eq. (3.135) and (3.136) we obtain the scalar Higgs potential:

$$\begin{aligned} V_{\text{NMSSM}}^{\text{H}} &= |\lambda|^2 |S|^2 \left(H_u^\dagger H_u + H_d^\dagger H_d \right) + \left| \lambda (H_u \cdot H_d) + \kappa S^2 \right|^2 \\ &\quad + \frac{1}{2} g_2^2 |H_u^\dagger H_d|^2 + \frac{g_1^2 + g_2^2}{8} \left(H_u^\dagger H_u - H_d^\dagger H_d \right)^2 \\ &\quad + m_{H_d}^2 |H_d|^2 + m_{H_u}^2 |H_u|^2 + m_S^2 |S|^2 \\ &\quad + \left(\frac{\kappa}{3} A_\kappa S^3 + \lambda A_\lambda H_u \cdot H_d S + \text{h.c.} \right). \end{aligned} \tag{3.137}$$

Following sec. 2.3, in the spontaneous symmetry breaking mechanism the

Higgs and the singlet develop VEVs

$$H_d = \begin{pmatrix} \frac{1}{\sqrt{2}}(v_d + H^0_{d\,\mathrm{Re}} + \mathrm{i}H^0_{d\,\mathrm{Im}}) \\ H^-_{d\ \mathrm{Re}} + \mathrm{i}H^-_{d\ \mathrm{Im}} \end{pmatrix} \qquad H_u = \begin{pmatrix} H^+_{u\ \mathrm{Re}} + \mathrm{i}H^+_{u\ \mathrm{Im}} \\ \frac{1}{\sqrt{2}}(v_u + H^0_{u\,\mathrm{Re}} + \mathrm{i}H^0_{u\,\mathrm{Im}}) \end{pmatrix}$$
$$S = \frac{1}{\sqrt{2}}(v_S + S_{\mathrm{Re}} + \mathrm{i}S_{\mathrm{Im}}) \tag{3.138}$$

where the VEVs, as in the sec. 2.3, can be set to be real and non-negative.

From the v_u and v_d VEVs, we can define the parameter $\tan\beta$:

$$\tan\beta = \frac{v_u}{v_d} \tag{3.139}$$

which is the same as in the MSSM.

We can find the relations between the three level masses $m^2_{H_d}$, $m^2_{H_u}$, m^2_S and the VEVs v_u, v_d, v_S plugging the expansions (3.138) of the fields around the VEVs into Eq. (3.137) and imposing that the resulting potential has an extremum at the vacuum:

$$\begin{gathered} \frac{\partial V^{\mathrm{H}}_{\mathrm{NMSSM}}}{\partial H^0_{d\,\mathrm{Re}}} = \frac{\partial V^{\mathrm{H}}_{\mathrm{NMSSM}}}{\partial H^0_{d\,\mathrm{Im}}} = \frac{\partial V^{\mathrm{H}}_{\mathrm{NMSSM}}}{\partial H^0_{u\,\mathrm{Re}}} = \frac{\partial V^{\mathrm{H}}_{\mathrm{NMSSM}}}{\partial H^0_{u\,\mathrm{Im}}} = 0 \\ \frac{\partial V^{\mathrm{H}}_{\mathrm{NMSSM}}}{\partial S_{\mathrm{Re}}} = \frac{\partial V^{\mathrm{H}}_{\mathrm{NMSSM}}}{\partial S_{\mathrm{Im}}} = 0 \end{gathered} \tag{3.140}$$

see [56]. These relations are called tadpole equations.

Finally, since the singlet mixes with the Higgs, the Higgs sector is modified respect to the MSSM: again from Eq. (3.137) expanding the Higgs and singlet around their VEVs, we can find the CP-even, -odd and charged Higgs mass matrices. In particular, from terms with field mass dimension of 2 we have

- 3 CP-even Higgs bosons containing a mixture of $H^0_{d\,\mathrm{Re}}$, $H^0_{u\,\mathrm{Re}}$ and S_{Re} fields;
- 3 CP-odd Higgs bosons containing a mixture of $H^0_{d\,\mathrm{Im}}$, $H^0_{u\,\mathrm{Im}}$ and S_{Im} fields;
- 2 charged Higgs bosons containing a mixture of H^-_d, $H^{-\dagger}_d$, H^+_u and $H^{+\dagger}_u$ fields.

Chapter 4

Matter-Antimatter asymmetry problem

Astrophysical observations reveal negligible presence of antimatter in the observable Universe. If antimatter abundance was comparable to matter abundance, that would imply particle-antiparticle annihilations that would be observed and identified as the consequence of the existence of antimatter in our observable Universe [57].

At the same time, no experimentally verified mechanism explains the observed predominance of matter over antimatter.

In astronomy matter that constitutes astronomical objects such as, for example, clouds of cold gas, black holes, stars, planets, comets and asteroids, is called baryonic matter because the main contribution to the mass comes from baryons. To have a quantitative definition of the predominance of baryonic matter over antibaryonic antimatter, we consider the baryon-antibaryon difference $n_B - n_{\bar{B}}$ where n_B is the baryonic number density in the Universe and $n_{\bar{B}}$ is the antibaryon number density in the Universe. We can quantify the baryon-antibaryon asymmetry of the Universe (BAU) with the ratio

$$\eta = \frac{n_B - n_{\bar{B}}}{n_\gamma} \tag{4.1}$$

where n_γ is the number density of cosmic background radiation photons.

From the experimental point of view, the parameter η can be measured from independent astrophysical observations. On the theoretical side, however, η can vary during the early Universe: indeed, as the Universe cools down, heavy particles annihilate and produce more photons while the number of baryons and antibaryons is not modified by these annihilation processes. For this reason, we introduce the baryon-antibaryon asymmetry parameter Y_B

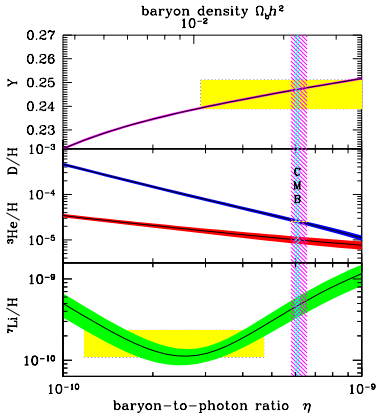

Figure 4.1: The coloured full bands represent, from top to bottom, the calculated primordial abundances of ^{4}H, ^{2}H, ^{3}H, and ^{7}Li relative to primordial abundance of H as function of η. The yellow boxes represent the observed primordial abundance of ^{4}H, ^{2}H and ^{7}Li. The ^{2}H observations are particularly precise. The wider violet vertical dashed band represents the range of η in which there is concordance between ^{2}H and ^{4}H data. The narrow light blue vertical dashed band represents the value of η deduced from CMB observations. The band widths represent the 95 % CL range. The plot shows a very good agreement between the η value from ^{2}H calculation, ^{2}H observations and CMB observations. [Figure taken from [59]].

that is defined as

$$Y_B = \frac{n_B - n_{\bar{B}}}{s} \tag{4.2}$$

where s is the entropy density of the Universe and remains approximately constant during the early Universe evolution. At the present time the baryon-antibaryon asymmetry Y_B can be related to η via the relation

$$s \simeq 7.04 n_\gamma \implies Y_B \simeq \frac{1}{7.04}\eta \tag{4.3}$$

see [58].

One way to measure η is from the standard big bang nucleosynthesis model (SBBN): during this process, η represents a key parameter of the model and determines the abundance of primordial elements such as ^{2}H, ^{3}H, ^{4}H and ^{7}Li. Different missions have measured these abundances, see [59], and η and thus Y_B can be inferred from the produced astrophysical data. The most precise value of η is given by the primordial abundance of ^{2}H and agrees with the η calculated from ^{3}H observations, see figure 4.1 and [60]. From this value of η and Eq. (4.3), the present value of Y_B can be inferred:

$$Y_B^{\text{exp}} = (8.2 - 9.4) \times 10^{-11} \ (95\% \text{ CL}) \ . \tag{4.4}$$

It is worth noting that the values of η from ^{7}Li observations shows a disagreement with the previous values of $2.4\,\sigma - 5.3\,\sigma$, according to which data is used, see [61]. This mismatch visible in Fig. 4.1, represents the so-called lithium problem and and may require physics beyond the SBBN.

Another independent way to calculate η is from the temperature anisotropy of the cosmic microwave background (CMB) [62]: using the analysis of the power spectrum of the CBD, the relative sizes of the Doppler peaks can be related to η. That is, the precise measurement of the CMB anisotropy provides another way, not directly related to the previous primordial abundance method, to determine the value of η and thus the value of Y_B:

$$Y_B^{\text{exp}} = 8.65 \pm 0.09 \times 10^{-11} \,. \tag{4.5}$$

The baryon-antibaryon asymmetry parameter Y_B obtained from the primordial abundance of ^{2}H, Eq. (4.4), and Y_B obtained from the CMB, Eq. (4.5), agree. The agreement between these two separate measurements represent a triumph of astrophysical observations and establish a reliable confirmation of the BAU.

4.1 Sakharov conditions

Even if there was a maximally allowed asymmetry before, inflation would have diluted it to a negligible amount [63]. This implies the necessity of a mechanism that, during the initial stages of the Universe, could have produced the observed BAU.

In general, such a mechanism has to satisfy three assumptions, known as Sakharov conditions for baryogenesis [64]:

1. violation of baryon number conservation (B violation);
2. violation of charge conjugation symmetry (C violation) and violation of the composition of charge and parity conjugation symmetries (CP violation);
3. departure from thermal equilibrium.

The first condition is obvious because after inflation the baryon asymmetry was many orders of magnitude smaller than today, consequently a baryogenesis mechanism cannot conserve $n_B - n_{\bar{B}}$.

To understand the need for the second condition consider a generic process and its C conjugate

$$X_{B=0} \to Y_{B=0} + B \tag{4.6}$$
$$\bar{X}_{B=0} \to \bar{Y}_{B=0} + \bar{B} \tag{4.7}$$

where $X_{B=0}$ and its C-conjugate $\bar{X}_{B=0}$ represent some initial state with vanishing baryon number, $Y_{B=0}$ and its C-conjugate $\bar{Y}_{B=0}$ are final states also with $B = 0$, and B and $\bar{B}$ represent the excess of baryons produced. If the charge conjugation is a symmetry, then both processes have the same rate Γ:

$$\Gamma_1(X \to Y + B) = \Gamma_2(\bar{X} \to \bar{Y} + \bar{B}) \ . \tag{4.8}$$

Now the difference $\Gamma_1 - \Gamma_2$ of these rates is proportional to the net rate of baryon production and is zero. Thus, to have a baryon production, the baryogenesis process must violate the C symmetry.

A similar argument also holds for the required CP violation [65]: a CP symmetry implies that for any process that produces an excess of baryons exists a complementary process which produces the same excess of antibaryons. Thus no net baryon-antibaryon asymmetry can be created.

Regarding the third condition, if a generic process such as the (4.6) is in thermal equilibrium, then, by definition, the rate for this process is equal to the rate for the inverse process $Y + B \to X$:

$$\Gamma(X \to Y + B) = \Gamma(Y + B \to X) \tag{4.9}$$

so, again, no net excess of baryons over antibaryons can be created. Thus, to explain the observed baryon-antibaryon asymmetry, we need a departure from thermal equilibrium.

The SM can, potentially, satisfy all the three Sakharov conditions. Gerard 't Hooft showed that the B violation is possible at very high temperature [66]. As said in sec. 2.5, however, the CP violation given by the CKM matrix, see sec. 2.3.3, is too small to account quantitatively for the observed baryon-antibaryon asymmetry (4.4) and (4.5), with the observed mass of the Higgs boson [39]. Alternatively, the departure from thermal equilibrium that would be enough to generate the observed baryon asymmetry requires the Higgs to have a mass $m_H \lesssim 75\,\text{GeV}$ [35], that is ruled out by experiment. Thus, to explain the BAU, we need physics BSM.

SUSY provides a good framework to resolve quantitatively the problem of the baryon over antibaryon excess. The first attempt in this direction employs the MSSM, see sec. 3.7. As in the SM, the B violation becomes possible at high temperature. Compared to the SM, in the MSSM there are many possible sources of CP violation such as, for example, the μ parameter. As noted in sec. 3.7.5, however, this CP violation is constrained by the electron electric dipole moment [51, 52]. Also, enough departure from thermal equilibrium implies a light stop, $m_{\tilde{t}} \lesssim 120\,\text{GeV}$, [53]. The NMSSM, see sec.3.8, supplies an ideal framework to study baryogenesis, see the published article in chapter 6 and references within it.

4.2 Electroweak baryogenesis outline

A mechanism that can produce a baryon-antibaryon asymmetry at the early stages of the Universe is called baryogenesis. Electroweak baryogenesis (EWBG) refers to such a mechanism that happens during the electroweak phase transition (EWPT).

EWBG can produce the BAU we observe today explaining the measured $Y_B^{\rm exp}$ values in Eq. (4.4) and (4.5). Schematically, EWBG consists of the following steps:

1. According to the big bang theory, the early Universe was filled with a cosmological plasma characterised by a very high energy density. High energies correspond to high temperatures and early times, while low energy corresponds to low temperatures and late times. At high temperature the Higgs potential shows a parabolic like potential, see fig. 2.1a, so that the $\mathrm{SU(2)_L}\otimes\mathrm{U(1)_Y}$ gauge symmetry is unbroken.

2. As the Universe cools down the shape of the Higgs potential changes, see fig. 4.2, and tends to the Mexican hat potential realised at zero temperature, see also fig. 2.1b and 2.1c. When the shape of the Higgs potential changes, the $\mathrm{SU(2)_L}\otimes\mathrm{U(1)_Y}$ symmetry breaks to the $\mathrm{U(1)_{em}}$, see sec. 2.2 and 2.3.

3. The plasma experience a phase transition from the so-called symmetric phase to the so-called broken phase. If the transition is a first-order phase transition, then it involves bubbles of broken phase expanding in the symmetric phase. In this way, each bubble divides space into 3 regions:

   (a) outside the bubble, where the system is still in the symmetric phase;

   (b) inside the bubble, where the system is in the broken phase;

   (c) the border between the symmetric and the broken phase, called bubble wall.

4. The bubbles expand, and as they expand:

   (a) bubble wall spread over the plasma interacting with it;

   (b) during the wall-plasma interaction, the moving wall hits and so scatters particles and antiparticles that constitute the plasma;

(c) because of CP-violating processes in the wall-plasma interaction, the reflection and refraction rates depend on the chirality of the particles;

(d) because of the different reflection and refraction rates, there is a CP asymmetry between the regions in front and behind the wall.

5. Due to the different vacuum expectation value (VEV) of the symmetric and broken phase, different processes happens outside and inside the bubble.

   (a) Outside the bubble, in the region described in step 3a, the vacuum structure of $\mathrm{SU(2)_L}$ consist of different vacua [67], see fig. 4.4. The high temperature allows thermal tunnelling to different $\mathrm{SU(2)_L}$ vacua of the symmetric phase. The transitions to different $\mathrm{SU(2)_L}$ vacua are non-perturbative processes that involve sphalerons that are unstable, static and finite-energy solutions of the classical field equations [68]. Importantly, sphaleron transitions violate B and L symmetry, transforming the CP asymmetry, created in step 4d, in front of the bubble to B asymmetry;

   (b) Inside the bubble, in the region described in step 3b, the non zero VEV of the broken phase suppresses the sphaleron processes preventing a violation of the B and L symmetry.

6. Bubbles keep on expanding, increasing the baryon excess continually according to the previous step 5a. During their expansion, the bubbles incorporate the baryon excess created in front of the bubble wall. Once the baryon excess is inside the bubble, it is frozen according to the step 5b. In this way, the bubbles accumulate baryon asymmetry inside themselves.

7. Eventually the bubbles extend over all the Universe so that all the Universe is in the broken phase with the baryon excess accumulated inside the bubbles.

The physics underlying the steps 1 and 2 is described in chapter 2. In the next sections, we analyse further the other steps.

4.3 Phase transitions

In this section we describe the physics underlying the step 3 in sec. 4.2.

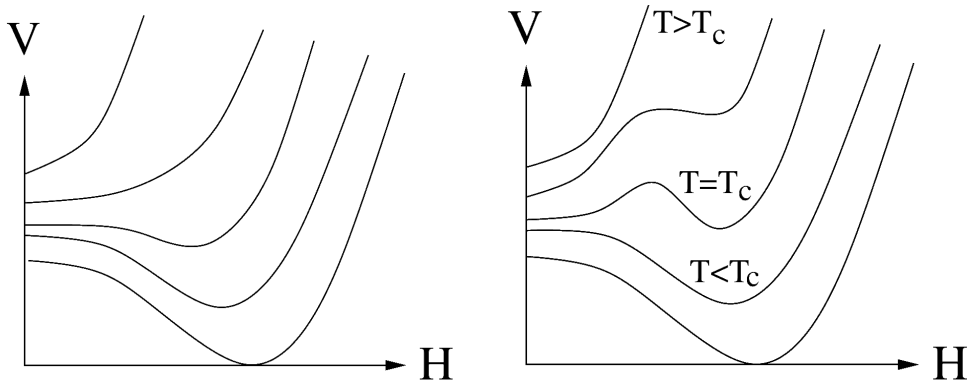

(a) *Second order phase transition* **(b)** *First order phase transition*

Figure 4.2: At high energy (high T and early times) the Higgs potential is parabolic-like. At low energy (low T and late times) the potential is Mexican-hat-like. Between the high and low energy, there are the intermediate states. The plot in (a) shows a second order phase transition where, during the intermediate states, from high to low energies, the minimum of the potential moves smoothly from the origin to the EW minimum. Alternatively, the plot in (b) shows a first order phase transition where, during the intermediate states, the potential develops a barrier and the minimum can transit from the origin to the EW minimum via tunnelling. In case (b), the temperature T_C where the minima are degenerate is called critical temperature. [Figure taken from [65]].

At high temperatures, the system is in an unbroken phase, and the minimum of the Higgs potential is at the origin. At low temperatures, the symmetry is broken, and the minimum of the Higgs potential is away from the origin. There are two different phase transitions that can take the system from the unbroken to the broken phase. These two different ways are shown in, and briefly described in the caption of fig. 4.2.

4.3.1 Second order phase transitions

In the case in which the Higgs potential do not develop a potential barrier, fig. 4.2a, while the temperature decreases the minimum of the Higgs potential can smoothly move from the origin and, at zero temperature, it ends to the observed EW vacuum that represents the vacuum expectation value of the Higgs field. This means that the transition of the system from the unbroken to the broken phase happens smoothly, following the minimum of the potential. There is no latent energy involved, and so the system does not release energy unless the temperature changes. This is a second-order phase transition also called continuous phase transition.

4.3.2 First order phase transitions

The second case, fig. 4.2b, starts as the previous case when at high temperatures the minimum is at the origin. However, when the temperature decreased, the Higgs potential develops a potential barrier, that traps the minimum at the origin. When the Universe reaches a critical temperature T_C, the Higgs potential shows two degenerate minima: one at the origin and one away from the origin.

After T_C, while the Universe keeps on cooling down, the global minimum is the one away from the origin, and the origin represents a point false vacuum. Still, the system is in the false vacuum state because the potential barrier prevents the system from moving to the true vacuum state. At this stage, the Universe is in a supercooled state. At a later time, progressively the energy difference between the false and the true vacuum becomes larger and larger, while the potential barrier drops. Eventually, thanks to the thermal energy, the system experiences a transition between the two states via thermal fluctuations over the barrier or via quantum tunnelling under it. In general, such a transition happens to a point in space that represents a nucleation seed.

Once a thermal seed is created, there is a competition between physical mechanisms that contribute to the expansion of the bubble and contrasting physical mechanisms that contribute to the collapse and disappearance of the

bubble. On the one hand, points surrounding the nucleation seed experience the same transition, passing from the false to the true vacuum. This happens because the transition from the false to the true vacuum decreases the free energy of the system and the free energy is proportional to the bubble volume. In a chain reaction, next surrounding points pass to the true vacuum as well pushing the bubble wall to expand, see [69–71]. On the other hand, for bubbles of small size, that is at the beginning of the bubble expansion, the bubble wall has a strong surface tension proportional to the bubble area that tends to shrink the bubble and eventually can make it disappear [72]. On top of that, these two competing mechanisms happen in the background of an expanding Universe. This means that the bubbles formation rate has to be compared with the Hubble rate [73]. The temperature at which the formation and growth of the bubbles is such that the fraction of the Universe in the symmetric phase is $\frac{1}{\mathrm{e}}$ is called nucleation temperature and indicated as T_N. In the literature, since the mechanisms that take part in the calculation of T_N are quite complex, the nucleation temperature T_N is often approximated with the critical temperature T_C.

This transition from the false to the true vacuum represents a first-order phase transition (FOPT). Such as, the system undergoes a violent transition in which latent energy is released. The system contains two different phases that are separated by the bubble wall: one phase outside the bubble in which the VEV of the Higgs field is still 0, and one phase inside the bubble with completed phase transition so that the VEV is different from 0. The bubble wall separates the internal symmetry-broken-phase regime from the external symmetry-unbroken-phase regime, see fig. 4.3.

The key characteristic of such a FOPT is the presence of a scalar field, not necessarily the Higgs field, that:

- is temperature-dependent;
- has a potential that is symmetric for high energy T_{high} and asymmetric for low energy T_{low};
- undergoes a symmetry breaking mechanism;
- has a potential that develops a feature from T_{high} to T_{low} that, for some time, freeze the system in a particular state, allowing a supercooled state.

4.4 Arising of CP asymmetry

In this section we expand the description of step 4 in sec. 4.2.

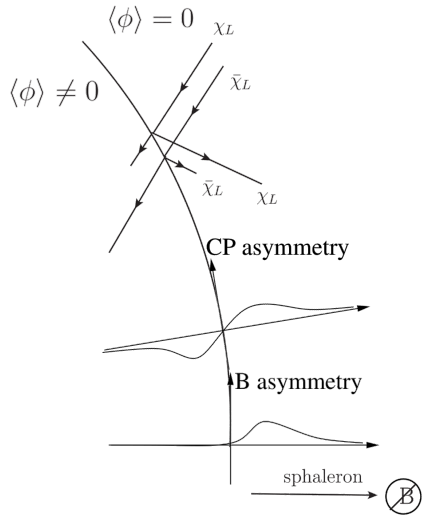

Figure 4.3: Matter predominance is created.

Once a bubble is nucleated, the bubble wall moves across the space that is filled with a plasma of hot particles. Since the particles interact with the Higgs field, they can detect the passage of the bubble wall and interact with it. The bubble wall has a velocity relative the plasma, so during the wall-particles interaction some particles are reflected in the direction of the wall velocity. This reflection is possible thanks to the latent heat that, during the interaction, is converted in kinetic energy of the scattered particle. Now, these interactions can, in general, violate the CP symmetry. Thus the quantum reflection depends on the chirality of the particle. A different reflection rate brings a CP asymmetry in the spaces in front and behind the wall, as schematically depicted in fig. 4.3. In particular, for the EWBG to produce the observed excess of matter over antimatter, this CP asymmetry inside and outside the bubble consist of

1. an excess of antiquarks over quarks in front of the wall, that is outside the bubble;

2. an opposite excess of quarks over antiquarks behind the wall, that is outside the bubble.

In other words, the CP violating interactions imply a wall-antiquark reflection rate bigger than the wall-quark reflection rate. Overall, however, different reflection rates cannot create B asymmetry: the excess of antiquarks outside the bubble $Y_B^{\text{out}} \propto n_B - n_{\bar{B}}$ is balanced by the opposite excess of quarks inside the bubble $Y_B^{\text{in}} = -Y_B^{\text{out}}$ without a net baryon number increase

$$Y_B^{\text{tot}} = Y_B^{\text{in}} + Y_B^{\text{out}} = 0 \, . \tag{4.10}$$

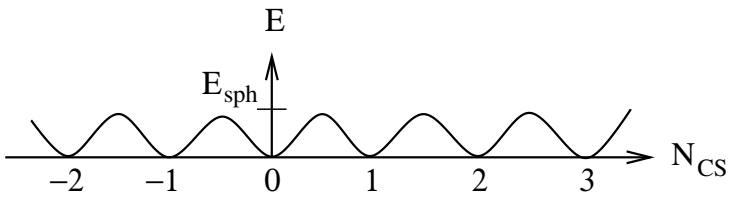

Figure 4.4: Vacuum structure of $SU(2)_L$. [Figure taken from [65]].

4.5 Sphaleron transitions

In this section we expand the description of step 5 in sec. 4.2.

The main idea is that the CP asymmetry, created according to the previous section, can be converted in B asymmetry thanks to the sphaleron processes that are active only outside the bubble. The vacua inside and outside the bubble are different. This difference leads to different physical phenomena inside and outside the bubble.

4.5.1 Outside the bubble

Outside the bubble, the symmetry is not broken. This case leads to the sphaleron transitions. Moreover, sphaleron transitions in a system with CP asymmetry lead to B violation.

Sphalerons

The vacuum structure of the non-Abelian SU(2) gauge group present many degenerate vacua [74, 75]. Each vacuum is separated by other vacua via an energy barrier, see fig. 4.4.

In general, the system is one specific vacuum but it tunnels to another vacuum. At low temperatures the transition rate is strongly suppressed [66]. However, at high temperatures, $T \gtrsim 100\,\text{GeV}$, the thermal energy increases significantly the energy of the system that becomes comparable to the energy barrier, see [76]. In this way, the tunnelling rate becomes significant and the system can move frequently from one minima to another. An estimation of the tunnelling rate per unit of volume is [77]

$$\frac{\Gamma_{\text{out}}}{V} \simeq cT^4 \tag{4.11}$$

where c is a constant that depends on the weak coupling α_w and has been calculated using lattice techniques [78, 79]:

$$c = (25.4 \pm 2.0)\alpha_w^5 \simeq (1.06 \pm 0.08) \times 10^{-6} \tag{4.12}$$

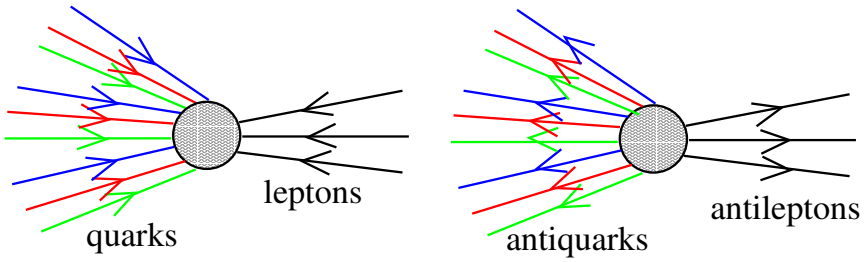

(a) *Sphaleron transition that converts quarks to leptons.*

(b) *Sphaleron transition that converts antiquarks to antileptons.*

Figure 4.5: Two examples of sphaleron transitions that change the B and L number. On the left there is the initial state and on the right the final state. In the middle, the sphaleron transition is represented as a blob. [Figure taken from [65]].

The passage from one minimum to another is a non-perturbative process called sphaleron transition. In this way, the tunnelling rate (4.11) represents the rate of sphaleron transitions. Importantly, as shown in [66], a sphaleron transition violates both baryon and lepton number by three units, where three is the number of generations, keeping the difference $B - L$ constant, see fig. 4.5.

B violation

Sphaleron transitions alone, however, are still not enough to explain today's observed excess of baryon over antibaryon. Indeed, sphaleron transitions can both decrease the baryon number, fig. 4.5a or increase the baryon number, fig. 4.5b.

At chemical equilibrium, the rate of sphaleron transitions that increase B is balanced by the rate of sphaleron transitions that decrease B. Since the system tends towards the chemical equilibrium, in the case of an excess of baryon over antibaryon, $n_B > n_{\bar{B}}$, the sphaleron processes tend to restore the baryon-antibaryon symmetry. The restoration happens because $n_B > n_{\bar{B}}$ and the probability of the transition that transform baryons in leptons $\Pr(B \to L)$ is equal to the probability of the transitions that transform antibaryons in antileptons: $\Pr(\bar{B} \to \bar{L}) = \Pr(B \to L)$. So there are more transitions $B \to L$ than transition $\bar{B} \to \bar{L}$ because there are more B than $\bar{B}$:

$$\Gamma_{\text{sph}}(B \to L) > \Gamma_{\text{sph}}(\bar{B} \to \bar{L}) \, . \tag{4.13}$$

This process of restoring the equilibrium is called relaxation.

The relaxation is also the reason why the baryon asymmetry, if taken as an initial condition of the Universe, cannot explain the observed BAU. In fact, in the early Universe, sphaleron transitions would relax any potential baryon asymmetry.

Outside the bubble, however, there is a CP asymmetry that plays an important role. From the previous sec 4.4, as seen in point 1 of the description of particle excesses, outside the bubble, there is an excess of antiquarks compared to quarks. Since there are more antiquarks than quarks, the rate of sphaleron processes that converts antiquarks to antileptons is bigger than the rate of sphaleron processes that converts quarks to leptons. In other words, the transitions depicted in fig. 4.5b happen more frequently than the transitions depicted in fig. 4.5a. The second transition increase the baryon number by three units destroying 3 antibaryons, $3\bar{B} \to 3\bar{L}$, and it is not balanced by the first transition that decreases the baryon number by three units destroying 3 baryons, $3B \to 3L$. Thus a net excess of baryons over antibaryon is created in front of the bubble wall.

Because the bubble wall moves, this continuously created excess of baryons is incorporated inside the bubble.

4.5.2 Inside the bubble

If the sphaleron mechanism were active inside the bubble, a precisely opposite excess of antimatter would be created inside the bubble, with no net baryon production. However, inside the bubble, the vacuum structure is different from the one outside the bubble: the vacuum structure does not have the many degenerate vacua seen in fig. 4.4, and the potential develops a VEV separated from the minimum at the origin by an energy potential, as in fig. 4.2b.

Because of this different vacuum structures, the sphaleron tunnelling rate given in Eq. (4.11) is no longer valid. Taking into account the broken symmetry inside the bubble, the sphaleron tunnelling rate is [65, 80, 81]

$$\frac{\Gamma_{\text{in}}}{V} \simeq c' \left[\frac{m_W(T)}{T}\right]^4 \left[\frac{E_{\text{sph}}(T)}{T}\right]^3 T^4 \mathrm{e}^{-\frac{E_{\text{sph}}(T)}{T}} \tag{4.14}$$

where m_W is the W boson mass at temperature T, E_{sph} is the height of the energy barrier and c' is a constant of order unity. Note that this rate is null in case the symmetry is unbroken and so $m_W = 0$, that is outside the bubble.

The energy barrier E_{sph} can be calculated as a function of the VEV $\mathfrak{h}(T)$ at temperature T [68]:

$$E_{\text{sph}} \simeq \sqrt{\frac{4\pi}{a_w}} f\left(\frac{\lambda}{a_w}\right) \mathfrak{h}(T) \tag{4.15}$$

where a_w is the weak coupling and $f(\frac{\lambda}{a_w})$ is a function of order unit that depend on the Higgs quartic coupling λ. Using

$$a_w = \frac{g_2^2}{4\pi} \simeq \frac{1}{30} \qquad f \simeq 2 \tag{4.16}$$

because f ranges as $1.5 \lesssim f \lesssim 2.7$ [68], from the previous Eq. (4.14) and (4.15) we can estimate the sphaleron tunnelling (4.14). We can see that the exponential

$$\sim \exp\left[-40\frac{\mathfrak{h}(T)}{T} \right] \tag{4.17}$$

strongly suppresses the transition rate inside the bubble.

Some antimatter inside the bubble is created according to the same sphaleron mechanism that is active outside the bubble and described in the previous sec. 4.5.1. That is, the sphaleron transitions tend to relax the CP asymmetry (that inside the bubble is opposite to the CP asymmetry outside the bubble). During this relaxation, sphaleron transitions create some antimatter (while an excess of matter is created outside the bubble). However, inside the bubble, the sphaleron tunnelling rate and so creation of antimatter is strongly suppressed according to Eq. (4.17).

4.6 Freezing out the B asymmetry

In this section we recap and finish the EWBG description in sec. 4.2 describing steps 7 and 6.

Since the bubble wall is moving, according to sec. 4.4, a CP asymmetry is continuously created inside and outside the bubble. As seen in the previous sec. 4.5.1 and 4.5.2, the CP asymmetry is converted in B asymmetry. Importantly, the conversion rate is very different. Indeed, considering Eq. (4.11), (4.14) and (4.15), we can calculate the ratio $\frac{\Gamma_{\text{out}}}{\Gamma_{\text{in}}}$:

$$\frac{\Gamma_{\text{out}}}{\Gamma_{\text{in}}} \propto \frac{T^7}{m_W^4 v^3} \exp\left[f\sqrt{4\pi 30}\,\frac{\mathfrak{h}(T)}{T} \right] . \tag{4.18}$$

The ratio in Eq. (4.18) shows that for temperatures in the order of the electroweak scale the excess of matter created outside the bubble is not balanced by the excess of antimatter inside the bubble. This imbalance is due to the different vacuum inside and outside the bubble that leads to the different sphaleron tunnelling rate (4.11) and (4.14) that lead to different amount of matter and antimatter inside and outside the bubble.

As the bubbles expand the excess of matter continuously falls inside the bubbles. Here, since the lack of antimatter production due to Eq. (4.18), only a tiny fraction of the matter is annihilated by antimatter. Moreover, since the sphaleron transitions are frozen out according to Eq. (4.17), the sphaleron cannot relax the excess of matter. That is the B asymmetry cannot decrease inside the bubbles.

This increase of B asymmetry goes on as the bubbles expand and it finishes only when the bubbles extend over all the Universe. At this point, the Universe consists of the inside regions of bubbles. Again, according to Eq. (4.17), in these regions, that is in the whole Universe, the excess of matter accumulated during the bubble expansion is not destroyed.

4.7 Phase transition strength

As we have seen, a FOPT is one of the important ingredients to achieve the EWBG: as shown in fig. 4.2, only a FOPT, and not a second order PT, shows the barrier potential $E_{\rm sph}$ and the VEV $\mathfrak{h}$ at T_C needed in Eq. (4.14) and (4.15). Using the outlined formalism we can quantify the excess of baryons over antibaryons during the EW phase transition, that is we can calculate the asymmetry parameter $Y_B^{\rm th}$. Then we can check $Y_B^{\rm th}$ against the measured one, $Y_B^{\rm exp}$ in Eq. (4.4) and (4.5).

The value of $Y_B^{\rm th}$ depends on the rate of the sphaleron processes. These processes involve sphalerons, respect the Sakharov conditions and can create a net amount of baryons. The rate of the sphaleron processes depends on the sphaleron energy $E_{\rm sph}(T_C)$ at the critical temperature T_C, see Eq. (4.11), (4.14) and (4.15). This is because the rate of sphaleron processes depends on the potential barrier in the scalar potential of a FOPT, see fig. 4.2b: the sphalerons energy is indeed given by the height of the barrier, while the rate of the sphaleron processes depends on the transition between the two minima.

4.7.1 Order parameter

In order to match the observed $Y_B^{\rm exp}$ the sphalerons have to have a minimum sphaleron energy [82]:

$$\frac{E_{\rm sph}(T_C)}{T_C} \gtrsim 45 \ . \tag{4.19}$$

Considering Eq. (4.15) and (4.16), the previous Eq. (4.19) gives a condition on the point of global minimum $\mathfrak{h}$ at the nucleation temperature T_N:

$$\gamma \equiv \frac{\mathfrak{h}}{T_N} \gtrsim 1 \ . \tag{4.20}$$

A FOPT that satisfy the previous condition (4.20) is called a strong first order phase transition (SFOPT) and γ is the order parameter quantifying the strength of the transition. From the definition (4.20) the order parameter γ measures the distance between the point of global minimum, representing the true vacuum, and the point of local minimum, representing the false vacuum.

In the case in which there are two Higgs SU(2) doublet, H_d and H_u, see for example the MSSM, tab. 3.1 and sec. 3.7, the strength of transition is given by the parameter $\gamma_{\rm EW}$:

$$\gamma_{\rm EW} = \frac{\sqrt{\left[\mathfrak{h}_d(T_N) - \mathfrak{h}'_d(T_N)\right]^2 + \left[\mathfrak{h}_u(T_N) - \mathfrak{h}'_u(T_N)\right]^2}}{T_N} \tag{4.21}$$

where $\left(\mathfrak{h}_d(T_N), \mathfrak{h}_u(T_N)\right)$ is the location of the global minimum of the scalar Higgs potential at the nucleation temperature T_N while $\left(\mathfrak{h}'_d(T_N), \mathfrak{h}'_u(T_N)\right)$ is the location of the local minimum at T_N. In models with an additional scalar singlet, see for example the NMSSM, tab. 3.2 and sec. 3.8, or the THDMS see Eq. (33) in the published material in sec. 6.1 at page 109, the relevant quantity for EWBG is again $\gamma_{\rm EW}$ [83] and the singlet VEV does not modify $\gamma_{\rm EW}$ in Eq. (4.21).

In this case $\mathfrak{h}_d(T_N)$ and $\mathfrak{h}_u(T_N)$ are two coordinate of the global minimum of the scalar fields at the nucleation temperature T_N while the local minimum is identified by prime coordinate such as $\mathfrak{h}'_d(T_N)$ and $\mathfrak{h}'_u(T_N)$. Again, a phase transition is considered strong when

$$\gamma_{\rm EW} \gtrsim 1 \tag{4.22}$$

so that the distance between the point of global minimum, representing the true vacuum, and the point of local minimum, representing the false vacuum is big enough to boost the baryon asymmetry and to explain the observed asymmetry parameter $Y_B^{\rm exp}$.

4.7.2 Strength of the transition

As said at the beginning of this section, the asymmetry parameter Y_B depends on the rate of sphaleron processes that depends on the sphaleron energy at the critical temperature $E_{\rm sph}(T_C)$ that, together with the strength parameter γ, is given by the potential barrier in a FOPT scalar potential, see fig. 4.2b. The potential barrier is originated from cubic terms in the scalar potential. At zero temperature, they are not present in models such as the SM or the MSSM, see Eq. (3.104). However, these terms enter in the scalar potential at loop level, see [84, 85], with the so-called Daisy corrections.

For model such as the MSSM, it has been showed that an agreement with the asymmetry parameter Y_B^{exp} implies an absolute upper bound on the stop mass, $m_{\tilde{t}} \lesssim 120\,\text{GeV}$, see [53], that that is hard to satisfy considering the current LHC limits [86]. This is because cubic terms represent a correction at the loop level, so they give, in this case, a too small contribution to the scalar potential. However, the contribution of cubic terms can easily be boosted and made consistent with Y_B^{exp} if the cubic terms appear in the potential at tree level. This is the case of the NMSSM or the THDMS, where cubic terms

$$\widehat{S}^3 \quad \text{and} \quad \widehat{S}\widehat{H}_u \cdot \widehat{H}_d \tag{4.23}$$

at tree-level are originated from the scalar singlet. For the NMSSM see Eq. (3.129) and for the effective field model THDMS see Eq. (10) in the published material in sec. 6.1 at page 109.

4.8 Effective potential

To achieve EWBG, we need a potential that can show a SFOPT, as in fig. 4.2b where $\gamma \gtrsim 1$. Moreover, to describe the conditions of the early Universe where the energy density is very high and decrease with time, we need to consider a temperature-dependent potential, see fig. We can use a perturbative approach in which the potential can be approximated as:

$$V_{\text{eff}} = V_{\text{tree}} + \Delta V_{\text{CW}} + \Delta V_T + V_{\text{daisy}} \tag{4.24}$$

where V_{tree} is the tree level potential, ΔV_{CW} is the one-loop or Coleman-Weinberg correction to the tree level potential, ΔV_T is the one-loop thermal correction and V_{daisy} is the daisy term.

The one-loop correction depend on the used gauge. In the R_ξ gauge, see sec. 2.4.3, the ΔV_{CW} expression is [87]

$$\begin{aligned}\Delta V_{\text{CW}} = \frac{1}{64\pi^2}\Bigg\{ &\sum_h n_h m_h^4(\xi)\left[\ln\left(\frac{m_h^2(\xi)}{Q^2}\right) - \frac{3}{2}\right] + \sum_V n_V m_V^4\left[\ln\left(\frac{m_V^2}{Q^2}\right) - \frac{5}{6}\right] \\ &- \sum_V \frac{1}{3} n_V (\xi m_V^2)^2\left[\ln\left(\frac{\xi m_V^2}{Q^2}\right) - \frac{3}{2}\right] - \sum_f n_f m_f^4\left[\ln\left(\frac{m_f^2}{Q^2}\right) - \frac{3}{2}\right]\Bigg\}\end{aligned} \tag{4.25}$$

where Q is the renormalization scale, m_i are field dependent masses and the n_i are the numbers of degrees of freedom for field i.

The one-loop thermal correction again in the R_ξ gauge is [87]

$$\Delta V_T = \sum_i \frac{T^4}{2\pi^2} n_i J_{\mathrm{B}} \left(\frac{m_i(\xi)^2}{T^2} \right) + \sum_j \frac{T^4}{2\pi^2} n_j J_{\mathrm{F}} \left(\frac{m_j^2}{T^2} \right) \tag{4.26}$$

where the nomenclature is the same as in the ΔV_{CW} and the J_{B} and J_{F} functions are defined as:

$$\mathrm{J_{B/F}} \left(\frac{m^2}{T^2} \right) = \pm \,\mathrm{Re} \int_0^\infty \mathrm{d}x \left[x^2 \ln \left(1 \mp \mathrm{e}^{-\sqrt{x^2 + \frac{m^2}{T^2}}} \right) \right] \tag{4.27}$$

where the upper sign is for bosons and the lower sign is for fermions.

The daisy terms are [84]

$$V_{\mathrm{daisy}} = -\frac{T}{12\pi} \left(\sum_h n_h \left[\left(\bar{m}_h^2 \right)^{\frac{3}{2}} - \left(m_h^2 \right)^{\frac{3}{2}} \right] + \sum_V \tfrac{1}{3} n_V \left[\left(\bar{m}_V^2 \right)^{\frac{3}{2}} - \left(m_V^2 \right)^{\frac{3}{2}} \right] \right), \tag{4.28}$$

where the $\bar{m}^2$ masses are field dependent mass eigenvalues that include Debye corrections to the tree-level masses in the mass matrices. The Debye corrections, that are active before the symmetry breaking, add additional T dependent terms and, following [88, 89], are of the form

$$c_\Phi T^2 |\Phi|^2 \qquad \text{for all complex scalar gauge eigenstates} \tag{4.29}$$

$$c_A T^2 A_\mu A^\mu \qquad \text{for all gauge bosons.} \tag{4.30}$$

In this way, we obtain the full one-loop finite temperature potential, which is a function of the fields and of the temperature T and can be used to study the EWBG, see chapter 6.

The terms V_{tree}, ΔV_{CW}, ΔV_T and V_{daisy} give different contributions to the potential V_{eff}. An example is in fig. 4.6. Here we used the NMSSM potential, as described in the published material in chapter 6. The full potential is a function of the VEV of H_d, H_u and S fields, but here we focus on the singlet VEV and set $v_d = v_u = 0$. The different terms have different contributions at different temperatures. However, we can see that the daisy terms V_{daisy} and the finite temperature corrections ΔV_T have an important contribution. The daisy terms cancel almost exactly the finite temperature corrections. The daisy terms indeed come from a resummation of leading infrared divergent graphs, see fig. 4.7, that correct the finite temperature corrections. As it is clear from lover temperatures, see the bottom right plot in fig. 4.6, the sum of the finite temperature corrections and daisy terms $\Delta V_T + V_{\mathrm{daisy}}$ have an important impact on the total potential. Indeed, the

magnitude of $\Delta V_T + V_{\text{daisy}}$ is comparable to the magnitude of the tree level potential V_{tree}. In contrast, the one loop corrections ΔV_{CW} are negligible compared to $\Delta V_T + V_{\text{daisy}}$.

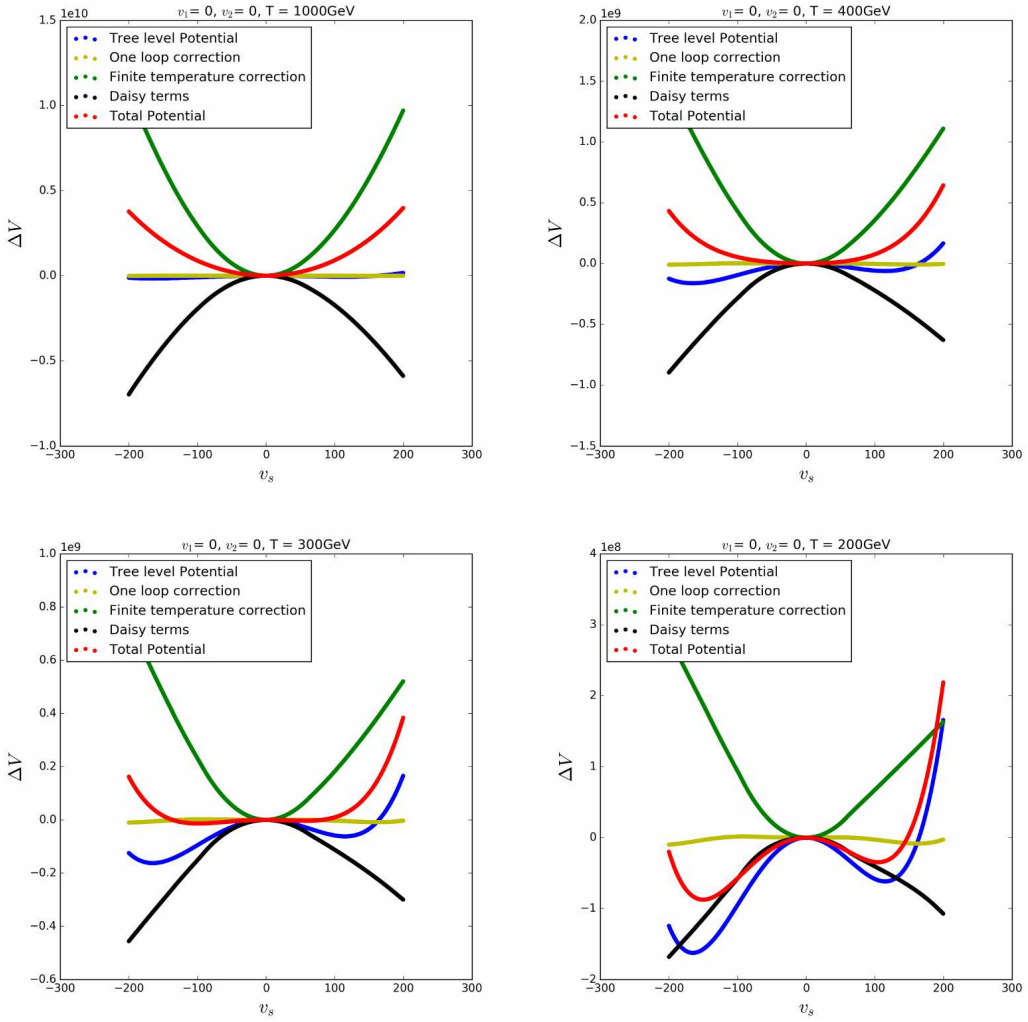

Figure 4.6: Different contributions to V_{eff}. The plots were produced during the work published in chapter 6, where we employ the NMSSM. We show the value of the potentials against the value of the singlet vev fixing the values of the H_d and H_u vevs to zero. The temperature are fixed in this way: the top left plot correspond to $T = 1\,\text{TeV}$, the top right plot correspond to $T = 400\,\text{GeV}$, the bottom left plot correspond to $T = 300\,\text{GeV}$ and the bottom right plot correspond to $T = 200\,\text{GeV}$. Referring to Eq. (4.24), the red line represent V_{eff}, the blue line represent V_{tree}, the yellow line represent ΔV_{CW}, the green line represent ΔV_T and the black line represent V_{daisy}. Thanks Yang Zhang for the images.

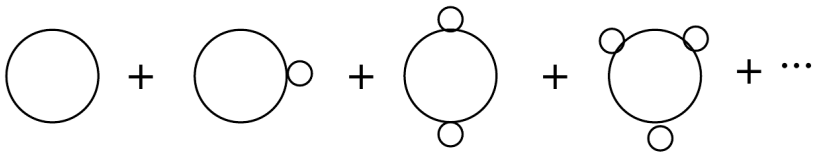

Figure 4.7: Graphs considered in the daisy corrections.

Chapter 5

Dark matter constraint from combined experiments

We collect astrophysical data mainly through the electromagnetic interaction: in other words, we obtain information about the Universe analysing the electromagnetic radiation that arrives to us. From this information, we know that the Universe consists of a variety of different objects, for example, dust, interstellar medium, planets, stars, star clusters, galaxies, galaxy groups, galaxy clusters, superclusters and galaxy filament. In general, each object is made of other objects that constitute it and is part of a collection that constitutes a bigger object. For example, galaxies are made of dust, interstellar medium, planets, stars and are part of galaxy clusters. We can observe the structure of these objects, that is their composition and how their components are organised inside them. For galaxies, in particular, we can observe the position, the velocity and the mass of the objects that are inside them.

Historically one of the first strongest evidence of dark matter came from data on different galaxies. The density and distribution of the detected matter and gas inside each galaxy was measured. Employing this data inside a Newtonian model, we can calculate the rotation curve, that is the velocity that an object at a specific distance from the galactic centre of mass has to have in order to be bound to the galaxy. We can thus observe the position and velocity of stars orbiting inside the galaxy. This data conspicuously disagree with the predicted rotation curve. To generate a rotation curve that agrees with the observed one, we need to assume the existence of a halo of DM, see fig. 5.1.

The presence of dark matter can also be deduced from galaxy clusters [91], colliding clusters of galaxies [92], structure formation [93], velocity dispersions [94], gravitational lensing [91, 95], cosmic microwave background [96], baryon acoustic oscillations [97] and measurement of the cosmological mass

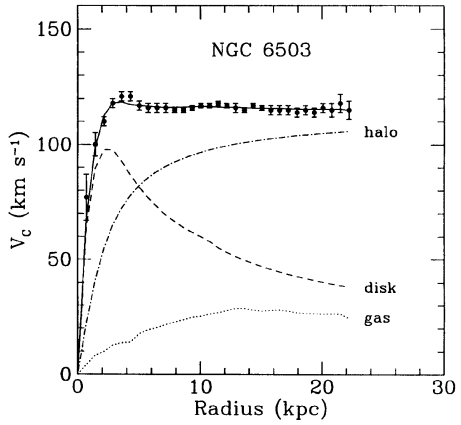

Figure 5.1: Rotation curve of NGC6503 Galaxy. The dashed and dotted curve represent the rotation curve expected, respectively, from the matter and gas observed inside the galaxy. These cannot match the observed data represented by dots with error. Assuming the presencean halo of dark matter given by the dot-dashed curve, the data match the solid total rotational curve. [Figure taken from [90]].

density from clustering [98]. All these observations make the existence of DM a widely accepted fact.

Since the DM cannot be made of SM particles [99], its explanation needs BSM physics. Many hypotheses have been made regarding the composition of DM [100]. However, until now, there is no widely accepted explanation of the DM nature. One of the possible and wide studied options is that the DM is made of sparticles. In sec. 3.7.3 we have seen that in the MSSM, to suppress baryon and lepton number violating terms, generally a discrete $\mathbb{Z}_2$ symmetry is imposed. This symmetry implies that the supersymmetric nature of sparticles is also conserved, that is sparticles cannot decay to SM particles. Thus, the lightest SUSY particle (LSP) must be stable. Assuming that the LSP is also weakly interacting and neutral, it represents a candidate for the DM.

Different sparticles can be considered as the LSP. In the following published work, we have considered the broadly investigated option that the lightest neutralino $\widetilde{\chi}_1^0$ is the LSP.

5.1 Published material

Physics Letters B 789 (2019) 582–591

Contents lists available at ScienceDirect

Physics Letters B

www.elsevier.com/locate/physletb

Constraining resonant dark matter with combined LHC electroweakino searches

Giancarlo Pozzo, Yang Zhang *

ARC Centre of Excellence for Particle Physics at the Tera-scale, School of Physics and Astronomy, Monash University, Melbourne, Victoria 3800, Australia

ARTICLE INFO

Article history:
Received 3 August 2018
Received in revised form 17 November 2018
Accepted 24 December 2018
Available online 2 January 2019
Editor: J. Hisano

ABSTRACT

In the Minimal Supersymmetric Standard Model light neutralinos can satisfy the dark matter (DM) abundance constraint by resonant annihilation via a Z or a light Higgs (h) boson. In this work we study the current and future status of this scenario by investigating relevant experimental constraints, including DM direct detection, measurements of Z and Higgs invisible decays, and direct searches at the Large Hadron Collider (LHC). To take full advantage of the LHC data, we combine the results of all relevant electroweakino searches performed by the Compact Muon Solenoid (CMS) Collaboration. Such combination increases the bound on the Higgsino mass parameter to $|\mu| > 390$ GeV, which is about 80 GeV stricter than the bound obtained from individual analyses. In a simplified model we find that the Z funnel region is on the brink of exclusion, the h funnel for $\mu < 0$ only survives if $\tan\beta < 7.4$, and the h funnel for $\mu > 0$ is the main surviving region. Future DM direct detection experiments, such as LUX and ZEPLIN, can explore the whole region, while the high luminosity LHC can exclude $\tan\beta > 8$ for $\mu > 0$ and $\tan\beta > 5.5$ for $\mu < 0$. After applying the muon anomalous magnetic moment constraint only a tiny part of the Z/h funnel region survives which will soon be probed by ongoing experiments.

1. Introduction

A wide range of astrophysical observations indicates the existence of dark matter (DM) at various length scales via gravitational effects. Motivated by this during the last decades considerable effort was made to detect DM particles at collider experiments (such as LEP [1] and the LHC [2,3]), in direct (by XENON1T [4], LUX [5] or PandaX [6]) and indirect (AMS-II [7], Fermi-LAT [8] or DAMPE [9]) detection experiments. Despite the lack of direct experimental evidence, the lightest neutralino of the R-parity conserving Minimal Supersymmetric Standard Model (MSSM) [10–12] remains an especially attractive DM candidate. This is because, beyond dark matter, the MSSM provides solutions to several problems of the Standard Model (SM): the lightness of the observed Higgs mass, a dynamical mechanism of electroweak symmetry breaking, the unification of particles and forces and beyond.

Supersymmetric (SUSY) global fits, which also include experimental constraints on DM particles, have delineated the most likely model parameter regions [10–31]. In global fits of the phenomenological MSSM, there is always a Z/h funnel region in which neutralino dark matter can achieve the right thermal relic density through Z or Higgs boson resonant annihilation. Consequently, in this region the DM mass is about half of the Z or Higgs boson mass. Comparing to other regions, the Z/h funnel region is an islet in the parameter space where some of the supersymmetric particles (sparticles) are relatively light. These characteristics make the sparticles in the Z/h funnel region the most promising candidates to be detected at the LHC and DM search experiments. More importantly, several modest excesses of data above the expected background were found in the signal regions of recent CMS and ATLAS electroweakino searches, including signal region `SR3ℓ_ISR` (3.02 σ deviation), `SR3ℓ_LOW` (2.13 σ deviation) and `SR2ℓ_ISR` (1.99 σ deviation) in ATLAS recursive jigsaw reconstruction analysis [32], `SR0D` (2.3 σ deviation) in ATLAS $\geq 4\ell + E_T^{miss}$ analysis [33], and the not-tt-like signal region for masses between 96 and 150 GeV (2.0σ deviation) in CMS $2\ell + E_T^{miss}$ analysis [34]. The global fit of the electroweakino sector performed by GAMBIT Collaboration shows that the Z/h funnel region is consistent with a new physics interpretation of these excesses [35,36]. Motivated by these results, in this work we carefully explore the present and future status of the Z/h funnel region.

* Corresponding author.
E-mail addresses: giancarlo.pozzo@monash.edu (G. Pozzo), yang.zhang@monash.edu (Y. Zhang).

https://doi.org/10.1016/j.physletb.2018.12.062

On the theoretical side, Z/h resonant annihilation is important in natural SUSY [37], especially in the natural MSSM, since it allows the lightest neutralino to achieve the observed thermal relic density [38]. In the natural Next-to-MSSM (NMSSM), although the inclusion of a singlet superfield relaxes the experimental constraints on the electroweakinos, the exclusion of the Z/h funnel region increases the lower limit on the DM mass from 20 GeV to 80 GeV [39–41]. The lower limit on the DM mass, in turn, is critical for any LHC sparticle search because under R-parity all sparticles decay to the lightest supersymmetric particle (LSP) $\tilde{\chi}_1^0$ and the LSP mass is folded into the analyses. Typically, stricter search limits arise in analyses with light neutralinos. In a simplified model, for instance, with first- and second-generation mass-degenerate squarks, squark masses below 1.6 TeV (1.4 TeV) are excluded for $m_{\tilde{\chi}_1^0} < 200$ GeV ($200\ \text{GeV} < m_{\tilde{\chi}_1^0} < 400$ GeV), but entirely survive if $m_{\tilde{\chi}_1^0} > 600$ GeV [42]. Therefore, in most cases, the exclusion of the Z/h funnel region affects the mass limits of all sparticles.

The MSSM Z/h funnel region has been examined in numerous recent papers [43–68]. The constraints from LHC Run-I SUSY direct searchers were implemented by requiring that the SUSY signal events do not exceed the 95% confidence level (C.L.) upper limit in the signal region with the best-expected exclusion power [44, 47,63,64]. At Run-I, due to relatively small backgrounds of leptonic processes, the signal region with the best-expected exclusion power for the Z/h funnel region comes from the "3ℓ" search for the $pp \to \tilde{\chi}_1^\pm \tilde{\chi}_2^0 \to W^\pm Z \tilde{\chi}_1^0 \tilde{\chi}_1^0 \to \ell\ell\nu\ell\tilde{\chi}_1^0\tilde{\chi}_1^0$ process [69]. However, with the increase of centre-of-mass-energy and integrated luminosity, the boosted jets can also be used to distinguish signals of heavy electroweakinos from background events. As a result, the sensitivities of searches for other decay modes will increase significantly, even surpassing the "3ℓ" search. An example is the "$1\ell 2b$" search for the $pp \to \tilde{\chi}_1^\pm \tilde{\chi}_2^0 \to W^\pm H \tilde{\chi}_1^0 \tilde{\chi}_1^0 \to b\bar{b}\nu\ell\tilde{\chi}_1^0\tilde{\chi}_1^0$ process with one lepton, two b-jets and E_T^{miss} final state. At the high luminosity LHC (HL-LHC), the 95% C.L. exclusion contour of "3ℓ" search reaches 1100 GeV in the case of the WZ-mediated simplified models [70], while the exclusion contour of "$1\ell 2b$" search reaches 1310 GeV in $\tilde{\chi}_1^\pm$, $\tilde{\chi}_2^0$ mass in the case of the Wh-mediated simplified models using the MVA technique [71]. At Run-II the impact of "$1\ell 2b$" search in the Z/h funnel region cannot be ignored, because $\tilde{\chi}_1^\pm$ decay exclusively to $\tilde{\chi}_1^0 W^\pm$ while $\text{BR}(\tilde{\chi}_2^0 \to \tilde{\chi}_1^0 h) + \text{BR}(\tilde{\chi}_3^0 \to \tilde{\chi}_1^0 h) \simeq 90\%$ [44]. A statistical combination of exclusive signal regions in these searches maximizes the discovery potential. For example, in the case of the WZ-mediated simplified models, the combination performed by CMS [72] improves on the "3ℓ" analysis yielding an observed lower limit of 150 GeV on the chargino mass.

In this work, we study the present status of Z/h funnel region under the constraint of $3l + E_T^{miss}$ [73], $2l + E_T^{miss}$ [34] and $1l + 2b + E_T^{miss}$ [74] searches using 13 TeV 35.9 fb^{-1} LHC data, as well as the latest DM direct detection results. The rest of paper is organized as follows. In Section 2 we briefly describe the electroweakino sector of MSSM, with focus on the properties of DM. We present the parameter space of the Z/h funnel region and related constraints in Section 3. The HL-LHC reach for the regions that survive the present LHC constraints is discussed in Section 4. In Section 5 we investigate the Z/h funnel region in a practical phenomenology model. Finally, we draw our conclusions in Section 6.

2. The Z/h-resonant neutralino dark mater

In this section we describe the MSSM electroweakino sector, that is the superpartners of the electroweak gauge bosons (Bino $\tilde{B}$ and Winos $\tilde{W}$) and the two Higgs doublets (Higgsinos $\tilde{H}$). After electroweak symmetry breaking the electroweakinos mix to form neutralino $\tilde{\chi}_i^0$ ($i = 1, 2, 3, 4$) and chargino $\tilde{\chi}_i^\pm$ ($i = 1, 2$) mass eigenstates. In the $\psi_\alpha = (\tilde{B}, \tilde{W}^0, \tilde{H}_d^0, \tilde{H}_u^0)$ basis neutralino masses are given by $-\frac{1}{2}[\psi_\alpha \mathcal{M}_{\tilde{\chi}'\alpha\beta}\psi_\beta + h.c.]$ with the non-diagonal, symmetric mass matrix

$$\mathcal{M}_{\tilde{\chi}^0} = \begin{pmatrix} M_1 & 0 & -M_Z s_W c_\beta & M_Z s_W s_\beta \\ 0 & M_2 & M_Z c_W c_\beta & -M_Z c_W s_\beta \\ -M_Z s_W c_\beta & M_Z c_W c_\beta & 0 & -\mu \\ M_Z s_W s_\beta & -M_Z c_W s_\beta & -\mu & 0 \end{pmatrix}. \tag{1}$$

Here M_1, M_2 and μ are the Bino, Wino and Higgsino masses, $s_\beta = \sin\beta$ and $c_\beta = \cos\beta$ where $\tan\beta = \langle H_u\rangle/\langle H_d\rangle$ is the ratio of the vacuum expectation values of the two Higgs doublets, M_Z is the Z boson mass, and s_W and c_W are the sine and cosine of the weak mixing angle θ_W. With the same notation, in the $(\tilde{W}^\pm, \tilde{H}^\pm)$ basis the chargino mass matrix is given by

$$\mathcal{M}_{\tilde{\chi}^\pm} = \begin{pmatrix} M_2 & \sqrt{2}c_\beta M_W \\ \sqrt{2}s_\beta M_W & \mu \end{pmatrix}, \tag{2}$$

where M_W is the W boson mass. The physical masses of the neutralinos and charginos are given by the eigenvalues of $\mathcal{M}_{\tilde{\chi}^0}$ and $\mathcal{M}_{\tilde{\chi}^\pm}$.

Due to the $m_{\tilde{\chi}_1^\pm} > 92$ GeV chargino mass limit from LEP [75], the Wino mass, M_2, and Higgsino mass, $|\mu|$, must be higher than about 100 GeV. As a result, the lightest neutralino, with mass $m_{\tilde{\chi}_1^0} \sim M_Z/2$ or $M_h/2$, must be Bino dominated. We demand it to be the LSP, and R-parity conservation renders it a DM candidate. The main annihilation mode for this DM proceeds via an s-channel Z or Higgs boson, and the corresponding annihilation cross section is given by [63]:

$$\begin{aligned}\sigma(\tilde{\chi}_1^0\tilde{\chi}_1^0 \to Z/h \to f\bar{f}) &\simeq \frac{1}{2}C_{Z/h}^2\sqrt{1-\frac{4m_{\tilde{\chi}_1^0}^2}{s}}\frac{1}{(s-M_{Z/h}^2)^2 + (M_{Z/h}\Gamma_{Z/h})^2}\frac{s}{M_{Z/h}} \\ &\times \Gamma_{Z/h\to f\bar{f}},\end{aligned} \tag{3}$$

where $C_{Z/h}$ is the coupling between $\tilde{\chi}_1^0$ and the Z/h boson, and $\Gamma_{Z/h}$ is the corresponding decay width. The couplings arise via neutralino mixing, as shown by the relevant Lagrangian term [76]:

$$\begin{aligned}\mathcal{L}_{\tilde{\chi}^0} = &\frac{e}{s_W}h\bar{\tilde{\chi}}_1^0(N_{12} - N_{11}\tan\theta_W)(\sin\alpha N_{13} + \cos\alpha N_{14})\tilde{\chi}_1^0 \\ &+ \frac{e}{s_W c_W}Z_\mu\bar{\tilde{\chi}}_i^0\gamma^\mu\Big[\frac{P_L}{2}(N_{14}^2 - N_{13}^2) + \frac{P_R}{2}(N_{14}^2 - N_{13}^2)\Big]\tilde{\chi}_j^0.\end{aligned} \tag{4}$$

Here α is the Higgs mixing angle, and N_{ij} are the elements of the 4×4 unitary matrix that diagonalizes the neutralino mass matrix $\mathcal{M}_{\tilde{\chi}^0}$ such that N_{11}^2, N_{12}^2 and $N_{13,14}^2$ are the Bino, Wino and Higgsino components of $\tilde{\chi}_1^0$, respectively. Equation (4) shows that the Higgsino components play an important role both in the $h\tilde{\chi}_1^0\tilde{\chi}_1^0$ and $Z\tilde{\chi}_1^0\tilde{\chi}_1^0$ interaction.

Considering the limit $M_1 < 100\ \text{GeV} < |\mu| \ll M_2$, the Higgsino components can be expressed as [44]

$$N_{13} = \frac{M_Z s_W}{\mu}\left(s_\beta + c_\beta\frac{M_1}{\mu}\right), \quad N_{14} = -\frac{M_Z s_W}{\mu}\left(c_\beta + s_\beta\frac{M_1}{\mu}\right), \tag{5}$$

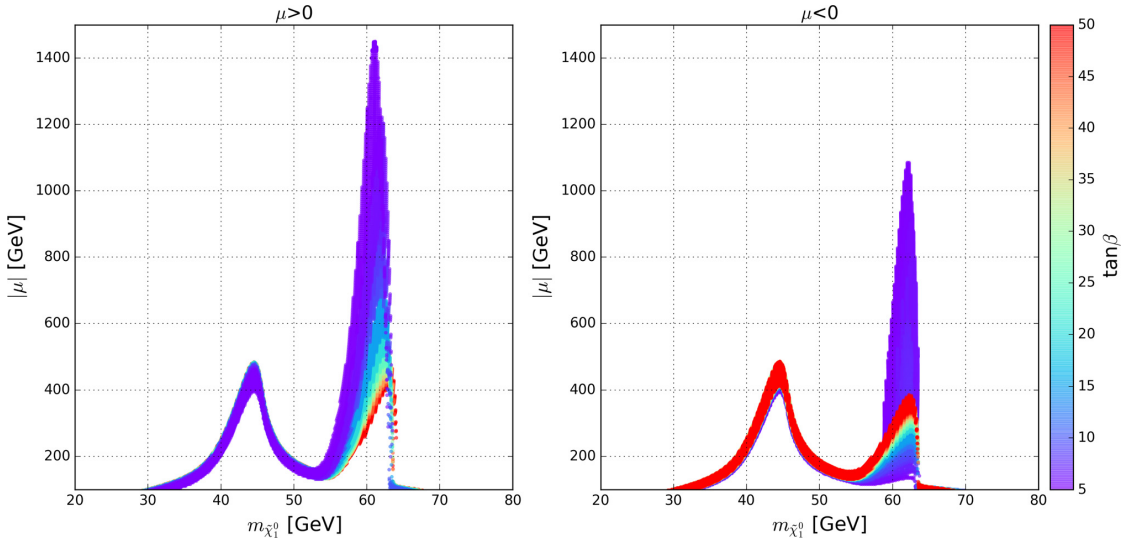

Fig. 1. Parameter regions allowed by the observed DM relic density ($0.0959 < \Omega h^2 < 0.1439$) on the Higgsino mass vs. lightest neutralino mass plane for $\mu > 0$ (left panel) and $\mu < 0$ (right panel). Colours show the value of $\tan\beta$. The masses of sparticles other than the electroweakinos are fixed at 3 TeV. The value of A_t is also fixed to obtain the observed Higgs mass: $A_t = 4.5$ TeV for $\tan\beta > 10$, $A_t = 5.0$ TeV for $7 < \tan\beta < 10$ and $A_t = 6.0$ TeV for $\tan\beta < 7$.

which decrease when the mass hierarchy between Higgsino and Bino increases. From equations (5) and (4), one can derive the couplings

$$C_Z = \frac{eM_Z^2}{\mu^2}\cos(2\beta)\left(1+\frac{M_1^2}{\mu^2}\right),$$
$$C_h = \frac{eM_Z}{\mu}\left[\cos(\beta+\alpha)+\sin(\beta-\alpha)\frac{M_1}{\mu}\right]. \quad (6)$$

Thus, the relic density of Z/h-resonant DM at tree level depends on M_1, μ and $\tan\beta$. We, therefore, perform a scan over M_1, μ and $\tan\beta$ to identify the parameter space where Z/h-resonant DM satisfies the observed DM abundance. Following that, we examine the impact of current and future experimental constraints on this parameter space.

3. The parameter space and constraints

To analyse the Z/h funnel region, we first study a simplified model that assumes the sfermion masses, wino mass M_2, gluino mass M_3 and CP-odd Higgs mass M_A are fixed at 3 TeV, heavy enough to decouple at LEP or the LHC. We set all the trilinear couplings except A_t to zero. To match the measured value of SM-like Higgs mass of 125.09 GeV [77], the trilinear coupling A_t is fixed at 4.5 TeV for $\tan\beta > 10$, at 5.0 TeV for $7 < \tan\beta < 10$ and at 6.0 TeV for $\tan\beta < 7$. Under these assumptions, we sample the following parameter space:

$$10\ \text{GeV} < M_1 < 100\ \text{GeV}, \qquad 50\ \text{GeV} < |\mu| < 1500\ \text{GeV},$$
$$5 < \tan\beta < 50. \quad (7)$$

We use `SUSY-HIT-1.5` [78] based on `SuSpect` [79], together with `SDECAY` [78,80] and `HDECAY` [81] to generate the mass spectrum and to calculate the Z/h boson decay branching ratios, `micrOMEGAs-4.3.5` [82,83] to calculate the DM observables, and `EasyScan_HEP` [17] to perform the scan. Due to the low dimensionality and simplicity of the parameter space we generate samples on a grid.

In Sections 3.1–3.4 we detail the relevant constraints on the Z/h-resonant DM. Here we ignore other observations, such as B-physics measurements, that tend to give mild constraints due to the high scale of the fixed SUSY parameters.

3.1. The thermal relic density of DM

From equations (6) and (3), we see that the measurement of the DM abundance by Planck [84] and WMAP [85] place severe restrictions on the relationship among M_1, μ and $\tan\beta$. We assume that the thermal relic density of the lightest neutralino is equal to the cold DM abundance $\Omega h^2 = 0.1199 \pm 0.0022$ at 2σ level with 10% theoretical uncertainty (cf. the `Plik` cross-half-mission likelihood in [84]). In Fig. 1 we project the allowed regions on the $(m_{\tilde{\chi}_1^0}, |\mu|)$ plane for both $\mu > 0$ and $\mu < 0$ with colours indicating the value of $\tan\beta$.

As sketched in Section 2, to achieve both the observed DM abundance and a sizeable coupling to the Z/h boson, the Bino-like $\tilde{\chi}_1^0$ must contain a certain amount of Higgsino component. This imposes limits on the Higgsino mass, shown in Fig. 1 by the coloured regions. The blank region above the coloured region leads to an overproduction of DM in the early universe, while the blank region below the coloured region has a relic density smaller than 0.096. Due to the resonance in equation (3), the Higgsino mass is enhanced when $m_{\tilde{\chi}_1^0}$ close to $M_{Z/h}$, therefore the allowed region features two clear peaks.

The Higgs resonances (the peaks around $m_h/2$) in the left ($\mu > 0$) and right ($\mu < 0$) panel of Fig. 1 show different dependence on $\tan\beta$ for a fixed $m_{\tilde{\chi}_1^0}$. This difference is caused by the sign of M_1/μ in the coupling between the $\tilde{\chi}_1^0$ and the Higgs boson. Taking the decoupling limit of the Higgs sector, $\beta - \alpha = \pi/2$, C_h in equation (6) can be written as

$$C_h = \frac{eM_Z}{\mu}\left(\sin 2\beta + \frac{M_1}{\mu}\right). \quad (8)$$

Therefore, for $M_1/\mu > 0$ and $M_1 \simeq M_h/2$ to keep the coupling C_h unchanged the Higgsino mass has to increase from 400 GeV to

1440 GeV and $\tan\beta$ has to decrease from 50 to 5. For the same reason, for $M_1/\mu < 0$ and $M_1 \simeq M_h/2$ the coupling is bracketed as $|\mu|$ decreases from 380 GeV to 130 GeV and $\tan\beta$ decreases from 50 to 7. For $M_1/\mu < 0$ and $\tan\beta < 7$ there are two separate regions corresponding to the observed relic density, divided by the so-called "blind spot" where $\sin 2\beta = M_1/\mu$ [40,52,86–88]. The coupling C_h changes sign between the two regions. For $\tan\beta = 5$ and $m_{\tilde{\chi}_1^0} = 52$ GeV, for example, the regions $\mu < -136$ GeV and -168 GeV $< \mu < -1085$ GeV both correspond to $\Omega h^2 < 0.14$.

The Z resonance, on the other hand, is independent of the sign of M_1/μ and it mildly depends on $\tan\beta$, as shown in equation (6). The Higgsino can be as heavy as about 470 GeV when DM annihilates via the Z resonance.

3.2. Dark matter direct detection experiments

Neutralinos with non-negligible Higgsino component can be directly detected via elastic scattering on nuclei mediated by Z or Higgs boson exchange [6,89–93]. The null result of the searches for such scattering by LUX [89], XENON1T [90,94] and PandaX-II [6] provides limits on the spin-independent (SI) neutralino-nucleon elastic cross section $\sigma^{\rm SI}_{\tilde{\chi}_1^0 n}$. In the $\tilde{\chi}_1^0$ mass region we consider the one-sided 90% C.L. upper limit on $\sigma^{\rm SI}_{\tilde{\chi}_1^0 n}$ is about 5×10pb [94]. The most sensitive constraints on spin-dependent (SD) DM-neutron elastic cross section $\sigma^{\rm SD}_{\tilde{\chi}_1^0 n}$ and DM-proton elastic cross section $\sigma^{\rm SD}_{\tilde{\chi}_1^0 p}$ come from LUX [93] and PICO-60 [95], respectively. In Fig. 2 we show current, as well as projected LUX-ZEPLIN (LZ) [96], constraints on $\sigma^{\rm SI}_{\tilde{\chi}_1^0 n}$ and $\sigma^{\rm SD}_{\tilde{\chi}_1^0 n}$ in the parameter regions that account for the observed DM abundance. The grey regions are excluded by either DM SI or SD scattering searches.

The top panels of Fig. 2 show the predicted $\sigma^{\rm SI}_{\tilde{\chi}_1^0 n}$ in the surviving region as a function of $m_{\tilde{\chi}_1^0}$. In the limit of heavy scalar superpartners, the dominant contribution of $\sigma^{\rm SI}_{\tilde{\chi}_1^0 n}$ comes from the t-channel exchange of a Higgs boson [52,88]:

$$\sigma^{\rm SI}_{\tilde{\chi}_1^0 n} \simeq \frac{4\mu_r^2}{\pi}\Big[\sum_{i=1}^{2}\frac{C_{h_i\tilde{\chi}_1^0\tilde{\chi}_1^0}C_{h_i NN}}{2M_{h_i}^2}\Big]^2. \tag{9}$$

Here μ_r is the neutralino-nucleus reduced mass, $C_{h_i NN}$ denotes the effective coupling between the Higgs and nucleon. As discussed in Subsection 3.1, in the vicinity of the Higgs resonance $C_{h\tilde{\chi}_1^0\tilde{\chi}_1^0}$ is restricted by the observed DM abundance. In this region $\sigma^{\rm SI}_{\tilde{\chi}_1^0 n}$ is practically independent of $\tan\beta$ and sign of μ, and it is large enough to be fully covered by the LZ projected limits. On the other hand, on the Z resonance the DM relic density is independent of $C_{h\tilde{\chi}_1^0\tilde{\chi}_1^0}$, and demands a fixed $|\mu|$ for certain $m_{\tilde{\chi}_1^0}$, such as $|\mu| \simeq 450$ GeV for $m_{\tilde{\chi}_1^0} = 45$ GeV. As a result, for $\mu > 0$ the $\sigma^{\rm SI}_{\tilde{\chi}_1^0 n}$ cross section decreases when $\tan\beta$ increases and will be detectable at LZ. For $\mu < 0$, however, due to the blind spot at $\sin 2\beta = M_1/\mu$, it is impossible to test Z-resonance DM for $\tan\beta = \tan[\arcsin(45/450)/2] \simeq 20$.

On the contrary, at tree level and in the heavy squark limit only the t-channel Z boson exchange diagram contributes to $\sigma^{\rm SD}_{\tilde{\chi}_1^0 n}$ and $\sigma^{\rm SD}_{\tilde{\chi}_1^0 p}$. Therefore, Z-resonant DM will be detected at LZ by SD DM-nucleon scattering, as shown in the bottom panels of Fig. 2. Since the 90% C.L. limit on the DM mass given by LUX [93] is about two times lower than the corresponding limit provided by PICO-60 [95], while in our model $\sigma^{\rm SD}_{\tilde{\chi}_1^0 n} = 0.76\sigma^{\rm SD}_{\tilde{\chi}_1^0 p}$, in the following we only study the SD DM-neutron elastic cross section.

In summary, a large part of the Z/h funnel region has been excluded by the current DM direct detection experimental constraints. The surviving regions require $m_{\tilde{\chi}_1^0} \in [41, 46] \cup [58, 63]$ GeV for positive μ and $m_{\tilde{\chi}_1^0} \in [40, 46] \cup [58, 63]$ GeV for negative μ. These regions will be probed by the SI and SD DM-nucleon scattering detection at LZ. We should keep in mind, however, that these regions are obtained under the assumption that the masses of all non-electroweakino sparticle masses are 3 TeV. If that is not the case, for example in the case of light squarks and a light non-SM-like CP-even Higgs, the SI DM-neutron cross section could reduce and modify the allowed regions.

3.3. Z and Higgs boson invisible decay

If $m_{\tilde{\chi}_1^0} < M_Z/2$, the decay of Z boson to a pair of neutralinos is kinematically allowed. The decay width of this process is given by [63]:

$$\Gamma(Z \to \tilde{\chi}_1^0\tilde{\chi}_1^0) = \frac{M_Z C^2_{Z\tilde{\chi}_1^0\tilde{\chi}_1^0}}{24\pi}\left(1 - \frac{4m^2_{\tilde{\chi}_1^0}}{M_Z^2}\right)^{\frac{3}{2}}. \tag{10}$$

45 GeV $> m_{\tilde{\chi}_1^0} >$ 40 GeV, in which DM direct detection is possible, equation (10) gives $\Gamma(Z \to \tilde{\chi}_1^0\tilde{\chi}_1^0) \lesssim 0.05$ MeV. This decay width is much below the LEP bound on the new physics contribution to $\Gamma(Z \to \text{invisible}) = 2$ MeV at 95% C.L. LEP bounds on electroweakino masses, $m_{\tilde{\chi}_1^\pm} > 92$ GeV and $m_{\tilde{\chi}_1^0} + m_{\tilde{\chi}_{2,3}^0} > 208$ GeV [97], are not constraining either in the surviving regions.

Similarly, for $m_{\tilde{\chi}_1^0} < M_h/2$, the Higgs boson decay width into a pair of neutralinos is:

$$\Gamma(h \to \tilde{\chi}_1^0\tilde{\chi}_1^0) = \frac{M_h C^2_{h\tilde{\chi}_1^0\tilde{\chi}_1^0}}{16\pi}\left(1 - \frac{4m^2_{\tilde{\chi}_1^0}}{M_h^2}\right)^{\frac{3}{2}}. \tag{11}$$

The combination of several searches performed by the ATLAS [98] and CMS [99,100] collaborations sets an upper limit of 0.24 at the 95% C.L. on BR($h \to \tilde{\chi}_1^0\tilde{\chi}_1^0$) for the 125 GeV Higgs boson. In Fig. 3, we show these limits in the $(m_{\tilde{\chi}_1^0}, |\mu|)$ logarithmic plane for different values of $\tan\beta$. It is clear that the limits become stronger as $\tan\beta$ decreases (increases) for $\mu > 0$ ($\mu < 0$), but they are always weaker than the DM direct detection limits. The global fit of Higgs couplings will provide a stricter constraint on the invisible Higgs decay width. However, the constraint from global fit can be relaxed by tuning the SUSY masses that here we fix at 3 TeV. For instance, the best fit point of global fit for Z/h funnel region in MSSM7 requires $m_{\tilde{t}_1} \simeq 2.1$ TeV and $M_A \simeq 1.8$ TeV [10]. Thus we do not impose the Higgs invisible decay constraint from global fit in simplified model. The projected limit on BR($h \to \tilde{\chi}_1^0\tilde{\chi}_1^0$), such as BR($h \to \tilde{\chi}_1^0\tilde{\chi}_1^0$) $> 0.4\%$ from ILC [101], can cover the whole Z funnel region, but not the h funnel [47,63].

3.4. Electroweakino searches at the 13 TeV LHC

The ATLAS [102–106] and CMS [34,72–74,107–109] collaborations performed numerous searches for direct production of electroweakinos at the 13 TeV LHC. In the simplified model in which the Wino-like $\tilde{\chi}_1^\pm$ ($\tilde{\chi}_2^0$) decays to a $W(Z)$ boson and a massless $\tilde{\chi}_1^0$, the search performed by ATLAS with 36 fb^{-1} data for final states involving two or three leptons excludes Wino masses up to 580 GeV [102]. The statistical combination of searches performed by CMS excludes the Wino below a mass of 650 GeV at the 95% C.L. [72]. The corresponding mass bounds for the Higgsino might

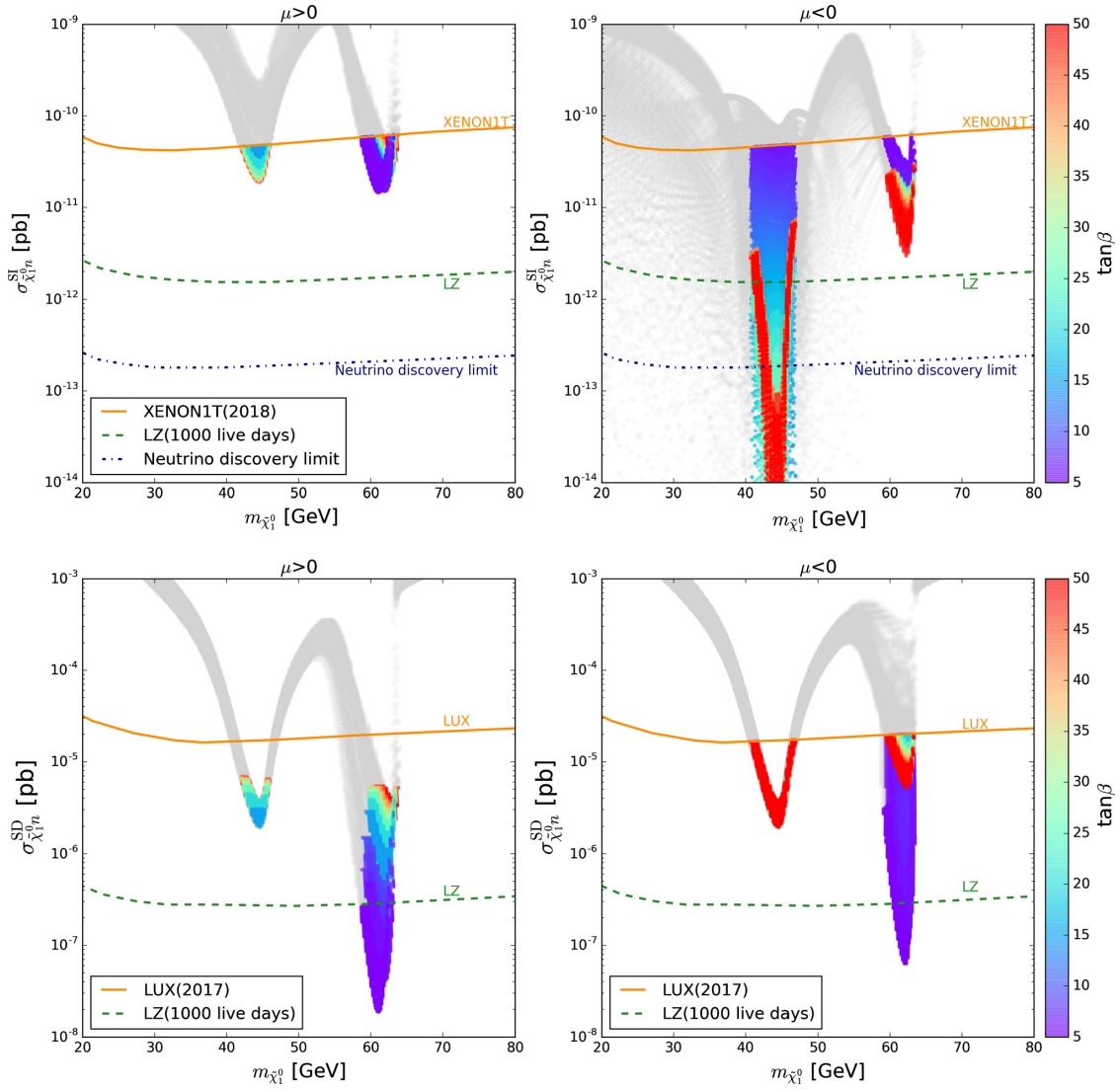

Fig. 2. Parameter regions allowed by the observed DM abundance ($0.0959 < \Omega h^2 < 0.1439$) on the $(m_{\tilde{\chi}^0_1}, \sigma^{SI}_{\tilde{\chi}^0_1 n})$ logarithmic plane (upper panels) and $(m_{\tilde{\chi}^0_1}, \sigma^{SD}_{\tilde{\chi}^0_1 n})$ logarithmic plane (lower panels) for $\mu > 0$ (left panels) and $\mu < 0$ (right panels). The orange solid lines mark the limit on $\sigma_{\tilde{\chi}^0_1 n}$ given by XENON1T [90,94] and LUX [93] experiments. The green dashed lines mark the projected limit of LUX-ZEPLIN [96]. The colours show the value of $\tan\beta$; grey regions are excluded by DM direct detection at 90% C.L.

be lower than that at least 100 GeV because the production rate of Higgsino-like chargino and neutralino pair is nearly half than the production rate of Wino-like chargino and neutralino pair [44]. Based on these surviving regions of Z/h-resonance DM could be excluded since the DM relic density imposes strict requirements on the Higgsino mass, as shown in Fig. 3. In the following, we assess the LHC constraints on the parameter space of interest by a detailed Monte Carlo simulation.

We use `MadGraph5_aMC@NLO_v2.6.1` [110] in combination with `Pythia6` [111] to generate events for the relevant processes:

$$pp \to \tilde{\chi}^{\pm}_1 \tilde{\chi}^0_{2,3}, \quad pp \to \tilde{\chi}^0_{2,3} \tilde{\chi}^0_{2,3}, \quad pp \to \tilde{\chi}^{\pm}_1 \tilde{\chi}^{\mp}_1, \tag{12}$$

where the production rate of the first process at the LHC is much larger than the others. Here $\tilde{\chi}^{\pm}_1$ decays 100% to a W boson and a $\tilde{\chi}^0_1$, $\tilde{\chi}^0_{2,3}$ decay to a Z boson and a $\tilde{\chi}^0_1$ or a h boson and $\tilde{\chi}^0_1$. Although the branching ratios $\mathrm{BR}(\tilde{\chi}^0_{2,3} \to \tilde{\chi}^0_1 Z)$ and $\mathrm{BR}(\tilde{\chi}^0_{2,3} \to \tilde{\chi}^0_1 h)$ depend on $\tan\beta$ and sign of μ, $\sum \mathrm{BR}(\tilde{\chi}^0_{2,3} \to \tilde{\chi}^0_1 Z)$ and $\sum \mathrm{BR}(\tilde{\chi}^0_{2,3} \to \tilde{\chi}^0_1 h)$ are roughly comparable for the whole parameter space [44]. The cross sections are normalized to next-to-leading order (NLO) computed by `PROSPINO2` [112]. Finally, we use `CheckMATE-2.0.7` [113] with `Delphes3.4.1` [114] to repeat the CMS analysis [72].

The CMS combined search related to our processes [72] included the following channels.

- The "$\geq 3\ell$" search for the $pp \to \tilde{\chi}^{\pm}_1 \tilde{\chi}^0_2 \to W^{\pm} Z \tilde{\chi}^0_1 \tilde{\chi}^0_1 \to \ell\ell\nu\ell \tilde{\chi}^0_1 \tilde{\chi}^0_1$ process, with three or more leptons and large E^{miss}_T in the final state [73]. In the several signal regions (SR) cat-

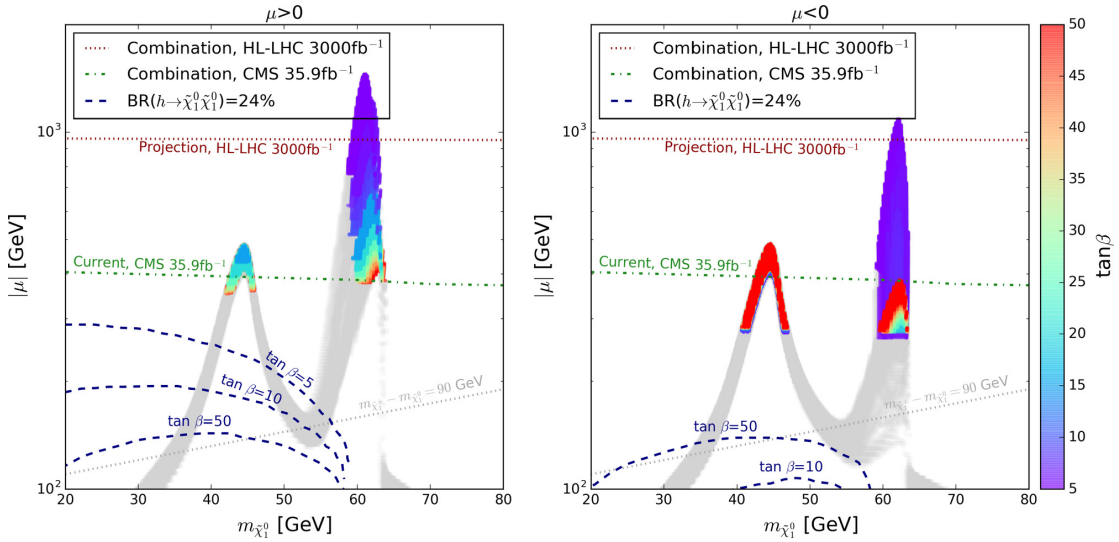

Fig. 3. Constraints on the relevant parameter regions from invisible decay limits. Regions excluded by DM direct detection are filled with grey colour. The blue dashed lines indicate the 95% C.L. upper limits on the invisible decay branching ratio of 125 GeV Higgs boson for different values of $\tan\beta$. The green dot-dashed lines and red dotted lines show the 95% C.L. upper limits from the combination of CMS searches for electroweakinos at the 13 TeV LHC with 35.9 fb^{-1} data and at the HL-LHC with 3000 fb^{-1} data, respectively. Regions below these lines are excluded by the corresponding experimental results.

egorized by the number of lepton and lepton flavour, SR-A targets the WZ topology. This is done by selecting events with three light-flavour leptons (e, μ), two of which form an opposite-sign, same-flavour (OSSF) pair. These events are further divided into 44 bins by the invariant mass of the pair $M_{\ell\ell}$, the transverse mass M_T of the third lepton and $E_T^{\rm miss}$. In [72], the categorization has been updated to improve the sensitivity for the region of $m_{\tilde{\chi}_2^0} - m_{\tilde{\chi}_1^0} \simeq M_Z$ by requiring H_T, the scalar p_T sum of the jets, with $p_T > 30$ GeV. However, compared to [73], the observed lower mass limit of the Wino-like $\tilde{\chi}_1^\pm$ for massless $m_{\tilde{\chi}_1^0}$ has also been improved from 450 GeV to 500 GeV. Here we adopt the improved bins of SR-A for the analysis, but the validation of cut-flows is based on [73] since the cut-flow in [72] has not been provided.

- The "2ℓ on-Z" search for the $pp \to \tilde{\chi}_1^\pm \tilde{\chi}_2^0 \to ZW^\pm \tilde{\chi}_1^0 \tilde{\chi}_1^0 \to \ell\ell jj \tilde{\chi}_1^0 \tilde{\chi}_1^0$ process, with exactly two OSSF leptons consistent with the Z boson mass, two non b-tagged jets consistent with the W boson mass and large $E_T^{\rm miss}$ in the final state [34]. The variable M_{T2} [115,116] is defined using $E_T^{\rm miss}$ and the two leptons are required to be more energetic than 80 GeV to reduce the $t\bar{t}$ background. Then four exclusive bins are defined based on $E_T^{\rm miss}$. The analysis probes Wino-like $\tilde{\chi}_1^\pm$ masses between approximately 160 and 610 GeV for $m_{\tilde{\chi}_1^0} = 0$ GeV and $\mathrm{BR}(\tilde{\chi}_1^\pm \to W^\pm \tilde{\chi}_1^0) = \mathrm{BR}(\tilde{\chi}_2^0 \to Z\tilde{\chi}_1^0) = 100\%$.
- The "$1\ell 2b$" search for the $pp \to \tilde{\chi}_1^\pm \tilde{\chi}_2^0 \to hW^\pm \tilde{\chi}_1^0 \tilde{\chi}_1^0 \to b\bar{b}\nu\ell \tilde{\chi}_1^0 \tilde{\chi}_1^0$ process, with exactly one lepton, exactly two b jets and large $E_T^{\rm miss}$ in the final state [74]. The invariant mass of the two b jets is required to be in the range [90, 150] GeV. The transverse mass of the lepton-$E_T^{\rm miss}$ system and the contransverse mass $M_{\rm CT}$ of the two b jets are used to suppress backgrounds, and the $E_T^{\rm miss}$ separates the SR into two exclusive bins. The result excludes $m_{\tilde{\chi}_1^\pm}$ between 220 GeV and 490 GeV at 95% C.L. when the $\tilde{\chi}_1^0$ is massless in the simplified model.

Additionally, there are "H($\gamma\gamma$)" searches for the $pp \to \tilde{\chi}_1^\pm \tilde{\chi}_2^0 \to hW^\pm \tilde{\chi}_1^0 \tilde{\chi}_1^0 \to \gamma\gamma\nu\ell \tilde{\chi}_1^0 \tilde{\chi}_1^0$ process, and "2ℓ soft" searches for the $pp \to \tilde{\chi}_1^\pm \tilde{\chi}_2^0 \to Z^* W^{\pm *} \tilde{\chi}_1^0 \tilde{\chi}_1^0 \to \ell\ell jj \tilde{\chi}_1^0 \tilde{\chi}_1^0$ process where Z^* and $W^{\pm *}$ are off-shell. But we do not include them in the analysis, further constraining the regions that survived DM direct detection limits, because the former can only exclude Wino below 170 GeV in a simplified model and the latter targets the situation of $m_{\tilde{\chi}_2^0} - m_{\tilde{\chi}_1^0} \simeq M_Z$.

As checked by CMS [72], these SRs are mutually exclusive, which means that they can be statistically combined to maximize the detection sensitivity. Thus, we combine them together though the modified frequentist approach, CL_s method [117], by `RooStats` [118]. The likelihood functions are written as

$$\mathcal{L}(\mu) = \prod_i^{N_{\rm ch}} \int d\mu' \int db_i' \frac{(\mu' s_i + b_j')^{n_i} e^{-(\mu' s_i + b_j')}}{n_i!} \times e^{\frac{-(\mu'-\mu)^2}{2\sigma_\mu^2}} \times e^{\frac{-(b_i'-b_i)^2}{2\sigma_{b_i}^2}}, \tag{13}$$

where μ is the parameter of interest, μ' and b_i' are nuisance parameters, and n_i and b_i are the number of signal and background events in the SRs. We take $\mu = 1$ for the signal hypothesis and $\mu = 0$ for the background only hypothesis. The background event numbers b_i and uncertainties σ_{b_i} are taken from the CMS reports, while the relative uncertainties of signal σ_μ are assumed to equal 5%. Covariance matrices are not included.

In Fig. 3 we show the 95% C.L. combined upper limits in the plane of $m_{\tilde{\chi}_1^0}$ and μ indicated by green dot-dash lines. They barely depend on $\tan\beta$ and the sign of μ, and slightly decrease with increasing $m_{\tilde{\chi}_1^\pm}$. To illustrate this, we choose four benchmark points of fixed $m_{\tilde{\chi}_1^\pm}$ as examples and show the details of the CL_s in Table 1. Comparing `BP1`, `BP2` and `BP3` we can see that the variation of $\tan\beta$ and sign of μ will affect the branching ratios of the Higgsino-like $\tilde{\chi}_{2,3}^0$, which can be easily obtained from equation (8), but hardly change $\mathrm{BR}(\tilde{\chi}_2^0 \to \tilde{\chi}_1^0 Z) + \mathrm{BR}(\tilde{\chi}_3^0 \to \tilde{\chi}_1^0 Z)$ and

Table 1
Benchmark points illustrating the result of the combined CMS electroweakino searches. The uncertainties in CL_s only represent the uncertainties from the CL_s calculation and do not include the uncertainties of the signal event generation.

	BP1	BP2	BP3	BP4
$\tan\beta$	30	10	30	30
M_1 (GeV)	50	50	50	80
μ (GeV)	390	390	−390	390
$m_{\tilde{\chi}_1^0}$ (GeV)	49.5	46.4	48.6	78.0
$m_{\tilde{\chi}_2^0}$ (GeV)	401	402	402	402
$m_{\tilde{\chi}_3^0}$ (GeV)	403	403	403	403
$m_{\tilde{\chi}_1^\pm}$ (GeV)	400	399	400	399
$\mathrm{BR}(\tilde{\chi}_2^0 \to \tilde{\chi}_1^0 Z)$	45%	39%	39%	33%
$\mathrm{BR}(\tilde{\chi}_2^0 \to \tilde{\chi}_1^0 h)$	55%	61%	61%	67%
$\mathrm{BR}(\tilde{\chi}_3^0 \to \tilde{\chi}_1^0 Z)$	63%	68%	69%	75%
$\mathrm{BR}(\tilde{\chi}_3^0 \to \tilde{\chi}_1^0 h)$	37%	32%	31%	35%
$\sigma_{\tilde{\chi}_{2,3}^0 \tilde{\chi}_1^\pm}$ (fb)	59.45	59.48	59.48	59.46
CL_s^{3l}	0.238 ± 0.007	0.240 ± 0.007	0.251 ± 0.007	0.265 ± 0.007
CL_s^{2l}	0.266 ± 0.018	0.246 ± 0.018	0.238 ± 0.017	0.231 ± 0.016
CL_s^{1l2b}	0.549 ± 0.009	0.552 ± 0.009	0.563 ± 0.009	0.553 ± 0.009
$\mathrm{CL}_s^{\mathrm{combine}}$	0.049 ± 0.005	0.051 ± 0.006	0.052 ± 0.005	0.054 ± 0.006

$\mathrm{BR}(\tilde{\chi}_2^0 \to \tilde{\chi}_1^0 h) + \mathrm{BR}(\tilde{\chi}_3^0 \to \tilde{\chi}_1^0 h)$. For BP4, a heavier Bino mass M_1 leads to a relatively compressed spectrum and hence smaller signal cut efficiencies.

In summary, for Z/h funnel DM, regions in which μ is smaller than about 390 GeV are excluded by LHC Run-II results, which limits are stricter than DM direct detection for negative μ and positive μ with $\tan\beta > 20$. The Z funnel region is on the verge of complete exclusion. In the case of $\mu < 0$, the h funnel region can only survive with $\tan\beta < 7.4$, while the h funnel region of $\mu > 0$ is the main surviving region. The h funnel regions for $\mu > 0$ and $\mu < 0$ are also shown in Fig. 4 on the $(\tan\beta, |\mu|)$ plane to display the surviving parameter space more clearly.

4. Electroweakino searches at the HL-LHC

Although the h funnel region of $\mu > 0$, that is the main region that survives the current experimental limits, will be fully probed by LZ [96], the HL-LHC reach is still worth investigating as a complementary test. We employ two electroweakino analyses at the HL-LHC proposed by ATLAS: the "3ℓ" search [70] and the "$1\ell 2b$" search [71]. Similar to the "$\geq 3\ell$" search at 13 TeV, the "3ℓ" search at the HL-LHC targets the $pp \to \tilde{\chi}_1^\pm \tilde{\chi}_2^0 \to W^\pm Z \tilde{\chi}_1^0 \tilde{\chi}_1^0 \to \ell\ell\nu\ell \tilde{\chi}_1^0 \tilde{\chi}_1^0$ process with three or more leptons and large E_T^{miss} in the final state. For 3000 fb^{-1} luminosity four signal regions, indicated by 'A', 'B', 'C', 'D', optimize the discovery and exclusion ability. The $1\ell 2b$ search for the $pp \to \tilde{\chi}_1^\pm \tilde{\chi}_2^0 \to W^\pm h \tilde{\chi}_1^0 \tilde{\chi}_1^0 \to \nu\ell b\bar{b} \tilde{\chi}_1^0 \tilde{\chi}_1^0$ process at the HL-LHC corresponds to two signal regions, 'C' and 'D'. Unlike the 13 TeV analysis, the signal regions at the HL-LHC are not exclusive. For example, in both analyses, the signal region C covers the signal region D. As a result, we choose the signal region with the best-expected exclusion power in each analysis, and then combine them together using the CL_s method described in Subsection 3.4.

The combined expected 95% C.L. upper limits on the Z/h funnel region are presented in Fig. 3 and Fig. 4 by red dot lines. We find that the combined result pushes the bound on μ to 960 GeV, which is 150 GeV stricter than the result of each individual analysis. There is no doubt that the Z funnel region will be completely excluded. The parameter space of h funnel region will be restricted to a very small region: $\tan\beta < 8$ for $\mu > 0$ and $\tan\beta < 5.5$ for $\mu < 0$. Such small $\tan\beta$, however, is highly disfavoured by experimental constraints, such as the SM-like Higgs data [119,120] and the muon anomalous magnetic moment.

5. The *Z/h* funnel in phenomenological MSSM

After exhibiting the status of the Z/h funnel region in simplified MSSM, it is desirable to investigate the situation when we get rid of the assumptions, such as the fixed sfermion masses and the ratio of neutralino DM to observed DM. In this section we briefly examine the Z/h funnel region in a wider model scope and with more experimental constraints. To this end, we study the light DM scenario of phenomenological MSSM (pMSSM) [76] by scanning the following parameter space:

$$\begin{gathered} 2 < \tan\beta < 60, \qquad 10\ \mathrm{GeV} < M_1 < 100\ \mathrm{GeV}, \\ 100\ \mathrm{GeV} < M_2 < 1000\ \mathrm{GeV}, \\ 100\ \mathrm{GeV} < \mu < 1500\ \mathrm{GeV}, \qquad 50\ \mathrm{GeV} < M_A < 2\ \mathrm{TeV}, \\ |A_t = A_b| < 5\ \mathrm{TeV}, \qquad 200\ \mathrm{GeV} < m_{Q_3}, \qquad m_{U_3} = m_{D_3} < 2\ \mathrm{TeV}, \\ 100\ \mathrm{GeV} < m_{L_{1,2,3}} = m_{E_{1,2,3}} = A_{E1,2,3} < 2\ \mathrm{TeV}. \end{gathered} \tag{14}$$

The mass of the gluino and the first two generation squarks are fixed to 2 TeV. In addition to the constraints described in Section 3, during the scan we implement the following experimental constraints at 95% C.L.:

- B-physics constraints, such as the precise measurements of $B \to X_s\gamma$, $B_s \to \mu^+\mu^-$, $B_d \to X_s\mu^+\mu^-$ and the mass differences ΔM_d and ΔM_s [97];
- the muon anomalous magnetic moment (a_μ), the measured value of which deviates from the SM prediction (a_μ^{SM}) [121, 122];
- global fit of the MSSM Higgs sector implemented by the packages `HiggsBounds` [123] and `HiggsSignals` [124];
- searches for direct production of charginos and neutralinos in events with $3\ell + E_T^{miss}$ [69] and $2\ell + E_T^{miss}$ [125] at LHC Run-I using `CheckMATE-2.0.23`.

We also require $m_{\tilde{l}} > 2.0\, m_{\tilde{\chi}_1^0}$ to discard the samples with DM co-annihilation through sleptons in the early universe. Since there may be other sources of DM, here we set only an upper bound on the DM relic density. Assuming that the other sources of the DM have no interaction with nuclei, this implies that we have to scale

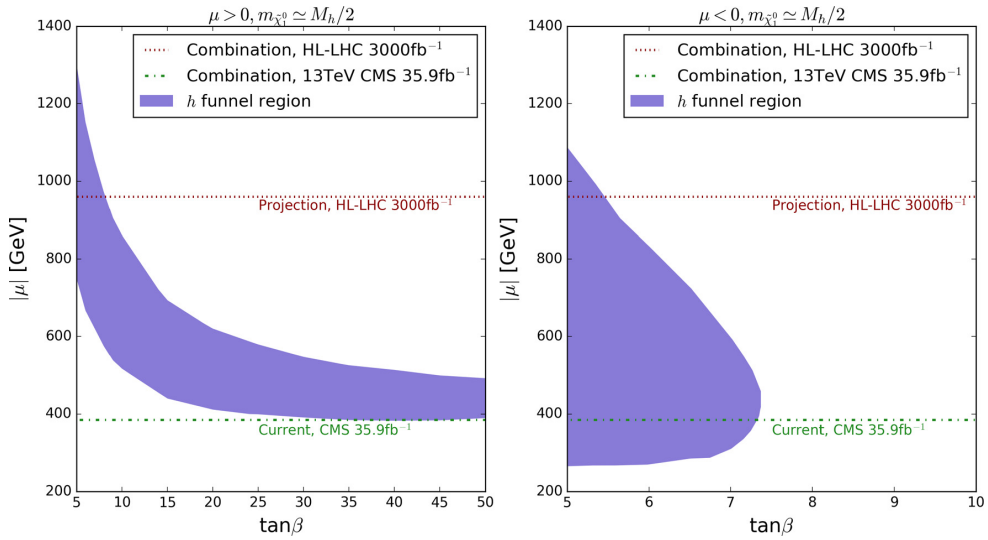

Fig. 4. The plots show, in the $(\tan\beta, |\mu|)$ plane, the h funnel region consistent with the observed DM abundance and DM direct detection limits. The green dot-dashed and red dotted lines show the 95% C.L. upper limits from combined CMS searches for electroweakinos at the 13 TeV LHC with 35.9 fb^{-1} data and limits by the HL-LHC with 3000 fb^{-1} data, respectively. Regions below the lines are excluded by the corresponding experimental results at 95% C.L.

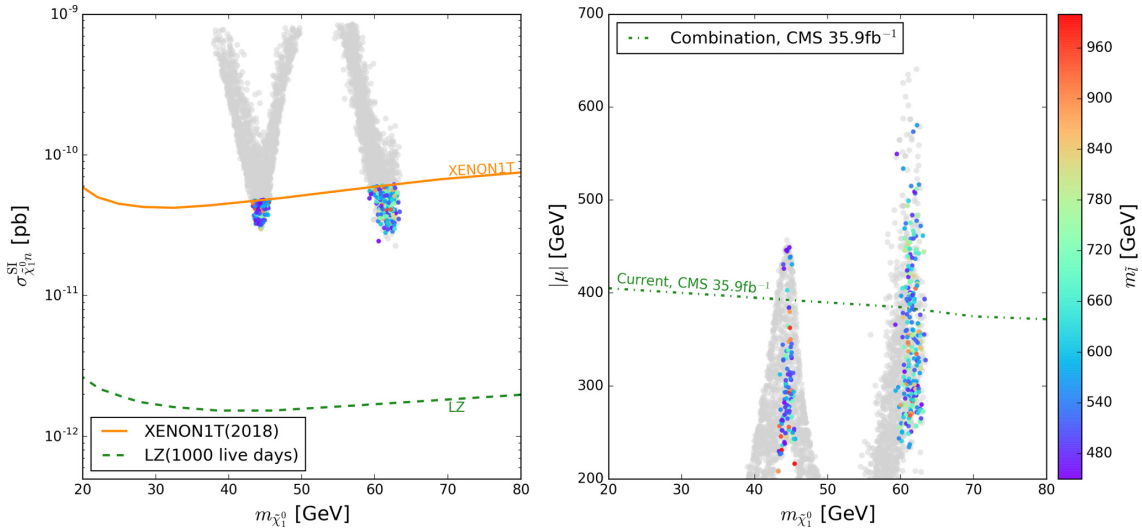

Fig. 5. Surviving parameter regions of pMSSM shown on the lightest neutralino mass vs. the SI DM-neutron elastic cross section (left panel) and vs. the Higgsino mass (right panel). Colours show the unified mass of sleptons, except for the grey samples that are excluded by DM direct detection at 90% C.L. or direct searches for sleptons at LHC at 95%C.L.

the DM-neutron elastic cross section by the ratio of neutralino DM relic density and observed DM abundance.

The surviving parameter regions of pMSSM are presented in Fig. 5 with grey points indicating the samples further excluded by DM SI/SD direct detection and direct searches for sleptons using 36 fb^{-1} data at LHC Run-II [102,126], and other colours indicating the unified mass of sleptons. The left panel is similar to the left top panel of Fig. 2, though now $\tilde{\chi}_1^0$ may represent only part of the total DM. Both the Z and h funnel regions are tightly restricted by the DM direct detection constraints that yield $m_{\tilde{\chi}_1^0} \in [43.1, 45.6]$ GeV or $[59.2, 63.6]$ GeV. In the right panel we find that the combination of electroweakino searches further excludes regions where the ratio of the neutralino DM relic density over the observed DM density is smaller than 58% (19%) for the Z (h) funnel region. Comparing the pMSSM model to the simplified model we find that the constraint on a_μ, which requires $\tan\beta > 9$, reduces the height of the h funnel region. Furthermore, a_μ also restricts the slepton masses [127]. As shown by the colours in Fig. 5, the surviving samples require either a light slepton or a light chargino. For Z/h resonances, the points of $m_{\tilde{l}} \lesssim 460$ GeV are excluded by the multi-lepton plus E_T^{miss} searches at LHC Run-II [102,126], which further reduce the height of the h funnel peak from 650 GeV to 580 GeV. Therefore, the detection of the whole Z/h funnel region in pMSSM will be much faster than the one in the simplified model, in the

joint result of future slepton searches and electroweakino searches at LHC. For example, if the exclusion limits on Higgsino mass and slepton mass are both improved by about 150 GeV, there would be no surviving point in pMSSM.

6. Summary

In this work we investigate the current and future status of the Z/h funnel region in the MSSM with the constraints from DM direct detection, measurements of Z/h invisible decay, direct searches for electroweakinos/sleptons at the LHC and muon g-2 measurement. Differently from previous studies in which the constraints from LHC were implemented by requiring the SUSY signal events in an individual signal region, we combine the results of all relevant electroweakino searches performed by the CMS, especially the "$1\ell 2b$" search. Such combination increases the bound on the Higgsino mass parameter to $|\mu| > 390$ GeV, which is about 80 GeV stricter than the bound obtained from individual analyses.

With such improvement, we find that in a simplified model the Z funnel region is on the brink of complete exclusion, the h funnel of $\mu < 0$ only survives if $\tan\beta < 7.4$, and the h funnel region of $\mu > 0$ is the main surviving region:

1. Z funnel region, $m_{\tilde{\chi}_1^0} \in [42.5, 45.8]$ GeV, $\mu \in [388, 484]$ GeV;
2. Z funnel region, $m_{\tilde{\chi}_1^0} \in [42.5, 45.8]$ GeV, $\mu \in [-388, -486]$ GeV;
3. h funnel region, $m_{\tilde{\chi}_1^0} \in [59.4, 63.4]$ GeV, $\mu \in [-386, -1089]$ GeV, $\tan\beta \in [5, 7.4]$;
4. h funnel region, $m_{\tilde{\chi}_1^0} \in [58.4, 63.6]$ GeV, $\mu \in [386, 1444]$ GeV.

They can be entirely detected by LZ, while regions 1 and 2, and most of the parameter space in region 3 and 4 can be excluded by the HL-LHC.

In the popular pMSSM, the surviving parameter space becomes smaller due to other constraints. Especially, the light sleptons required by the muon anomalous magnetic moment will accelerate the exclusion of Z/h funnel region at the LHC. Only a tiny part of the parameter space can survive the current experimental constraints. Though the modest excesses in recent electroweakino searches prefer light electroweakino, the Z/h funnel region in MSSM is not an ideal interpretation; this is particularly true in view of a plausible improvement of the bounds on $\sigma^{\mathrm{SI}}_{\tilde{\chi}_1^0 n}$ expected by the on-going DM direct detection experiments, or also in view of the increase of the limits on slepton and electroweakino in non-compressed region by the forthcoming LHC 80 fb^{-1} results.

Acknowledgements

We thank Csaba Balazs for useful comments on the draft. This research was supported by the ARC Centre of Excellence for Particle Physics at the Tera-scale, under the grant CE110001004.

References

[1] J. Abdallah, et al., DELPHI, Eur. Phys. J. C 38 (2005) 395, arXiv:hep-ex/0406019 [hep-ex].
[2] M. Aaboud, et al., ATLAS, J. High Energy Phys. 01 (2018) 126, arXiv:1711.03301 [hep-ex].
[3] A.M. Sirunyan, et al., CMS, J. High Energy Phys. 07 (2017) 014, arXiv:1703.01651 [hep-ex].
[4] E. Aprile, et al., XENON, Eur. Phys. J. C 77 (2017) 881, arXiv:1708.07051 [astro-ph.IM].
[5] D.S. Akerib, et al., LUX, Phys. Rev. D 93 (2016) 072009, arXiv:1512.03133 [physics.ins-det].
[6] X. Cui, et al., PandaX-II, Phys. Rev. Lett. 119 (2017) 181302, arXiv:1708.06917 [astro-ph.CO].
[7] M. Aguilar, et al., AMS, Phys. Rev. Lett. 110 (2013) 141102.
[8] M. Ackermann, et al., Fermi-LAT, Phys. Rev. Lett. 115 (2015) 231301, arXiv:1503.02641 [astro-ph.HE].
[9] J. Chang, et al., DAMPE, Astropart. Phys. 95 (2017) 6, arXiv:1706.08453 [astro-ph.IM].
[10] P. Athron, et al., GAMBIT, Eur. Phys. J. C 77 (2017) 879, arXiv:1705.07917 [hep-ph].
[11] E. Bagnaschi, et al., Eur. Phys. J. C 78 (2018) 256, arXiv:1710.11091 [hep-ph].
[12] G. Aad, et al., ATLAS, J. High Energy Phys. 10 (2015) 134, arXiv:1508.06608 [hep-ex].
[13] P. Athron, et al., GAMBIT, Eur. Phys. J. C 77 (2017) 824, arXiv:1705.07935 [hep-ph].
[14] P. Athron, GAMBIT, in: 5th Large Hadron Collider Physics Conference (LHCP 2017), Shanghai, China, May 15–20, 2017, 2017, arXiv:1708.07594 [hep-ph].
[15] P. Athron, et al., GAMBIT, Eur. Phys. J. C 77 (2017) 784, Addendum: Eur. Phys. J. C 78 (2) (2018) 98, arXiv:1705.07908 [hep-ph].
[16] M.A. Ajaib, I. Gogoladze, arXiv:1710.07842 [hep-ph], 2017.
[17] C. Han, K.-i. Hikasa, L. Wu, J.M. Yang, Y. Zhang, Phys. Lett. B 769 (2017) 470, arXiv:1612.02296 [hep-ph].
[18] P. Bechtle, et al., Eur. Phys. J. C 76 (2016) 96, arXiv:1508.05951 [hep-ph].
[19] E.A. Bagnaschi, et al., Eur. Phys. J. C 75 (2015) 500, arXiv:1508.01173 [hep-ph].
[20] C. Balazs, A. Buckley, D. Carter, B. Farmer, M. White, Eur. Phys. J. C 73 (2013) 2563, arXiv:1205.1568 [hep-ph].
[21] A. Fowlie, M. Kazana, K. Kowalska, S. Munir, L. Roszkowski, E.M. Sessolo, S. Trojanowski, Y.-L.S. Tsai, Phys. Rev. D 86 (2012) 075010, arXiv:1206.0264 [hep-ph].
[22] O. Buchmueller, et al., Eur. Phys. J. C 72 (2012) 2243, arXiv:1207.7315 [hep-ph].
[23] C. Strege, G. Bertone, F. Feroz, M. Fornasa, R. Ruiz de Austri, R. Trotta, J. Cosmol. Astropart. Phys. 1304 (2013) 013, arXiv:1212.2636 [hep-ph].
[24] M. Citron, J. Ellis, F. Luo, J. Marrouche, K.A. Olive, K.J. de Vries, Phys. Rev. D 87 (2013) 036012, arXiv:1212.2886 [hep-ph].
[25] N. Bornhauser, M. Drees, Phys. Rev. D 88 (2013) 075016, arXiv:1307.3383 [hep-ph].
[26] S. Henrot-Versillé, R. Lafaye, T. Plehn, M. Rauch, D. Zerwas, S. Plaszczynski, B. Rouillé d'Orfeuil, M. Spinelli, Phys. Rev. D 89 (2014) 055017, arXiv:1309.6958 [hep-ph].
[27] P. Bechtle, et al., in: Proceedings, 2013 European Physical Society Conference on High Energy Physics (EPS-HEP 2013), Stockholm, Sweden, July 18–24, 2013, in: PoS, vol. EPS-HEP2013, 2013, p. 313, arXiv:1310.3045 [hep-ph].
[28] O. Buchmueller, et al., Eur. Phys. J. C 74 (2014) 2922, arXiv:1312.5250 [hep-ph].
[29] J. Ellis, Eur. Phys. J. C 74 (2014) 2732, arXiv:1312.5426 [hep-ph].
[30] P. Bechtle, et al., in: Proceedings, 37th International Conference on High Energy Physics (ICHEP 2014), Valencia, Spain, July 2–9, 2014, Nucl. Part. Phys. Proc. 273–275 (2016) 589, arXiv:1410.6035 [hep-ph].
[31] P. Bechtle, et al., J. High Energy Phys. 06 (2012) 098, arXiv:1204.4199 [hep-ph].
[32] M. Aaboud, et al., ATLAS, arXiv:1806.02293 [hep-ex], 2018.
[33] M. Aaboud, et al., ATLAS, Phys. Rev. D 98 (2018) 032009, arXiv:1804.03602 [hep-ex].
[34] A.M. Sirunyan, et al., CMS, J. High Energy Phys. 03 (2018) 076, arXiv:1709.08908 [hep-ex].
[35] A. Kvellestad, GAMBIT, in: 39th International Conference on High Energy Physics (ICHEP 2018), Seoul, Gangnam-Gu, Korea, Republic of, July 4–11, 2018, 2018, arXiv:1807.03208 [hep-ph].
[36] P. Athron, et al., GAMBIT, arXiv:1809.02097 [hep-ph], 2018.
[37] H. Baer, V. Barger, P. Huang, A. Mustafayev, X. Tata, Phys. Rev. Lett. 109 (2012) 161802, arXiv:1207.3343 [hep-ph].
[38] M. Abdughani, L. Wu, J.M. Yang, Eur. Phys. J. C 78 (2018) 4, arXiv:1705.09164 [hep-ph].
[39] J. Cao, Y. He, L. Shang, W. Su, Y. Zhang, J. High Energy Phys. 08 (2016) 037, arXiv:1606.04416 [hep-ph].
[40] J. Cao, Y. He, L. Shang, W. Su, P. Wu, Y. Zhang, J. High Energy Phys. 10 (2016) 136, arXiv:1609.00204 [hep-ph].
[41] U. Ellwanger, J. High Energy Phys. 02 (2017) 051, arXiv:1612.06574 [hep-ph].
[42] M. Aaboud, et al., ATLAS, arXiv:1712.02332 [hep-ex], 2017.
[43] T. Han, F. Kling, S. Su, Y. Wu, J. High Energy Phys. 02 (2017) 057, arXiv:1612.02387 [hep-ph].
[44] L. Calibbi, J.M. Lindert, T. Ota, Y. Takanishi, J. High Energy Phys. 11 (2014) 106, arXiv:1410.5730 [hep-ph].
[45] M. van Beekveld, W. Beenakker, S. Caron, R. Peeters, R. Ruiz de Austri, Phys. Rev. D 96 (2017) 035015, arXiv:1612.06333 [hep-ph].
[46] A. Achterberg, S. Amoroso, S. Caron, L. Hendriks, R. Ruiz de Austri, C. Weniger, J. Cosmol. Astropart. Phys. 1508 (2015) 006, arXiv:1502.05703 [hep-ph].
[47] R.K. Barman, G. Belanger, B. Bhattacherjee, R. Godbole, G. Mendiratta, D. Sengupta, Phys. Rev. D 95 (2017) 095018, arXiv:1703.03838 [hep-ph].
[48] J. Bramante, N. Desai, P. Fox, A. Martin, B. Ostdiek, T. Plehn, Phys. Rev. D 93 (2016) 063525, arXiv:1510.03460 [hep-ph].

[49] M. Chakraborti, A. Datta, N. Ganguly, S. Poddar, J. High Energy Phys. 11 (2017) 117, arXiv:1707.04410 [hep-ph].
[50] M. Badziak, M. Olechowski, P. Szczerbiak, J. High Energy Phys. 07 (2017) 050, arXiv:1705.00227 [hep-ph].
[51] T. Han, S. Padhi, S. Su, Phys. Rev. D 88 (2013) 115010, arXiv:1309.5966 [hep-ph].
[52] M. Badziak, M. Olechowski, P. Szczerbiak, J. High Energy Phys. 03 (2016) 179, arXiv:1512.02472 [hep-ph].
[53] A. Choudhury, S. Rao, L. Roszkowski, Phys. Rev. D 96 (2017) 075046, arXiv:1708.05675 [hep-ph].
[54] M. Chakraborti, U. Chattopadhyay, S. Poddar, J. High Energy Phys. 09 (2017) 064, arXiv:1702.03954 [hep-ph].
[55] A. Kobakhidze, M. Talia, L. Wu, Phys. Rev. D 95 (2017) 055023, arXiv:1608.03641 [hep-ph].
[56] A. Choudhury, S. Mondal, Phys. Rev. D 94 (2016) 055024, arXiv:1603.05502 [hep-ph].
[57] M. van Beekveld, W. Beenakker, S. Caron, R. Ruiz de Austri, J. High Energy Phys. 04 (2016) 154, arXiv:1602.00590 [hep-ph].
[58] S. Profumo, T. Stefaniak, L. Stephenson Haskins, Phys. Rev. D 96 (2017) 055018, arXiv:1706.08537 [hep-ph].
[59] L. Calibbi, T. Ota, Y. Takanishi, J. High Energy Phys. 07 (2011) 013, arXiv:1104.1134 [hep-ph].
[60] G. Belanger, F. Boudjema, A. Cottrant, R.M. Godbole, A. Semenov, Phys. Lett. B 519 (2001) 93, arXiv:hep-ph/0106275 [hep-ph].
[61] T. Han, Z. Liu, A. Natarajan, J. High Energy Phys. 11 (2013) 008, arXiv:1303.3040 [hep-ph].
[62] Q.-F. Xiang, X.-J. Bi, P.-F. Yin, Z.-H. Yu, Phys. Rev. D 94 (2016) 055031, arXiv:1606.02149 [hep-ph].
[63] K. Hamaguchi, K. Ishikawa, Phys. Rev. D 93 (2016) 055009, arXiv:1510.05378 [hep-ph].
[64] C. Han, Int. J. Mod. Phys. A 32 (2017) 1745003, arXiv:1409.7000 [hep-ph].
[65] E. Bernreuther, J. Horak, T. Plehn, A. Butter, arXiv:1805.11637 [hep-ph], 2018.
[66] C. Arina, M. Chala, V. Martin-Lozano, G. Nardini, J. High Energy Phys. 12 (2016) 149, arXiv:1610.03822 [hep-ph].
[67] T.A.W. Martin, D. Morrissey, J. High Energy Phys. 12 (2014) 168, arXiv:1409.6322 [hep-ph].
[68] D. Barducci, A. Belyaev, A.K.M. Bharucha, W. Porod, V. Sanz, J. High Energy Phys. 07 (2015) 066, arXiv:1504.02472 [hep-ph].
[69] G. Aad, et al., ATLAS, J. High Energy Phys. 04 (2014) 169, arXiv:1402.7029 [hep-ex].
[70] Search for Supersymmetry at the High Luminosity LHC with the ATLAS Experiment, Tech. Rep. ATL-PHYS-PUB-2014-010, CERN, Geneva, 2014.
[71] Prospect for a Search for Direct Pair Production of a Chargino and a Neutralino Decaying Via a W Boson and the Lightest Higgs Boson in Final States with One Lepton, Two B-Jets and Missing Transverse Momentum at the High Luminosity LHC with the ATLAS Detector, Tech. Rep. ATL-PHYS-PUB-2015-032, CERN, Geneva, 2015.
[72] A.M. Sirunyan, et al., CMS, arXiv:1801.03957 [hep-ex], 2018.
[73] A.M. Sirunyan, et al., CMS, arXiv:1709.05406 [hep-ex], 2017.
[74] A.M. Sirunyan, et al., CMS, J. High Energy Phys. 11 (2017) 029, arXiv:1706.09933 [hep-ex].
[75] Lepsusywg, aleph, delphi, l3 and opal experiments, note lepsusywg/02-04.1, note lepsusywg/01-03.1, http://lepsusy.web.cern.ch/lepsusy.
[76] J. Cao, Y. He, L. Shang, W. Su, Y. Zhang, J. High Energy Phys. 03 (2016) 207, arXiv:1511.05386 [hep-ph].
[77] G. Aad, et al., CMS, ATLAS, Phys. Rev. Lett. 114 (2015) 191803, arXiv:1503.07589 [hep-ex].
[78] A. Djouadi, M.M. Muhlleitner, M. Spira, Physics at LHC, in: Proceedings, 3rd Conference, Cracow, Poland, July 3–8, 2006, Acta Phys. Pol. B 38 (2007) 635, arXiv:hep-ph/0609292 [hep-ph].
[79] A. Djouadi, J.-L. Kneur, G. Moultaka, Comput. Phys. Commun. 176 (2007) 426, arXiv:hep-ph/0211331 [hep-ph].
[80] M. Muhlleitner, Linear colliders, in: Proceedings, International Conference, LCWS 2004, Paris, France, April 19–23, 2004, Acta Phys. Pol. B 35 (2004) 2753, hep-ph/0409200 [hep-ph].
[81] A. Djouadi, J. Kalinowski, M. Spira, Comput. Phys. Commun. 108 (1998) 56, arXiv:hep-ph/9704448 [hep-ph].
[82] G. Belanger, F. Boudjema, A. Pukhov, A. Semenov, Comput. Phys. Commun. 149 (2002) 103, arXiv:hep-ph/0112278 [hep-ph].
[83] D. Barducci, G. Belanger, J. Bernon, F. Boudjema, J. Da Silva, S. Kraml, U. Laa, A. Pukhov, arXiv:1606.03834 [hep-ph], 2016.
[84] P.A.R. Ade, et al., Planck, Astron. Astrophys. 594 (2016) A13, arXiv:1502.01589 [astro-ph.CO].
[85] J. Dunkley, et al., WMAP, Astrophys. J. Suppl. 180 (2009) 306, arXiv:0803.0586 [astro-ph].
[86] C. Cheung, L.J. Hall, D. Pinner, J.T. Ruderman, J. High Energy Phys. 05 (2013) 100, arXiv:1211.4873 [hep-ph].
[87] P. Huang, C.E.M. Wagner, Phys. Rev. D 90 (2014) 015018, arXiv:1404.0392 [hep-ph].
[88] M. Badziak, M. Olechowski, P. Szczerbiak, in: Proceedings, 18th International Conference from the Planck Scale to the Electroweak Scale (Planck 2015), Ioannina, Greece, May 25–29, 2015, PoS PLANCK2015 (2015) 130, arXiv:1601.00768 [hep-ph].
[89] D.S. Akerib, et al., LUX, Phys. Rev. Lett. 118 (2017) 021303, arXiv:1608.07648 [astro-ph.CO].
[90] E. Aprile, et al., XENON, Phys. Rev. Lett. 119 (2017) 181301, arXiv:1705.06655 [astro-ph.CO].
[91] C. Fu, et al., PandaX-II, Erratum, Phys. Rev. Lett. 118 (2017) 071301, Phys. Rev. Lett. 120 (4) (2018) 049902, arXiv:1611.06553 [hep-ex].
[92] E. Aprile, et al., XENON100, Phys. Rev. D 94 (2016) 122001, arXiv:1609.06154 [astro-ph.CO].
[93] D.S. Akerib, et al., LUX, Phys. Rev. Lett. 118 (2017) 251302, arXiv:1705.03380 [astro-ph.CO].
[94] XENON1T, https://science.purdue.edu/xenon1t/?p=1080.
[95] C. Amole, et al., PICO, Phys. Rev. Lett. 118 (2017) 251301, arXiv:1702.07666 [astro-ph.CO].
[96] D.S. Akerib, et al., LUX-ZEPLIN, arXiv:1802.06039 [astro-ph.IM], 2018.
[97] C. Patrignani, et al., Particle Data Group, Chin. Phys. C 40 (2016) 100001.
[98] G. Aad, et al., ATLAS, J. High Energy Phys. 11 (2015) 206, arXiv:1509.00672 [hep-ex].
[99] V. Khachatryan, et al., CMS, J. High Energy Phys. 02 (2017) 135, arXiv:1610.09218 [hep-ex].
[100] Search for Invisible Decays of the Higgs Boson Produced Through Vector Boson Fusion at $\sqrt{s} = 13$ TeV, Tech. Rep. CMS-PAS-HIG-17-023, CERN, Geneva, 2018.
[101] D.M. Asner, et al., in: Proceedings, 2013 Community Summer Study on the Future of U.S. Particle Physics: Snowmass on the Mississippi (CSS2013), Minneapolis, MN, USA, July 29-August 6, 2013, 2013, arXiv:1310.0763 [hep-ph].
[102] M. Aaboud, et al., ATLAS, arXiv:1803.02762 [hep-ex], 2018.
[103] M. Aaboud, et al., ATLAS, arXiv:1802.03158 [hep-ex], 2018.
[104] M. Aaboud, et al., ATLAS, Phys. Rev. D 97 (2018) 052010, arXiv:1712.08119 [hep-ex].
[105] M. Aaboud, et al., ATLAS, arXiv:1712.02118 [hep-ex], 2017.
[106] M. Aaboud, et al., ATLAS, Eur. Phys. J. C 78 (2018) 154, arXiv:1708.07875 [hep-ex].
[107] A.M. Sirunyan, et al., CMS, Phys. Rev. D 97 (2018) 032007, arXiv:1709.04896 [hep-ex].
[108] A.M. Sirunyan, et al., CMS, Phys. Lett. B 779 (2018) 166, arXiv:1709.00384 [hep-ex].
[109] A.M. Sirunyan, et al., CMS, arXiv:1801.01846 [hep-ex], 2018.
[110] J. Alwall, R. Frederix, S. Frixione, V. Hirschi, F. Maltoni, O. Mattelaer, H.S. Shao, T. Stelzer, P. Torrielli, M. Zaro, J. High Energy Phys. 07 (2014) 079, arXiv:1405.0301 [hep-ph].
[111] P. Torrielli, S. Frixione, J. High Energy Phys. 04 (2010) 110, arXiv:1002.4293 [hep-ph].
[112] W. Beenakker, R. Hopker, M. Spira, arXiv:hep-ph/9611232 [hep-ph], 1996.
[113] D. Dercks, N. Desai, J.S. Kim, K. Rolbiecki, J. Tattersall, T. Weber, Comput. Phys. Commun. 221 (2017) 383, arXiv:1611.09856 [hep-ph].
[114] J. de Favereau, C. Delaere, P. Demin, A. Giammanco, V. Lemaître, A. Mertens, M. Selvaggi, DELPHES 3, J. High Energy Phys. 02 (2014) 057, arXiv:1307.6346 [hep-ex].
[115] C.G. Lester, B. Nachman, J. High Energy Phys. 03 (2015) 100, arXiv:1411.4312 [hep-ph].
[116] C.G. Lester, D.J. Summers, Phys. Lett. B 463 (1999) 99, arXiv:hep-ph/9906349 [hep-ph].
[117] A.L. Read, J. Phys. G, Nucl. Part. Phys. 28 (2002) 2693.
[118] G. Schott, RooStats Team, in: Proceedings, PHYSTAT 2011 Workshop on Statistical Issues Related to Discovery Claims in Search Experiments and Unfolding, CERN, Geneva, Switzerland 17-20 January 2011, CERN, Geneva, 2011, pp. 199–208, arXiv:1203.1547 [physics.data-an].
[119] J.A. Casas, J.M. Moreno, K. Rolbiecki, B. Zaldivar, J. High Energy Phys. 09 (2013) 099, arXiv:1305.3274 [hep-ph].
[120] C. Arina, V. Martin-Lozano, G. Nardini, J. High Energy Phys. 08 (2014) 015, arXiv:1403.6434 [hep-ph].
[121] G.W. Bennett, et al., Muon g-2, Phys. Rev. D 73 (2006) 072003, arXiv:hep-ex/0602035 [hep-ex].
[122] M. Davier, A. Hoecker, B. Malaescu, Z. Zhang, Eur. Phys. J. C 71 (2011) 1515, Erratum: Eur. Phys. J. C 72 (2012) 1874, arXiv:1010.4180 [hep-ph].
[123] P. Bechtle, O. Brein, S. Heinemeyer, O. Stål, T. Stefaniak, G. Weiglein, K.E. Williams, Eur. Phys. J. C 74 (2014) 2693, arXiv:1311.0055 [hep-ph].
[124] P. Bechtle, S. Heinemeyer, O. Stål, T. Stefaniak, G. Weiglein, Eur. Phys. J. C 74 (2014) 2711, arXiv:1305.1933 [hep-ph].
[125] G. Aad, et al., ATLAS, J. High Energy Phys. 05 (2014) 071, arXiv:1403.5294 [hep-ex].
[126] A.M. Sirunyan, et al., CMS, Phys. Lett. B (2019), https://doi.org/10.1016/j.physletb.2019.01.005, arXiv:1806.05264 [hep-ex].
[127] P. Cox, C. Han, T.T. Yanagida, arXiv:1805.02802 [hep-ph], 2018.

Chapter 6

Electroweak phase transition in the NMSSM

As we have seen in the previous chapter 4, the baryon asymmetry of the universe is one of the main problems in physics whose explanation requires BSM physics. The NMSSM, studied in sec. 3.8, provides a SUSY model in which EWBG, can generate the amount of matter that we observe in the Universe, see sec. 4.2. The NMSSM includes all the particles of the MSSM plus a scalar singlet S, see tab. 3.2. The presence of the singlet is fundamental because it introduces cubic terms, see Eq. (4.23), that contribute at tree level to the potential barrier of the first order phase transition, see fig. 4.2b, boosting the asymmetry parameter Y_B to have the measured value (4.4)-(4.5).

In the following published work, we study phase transitions, see sec. 4.3 and 4.7, that are compatible with the currently observed characteristics of the Universe. For this study, we considered the Higgs sector, described in sec. 3.8.2. To make gauge independent calculations, we used the R_ξ gauges described in sec. 2.4.3. To make precise calculation we used the two Higgs doublet model with a scalar singlet (THDMS) that is a model which can be an effective field theory of the NMSSM at low energies. Finally, we utilised a perturbative approach with Coleman-Weinberg corrections, one-loop thermal corrections and daisy terms as described in sec. 4.8.

6.1 Published material

JHEP

Published for SISSA by Springer

Received: September 5, 2019
Revised: October 24, 2019
Accepted: November 10, 2019
Published: November 26, 2019

Strong first-order phase transitions in the NMSSM — a comprehensive survey

Peter Athron,[a] **Csaba Balazs,**[a] **Andrew Fowlie,**[a,b] **Giancarlo Pozzo,**[a] **Graham White**[c] **and Yang Zhang**[a]

[a] *ARC Centre of Excellence for Particle Physics at the Terascale, School of Physics and Astronomy, Monash University, Victoria 3800, Australia*

[b] *Department of Physics and Institute of Theoretical Physics, Nanjing Normal University, Nanjing, 210023, China*

[c] *TRIUMF, 4004 Wesbrook Mall, Vancouver, British Columbia V6T 2A3, Canada*

E-mail: peter.athron@coepp.org.au, csaba.balazs@monash.edu, andrew.j.fowlie@qq.com, giancarlo.pozzo@monash.edu, gwhite@triumf.ca, yang.zhang@monash.edu

Abstract: Motivated by the fact that the Next-to-Minimal Supersymmetric Standard Model is one of the most plausible models that can accommodate electroweak baryogenesis, we analyze its phase structure by tracing the temperature dependence of the minima of the effective potential. Our results reveal rich patterns of phase structure that end in the observed electroweak symmetry breaking vacuum. We classify these patterns according to the first transition in their history and show the strong first-order phase transitions that may be possible in each type of pattern. These could allow for the generation of the matter-antimatter asymmetry or potentially observable gravitational waves. For a selection of benchmark points, we checked that the phase transitions completed and calculated the nucleation temperatures. We furthermore present samples that feature strong first-order phase transitions from an extensive scan of the whole parameter space. We highlight common features of our samples, including the fact that the Standard Model like Higgs is often not the lightest Higgs in the model.

Keywords: Supersymmetry Phenomenology

ArXiv ePrint: 1908.11847

https://doi.org/10.1007/JHEP11(2019)151

JHEP11(2019)151

Contents

1 Introduction **1**

2 NMSSM **3**
2.1 Matching to the THDMS 4

3 Effective potential **5**
3.1 Effective potential at zero temperature 5
3.2 Effective potential at finite temperature 7

4 First-order phase transitions **8**

5 Results **10**
5.1 Parameter space, constraints and sampling strategy 10
5.2 Classification of phase transitions 12
5.3 Benchmark points 13
5.4 Reaching the observed SM vacuum 16
5.4.1 The strongest FOPT ends in the SM vacuum 16
5.4.2 The strongest FOPT does not end in the SM vacuum 21
5.5 Properties of the Higgs bosons 27

6 Conclusions **28**

A Field dependent masses **30**

B Numerical methods for FOPTs **32**

JHEP11(2019)151

1 Introduction

One of the enduring problems in modern physics is the origin of the baryon asymmetry of the Universe (BAU) [1–3]. This asymmetry cannot be an initial condition in any cosmology that includes inflation, as that would wash out any initial asymmetry.[1] Therefore baryon asymmetry must be produced; however, as yet there is no experimental confirmation of any production mechanism. Any mechanism that produces the BAU must satisfy three criteria [5]:

1. charge (C) and charge-parity (CP) violation,
2. baryon number (B) violation, and
3. departure from equilibrium.

[1] For an exception to this rule of thumb see ref. [4].

The Standard Model (SM) has the ingredients to satisfy all three criteria: there is a CP violating phase in the CKM matrix, B is violated through sphalerons which are unsuppressed at high temperature and there could be departures from equilibrium following two phase transitions (PTs) that occur in the SM vacuum as it cools — the electroweak (EW) and the QCD transition. Quantitatively, however, the CP violating phase in the CKM matrix is far too feeble to produce enough baryon asymmetry. Furthermore the two transitions that occur in the SM at high temperature are both crossover transitions rather than first-order phase transitions (FOPTs) and therefore do not provide a large enough departure from equilibrium (see e.g., ref. [6]). As such one has to look beyond the SM for explanations.

While the origin of the baryon asymmetry is a mystery, its measurement is on a firm foundation. During big bang nucleosynthesis, the baryon asymmetry is an input to the set of Boltzmann equations that govern the production of primordial light elements. Since we can measure some of these primordial abundances (deuterium in particular) with high accuracy, this constrains the baryon asymmetry[2] to be [7]

$$Y_B \equiv \frac{n_B}{s} = 8.2 - 9.4 \times 10^{-11} \text{ (95\% CL)}. \tag{1.1}$$

Furthermore the baryon asymmetry produces acoustic oscillations in the power spectrum of the cosmic microwave background (CMB) [8]. Observing these oscillations gives an even tighter bound on the BAU,

$$Y_B = 8.65 \pm 0.09 \times 10^{-11}. \tag{1.2}$$

The fact that there is a concordance between these two unrelated measurement approaches is a triumph of cosmology. Along with dark matter and inflation, the origin of the BAU is a powerful cosmological argument for physics beyond the SM.

Electroweak baryogenesis is a minimal and natural explanation for the origin of the baryon asymmetry in the Universe [3, 9–44]. It utilizes the electroweak phase transition (EWPT) which is known to have occurred in our cosmic history providing the reheating temperature was not unnaturally small. Although this transition is a crossover in the SM, its character may be modified by the introduction of new weak scale bosons such that the transition becomes a strongly FOPT (SFOPT) and proceeds by bubble nucleation. Such a phenomenon is all the more interesting because it might directly be probed by future gravitational wave detectors [45–50].

This mechanism can be in principle realized within supersymmetry. In the Minimal Supersymmetric Standard Model (MSSM) a barrier between the EW symmetric and broken vacuums arises from thermal corrections from stops; however, one requires light stops to catalyze the PT such that it is sufficiently strongly first order [51, 52]. This is all but ruled out by LHC constraints on stop masses [53]. Much more attractive is the possibility of the Next-to-Minimal Supersymmetric Standard Model (NMSSM) [54, 55] where a light singlet scalar can catalyze a strongly first order EWPT [16, 25, 56]. Unlike the stop which catalyzes the PT through thermal effects, the singlet can change the potential such that there is a barrier even at zero temperature.

[2]We convert measurements of the photon-baryon ratio to Y_B by ref. [2]

$$Y_B \equiv \frac{n_B}{s} \approx \frac{1}{7.04}\frac{n_B}{n_\gamma}.$$

JHEP11(2019)151

Electroweak baryogenesis was recently considered within the NMSSM [15, 57–61] and it was found that the baryon asymmetry can vary by an order of magnitude depending on whether the singlet acquires a vacuum expectation value (VEV) before or during the EWPT (with a simultaneous transition providing more efficient baryon production) [59]. Furthermore the baryon yield is proportional to the maximal variation of the ratio of the two Higgs VEVs, $\Delta\beta$, and it was shown in refs. [15, 30, 62–65] that $\Delta\beta$ can be an order of magnitude larger in the NMSSM compared to the MSSM.

In this work we explore the plausibility of EW baryogenesis within the NMSSM, focusing on the PT and leaving CP violation to future work (see [57, 66–78] for various approaches to generating CP violation). We consider the case where the superpartners are all heavy enough to have their thermal contributions Boltzmann suppressed during the transition. Thus we can match our model to a two Higgs doublet model plus a singlet (THDMS). We sample the parameter space to find points with an EW SFOPT. For such points, we investigate the phase structure, that is the evolution of the minima of the effective potential as the Universe cools. This investigation includes determining whether the singlet acquires a VEV during or before the EWPT and it also involves calculating the strength of the PT.

As we focus on the third Sakharov condition (a departure from thermal equilibrium), we do not consider explicit or spontaneous CP violation in the Higgs sector. We instead assume that CP violation enters the Higgs sector radiatively, though remain agnostic about the exact source of CP violation and do not examine constraints on complex phases (such as electric dipole moments). This simplification allows us to focus only on PTs between the ground states of CP-even fields, easing the numerical problem of finding vacua of a multifield scalar potential.

The structure of this paper is as follows. In section 2 we introduce the NMSSM and the THDMS, fixing the notation we will use in the paper. Following this, in section 3 we describe the radiative and finite temperature corrections that we include in our analysis. Then in section 4 we outline the procedure we use to determine if a point in the parameter space has a FOPT or not, and if so calculate the critical temperature and transition strength. The results of our scan are presented in section 5 and finally our conclusions are given in section 6.

2 NMSSM

The NMSSM extends the MSSM particle content by adding one singlet superfield, $\hat{S}$. Here we work in the $\mathbb{Z}_3$ symmetric NMSSM where the μ-term of the MSSM is forbidden and instead an effective μ-term, $\mu_{\text{eff}} = \lambda\langle S\rangle$, is generated when the singlet develops a VEV, thus solving the μ-problem of the MSSM. The superpotential is given by

$$\mathcal{W}_{\text{NMSSM}} = (Y_u)_{ij}\,\hat{Q}_i\cdot\hat{H}_u\,\hat{u}^c_j + (Y_d)_{ij}\,\hat{Q}_i\cdot\hat{H}_d\,\hat{d}^c_j + (Y_e)_{ij}\,\hat{L}_i\cdot\hat{H}_d\,\hat{e}^c_j, + \lambda\,\hat{S}\,\hat{H}_u\cdot\hat{H}_d + \frac{1}{3}\kappa\,\hat{S}^3, \quad (2.1)$$

where a hat is used for superfields, $i, j \in \{1, 2, 3\}$ are family indices, and we have introduced the $\text{SU}(2)_L$ dot product, $A\cdot B = A^1B^2 - A^2B^1$. The discrete $\mathbb{Z}_3$ symmetry is spontaneously

JHEP11(2019)151

broken when the Higgs fields or singlet obtain a VEV. We assume that following the strategies of refs. [79–81] domain wall problems can in principle be avoided without impacting any phenomenology.

Under the SM gauge group $G_{\rm SM} = {\rm SU}(3)_C \times {\rm SU}(2)_L \times {\rm U}(1)_Y$ the superfields transform as

$$\begin{aligned} &\hat{Q} : (\mathbf{3}, \mathbf{2}, \tfrac{1}{6}), \quad \hat{u}^c : (\bar{\mathbf{3}}, \mathbf{1}, -\tfrac{2}{3}), \quad \hat{d}^c : (\bar{\mathbf{3}}, \mathbf{1}, \tfrac{1}{3}), \quad \hat{L} : (\mathbf{1}, \mathbf{2}, -\tfrac{1}{2}), \quad \hat{e}^c : (\mathbf{1}, \mathbf{1}, 1), \\ &\hat{H}_d : (\mathbf{1}, \mathbf{2}, -\tfrac{1}{2}), \quad \hat{H}_u : (\mathbf{1}, \mathbf{2}, \tfrac{1}{2}), \quad \hat{S} : (\mathbf{1}, \mathbf{1}, 0) \end{aligned} \tag{2.2}$$

where the first two entries inside the parentheses give the representation under $\mathrm{SU}(3)_C$ and $\mathrm{SU}(2)_L$, respectively, while the third entry gives the $\mathrm{U}(1)_Y$ hypercharges without GUT normalization.

There are three contributions to the tree-level Higgs potential of the NMSSM:

$$V_{\rm NMSSM} = V_F + V_D + V_{\rm soft}. \tag{2.3}$$

Here the F- and D-term contributions are

$$V_F = |\lambda S|^2 \left(|H_u|^2 + |H_d|^2\right) + \left|\lambda H_u \cdot H_d + \kappa S^2\right|^2, \tag{2.4}$$

$$V_D = \frac{1}{8}(g^2 + g'^2)(|H_u|^2 - |H_d|^2)^2 + \frac{1}{2}g^2|H_u^\dagger H_d|^2, \tag{2.5}$$

where g and g' are respectively the $\mathrm{SU}(2)_L$ and $\mathrm{U}(1)_Y$ gauge couplings without GUT normalization. Finally, the soft-breaking terms are

$$V_{\rm soft} = m_{H_u}^2|H_u|^2 + m_{H_d}^2|H_d|^2 + m_S^2|S|^2 + \left[\lambda A_\lambda S H_u \cdot H_d + \frac{1}{3}\kappa A_\kappa S^3 + \text{h.c.}\right]. \tag{2.6}$$

The couplings λ and κ and the corresponding trilinears, A_λ and A_κ, are in general complex. Three of the four phases, however, may be removed through field redefinitions of H_u, H_d and S. Since current LHC limits and the 125 GeV Higgs mass measurements require squarks and gluinos to be TeV-scale, the mass spectrum of the NMSSM must contain a large hierarchy between the SM particles and colored sparticles. Furthermore the states with the largest couplings include both heavy sparticles and light SM particles, i.e., stops and the top quark. Therefore higher-order corrections will always include large logarithms since one cannot choose the renormalization scale Q to simultaneously minimize $\ln m_t/Q$ and $\ln M_{\rm SUSY}/Q$. This makes it challenging to perform precise calculations when working in the full theory. To improve the precision of our calculations we will integrate out the heavy superpartners and use an effective field theory (EFT) which contains only the light states. This makes it possible run to $Q = m_t$ and perform calculations in the EFT which are free from large logarithms.

2.1 Matching to the THDMS

Since we want to consider scenarios in which all superpartners are too heavy to impact the PT, we match the NMSSM to a two Higgs doublet model plus a singlet (THDMS), which in this context is an effective field theory of the full NMSSM theory valid below $M_{\rm SUSY}$.[3]

[3]This is also the approach taken in refs. [15, 82–84].

JHEP11(2019)151

The tree-level potential of a $\mathbb{Z}_3$ symmetric THDMS model is

$$\begin{aligned} V^{\text{tree}}_{\text{THDMS}} = &\frac{1}{2}\lambda_1|H_d|^4+\frac{1}{2}\lambda_2|H_u|^4+(\lambda_3+\lambda_4)|H_u|^2|H_d|^2-\lambda_4|H_u^\dagger H_d|^2 \\ &+\lambda_5|S|^2|H_d|^2+\lambda_6|S|^2|H_u|^2+(\lambda_7 S^{*2}H_d\cdot H_u+\text{h.c.})+\lambda_8|S|^4 \\ &+m_1^2|H_d|^2+m_2^2|H_u|^2+m_3^2|S|^2-(m_4 S H_d\cdot H_u+\text{h.c.})-\frac{1}{3}(m_5 S^3+\text{h.c.}), \end{aligned} \tag{2.7}$$

where the couplings λ_7, m_4 and m_5 may be complex. Two of the three phases, however, may be removed by redefinitions of H_u, H_d and S, leaving a single complex phase, as in the NMSSM. In (2.7) we follow the conventions in refs. [15, 82–84]; in particular the $|H_u|^2|H_d|^2$ coefficient is $\lambda_3+\lambda_4$. We match the NMSSM to the THDMS at the scale M_{SUSY} by identifying the tree-level conditions

$$\begin{aligned} &\lambda_1 = \frac{1}{4}\left(g'^2+g^2\right), \quad \lambda_2 = \frac{1}{4}\left(g'^2+g^2\right)+\Delta\lambda_2, \quad \lambda_3 = \frac{1}{4}\left(g^2-g'^2\right), \\ &\lambda_4 = \frac{1}{2}\left(2|\lambda|^2-g^2\right), \quad \lambda_5 = \lambda_6 = |\lambda|^2, \quad \lambda_7 = -\lambda\kappa^*, \quad \lambda_8 = |\kappa|^2, \\ &m_1^2 = m_{H_d}^2, \quad m_2^2 = m_{H_u}^2, \quad m_3^2 = m_S^2, \quad m_4 = A_\lambda\lambda, \quad m_5 = -A_\kappa\kappa. \end{aligned} \tag{2.8}$$

We furthermore included a dominant one-loop threshold correction to the matching for λ_2,

$$\Delta\lambda_2 = \frac{3y_t^4 A_t^2}{8\pi^2 M_{\text{SUSY}}^2}\left(1-\frac{A_t^2}{12M_{\text{SUSY}}^2}\right). \tag{2.9}$$

Although we stated the potential and matching conditions for λ_7, m_4 and m_5 without loss of generality, we later consider only real, CP conserving parameters. As discussed in section 1 we assume that the CP violation demanded by Sakharov's first condition originates in a different sector of the NMSSM, e.g., the squark sector. Although CP violation must enter the Higgs sector through loops, since we only consider the dominant one-loop corrections in the matching, CP violating phases that may appear outside of the Higgs sector do not enter our calculation. At higher orders, however, we would be forced to consider complex parameters and consequently (as later discussed) PTs involving CP-odd fields. An examination of the potential impact this could have is left for future study. Since we match the NMSSM to a THDMS, our results are also applicable to a subspace of the THDMS, which is well-motivated even in the absence of supersymmetry.

3 Effective potential

3.1 Effective potential at zero temperature

In the R_ξ gauge the one-loop corrections to the potential, ΔV, are given by [85]

$$\begin{aligned} \Delta V = \frac{1}{64\pi^2}\Bigg(&\sum_h n_h m_h^4(\xi)\left[\ln\left(\frac{m_h^2(\xi)}{Q^2}\right)-3/2\right]+\sum_V n_V m_V^4\left[\ln\left(\frac{m_V^2}{Q^2}\right)-5/6\right] \\ &-\sum_V \tfrac{1}{3}n_V(\xi m_V^2)^2\left[\ln\left(\frac{\xi m_V^2}{Q^2}\right)-3/2\right]-\sum_f n_f m_f^4\left[\ln\left(\frac{m_f^2}{Q^2}\right)-3/2\right]\Bigg). \end{aligned} \tag{3.1}$$

where Q is the renormalization scale, m_i are field dependent $\overline{\text{MS}}$ masses and the n_i are the numbers of degrees of freedom for field i. The first term sums fluctuations of scalar fields, which at the EW breaking minimum can be separated into physical Higgs bosons and Goldstone bosons, the second term sums transverse and longitudinal massive gauge bosons, the third one scalar gauge boson fluctuations, and the final one fermions.

We neglect contributions to the vacuum energy. The numbers of degree of freedom for the particles that we include are

$$n_{h_i^0} = n_{A_i^0} = n_{H_i^+} = n_{H_i^-} = 1, \tag{3.2}$$

$$n_{W^+} = n_{W^-} = n_Z = 3, \tag{3.3}$$

$$n_t = n_b = 12,\ n_\tau = 4 \tag{3.4}$$

for the real scalar, vector and Dirac fermion fields in our model, where A_i^0, H_i^+ and H_i^- include the physical Higgs states and the Goldstone bosons.

At zero temperature, the minimum of the one-loop potential lies at non-zero values for the Higgs fields, which we refer to as VEVs, and assume may always be written as

$$\langle H_u \rangle = \frac{1}{\sqrt{2}} \begin{pmatrix} 0 \\ v_u \end{pmatrix}, \qquad \langle H_d \rangle = \frac{1}{\sqrt{2}} \begin{pmatrix} v_d \\ 0 \end{pmatrix}, \qquad \langle S \rangle = \frac{1}{\sqrt{2}} v_S, \tag{3.5}$$

where v_u, v_d and v_S are real, i.e., we do not consider charge or CP breaking VEVs.[4] As we assume that the VEVs are CP conserving, a tadpole condition forces CP violating phases in the potential to vanish.

To construct the field dependent masses appearing in (3.1), we consider the potential as a function of the fields corresponding to the VEVs, i.e., we consider the h_u, h_d and s components of the fields,

$$H_u = \begin{pmatrix} H_u^+ \\ \frac{1}{\sqrt{2}} (h_u + i a_u) \end{pmatrix}, \qquad H_d = \begin{pmatrix} \frac{1}{\sqrt{2}} (h_d + i a_d) \\ H_d^- \end{pmatrix}, \qquad S = \frac{1}{\sqrt{2}} (s + i\sigma), \tag{3.6}$$

where h_u, h_d and s are real. The field dependent masses are functions of h_u, h_d and s. In principle, we could consider variation of the charged and CP-odd fields which cannot all be eliminated by gauge fixing. However, because we consider PTs only between charge and CP conserving vacua, we set charged and CP-odd Higgs fields to zero in the field dependent masses. The expressions for the field dependent masses are given in appendix A.

The effective potential also contains explicit dependence on the gauge parameter ξ. The physical, gauge-independent content of the effective potential may be found through Nielsen identities [88], which express the fact that at extrema, $\mathfrak{h}$, the gauge dependence of the effective potential vanishes, since

$$\frac{\partial V_{\text{eff}}(h, \xi)}{\partial \xi} \propto \frac{\partial V_{\text{eff}}(h, \xi)}{\partial h}, \tag{3.7}$$

[4] Spontaneous charge and CP violation are impossible at tree-level in our THDMS model with NMSSM matching conditions [86]. See, however, ref. [87] for a recent discussion of this issue in a general THDMS model.

JHEP11(2019)151

and thus

$$\frac{\mathrm{d}V_{\rm eff}(\mathfrak{h},\xi)}{\mathrm{d}\xi} = \frac{\partial V_{\rm eff}(\mathfrak{h},\xi)}{\partial \xi} + \frac{\partial \mathfrak{h}}{\partial \xi}\frac{\partial V_{\rm eff}(\mathfrak{h},\xi)}{\partial h} = 0. \tag{3.8}$$

The location of the extrema, however, are gauge dependent, i.e., $\partial\mathfrak{h}/\partial\xi \neq 0$. See e.g., refs. [85, 89] for further discussion of this issue. We work in the $\xi = 1$ (Feynman) gauge. The effective potential furthermore depends on a choice of renormalization scale, which could in fact have greater impact than gauge ambiguities [90].

3.2 Effective potential at finite temperature

To describe the conditions of the early Universe we need to take into account temperature corrections. We calculate one-loop finite temperature corrections including daisy terms using the Arnold-Espinosa method [91] in the $\xi = 1$ (Feynman) gauge. The effective potential can be written as a sum of zero temperature and finite temperature pieces

$$V_{\rm eff} = V^{\rm tree}_{\rm THDMS} + \Delta V_{\rm THDMS} + \Delta V_T + V_{\rm daisy}. \tag{3.9}$$

The one-loop thermal corrections in the R_ξ gauge are [85]

$$\begin{aligned}\Delta V_T = \frac{T^4}{2\pi^2}\Bigg[&\sum_h n_h J_{\rm B}\left(\frac{m_h^2(\xi)}{T^2}\right) + \sum_V n_V J_{\rm B}\left(\frac{m_V^2}{T^2}\right)\\ &- \sum_V \tfrac{1}{3} n_V J_{\rm B}\left(\frac{\xi m_V^2}{T^2}\right) + \sum_f n_f J_{\rm F}\left(\frac{m_f^2}{T^2}\right)\Bigg],\end{aligned} \tag{3.10}$$

where the field dependent masses are the same as those appearing in (3.1) in the previous section, and the expressions for them are given in appendix A. The degrees of freedom, n, are as in (3.2); we again neglect contributions to the vacuum energy and the thermal functions are

$$J_{\rm B/F}(y^2) = \pm\,\mathrm{Re}\int_0^\infty x^2 \ln\left(1 \mp e^{-\sqrt{x^2+y^2}}\right)\mathrm{d}x. \tag{3.11}$$

Here the upper/lower signs are for bosons/fermions. For $m^2 \gg T^2$ the thermal functions are exponentially suppressed by a Boltzmann factor. This ensures that the massive supersymmetric particles that we integrated out do not impact the finite temperature corrections.

The daisy terms are

$$V_{\rm daisy} = -\frac{T}{12\pi}\left(\sum_h n_h\left[\left(\bar{m}_h^2\right)^{\frac{3}{2}} - \left(m_h^2\right)^{\frac{3}{2}}\right] + \sum_V \tfrac{1}{3} n_V\left[\left(\bar{m}_V^2\right)^{\frac{3}{2}} - \left(m_V^2\right)^{\frac{3}{2}}\right]\right), \tag{3.12}$$

where we sum over the Higgs fields (including Goldstone bosons) and massive gauge bosons, and $\bar{m}^2$ are field dependent mass eigenvalues that include Debye corrections to the tree-level masses in the mass matrices. The Debye corrections add additional T dependent terms of the form $c_\Phi T^2|\Phi|^2$ for all complex scalar gauge eigenstates and $c_A T^2 A_\mu A^\mu$ for all gauge bosons associated with the original gauge symmetries before EWSB. For the

JHEP11(2019)151

THDMS we find,

$$c_{H_u} = \tfrac{1}{48}\left(3g'^2 + 9g^2 + 12y_t^2 + 12\lambda_2 + 8\lambda_3 + 4\lambda_4 + 4\lambda_6\right), \tag{3.13}$$

$$c_{H_d} = \tfrac{1}{48}\left(3g'^2 + 9g^2 + 12y_b^2 + 4y_\tau^2 + 12\lambda_1 + 8\lambda_3 + 4\lambda_4 + 4\lambda_5\right), \tag{3.14}$$

$$c_S = \tfrac{1}{48}\left(8\lambda_5 + 8\lambda_6 + 16\lambda_8\right), \tag{3.15}$$

$$c_{W_{1,2,3}} = 2g^2, \tag{3.16}$$

$$c_B = 2g'^2, \tag{3.17}$$

where the couplings g', g, y_t, y_b and y_τ are as in (A.1). The corrections for the gauge bosons are in the gauge basis before symmetry breaking and every component of a gauge representation receives the same Debye correction. The scalar coefficients are gauge independent, as they originate from a high-temperature expansion of (3.10), in which the dependence on ξ cancels,

$$c_{ij} = \frac{1}{T^2}\frac{\partial^2 \Delta V_T}{\partial\phi_i \partial\phi_j}\bigg|_{T^2 \gg m^2}. \tag{3.18}$$

The coefficents for the gauge bosons are the same as those of the two-Higgs doublet model, which can be found in the literature [92]. We cross-checked our results in (3.13) – (3.17) against general expressions in ref. [93]. Thus we have described the full finite temperature potential, which is a function of the fields h_u, h_d and s and the temperature, T.

4 First-order phase transitions

Having constructed the finite temperature effective potential, we investigated whether there was a FOPT in which the vacuum of the potential changed abruptly as the Universe cooled. For such a transition to occur, the potential must exhibit two minima separated by a barrier. The temperature at which the two minima are exactly degenerate is known as the critical temperature. That is, at the critical temperature, T_C, there are minima such that

$$V_{\text{eff}}(\mathfrak{h}_u, \mathfrak{h}_d, \mathfrak{s}, T_C) = V_{\text{eff}}(\mathfrak{h}'_u, \mathfrak{h}'_d, \mathfrak{s}', T_C) \tag{4.1}$$

where caligraphic fonts, $\mathfrak{h}_u$ etc, indicate a minimum of the scalar potential, i.e.,

$$\partial_{h_u} V_{\text{eff}}(\mathfrak{h}_u, \mathfrak{h}_d, \mathfrak{s}) = \partial_{h_d} V_{\text{eff}}(\mathfrak{h}_u, \mathfrak{h}_d, \mathfrak{s}) = \partial_s V_{\text{eff}}(\mathfrak{h}_u, \mathfrak{h}_d, \mathfrak{s}) = 0. \tag{4.2}$$

Below the critical temperature, the potential develops a minimum that is deeper than the other minima. The system may tunnel through the barrier to the new vacuum state with the lower minimum [94–96]. As discussed below, however, the transition might not complete.

We developed a C++ program, `PhaseTracer`, to map the temperature dependence of the minima of the effective potential and to find potential PTs between them. It enhances the algorithm that was developed in `CosmoTransitions` [97] to map out the phase structure, and to find out possible PTs between every phase. The numerical method coded in `PhaseTracer` is briefly described in appendix B. This method is different from the one applied in the code `BSMPT` [93] and previous works on SFOPTs in the NMSSM [61], which

JHEP11(2019)151

may only find a single PT between the EW symmetric vacuum and the observed EWSB vacuum. Our method is able to map out a more complicated phase structure and find multiple PTs in it. Of equal importance, by analyzing the phase structure obtained by `PhaseTracer`, we confirmed that not all potential tunnelings actually take place in the early Universe. This may happen because the tunneling rate is too slow or because the PT is located on a branch of the phase structure that the system never utilizes because it evolved in a different direction.

To exhibit spontaneous EWSB as the Universe cooled, the vacuum of the finite temperature effective potential (3.9) should respect EW symmetry at high temperature, which is 1 TeV in this work, and should violate it at zero temperature. Thus at high temperature the global minimum should lie at the origin, $h_u = 0$ and $h_d = 0$, and at zero temperature the deepest minimum should lie at the observed EWSB VEV. We can use this information to fix the boundaries of the phase structure by finding all minima of the potential at $T = 0$ and $T = 1\,\text{TeV}$ and checking that spontaneous symmetry breaking occurs. Starting from $T = 0$ then we can use `PhaseTracer` to find all possible PTs.

The strength of such a transition is described by an order parameter. For baryogenesis, we consider the order parameter

$$\gamma_{\text{EW}} \equiv \frac{\sqrt{(\mathfrak{h}_u - \mathfrak{h}'_u)^2 + (\mathfrak{h}_d - \mathfrak{h}'_d)^2}}{T_C}. \tag{4.3}$$

The singlet VEV is not included here because it does not affect EW sphalerons. Order parameters of about $\gamma_{\text{EW}} \gtrsim 1$ are considered strong and could catalyze baryogenesis.

The Nielsen identities in (3.8) imply that the critical temperature is gauge independent, since the effective potential is gauge independent at extrema. Our one-loop truncation of the effective potential, however, means that it is gauge independent only at the tree-level extrema. Thus the critical temperature, which we find from the effective potential at the one-loop minima, is gauge dependent. See ref. [85] for further discussion and a procedure that may enforce gauge independence. The location of the minima, furthermore, and thus the order parameter, always depend on the gauge parameter ξ.

A first order transition occurs through bubble nucleation and there is a finite probability per unit time and volume for tunneling to a new phase. The new phase dominates once the following condition is satisfied [98, 99],

$$\frac{S_E(T_N)}{T_N} \simeq 140, \tag{4.4}$$

where S_E stands for the Euclidean bubble action, and T_N is the so-called nucleation temperature. If there is no solution, we conclude that the transition cannot complete. During the scan, we identify all possible PTs without checking whether they successfully nucleate. After classifying phase structures, we check nucleation temperatures for a subset of our samples using `CosmoTransitions` [97].

JHEP11(2019)151

5 Results

5.1 Parameter space, constraints and sampling strategy

To explore all possible PTs in the NMSSM, including strong EWPTs, we sampled the parameter space of the model within the ranges shown in table 1. The first four parameters, λ, κ, A_λ and A_κ are from the tree-level NMSSM potential and enter the matching conditions at tree-level (2.8), while the fifth parameter, the stop trilinear A_t enters at the one-loop level (2.9). These parameters are all defined at the matching scale m_{SUSY} which we also take as an input and represents the geometric mean of the left and right soft SUSY breaking masses of the stops, which have been integrated out, i.e.

$$m_{\text{SUSY}} = \sqrt{m_{\tilde{t}_L} m_{\tilde{t}_R}}. \tag{5.1}$$

The final two parameters are the ratio of the Higgs VEVs $\tan\beta \equiv v_u/v_d$ and the singlet VEV, v_S, which are defined at the top quark mass, $m_t = 173.1\,\text{GeV}$. Therefore our model has eight free parameters.

From these inputs the parameters of the THDMS at m_t are obtained using `FlexibleSUSY-2.1.0` [100, 101], coupled with[5] `SARAH-4.12.3` [104–107], which implements the matching and running procedure described in section 2.1, with (2.8) specified as a boundary condition in the `FlexibleSUSY` model file.[6] Since all running and effective potential calculations are performed in the THDMS it is not necessary to specify any further soft-breaking masses in the NMSSM. Because the quartic coupling λ can always be made positive through field redefinitions, we do not consider negative values for it, but we do consider both negative and positive values for the soft trilinears, κ and v_S. Lastly, as discussed earlier, for self-consistency we only consider real parameters.

The field dependent masses which enter the one-loop corrections to potential are calculated with `FlexibleSUSY`, and the thermal functions are evaluated using the implementation described in ref. [108]. We use `PhaseTracer` to find the phases and critical temperatures by exploring the finite temperature potential between $T = 0$ and $T = 1\,\text{TeV}$, as described in section 4. Since this involves varying the field values that enter the field-dependent masses, in principle it is possible that this could re-introduce large logarithms and lead to perturbativity problems, therefore we do not consider VEVs greater than 1.6 TeV. In practice in all our results the VEVs are significantly smaller than this, and are less than 300 GeV in all but one very special category of points, therefore this restriction does not have an impact on our results.[7]

The main experimental constraints on the parameter region of interest come from LEP chargino searches and the observed Higgs properties. The Higgs sector of our model must be compatible with observations of an SM-like Higgs boson with a mass close to 125 GeV. The observed Higgs, however, could correspond to any one of the three neutral Higgs bosons in our model. We calculated tree-level reduced couplings between the neutral

[5] Internally `FlexibleSUSY` also uses some numerical routines from `SOFTSUSY` [102, 103].

[6] The `SARAH` and `FlexibleSUSY` model files we wrote for this are provided as supplementary material to this paper published on JHEP.

[7] This category of points will be introduced later and can be seen in the bottom left plot of figure 7.

JHEP11(2019)151

Parameter	Range	Metric
λ	0, $\pi/2$	flat
$\lvert\kappa\rvert$	0, $\pi/2$	flat
$\lvert A_\lambda\rvert$	0, 10 TeV	hybrid
$\lvert A_\kappa\rvert$	0, 10 TeV	hybrid
$\lvert A_t\rvert$	0, 10 TeV	hybrid
m_{SUSY}	1, 10 TeV	log
$\lvert v_S\rvert$	0, 10 TeV	hybrid
$\tan\beta$	1, 60	log

Table 1. Ranges and metric of parameters that we scanned in the NMSSM at the SUSY scale. We considered positive and negative κ, v_S and trilinear couplings. The "hybrid" metric is flat below 10 GeV, and logarithmic elsewhere. The top mass was fixed to its measured value 173.1 GeV [7].

Higgs bosons and SM fermions by taking into account mixing between the neutral Higgs bosons. We furthermore calculated one-loop reduced couplings between the Higgs bosons and photons and gluons using `FlexibleSUSY` routines developed in ref. [109]. By passing this information and the Higgs masses to `Lilith-1.1.4_DB-17.05` [110], we find a chi-squared, χ^2_{Higgs}, for our Higgs sector from Run I and II measurements of the Higgs boson at the LHC.

We penalized points in tension with LEP bounds on charginos [7] by introducing a chi-squared for the effective μ-parameter

$$\chi^2_{\text{LEP}} \equiv \begin{cases} 0 & \mu_{\text{eff}} \geq 100\,\text{GeV}, \\ \left(\frac{\mu_{\text{eff}} - 100\,\text{GeV}}{5\,\text{GeV}}\right)^2 & \mu_{\text{eff}} < 100\,\text{GeV}. \end{cases} \tag{5.2}$$

We constructed this function to guide our sampling algorithm towards acceptable solutions with $m_{\tilde{\chi}_1^\pm} \gtrsim 100\,\text{GeV}$, rather than precisely reflect experimental constraints from LEP. We furthermore penalized points without an SFOPT by the chi-squared

$$\chi^2_{\text{SFOPT}} \equiv \left(\frac{\log_{10}\gamma_{\text{EW}}}{0.2}\right)^2. \tag{5.3}$$

The role of this term is to focus our sampling algorithm on SFOPT with $\gamma_{\text{EW}} \simeq 1$; it is in fact equivalent to a Gaussian penalty $\log_{10}\gamma_{\text{EW}} = 0 \pm 0.2$.

Since the parameter space shown in table 1 is eight-dimensional we sampled points from our model using `MultiNest-3.10` [111–113] with a chi-squared

$$\chi^2 = \chi^2_{\text{Higgs}} + \chi^2_{\text{SFOPT}} + \chi^2_{\text{LEP}}. \tag{5.4}$$

We saved and considered all points evaluated by `MultiNest`, i.e., we disabled the cuts ordinarily placed on saved points by the `MultiNest` algorithm. To be consistent with the LHC Higgs measurements and LEP bounds on charginos [7], and to satisfy our SFOPT requirement, we select points with

$$\chi^2_{\text{Higgs}} - \min\chi^2_{\text{Higgs}} \leq 6.18,\ \mu_{\text{eff}} \geq 100\,\text{GeV} \text{ and } \gamma_{\text{EW}} \geq 1, \tag{5.5}$$

JHEP11(2019)151

where $\min \chi^2_{\rm Higgs} = 22.3$ was the minimum $\chi^2_{\rm Higgs}$ found in our scan. After that, we further required that remaining points satisfied LHC and LEP bounds on BSM Higgs bosons using `HiggsBounds-5.3.2beta` [114–118], which we interfaced via `NMSSMCALC` [119].

5.2 Classification of phase transitions

After collecting more than three million valid points, we found that the possible phase structures in the NMSSM harbored rich and novel phenomenology. To reflect this phenomenology, we classify these points into three categories that differ by the nature of the first possible PT in the cosmological history:

1. `Type-H-and-S`: EW symmetry is spontaneously broken such that at least one Higgs field and the singlet field obtain non-vanishing VEVs simultaneously.
2. `Type-Only-H`: EW symmetry is spontaneously broken by one or both Higgs fields obtaining VEVs, but the singlet VEV remains zero.
3. `Type-Only-S`: EW symmetry remains unbroken, but the singlet field obtains a VEV. The Higgs obtain non-vanishing VEVs in a SFOPT afterwards, during which the sign of singlet VEV may be maintained or flipped. Thus we further classify this type into two subcategories:
   - `Type-Only-S(maintain)`: the strongest PT maintains the sign of singlet VEV.
   - `Type-Only-S(flip)`: the strongest PT flips the sign of singlet VEV.

It is important to understand that at this stage we do not have the means to ensure that a PT is definitely part of the cosmological history. More precisely, for such an extensive sample of parameter points, we are not in the position to calculate nucleation temperatures, actions, decay rates, etc. for each potential transition in the phase structure. For this reason, unless specified otherwise when we say 'PT' we typically mean '*possible* PT'.

To simplify our discussion of this non-trivial structure, we introduce the following shorthand notation:

- We denote the minimum value of the potential in a given direction with a calligraphic font. For example, $\mathfrak{s}$ is a value of singlet field s at a minimum of the scalar potential.
- By the triplet of values e.g., $(100, 200, 300)$, we mean $\mathfrak{h}_u = 100\,\text{GeV}$, $\mathfrak{h}_d = 200\,\text{GeV}$, and $\mathfrak{s} = 300\,\text{GeV}$.
- At a critical temperature, two vacua are degenerate. However, we always define the true vacuum to be the deepest of these vacua just below the critical temperature, and the other one is the false vacuum in our notation.
- In case of multiple SFOPTs we refer to the SFOPT with the greatest $\gamma_{\rm EW}$ as the strongest one.
- We define
$$\mathfrak{h} \equiv \text{sign}(\mathfrak{h}_u \mathfrak{h}_d)\sqrt{\mathfrak{h}_u^2 + \mathfrak{h}_d^2}, \tag{5.6}$$
as the signed geometric mean of the Higgs fields.

JHEP11(2019)151

5.3 Benchmark points

In figure 1, we present a phase history for a typical point in each category. For these benchmark points, we checked our results with `CosmoTransitions` and calculated the nucleation temperature for every possible FOPT. The corresponding input parameters, Higgs properties and transition information are shown in table 2. On each panel, the lines show the signed geometric mean of the Higgs fields (left) or the singlet field (right) at a minimum of the potential as a function of temperature.[8] Two phases linked by an arrow at a given temperature are degenerate and thus a FOPT could occur in the direction indicated by the arrow (i.e., below the critical temperature, the phase at the end of the arrow contains a deeper minimum). When there is more than one possible sequence of FOPTs that leads from the origin at $T = 1\,\text{TeV}$ to the observed vacuum at $T = 0$, we show the FOPTs that belong to the sequence that includes the strongest FOPT by black arrows, and PTs that are not part of that history by gray arrows. Note though that other possible FOPTs between phases that are never degenerate are not marked. For example, in the upper left panel, the minima in phase 2, which appears at about $T = 88\,\text{GeV}$, always lies shallower than that in phase 3. A FOPT between them is possible, although there is no critical temperature.

From figure 1 we can see that in all categories at high temperature, $T > 400\,\text{GeV}$, the true vacuum is always at the origin (as described in section 4 this is a requirement in our scan). In the upper left panel, the first (and only) PT occurs at $T \lesssim 145\,\text{GeV}$ between $(0, 0, 0)$ and $(106, 117, 276)$ with $\gamma_{\text{EW}} = 1.09$ and nucleation temperature $T_N = 116\,\text{GeV}$. Thus it is classified as `Type-H-and-S`.

In the upper right panel, only one of the Higgs fields, h_u, develops a VEV during the first crossover transition at $T = 155\,\text{GeV}$. The first transition in the cosmological history was never first order in our `Type-Only-H` samples. As the Universe cools, however, a deeper minimum exists between $T = 151\,\text{GeV}$ and $T = 124\,\text{GeV}$ at about $(0, 0, 450)$, which belongs to phase 2. The FOPT to this deeper minimum would (temporarily) restore EW symmetry; however, we find that it cannot complete as (4.4) cannot be satisfied. If it completed, EW symmetry would subsequently be permanently broken by another SFOPT at $T \lesssim 123.6\,\text{GeV}$ which would complete, from $(0, 0, 463)$ to $(91, 162, 274)$ with $\gamma_{\text{EW}} = 1.5$ and $T_N = 119\,\text{GeV}$. Indeed, in all the `Type-Only-H` samples that we found, EW symmetry was broken, possibly restored and finally broken again, and the *final* FOPT would be the strongest, just as in this example. However, these sequences of transitions are impossible, as the actions for the transitions that restore EW symmetry are always so large that bubbles cannot nucleate properly. Thus although there appear to be SFOPTs with $\gamma_{\text{EW}} > 1$ and nucleation temperatures in the `Type-Only-H` samples, they cannot explain the observed baryon asymmetry of the Universe, as a previous transition in the cosmological history would not complete.

For the `Type-Only-S(maintain)` point (lower left panel) in the first transition at $T = 233\,\text{GeV}$ only the singlet obtains a positive VEV; EW symmetry is broken with the

[8] Note though that two phases connected by crossover PTs are merged into one phase in order to simplify the phase structure.

JHEP11(2019)151

	Type-H-and-S	Type-Only-H	Type-Only-S (maintain)	Type-Only-S (flip)
λ	0.618	0.607	0.601	0.935
κ	0.229	0.191	0.175	1.137
A_λ	160.1	160.5	170.0	147.4
A_κ	-93.7	-117.5	-25.2	61.4
A_t	-21.4	38.3	-24.6	-478.6
$m_{\rm SUSY}$	6374.7	3463.1	5857.5	4164.3
v_S	307.9	247.5	245.7	183.1
$\tan\beta$	1.2	2.0	2.6	3.2
m_{H_1}	91.7	47.9	45.6	126.2
m_{H_2}	127.4	124.6	125.1	184.4
m_{H_3}	237.6	226.6	252.7	366.5
m_{A_1}	167.3	145.9	103.8	145.4
m_{A_2}	229.7	225.9	248.2	325.8
$m_{H^\pm}$	214.2	206.7	233.1	294.3
$\chi^2_{\rm Higgs}$	27.0	25.6	26.2	26.4
First PT				
Order	1st	2nd at $T = 155$	1st	1st
False vac.	$(0, 0, 0)$	$(0, 0, 0)$	$(0, 0, 0)$	$(0, 0, 0)$
True vac.	$(106, 117, 276)$	$(0, +\text{ve}, 0)$	$(0, 0, 182)$	$(0, 0, -12)$
T_C	145	N/A	233	368
T_N	116	N/A	230	367
Strongest FOPT				
False vac.	Same as above	$(0, 0, 463)$	$(0, 0, 400)$	$(0, 0, -188)$
True vac.		$(91, 162, 274)$	$(59, 114, 349)$	$(66, 209, 179)$
T_C		124	121	104
T_N		119	119	N/A; no nuc.
$\gamma_{\rm EW}$	1.1	1.5	1.1	2.1
Ends at SM vac.	Yes	Yes	Yes	Yes
Possible	Yes	No; prior PT fails	Yes	No; no nuc.

Table 2. Benchmark points for our four scenarios. All dimensionful quantities are in GeV. The abbreviation vac. is for vacuum and nuc. is for nucleation. The +ve in `Type-Only-H` means that the field value of vacuum during the 2nd order phase transition is shifted to positive direction.

JHEP11(2019)151

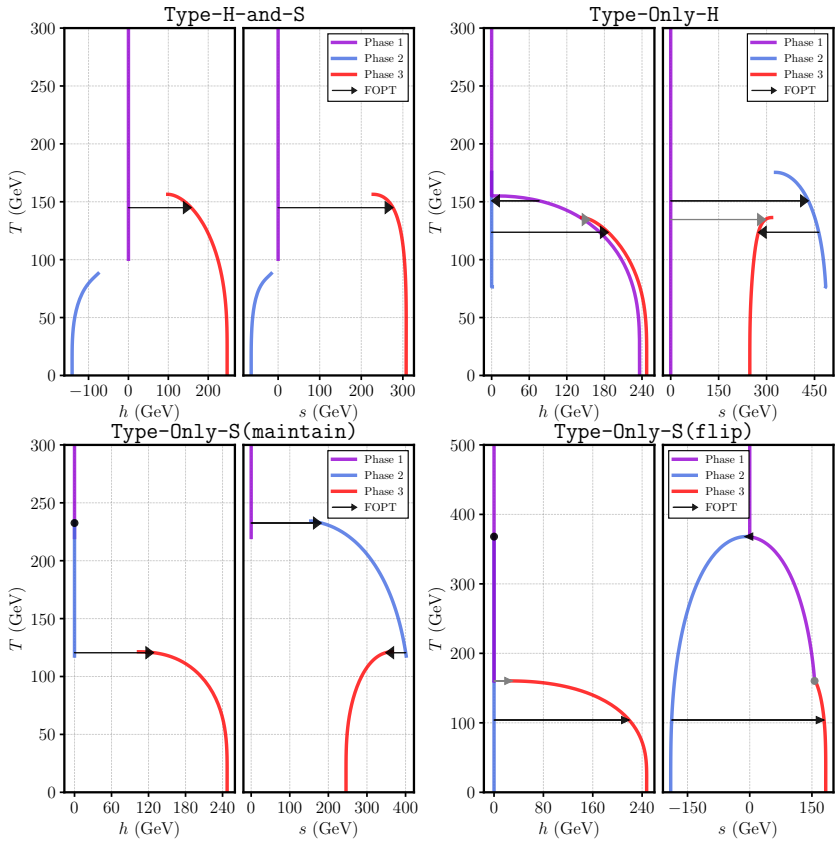

Figure 1. Phase structures for typical points in the categories `Type-H-and-S` (upper left), `Type-Only-H` (upper right), `Type-Only-S(maintain)` (lower left) and `Type-Only-S(flip)` (lower right). The lines show the field values at a particular minimum as a function of temperature. The arrows indicate that at that temperature the two phases linked by the arrows are degenerate and thus that a FOPT could occur in the direction of the arrow. The dots in the lower panels represent transitions that do not change the corresponding field values. The black arrows and dots show a path that includes the strongest EW FOPT, while the gray ones are not in that path.

sign of singlet VEV maintained in the second (and final) PT at $T = 121\,\text{GeV}$. Both of the transitions are strongly first order and complete. Although transitions in which only the singlet obtains a VEV cannot precipitate baryogenesis, they might nevertheless result in interesting gravitational wave signatures.

Finally, we consider a `Type-Only-S(flip)` point (lower right panel). The singlet field develops a negative value during the first transition at $T = 368\,\text{GeV}$, which is first-order and completes at $T_N = 367\,\text{GeV}$. At $T \lesssim 368\,\text{GeV}$, just below the critical temperature of the first transition, a phase with positive $\mathfrak{s}$ develops, which is approximately symmetric

JHEP11(2019)151

with respect to the phase with negative $\mathfrak{s}$. Eventually, a second first-order transition at $T = 104\,\text{GeV}$ breaks EW symmetry and flips the sign of the singlet by transitioning to this approximately symmetric phase. Although this is the strongest PT, it cannot complete, as the barrier between the phases means that the tunneling action is too large for (4.4) to be satisfied. This phenomenon appears in a large fraction of our `Type-Only-S(flip)` samples.

Phase histories of types `Type-H-and-S` and `Type-Only-S(maintain)` were previously investigated in refs. [15, 59–61]; however, the richer phase histories in `Type-Only-H` and `Type-Only-S(flip)` have not been discussed in the literature as far as we are aware. Note that the barrier between the minima in the `Type-Only-H` and `Type-Only-S(flip)` are usually so high that the tunneling may not happen. This shows the importance of studying phase structure as well as calculating the transition strength.

We also checked the robustness of our results against the change of the renormalization scale. For the `Type-H-and-S` benchmark point in table 2, we found a mild (1% – 2%) variation of the critical temperature and the transition strength as the renormalization scale changes in the $(m_t/2, 2m_t)$ range. We furthermore checked gauge dependence by repeating our calculations for our benchmark points in the $\xi = 0$ (Landau) gauge. We found, as anticipated, that gauge dependence was present but typically mild, especially for the critical temperatures. The gauge dependence could, nevertheless, motivate the application of gauge independent techniques in future works.

5.4 Reaching the observed SM vacuum

During the scan we required that the deepest minimum at zero temperature agreed with the observed VEV, $\mathfrak{h} = 246\,\text{GeV}$. We call the phase associated with the observed VEV the SM vacuum. We split our samples by two ways of reaching the SM vacuum. First, in section 5.4.1 we consider samples for which the strongest SFOPT ends in the SM vacuum, which changes smoothly to $\mathfrak{h} = 246\,\text{GeV}$ at $T = 0$. Second, in section 5.4.2 we consider samples for which the strongest FOPT does not end in the SM vacuum. As we discuss, such samples must feature at least one further FOPT that ultimately ends in the observed vacuum at $T = 0$. In both cases, the `Type-Only-H` scenario was by far the rarest, with noticeably few samples shown in the following scatter plots.

5.4.1 The strongest FOPT ends in the SM vacuum

We selected samples in which the strongest FOPT ended in the SM vacuum. For our samples, it was sufficient to check that $\mathfrak{h}_u > 0\,\text{GeV}$ and $\mathfrak{h}_d > 0\,\text{GeV}$ for the true vacuum of strongest FOPT. All of our benchmark points in table 2 are in this category. In figure 2, we present the true and false minima of the *strongest* FOPT at the critical temperature. It demonstrates some features of each of the types of point that we described above. For `Type-H-and-S`, the *first* transition, in which the Higgs and singlet fields acquire VEVs, is usually also the *strongest* FOPT. There are however three exceptional points where the singlet field values at the false minimum are non-zero. They have similar phase structures to the upper right panel of figure 1 except that the minima of phase 1 is always deeper than the minima of phase 2 in all three cases. Thus there is no critical temperature between these phases, and so the strongest FOPT for these three points is not in the cosmological history.

JHEP11(2019)151

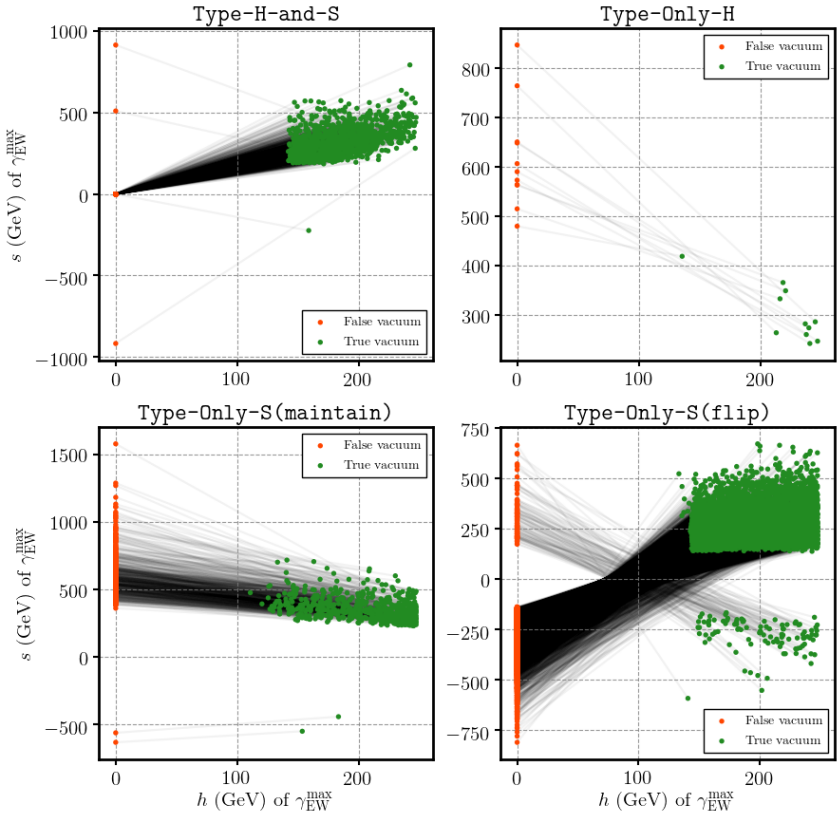

Figure 2. The Higgs and singlet field values at the true and false minima at the critical temperature of the strongest FOPT for samples for which the strongest FOPT ends in the SM vacuum.

According to the definition of `Type-Only-H`, only the Higgs fields obtain VEVs in the first transition in the history, while the upper right panel of figure 2 shows that the false vacuums of strongest FOPT have zero Higgs VEVs, $\mathfrak{h}_u = \mathfrak{h}_d = 0$, but a non-vanishing singlet VEV, $\mathfrak{s} \neq 0$. This means that there must be an intermediate transition that restores EW symmetry and generates a singlet VEV. Since the number of `Type-Only-H` scenarios that we found are quite small, we checked each one in detail. We found that this intermediate transition exists for all `Type-Only-H` samples, but the corresponding tunneling probabilities are too small. Nonetheless it is possible that there exist scenarios of this type where the transition does complete.

The lower panels of figure 2 display samples of `Type-Only-S` where the strongest FOPT maintains (left) or flips (right) the sign of the singlet VEV. We see that the singlet VEV can evolve to up to 1.6 TeV after the first transition, and then shifts to about 150 GeV to 650 GeV during the strongest FOPT. The singlet VEV $\mathfrak{s}$ of the true vacuum can be both

JHEP11(2019)151

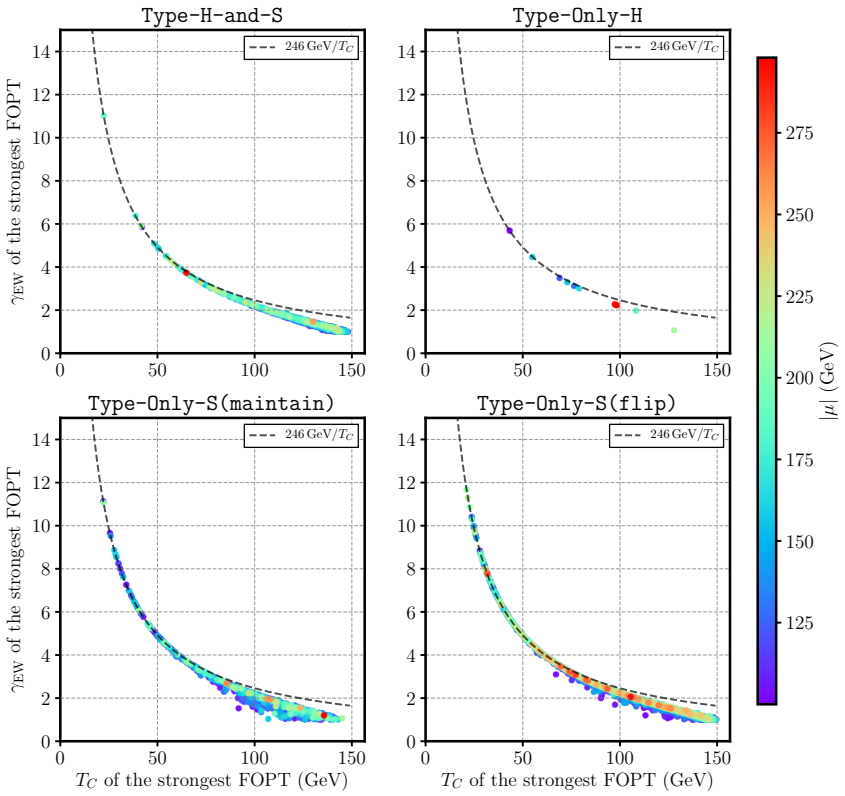

Figure 3. The critical temperature and order parameter for the strongest PTs for samples for which the strongest FOPT ends in the SM vacuum. The points are colored by the effective μ-parameter.

positive or negative, because the input v_S includes both signs. We have checked that the singlet VEV at the true vacuum has the same sign as the input v_S.

In all scenarios, the spread in the possible true vacuum for the Higgs fields at the critical temperature is small, and typically it matches and rarely exceeds the input EWSB vacuum, i.e., $\mathfrak{h} \lesssim 246\,\text{GeV}$. This can be further seen in figure 3, which shows the FOPT strength against the critical temperature. The strength lies close to what it would be if $\mathfrak{h} = 246\,\text{GeV}$ (dashed gray line). For higher critical temperatures, however, deviations from the gray line are visible, as the thermal loop-corrections are relevant. The thermal loop-corrections tend to make the potential more convex, thus decreasing $\mathfrak{h}$ at the critical temperature and the strength of the PT.

We now delineate the regions of the NMSSM parameter space in which our four scenarios occur. We checked that in all scenarios the stops were truly decoupled by checking stop mixing, $X_t = A_t - \mu_{\text{eff}} \cot\beta$, which could potentially split the stop mass eigenvalues making one of them light. We found that most samples were actually concentrated within

JHEP11(2019)151

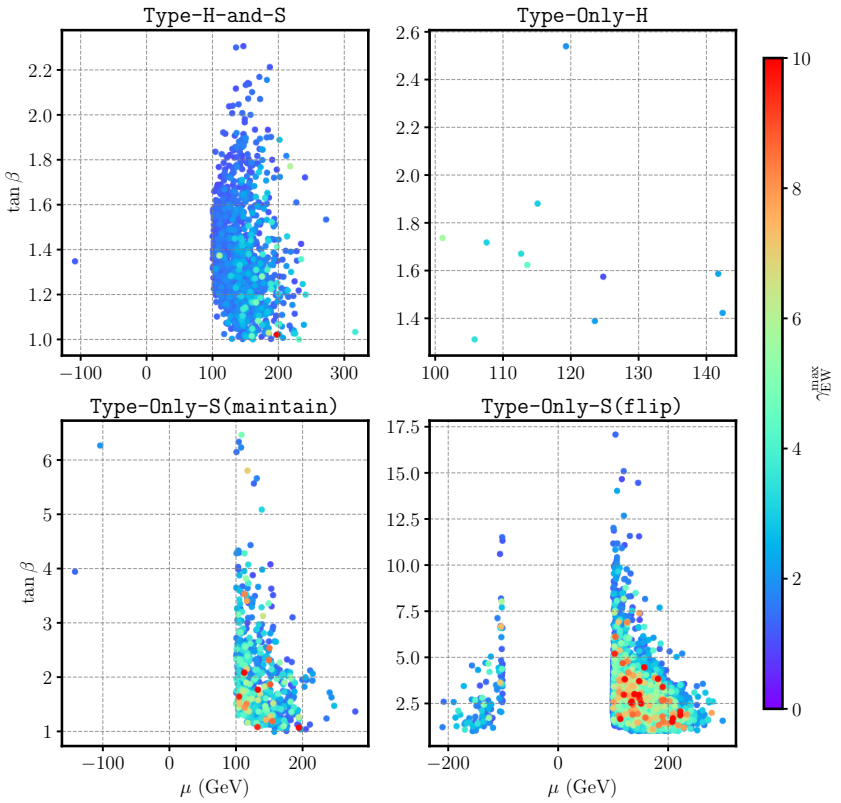

Figure 4. The parameters $(\mu_{\rm eff}, \tan\beta)$ for samples for which the strongest FOPT ends in the SM vacuum. The points are colored by the $\gamma_{\rm EW}$ of the strongest FOPT.

the range $-m_{\rm SUSY} \leq X_t \leq m_{\rm SUSY}$ and no particular value of $m_{\rm SUSY}$ was preferred by our samples.

In figure 4 we show that the Higgs sector parameters ($\mu_{\rm eff}$, $\tan\beta$) are severely constrained. Indeed, the `Type-H-and-S` and `Type-Only-H` scenarios require $\tan\beta \lesssim 3$, whereas the `Type-Only-S(maintain)` and `Type-Only-S(flip)` scenarios permit $\tan\beta \lesssim 7$ and $\tan\beta \lesssim 17$, respectively. For all types, the upper limit of $\tan\beta$ decreases with $\mu_{\rm eff}$ increasing. The effective μ-parameter, and thus the higgsinos, are always light, $|\mu_{\rm eff}| \lesssim 300\,\text{GeV}$. Thus we find further motivation for scenarios with small $\mu_{\rm eff} \lesssim 1\,\text{TeV}$, which are also motivated by naturalness, and we anticipate that the searches for higgsinos at the LHC could be sensitive to our models. Samples with $\mu_{\rm eff} < 0$ were extremely rare in the `Type-H-and-S` and `Type-Only-S(maintain)` scenarios, and not present in the `Type-Only-H` samples.

We see, furthermore, in figure 5, that quartic couplings of around $\lambda \approx 0.6$ and $\kappa \approx 0.2$ could result in an SFOPT in all our scenarios, though a broad range of couplings result in SFOPTs in `Type-Only-S(flip)` scenario, including couplings with values far above the

JHEP11(2019)151

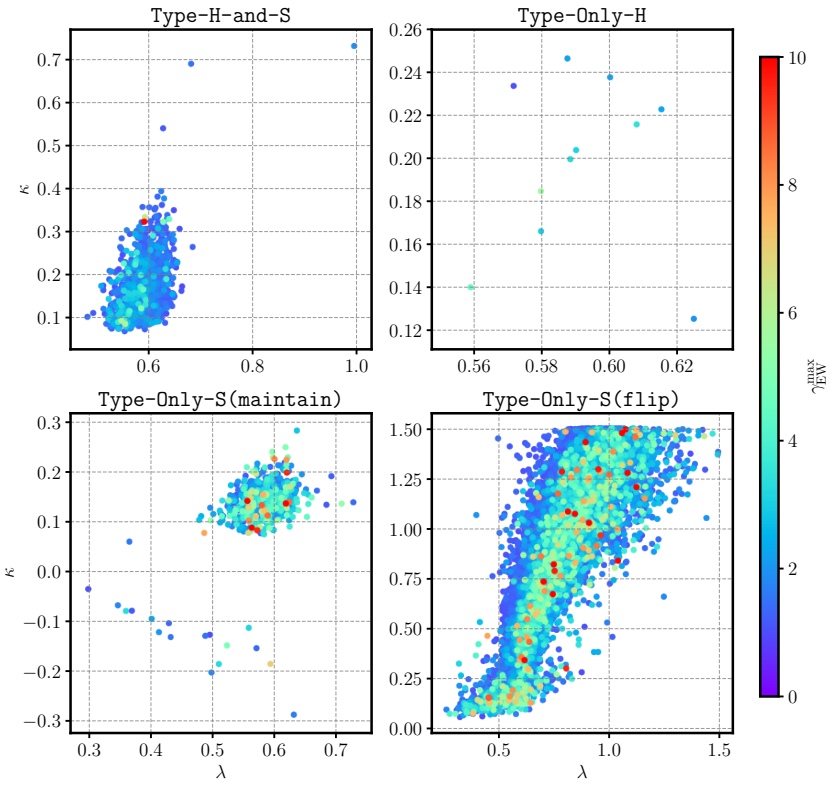

Figure 5. The quartics (λ, κ) for samples for which the strongest FOPT ends in the SM vacuum. The points are colored by the $\gamma_{\rm EW}$ of the strongest FOPT.

limits that would be set if we required perturbativity up to the GUT scale. The constraints strongly prefer that $\lambda\kappa > 0$, a combination that is invariant under the field redefinition $S \to -S$. Since we worked in a $\lambda > 0$ convention, the inequality $\lambda\kappa > 0$ is equivalent to $\kappa > 0$. In the `Type-Only-S(maintain)` scenarios, however, we find a few solutions for which $\kappa < 0$.

Figure 6 shows the trilinear couplings $(A_\lambda,\ A_\kappa)$ with the quartic coupling κ shown by the color bar. The trilinears play an important role. As different types of sample require different sign of singlet VEV at low temperatures, the parameter space of each type shows distinguishable tendency. The samples in `Type-H-and-S`, `Type-Only-H` and `Type-Only-S(maintain)` scenarios are concentrated at negative A_κ with positive κ or positive A_κ with negative κ, as well as a horizontal slice of points at $A_\kappa \approx 10\,\text{GeV}$ for `Type-H-and-S` and `Type-Only-S(maintain)`. On the other hand, A_λ is typically positive but $\lesssim 500\,\text{GeV}$. The one point with negative A_λ in `Type-H-and-S` and the two points with negative A_λ in `Type-Only-S(maintain)` correspond the point of negative $\mu_{\rm eff}$ in

JHEP11(2019)151

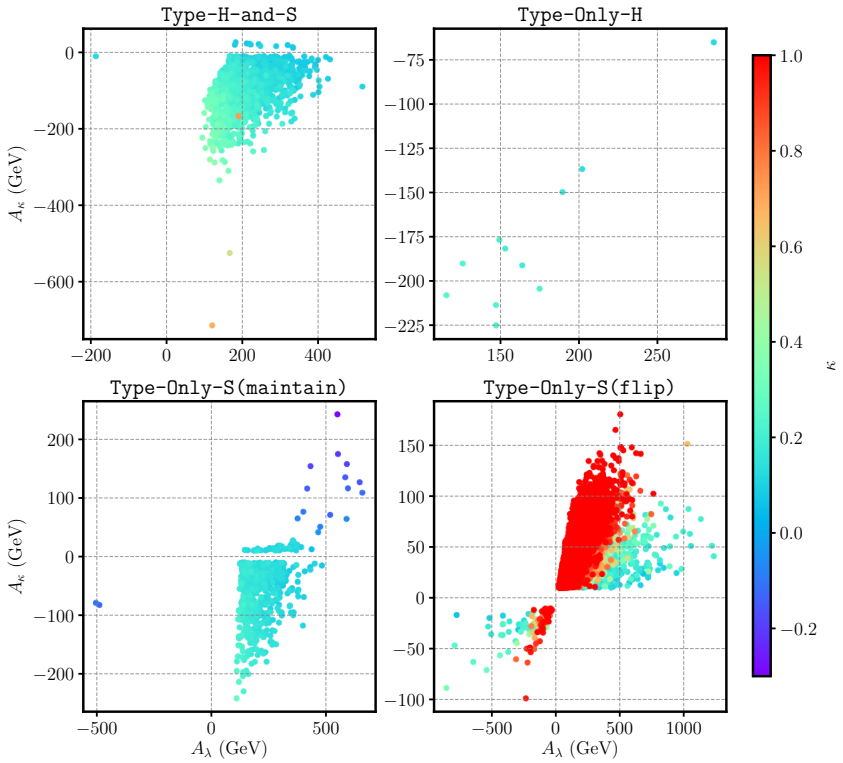

Figure 6. The trilinears (A_λ, A_κ) for samples for which the strongest FOPT ends in the SM vacuum. The points are colored by the parameter κ.

figure 4. The distinction between `Type-H-and-S` and `Type-Only-S(maintain)` is that `Type-Only-S(maintain)` favors smaller A_κ and A_λ. Finally, `Type-Only-S(flip)` shows two approximately symmetric regions that were previously identified in figure 4 by the sign of μ_{eff}. The region of positive (negative) A_λ and A_κ corresponds to positive (negative) μ_{eff}.

We emphasize again that the parameter spaces shown in figure 4, figure 5 and figure 6 can only ensure the existence of a SFOPT with $\gamma_{\text{EW}} \gtrsim 1$. Establishing whether this SFOPT is definitely part of the cosmological history requires further investigation, which we only present for our benchmark points.

5.4.2 The strongest FOPT does not end in the SM vacuum

Other than the scenario discussed above, we have plenty of samples in which the strongest FOPT does not end in the SM vacuum, as shown in figure 7. In these samples, in the true vacuum for the strongest FOPT, $\mathfrak{h}$ is always negative and $\mathfrak{s}$ is either zero or has a different sign to μ_{eff}, so this almost certainly does not belong to the SM vacuum in which $\mathfrak{h} = 246\,\text{GeV}$. The spread in the possible true vacuum for the Higgs fields at the critical

JHEP11(2019)151

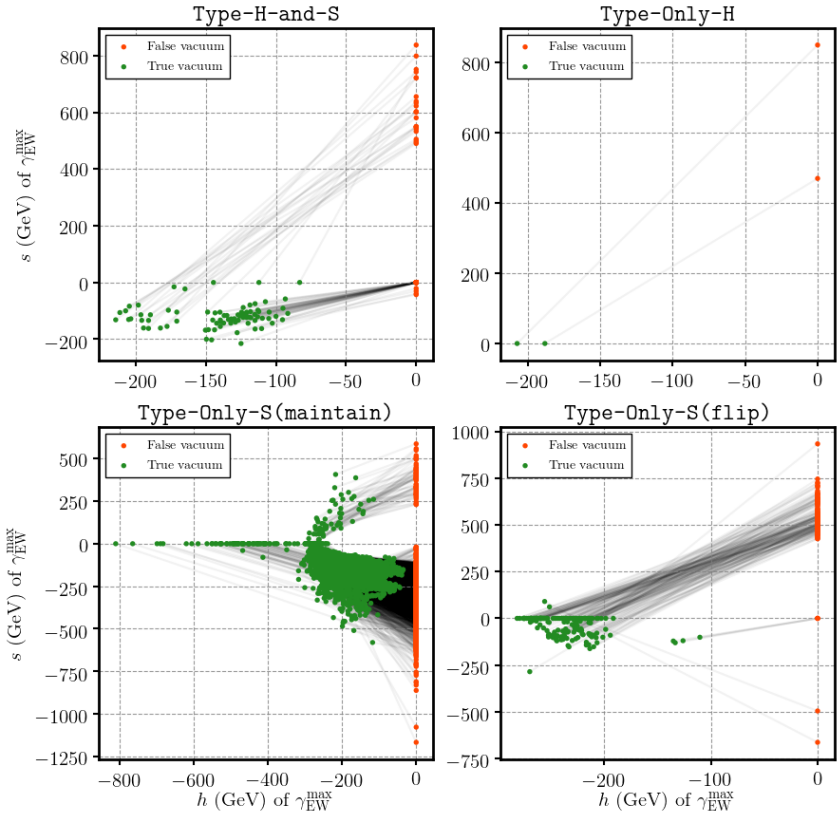

Figure 7. The Higgs and singlet fields at the critical temperature of the strongest FOPT for samples for which the strongest FOPT does not end in the SM vacuum.

temperature is substantial, and could differ considerably from the observed EW vacuum. Because of this, we no longer find that $\mathfrak{h} \approx 246\,\text{GeV}$, allowing enhancement or suppression of the strength of the PT in figure 8, which differs markedly from figure 3. Indeed, in the `Type-Only-S(maintain)` scenario, SFOPTs are possible for substantial critical temperatures of up to $T_C \lesssim 500\,\text{GeV}$.

At first glance, these points might seem uninteresting, as they do not end in the correct zero-temperature vacuum. They may be especially interesting, however, as this means that in order for such samples to achieve the correct zero-temperature vacuum, there must be another EW FOPT transition or sequence of transitions that complete and end in the correct vacuum. Thus in figure 9 we histogram the number of possible FOPTs with $\gamma_{\rm EW} \gtrsim 1$ for each sample. Let us stress that strictly speaking, we count the number of temperatures at which two vacua are degenerate. This differs from the number of FOPTs that can take place in one cosmological history, since only particular routes through the

JHEP11(2019)151

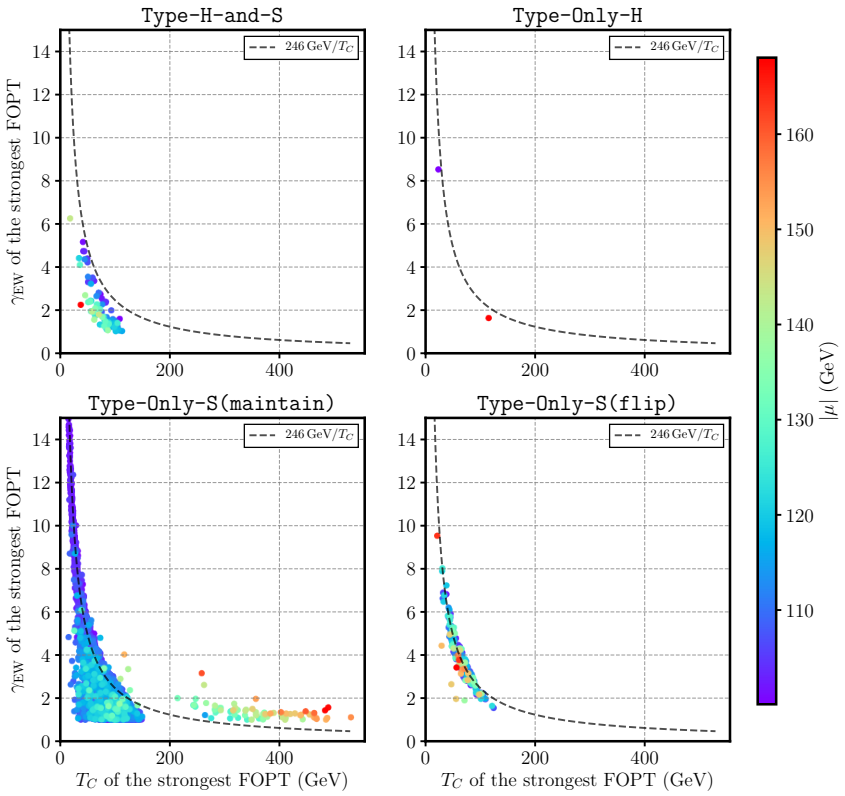

Figure 8. The critical temperature and order parameter for the strongest PTs for samples for which the strongest FOPT does not end in the SM vacuum. The points are colored by the effective μ-parameter.

phases are possible. For example the upper right panel of figure 1 exhibits one or two FOPTs from phase 1 to phase 3, but we would count this though as three. Furthermore FOPTs may also occur between phases that were never degenerate, but such possibilities are not included in our count.

For the samples that end in the SM vacuum (left panel), there is usually a single FOPT with $\gamma_{\rm EW} > 1$, except in the `Type-Only-H` scenario, in which there are often two FOPTs with $\gamma_{\rm EW} > 1$. For the samples that do not end in the SM vacuum (right panel), almost all of `Type-Only-H` and `Type-Only-S(maintain)` samples and about half the `Type-H-and-S` samples have more than one EW SFOPTs. We also checked that for most of them the second strongest FOPT *does* end in the SM vacuum.

Thus, without further calculations, the samples for which the strongest FOPT does not end in the SM vacuum could still potentially explain the observed baryon asymmetry. We display the parameter spaces in figure 10, figure 11 and figure 12. Compared to the

JHEP11(2019)151

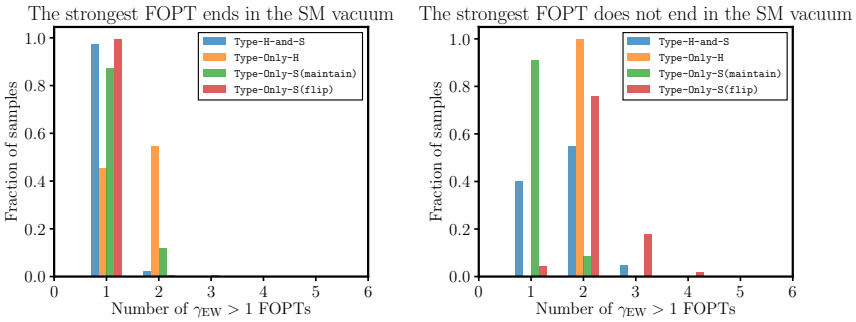

Figure 9. Number of FOPTs with $\gamma_{\rm EW} \gtrsim 1$ per point, for points for which the strongest FOPT ends in the SM vacuum (left panel) and does not end in the SM vacuum (right panel).

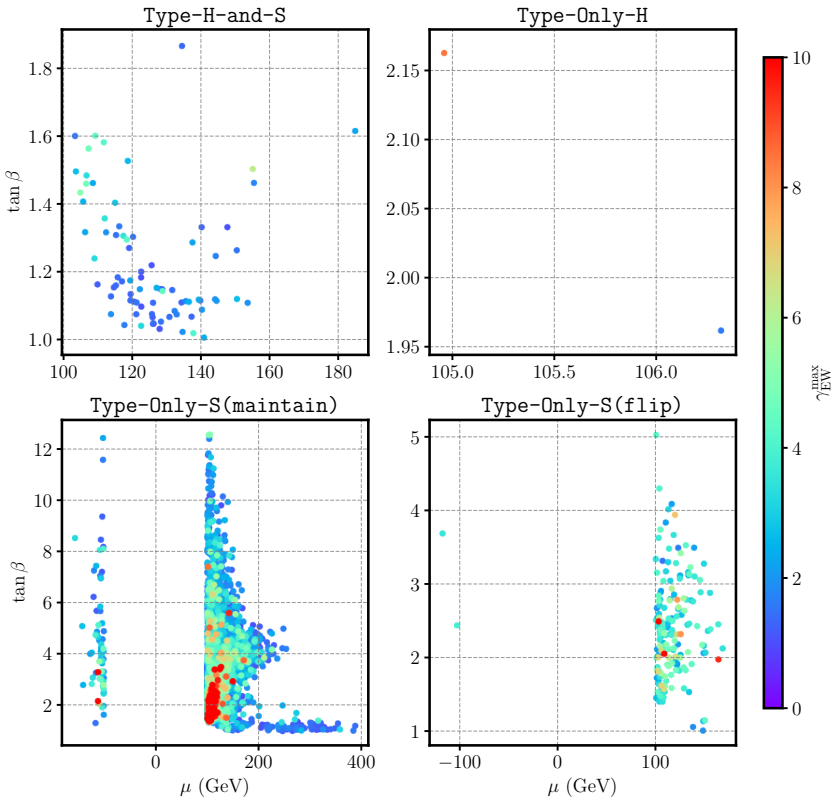

Figure 10. $(\mu_{\rm eff}, \tan\beta)$ for samples for which the strongest FOPT does not end in the SM vacuum. The points are colored by the $\gamma_{\rm EW}$ of the strongest FOPT.

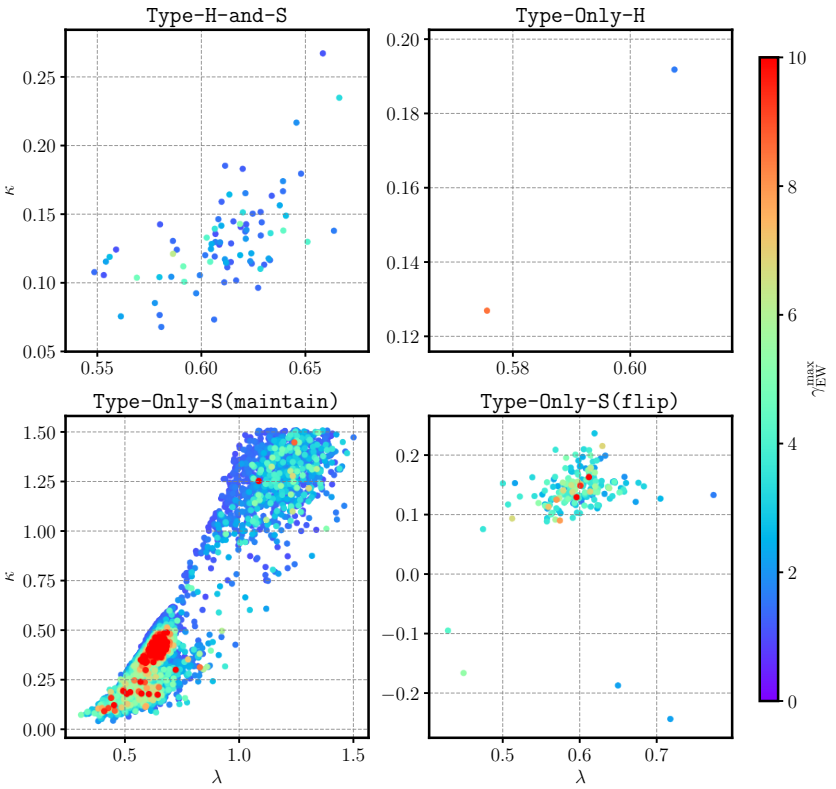

Figure 11. (λ, κ) for samples for which the strongest FOPT does not end in the SM vacuum. The points are colored by the $\gamma_{\rm EW}$ of the strongest FOPT.

scenario in which the strongest FOPT ends in the SM vacuum, the parameter spaces of `Type-H-and-S` and `Type-Only-H` are roughly unchanged, while `Type-Only-S(maintain)` and `Type-Only-S(flip)` exchange parameter spaces with each other. This is because here the `Type-Only-S(maintain)` (`Type-Only-S(flip)`) requires a minimum on the singlet axis with $\mathfrak{s} < 0$ ($\mathfrak{s} > 0$), opposite to the `Type-Only-S(maintain)` (`Type-Only-S(flip)`) scenarios in which the strongest FOPT ends in the SM vacuum.

From figure 10 we see that the constraints on the effective μ-parameter are stricter than they are in the scenario in which the strongest FOPT ends in the SM vacuum, especially for small $\tan\beta$. The `Type-H-and-S`, `Type-Only-H` and `Type-Only-S(flip)` scenarios require an effective μ-parameter smaller than about 200 GeV, whereas the `Type-Only-S(maintain)` permits $\mu_{\rm eff} \lesssim 400\,\text{GeV}$. The slender bar in the `Type-Only-S(maintain)` scenario at $\tan\beta \simeq 1$ and $\mu_{\rm eff} \in [200, 400]\,\text{GeV}$ corresponds to samples with $T_C \gtrsim 200\,\text{GeV}$ for the strongest FOPT, displayed in the lower left panel of figure 8.

In figure 11, a visible difference appears in `Type-Only-S(maintain)` compared to figure 5. The parameter space of λ and κ splits into two separate regions, and relatively

JHEP11(2019)151

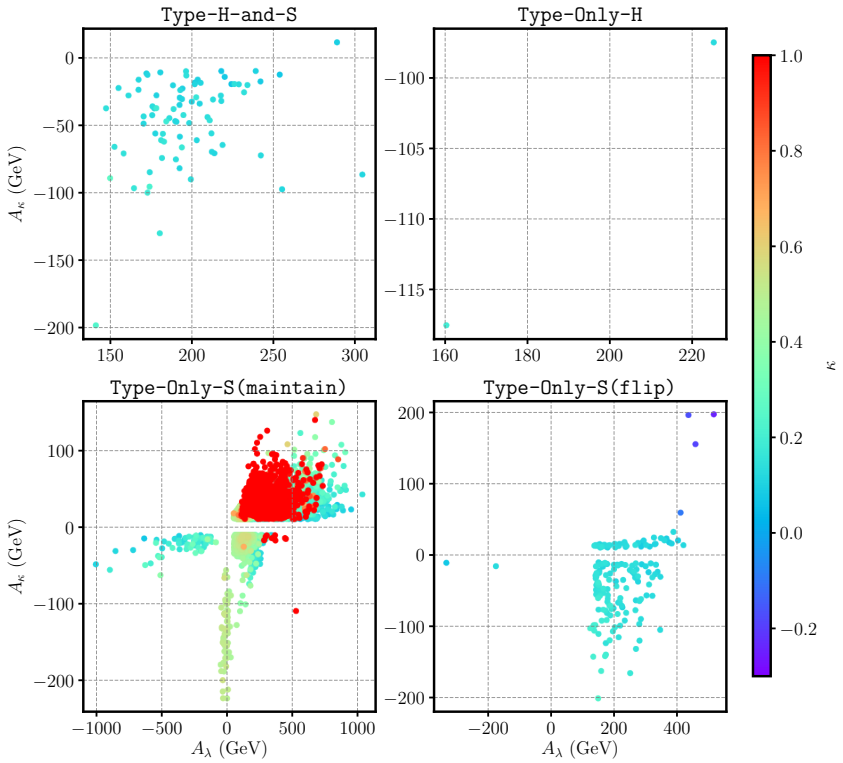

Figure 12. (A_λ, A_κ) for samples for which the strongest FOPT does not end in the SM vacuum. The points are colored by the κ-parameter.

large $\lambda \gtrsim 0.5$ is favored. For instance, when $\kappa \simeq 1.4$, here λ is always larger than 1, whereas in lower left panel of figure 5 λ can be as low as 0.5.

On the trilinear couplings (A_λ, A_κ) plane, there are two additional regions in the `Type-Only-S(maintain)` scenario (lower left, figure 12) compared to the `Type-Only-S(flip)` samples for which the strongest FOPT end in the SM vacuum (lower right, figure 6). First, there is an additional region at $A_\lambda \simeq 0\,\text{GeV}$. This region corresponds to the previously mentioned region at $\tan\beta \simeq 1$ and $\mu_{\text{eff}} \in [200, 400]\,\text{GeV}$, with $T_C \gtrsim 200\,\text{GeV}$ for the strongest FOPT. Second, there is an additional region at $A_\kappa \simeq -50\,\text{GeV}$ and $A_\lambda > 0$. This region is similar to one in the `Type-Only-S(flip)` scenario (lower right, figure 12). Indeed, for this region, as well as the strongest FOPT that maintains the sign of singlet, there is another weaker FOPT that flips the sign of singlet.

In summary, the scenario in which the strongest FOPT does not end in the SM vacuum introduces new interesting regions of parameter space that were not covered by the scenarios in which the strongest FOPT ends in the SM vacuum. These scenarios may be especially interesting because they could be followed by additional FOPTs. However, at the same

JHEP11(2019)151

time there is an additional requirements to ensure that the subsequent transitions actually lead to the EW breaking phase we observe today, which we have not checked.

5.5 Properties of the Higgs bosons

As shown by our benchmark points, although our points pass experimental constraints from LEP and the LHC, our scenarios are not in a decoupling regime in which Higgses other than the 125 GeV one are heavy. This is not surprising since it is well known that in the NMSSM a light singlet Higgs state plays an important role in generating a FOPT that breaks EW symmetry [16, 25, 56], without the need for light stops which are heavily constrained by LHC searches [120, 121]. In fact, in all our benchmarks, all Higgs bosons are lighter than about 400 GeV, while there are always at least two CP even Higgs states with masses below 600 GeV in the samples from our scan, with the SM-like Higgs being either h_1 or h_2.

In figure 13 we show the masses of the non-SM-like CP even neutral Higgs bosons in our four scenarios by plotting the mass of h_3, which is never SM-like, against the mass of the Higgs (either h_1 or h_2) that did not play the role of the SM-like Higgs. Samples that are allowed by experimental constraints are shown by green points. We also show excluded samples to aid explanations (gray and blue points).

For the samples where the strongest FOPT ends in the SM vacuum we see that the SM-like Higgs is actually the next to lightest CP even Higgs for almost all allowed samples (green points) in `Type-H-and-S`, `Type-Only-H` and `Type-Only-S(maintain)`, with just three exceptions that all appear in the `Type-H-and-S` samples. In contrast, in the `Type-Only-S(flip)` scenarios, the SM-like Higgs can be either the lightest Higgs or the next to lightest Higgs. The samples where the strongest FOPT does not end in the SM vacuum show very similar results, but as usual the patterns of the `Type-Only-S(maintain)` and `Type-Only-S(flip)` scenarios are exchanged.

The reason we see so few samples where the SM-like Higgs is the lightest state for the categories mentioned above seems to be the constraints on the observed Higgs. We note that, although it is not clear in the plot, for these types of scenarios there are already a significantly larger number of gray points where the SM-like Higgs is the second lightest CP even Higgs boson than there are for the case where it is the lightest. Applying the constraints on the SM-like Higgs from `Lilith-1.1.4_DB-17.05` then reduces the number of samples where it is the lightest to almost zero. The samples excluded by `HiggsBounds-5.3.2beta` in `Type-Only-S(flip)` scenario for which the strongest FOPT ends in the SM vacuum and `Type-Only-S(maintain)` scenario for which the strongest FOPT does not end in the SM vacuum (shown by blue points) are mainly excluded by an LHC search for a scalar resonance decaying to a pair of Z bosons [122]. It is also worth noting that even without the requirement of an SFOPT, similar observations have been made in the NMSSM previously. A preference for the SM-like Higgs being the next to lightest one was also found in a global analysis of the NMSSM [123] that did not consider PTs.

Lastly, we note that many of the panels in figure 13 appear to indicate an upper bound on the mass of the heaviest Higgs, m_{h_3}, in each scenario. For example, for the `Type-H-and-S` scenario in which the strongest FOPT ends in the SM vacuum, the samples allowed

JHEP11(2019)151

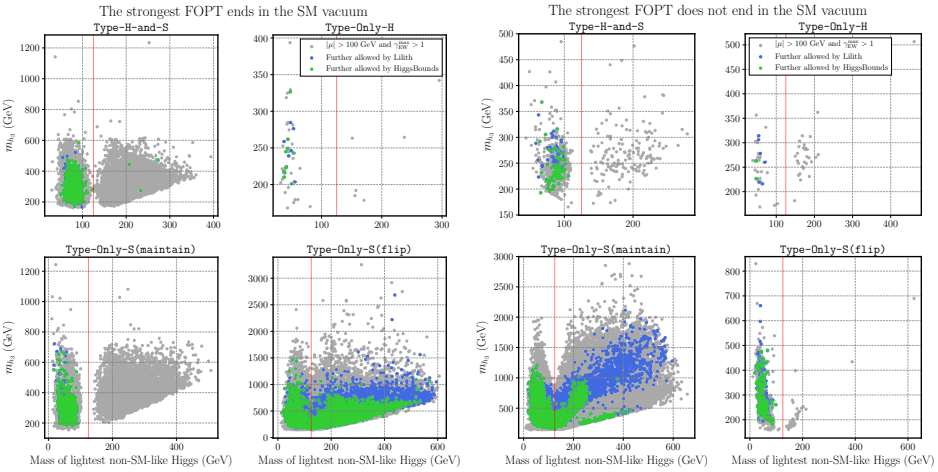

Figure 13. Masses of the non-SM-like Higgs bosons in our four scenarios, for points for which the strongest FOPT ends in the SM vacuum (left block of four plots) and does not end in the SM vacuum (right block of four plots). We show points satisfying $\mu > 100\,\text{GeV}$ and $\gamma_{\text{EW}} > 1$ (gray), further allowed by `Lilith-1.1.4_DB-17.05` [110] constraints on the SM-like Higgs (blue), and by `HiggsBounds-5.3.2beta` [114–118] constraints on non-SM-like Higgses (green). The vertical red line indicates $m_h = 125\,\text{GeV}$ in each panel.

by collider constraints on Higgs bosons (green points) stop at about $m_{h_3} \lesssim 500\,\text{GeV}$. However, despite collecting more than three million samples, we judged our coverage at the largest Higgs masses to be inadequate to reliably address the question of whether upper bounds on the Higgs masses exist, as large masses may just be rare with our sampling strategy. We checked, however, that experimental constraints on the Higgs sector appear to be (at most) weakly sensitive to m_{h_3}. We thus anticipate that there is in fact no upper bound on the mass of the heaviest Higgs, as we suspect that it can be arbitrarily heavy without impacting the phase structure or Higgs observables.

6 Conclusions

Motivated by EW baryogenesis and gravitational wave experiments, in this article we investigated the properties of PTs in the NMSSM. We employed an effective field theory approach to calculate the finite temperature effective potential by matching the NMSSM to the THDMS. By tracing the change in the minima of the effective potential with temperature, we mapped out the phase structure and computed the strengths of any EWPTs, γ_{EW}. By scanning the parameter space of the NMSSM, we obtained millions of samples that featured an SFOPT with $\gamma_{\text{EW}} > 1$ and satisfied the constraints from LHC Higgs measurements and LEP bounds on charginos.

We classified them into three categories, `Type-H-and-S`, `Type-Only-H` and `Type-Only-S`, based on the nature of the first PT in their cosmological histories. The `Type-`

JHEP11(2019)151

Only-S samples were further divided into Type-Only-S(maintain) and Type-Only-S (flip) according to whether the singlet VEV changed sign during the strongest EWPT. In the Type-H-and-S samples, the first PT in the cosmological history breaks EW symmetry and gives the singlet a VEV at the same time. This transition is usually the strongest one.

The Type-Only-H samples, on the other hand, go through a series of PTs that break, restore and break again EW symmetry. The first one is a crossover transition during which only the h_d field obtains a non-vanishing VEV, and the last one is the strongest EW FOPT. This scenario was by far the rarest in our scan. For the Type-Only-S(maintain) samples, during the first transition EW symmetry remains unbroken, but the singlet field obtains a non-vanishing VEV. Then EW symmetry breaks through a subsequent FOPT. Both of the transitions can be SFOPTs, which could give interesting gravitational wave signatures [124] as well as triggering an EW baryogenesis mechanism. The first PT of the Type-Only-S(flip) samples is usually a FOPT with very small γ, and the following strongest FOPT flips the sign of the singlet VEV. We found, however, that the tunneling rates in Type-Only-H and Type-Only-S(flip) scenarios could be problematic. For our benchmarks, the SFOPT in the Type-Only-H scenario did not complete, and in the Type-Only-S(flip) scenario, a preceding PT required to reach the SFOPT did not complete. Thus, unfortunately, these scenarios might not help EW baryogenesis.

The regions of NMSSM parameter space in which the four scenarios occur show different features. In the samples for which the strongest FOPT ends in the observed zero temperature phase:

- The observed 125 GeV Higgs is often the second lightest Higgs in the model, not the lightest one.
- All of the input parameters are severely constrained, except the SUSY scale m_{SUSY} and stop trilinear A_t.
- Quartic couplings of around $\lambda \simeq 0.6$ and $\kappa \simeq 0.2$ could result in an SFOPT in all our scenarios, though a broad range of couplings result in SFOPTs in the Type-Only-S (flip) scenario, including couplings far away from limits on perturbativity.
- The scenarios predict different trilinear couplings, i.e., they are distinguishable on the (A_λ, A_κ) plane. The A_λ and A_κ of the Type-Only-S(flip) samples always have the same sign, while in the other scenarios the samples are concentrated in the quadrant of negative A_κ and positive A_λ. Compared to the Type-H-and-S scenario, the Type-Only-S(maintain) scenario favors smaller $|A_\kappa|$ and A_λ.

In addition we found substantial samples for which the strongest FOPT does not end in the SM vacuum. The regions of parameter space are similar to the samples for which the strongest FOPT ends in the SM vacuum, except that Type-Only-S(maintain) and Type-Only-S(flip) exchange parameter spaces with each other. There are, furthermore, two additional regions that appear in the Type-Only-S(maintain) scenario, and one of them results in critical temperatures higher than 200 GeV.

JHEP11(2019)151

In summary, we mapped out and classified intricate patterns of symmetry breaking that are possible in the NMSSM, and checked which scenarios could in principle help provide a viable theory of EW baryogenesis or potentially lead to a gravitational wave signal. We found viable scenarios in which the Higgs fields and singlet or only singlet first acquired VEVs. We checked that the sequences of required PTs actually nucleated, contained a SFOPT, and that the model satisfied constraints from LEP and the LHC. The combination of constraints lead to the predictions that $\lambda \simeq 0.6$, $\kappa \simeq 0.2$ and that the observed 125 GeV Higgs tends to be the second lightest Higgs in the model.

Acknowledgments

We thank Sujeet Akula for early collaboration on the paper. We are grateful for Margarete Mühlleitner and Jonathan Kozaczuk for responding to queries regarding previous work and Junjie Cao for helpful remarks. TRIUMF receives federal funding via a contribution agreement with the National Research Council of Canada and the Natural Science and Engineering Research Council of Canada. The work of P.A. is supported by the Australian Research Council Future Fellowship grant FT160100274. The work of C.B. was supported by the Australian Research Council through the ARC Centre of Excellence for Particle Physics at the Terascale (grant CE110001104). The work of P.A. and C.B. are also supported with the Australian Research Council Discovery Project grant DP180102209.

A Field dependent masses

When exploring the potential away from minima we need to account for the Higgs field dependence of the $\overline{\text{MS}}$ mass eigenstates in (3.1). Therefore here we present the so-called field dependent masses of the THDMS.

The field dependent masses of the gauge bosons and top, bottom and tau fermions are given by the simple tree-level expressions

$$\begin{gathered} M_W^2 = \tfrac{1}{4}g^2\left(h_u^2+h_d^2\right), \quad M_Z^2 = \tfrac{1}{4}\left(g'^2+g^2\right)\left(h_u^2+h_d^2\right), \\ m_t = \tfrac{1}{\sqrt{2}}y_t h_u, \quad m_b = \tfrac{1}{\sqrt{2}}y_b h_d, \quad m_\tau = \tfrac{1}{\sqrt{2}}y_\tau h_d, \end{gathered} \tag{A.1}$$

where the gauge couplings are without GUT normalization, and the y_t, y_b and y_τ are the $(3,3)$ elements of the corresponding Yukawa matrices.

Since the Higgs states mix, the CP even, CP odd and charged $\overline{\text{MS}}$ Higgs masses are the eigenvalues of the corresponding CP even, CP odd and charged mass matrices. The mass matrix for the CP even neutral Higgs bosons, in the basis $\{H_d, H_u, S\}$, is

$$\begin{aligned} \left(M_{H^0}^2\right)_{11} &= \overline{m}_1^2 + \frac{3}{2}\lambda_1 h_d^2 + \frac{1}{2}\lambda_5 s^2 + \frac{1}{2}(\lambda_3+\lambda_4)h_u^2, \\ \left(M_{H^0}^2\right)_{22} &= \overline{m}_2^2 + \frac{3}{2}\lambda_2 h_u^2 + \frac{1}{2}\lambda_6 s^2 + \frac{1}{2}(\lambda_3+\lambda_4)h_d^2, \\ \left(M_{H^0}^2\right)_{33} &= \overline{m}_S^2 - \sqrt{2}\,\mathrm{Re}(m_5)s + \frac{1}{2}\lambda_5 h_d^2 + \mathrm{Re}(\lambda_7)h_u h_d + \frac{1}{2}\lambda_6 h_u^2 + 3\lambda_8 s^2, \\ \left(M_{H^0}^2\right)_{12} &= \left(M_{H^0}^2\right)_{21} = -\frac{1}{\sqrt{2}}\,\mathrm{Re}(m_4)s + \frac{1}{2}\,\mathrm{Re}(\lambda_7)s^2 + (\lambda_3+\lambda_4)h_u h_d, \end{aligned}$$

JHEP11(2019)151

$$\begin{aligned}
\left(M^2_{H^0}\right)_{13} &= \left(M^2_{H^0}\right)_{31} = -\frac{1}{\sqrt{2}}\,\mathrm{Re}(m_4)h_u + \lambda_5 h_d s + \mathrm{Re}(\lambda_7)h_u s,\\
\left(M^2_{H^0}\right)_{23} &= \left(M^2_{H^0}\right)_{32} = -\frac{1}{\sqrt{2}}\,\mathrm{Re}(m_4)h_d + \mathrm{Re}(\lambda_7)h_d s + \lambda_6 h_u s.
\end{aligned} \tag{A.2}$$

where we have written $\overline{m}_1^2$, $\overline{m}_2^2$ and $\overline{m}_S^2$ with a bar to denote the fact that in this context these are fixed to fulfill the following tree-level EW symmetry breaking (EWSB) conditions

$$\begin{aligned}
\overline{m}_1^2 &= -\frac{1}{2}(\lambda_3+\lambda_4)v_u^2 - \frac{1}{2}\lambda_1 v_d^2 - \frac{1}{2}\lambda_5 v_S^2 - \frac{1}{2}\,\mathrm{Re}(\lambda_7)\frac{v_u v_S^2}{v_d} + \frac{1}{\sqrt{2}}\,\mathrm{Re}(m_4)\frac{v_u v_S}{v_d},\\
\overline{m}_2^2 &= -\frac{1}{2}\lambda_2 v_u^2 - \frac{1}{2}(\lambda_3+\lambda_4)v_d^2 - \frac{1}{2}\lambda_6 v_S^2 - \frac{1}{2}\,\mathrm{Re}(\lambda_7)\frac{v_d v_S^2}{v_u} + \frac{1}{\sqrt{2}}\,\mathrm{Re}(m_4)\frac{v_d v_S}{v_u},\\
\overline{m}_S^2 &= -\frac{1}{2}\lambda_6 v_u^2 - \frac{1}{2}\lambda_5 v_d^2 - \lambda_8 v_S^2 - \mathrm{Re}(\lambda_7)v_d v_u + \frac{1}{\sqrt{2}}\,\mathrm{Re}(m_4)\frac{v_u v_d}{v_S} + \frac{1}{\sqrt{2}}\,\mathrm{Re}(m_5)v_S.
\end{aligned} \tag{A.3}$$

Note that the VEVs appearing on the right hand side are the zero temperature VEVs, so $\overline{m}_1^2$, $\overline{m}_2^2$ and $\overline{m}_S^2$ do not vary with either temperature or with the fields. If we permit a complex phase in the THDMS parameters, there is in fact an additional tadpole equation relating it to complex phases in the VEVs. As we assume real, CP conserving VEVs, however, this extra tadpole simply forces the complex phase in the THDMS parameters to vanish. The three CP even mass eigenstates, h_1, h_2 and h_3, are then found by diagonalizing $M^2_{H^0}$.

Similarly, the CP odd mass matrix is

$$\begin{aligned}
\left(M^2_A\right)_{11} &= \overline{m}_1^2 + \frac{1}{2}\lambda_1 h_d^2 + \frac{1}{2}\lambda_5 s^2 + \frac{1}{2}(\lambda_3+\lambda_4)h_u^2,\\
\left(M^2_A\right)_{22} &= \overline{m}_2^2 + \frac{1}{2}\lambda_2 h_u^2 + \frac{1}{2}\lambda_6 s^2 + \frac{1}{2}(\lambda_3+\lambda_4)h_d^2,\\
\left(M^2_A\right)_{33} &= \overline{m}_S^2 + \sqrt{2}\,\mathrm{Re}(m_5)s + \frac{1}{2}\lambda_5 h_d^2 - \mathrm{Re}(\lambda_7)h_u h_d + \frac{1}{2}\lambda_6 h_u^2 + \lambda_8 s^2,\\
\left(M^2_A\right)_{12} &= \left(M^2_A\right)_{21} = \frac{1}{\sqrt{2}}\,\mathrm{Re}(m_4)s - \frac{1}{2}\,\mathrm{Re}(\lambda_7)s^2,\\
\left(M^2_A\right)_{13} &= \left(M^2_A\right)_{31} = \frac{1}{\sqrt{2}}\,\mathrm{Re}(m_4)h_u + \mathrm{Re}(\lambda_7)h_u s,\\
\left(M^2_A\right)_{23} &= \left(M^2_A\right)_{32} = \frac{1}{\sqrt{2}}\,\mathrm{Re}(m_4)h_d + \mathrm{Re}(\lambda_7)h_d s.
\end{aligned} \tag{A.4}$$

Diagonalizing it results in a neutral Goldstone boson G^0 and the two physical CP odd Higgs bosons, A_1 and A_2. The field dependent Goldstone masses are only zero at extrema of the tree-level potential. Thus, away from extrema, we cannot easily distinguish Goldstone bosons from physical Higgs bosons. In the $\xi = 1$ gauge, however, they are treated on an equal footing and we do not need to identify Goldstones.

Finally, the charged Higgs mass matrix is

$$\begin{aligned}
\left(M^2_{H^\pm}\right)_{11} &= \overline{m}_1^2 + \frac{1}{2}\lambda_5 s^2 + \frac{1}{2}\lambda_1 h_d^2 + \frac{1}{2}\lambda_3 h_u^2,\\
\left(M^2_{H^\pm}\right)_{22} &= \overline{m}_2^2 + \frac{1}{2}\lambda_6 s^2 + \frac{1}{2}\lambda_3 h_d^2 + \frac{1}{2}\lambda_2 h_u^2,\\
\left(M^2_{H^\pm}\right)_{21} &= \left(M^2_{H^\pm}\right)^*_{12} = \frac{1}{\sqrt{2}}m_4 s - \frac{1}{2}\lambda_7 s^2 - \frac{1}{2}\lambda_4 h_d h_u.
\end{aligned} \tag{A.5}$$

Diagonalizing it results in the charged Higgs boson, $H^\pm$ and the charged Goldstone boson $G^\pm$.

JHEP11(2019)151

Gauge-fixing, however, alters the tree-level mass matrices, such that the field dependent scalar masses are gauge dependent. The CP even mass matrix receives no gauge-fixing contribution but the CP odd and charged mass matrices receive additional contributions in the R_ξ gauge,

$$\begin{aligned}
\left(M_A^2\right)_{11} &\to \left(M_A^2\right)_{11} + \frac{1}{4}\xi(g^2+g'^2)h_d^2, \\
\left(M_A^2\right)_{12} &\to \left(M_A^2\right)_{12} - \frac{1}{4}\xi(g^2+g'^2)h_d h_u, \\
\left(M_A^2\right)_{22} &\to \left(M_A^2\right)_{22} + \frac{1}{4}\xi(g^2+g'^2)h_u^2, \\
\left(M_{H^\pm}^2\right)_{11} &\to \left(M_{H^\pm}^2\right)_{11} + \frac{1}{4}\xi g^2 h_d^2, \\
\left(M_{H^\pm}^2\right)_{12} &\to \left(M_{H^\pm}^2\right)_{12} - \frac{1}{4}\xi g^2 h_d h_u, \\
\left(M_{H^\pm}^2\right)_{22} &\to \left(M_{H^\pm}^2\right)_{22} + \frac{1}{4}\xi g^2 h_u^2.
\end{aligned} \tag{A.6}$$

The elements involving the singlet are unaffected. At the tree-level minimum, in which the Goldstone bosons are otherwise massless, the gauge-fixing contributions do not affect the masses of the physical Higgs bosons but result in Goldstone masses

$$\begin{aligned}
M_{G^0}^2 &= \xi M_Z^2, \\
M_{G^\pm}^2 &= \xi M_W^2,
\end{aligned} \tag{A.7}$$

where M_W and M_Z are the masses of the W and Z bosons.

B Numerical methods for FOPTs

We first find all minima of the potential at $T = 0$ and $T = 1\,\text{TeV}$ to check that spontaneous symmetry breaking occurs,[9] where in particular we reject points where the deepest $T = 0$ minima is not the observed SM vacuum. If it occurs, we trace the trajectory with temperature of every $T = 0$ and $T = 1\,\text{TeV}$ minima. We call the trajectory of a particular minima a phase (note though this definition cannot distinguish phases linked by second-order or crossover transitions). A phase ends at the temperature at which the minima disappears. If two phases coexist at the same temperature, there may exist a critical temperature at which they are degenerate.

We apply an algorithm developed in `CosmoTransitions` [97] to trace phases in steps no greater than ΔT:

0. We select a minima $\mathfrak{m} \equiv (\mathfrak{h}_u, \mathfrak{h}_d, \mathfrak{s})$ at temperature T to trace.

1. We use a local minimum finding algorithm, such as Nelder-Mead [125], to find the minimum $\mathfrak{m}'$ at $T' = T + \Delta T$.

2. We check that the new minimum $\mathfrak{m}'$ lies close to that expected from a shift caused by thermal corrections.

[9] Our search for minima is restricted to field values within the range $-1.6\,\text{TeV}$ to $1.6\,\text{TeV}$.

JHEP11(2019)151

We calculate the difference

$$R = \max\left(\left\|\mathfrak{m} + \left.\frac{\partial \mathfrak{m}}{\partial T}\right|_{\mathfrak{m}} \Delta T - \mathfrak{m}'\right\|, \left\|\mathfrak{m}' - \left.\frac{\partial \mathfrak{m}}{\partial T}\right|_{\mathfrak{m}'} \Delta T - \mathfrak{m}\right\|\right). \tag{B.1}$$

3. If $R \leq \max R$, where $\max R$ governs the maximum acceptable changes in the field, we accept that the minima $\mathfrak{m}'$ at temperature T' belongs to the same phase as the minima $\mathfrak{m}$ at temperature T. We continue to trace the phase by returning to step 1 with $\mathfrak{m} \to \mathfrak{m}'$ and $T \to T'$, and we reset any changes to ΔT.

   If $R > \max R$, we assume that the change in temperature dramatically changed the potential. We reduce the change in temperature by a factor of two, $\Delta T \to \Delta T/2$, and return to 1.

   If, however, $R > \max R$ and $|\Delta T| < \min \Delta T$, where $\min \Delta T$ governs the smallest permissible step in temperature, we conclude that the phase must have ended, as the minima appears to change abruptly with a small change in temperature.

We save the sequence of minima and temperature found through this process — this is a phase. We find all the phases by tracing all $T = 0$ minima up to at most 1 TeV (the phase may end earlier) and all $T = 1$ TeV minima down to $T = 0$ (in which case $\Delta T < 0$). After removing degenerate phases, we denote the i-th phase by $\mathfrak{m}_i(T)$.

If any two of the phases, e.g., the i-th and j-th phase, coexist between temperatures T_1 and T_2, and if

$$V_{\text{eff}}(\mathfrak{m}_i(T_1), T_1) > V_{\text{eff}}(\mathfrak{m}_j(T_1), T_1) \tag{B.2}$$

$$V_{\text{eff}}(\mathfrak{m}_i(T_2), T_2) < V_{\text{eff}}(\mathfrak{m}_j(T_2), T_2) \tag{B.3}$$

there must exit a critical temperature, T_C, between temperatures T_1 and T_2 at which they are degenerate,

$$V_{\text{eff}}(\mathfrak{m}_i(T_C), T_C) = V_{\text{eff}}(\mathfrak{m}_j(T_C), T_C). \tag{B.4}$$

We calculate the critical temperature using bisection, and find properties of the transition, e.g., the strength of transition from (4.3).

References

[1] D.E. Morrissey and M.J. Ramsey-Musolf, *Electroweak baryogenesis*, *New J. Phys.* **14** (2012) 125003 [arXiv:1206.2942] [INSPIRE].

[2] J.M. Cline, *Baryogenesis*, in *Les Houches Summer School — Session 86: Particle Physics and Cosmology: The Fabric of Spacetime Les Houches, France, July 31 – August 25, 2006*, 2006, hep-ph/0609145 [INSPIRE].

[3] G.A. White, *A Pedagogical Introduction to Electroweak Baryogenesis*, Morgan & Claypool Publishers, (2016), pp. 2053–2571, [https://doi.org/10.1088/978-1-6817-4457-5].

JHEP11(2019)151

[4] G. Krnjaic, *Can the Baryon Asymmetry Arise From Initial Conditions?*, *Phys. Rev.* **D 96** (2017) 035041 [arXiv:1606.05344] [INSPIRE].

[5] A.D. Sakharov, *Violation of CP invariance, C asymmetry, and baryon asymmetry of the universe*, *Pis'ma Zh. Eksp. Teor. Fiz.* **5** (1967) 32.

[6] M. D'Onofrio and K. Rummukainen, *Standard model cross-over on the lattice*, *Phys. Rev.* **D 93** (2016) 025003 [arXiv:1508.07161] [INSPIRE].

[7] Particle Data Group collaboration, *Review of Particle Physics*, *Chin. Phys.* **C 40** (2016) 100001 [INSPIRE].

[8] Planck collaboration, *Planck 2015 results. XIII. Cosmological parameters*, *Astron. Astrophys.* **594** (2016) A13 [arXiv:1502.01589] [INSPIRE].

[9] M. Trodden, *Electroweak baryogenesis*, *Rev. Mod. Phys.* **71** (1999) 1463 [hep-ph/9803479] [INSPIRE].

[10] J.M. Cline, M. Jarvinen and F. Sannino, *The Electroweak Phase Transition in Nearly Conformal Technicolor*, *Phys. Rev.* **D 78** (2008) 075027 [arXiv:0808.1512] [INSPIRE].

[11] J.M. Cline, G. Laporte, H. Yamashita and S. Kraml, *Electroweak Phase Transition and LHC Signatures in the Singlet Majoron Model*, *JHEP* **07** (2009) 040 [arXiv:0905.2559] [INSPIRE].

[12] D. Borah and J.M. Cline, *Inert Doublet Dark Matter with Strong Electroweak Phase Transition*, *Phys. Rev.* **D 86** (2012) 055001 [arXiv:1204.4722] [INSPIRE].

[13] J.M. Cline and K. Kainulainen, *Improved Electroweak Phase Transition with Subdominant Inert Doublet Dark Matter*, *Phys. Rev.* **D 87** (2013) 071701 [arXiv:1302.2614] [INSPIRE].

[14] T. Konstandin, *Quantum Transport and Electroweak Baryogenesis*, *Phys. Usp.* **56** (2013) 747 [arXiv:1302.6713] [INSPIRE].

[15] J. Kozaczuk, S. Profumo, L.S. Haskins and C.L. Wainwright, *Cosmological Phase Transitions and their Properties in the NMSSM*, *JHEP* **01** (2015) 144 [arXiv:1407.4134] [INSPIRE].

[16] S. Profumo, M.J. Ramsey-Musolf, C.L. Wainwright and P. Winslow, *Singlet-catalyzed electroweak phase transitions and precision Higgs boson studies*, *Phys. Rev.* **D 91** (2015) 035018 [arXiv:1407.5342] [INSPIRE].

[17] D. Curtin, P. Meade and C.-T. Yu, *Testing Electroweak Baryogenesis with Future Colliders*, *JHEP* **11** (2014) 127 [arXiv:1409.0005] [INSPIRE].

[18] F.P. Huang and C.S. Li, *Electroweak baryogenesis in the framework of the effective field theory*, *Phys. Rev.* **D 92** (2015) 075014 [arXiv:1507.08168] [INSPIRE].

[19] S. Inoue, G. Ovanesyan and M.J. Ramsey-Musolf, *Two-Step Electroweak Baryogenesis*, *Phys. Rev.* **D 93** (2016) 015013 [arXiv:1508.05404] [INSPIRE].

[20] A. Katz, M. Perelstein, M.J. Ramsey-Musolf and P. Winslow, *Stop-Catalyzed Baryogenesis Beyond the MSSM*, *Phys. Rev.* **D 92** (2015) 095019 [arXiv:1509.02934] [INSPIRE].

[21] K. Fuyuto, J. Hisano and E. Senaha, *Toward verification of electroweak baryogenesis by electric dipole moments*, *Phys. Lett.* **B 755** (2016) 491 [arXiv:1510.04485] [INSPIRE].

[22] F.P. Huang, P.-H. Gu, P.-F. Yin, Z.-H. Yu and X. Zhang, *Testing the electroweak phase transition and electroweak baryogenesis at the LHC and a circular electron-positron collider*, *Phys. Rev.* **D 93** (2016) 103515 [arXiv:1511.03969] [INSPIRE].

JHEP11(2019)151

[23] A. Kobakhidze, L. Wu and J. Yue, *Electroweak Baryogenesis with Anomalous Higgs Couplings*, *JHEP* **04** (2016) 011 [arXiv:1512.08922] [INSPIRE].

[24] F.P. Huang, Y. Wan, D.-G. Wang, Y.-F. Cai and X. Zhang, *Hearing the echoes of electroweak baryogenesis with gravitational wave detectors*, *Phys. Rev.* **D 94** (2016) 041702 [arXiv:1601.01640] [INSPIRE].

[25] A.V. Kotwal, M.J. Ramsey-Musolf, J.M. No and P. Winslow, *Singlet-catalyzed electroweak phase transitions in the 100 TeV frontier*, *Phys. Rev.* **D 94** (2016) 035022 [arXiv:1605.06123] [INSPIRE].

[26] V. Vaskonen, *Electroweak baryogenesis and gravitational waves from a real scalar singlet*, *Phys. Rev.* **D 95** (2017) 123515 [arXiv:1611.02073] [INSPIRE].

[27] C. Balázs, G. White and J. Yue, *Effective field theory, electric dipole moments and electroweak baryogenesis*, *JHEP* **03** (2017) 030 [arXiv:1612.01270] [INSPIRE].

[28] A. Beniwal, M. Lewicki, J.D. Wells, M. White and A.G. Williams, *Gravitational wave, collider and dark matter signals from a scalar singlet electroweak baryogenesis*, *JHEP* **08** (2017) 108 [arXiv:1702.06124] [INSPIRE].

[29] G. Kurup and M. Perelstein, *Dynamics of Electroweak Phase Transition In Singlet-Scalar Extension of the Standard Model*, *Phys. Rev.* **D 96** (2017) 015036 [arXiv:1704.03381] [INSPIRE].

[30] S. Akula, C. Balázs, L. Dunn and G. White, *Electroweak baryogenesis in the $\mathbb{Z}_3$-invariant NMSSM*, *JHEP* **11** (2017) 051 [arXiv:1706.09898] [INSPIRE].

[31] C.-W. Chiang, M.J. Ramsey-Musolf and E. Senaha, *Standard Model with a Complex Scalar Singlet: Cosmological Implications and Theoretical Considerations*, *Phys. Rev.* **D 97** (2018) 015005 [arXiv:1707.09960] [INSPIRE].

[32] Q.-H. Cao, F.P. Huang, K.-P. Xie and X. Zhang, *Testing the electroweak phase transition in scalar extension models at lepton colliders*, *Chin. Phys.* **C 42** (2018) 023103 [arXiv:1708.04737] [INSPIRE].

[33] M.J. Ramsey-Musolf, P. Winslow and G. White, *Color Breaking Baryogenesis*, *Phys. Rev.* **D 97** (2018) 123509 [arXiv:1708.07511] [INSPIRE].

[34] F.P. Huang and C.S. Li, *Probing the baryogenesis and dark matter relaxed in phase transition by gravitational waves and colliders*, *Phys. Rev.* **D 96** (2017) 095028 [arXiv:1709.09691] [INSPIRE].

[35] J. de Vries, M. Postma, J. van de Vis and G. White, *Electroweak Baryogenesis and the Standard Model Effective Field Theory*, *JHEP* **01** (2018) 089 [arXiv:1710.04061] [INSPIRE].

[36] L. Niemi, H.H. Patel, M.J. Ramsey-Musolf, T.V.I. Tenkanen and D.J. Weir, *Electroweak phase transition in the real triplet extension of the SM: Dimensional reduction*, *Phys. Rev.* **D 100** (2019) 035002 [arXiv:1802.10500] [INSPIRE].

[37] T. Modak and E. Senaha, *Electroweak baryogenesis via bottom transport*, *Phys. Rev.* **D 99** (2019) 115022 [arXiv:1811.08088] [INSPIRE].

[38] M. Carena, M. Quirós and Y. Zhang, *Electroweak Baryogenesis from Dark-Sector CP-violation*, *Phys. Rev. Lett.* **122** (2019) 201802 [arXiv:1811.09719] [INSPIRE].

[39] M. Chala, M. Ramos and M. Spannowsky, *Gravitational wave and collider probes of a triplet Higgs sector with a low cutoff*, *Eur. Phys. J.* **C 79** (2019) 156 [arXiv:1812.01901] [INSPIRE].

JHEP11(2019)151

[40] R. Zhou, W. Cheng, X. Deng, L. Bian and Y. Wu, *Electroweak phase transition and Higgs phenomenology in the Georgi-Machacek model*, *JHEP* **01** (2019) 216 [arXiv:1812.06217] [INSPIRE].

[41] A. Alves, T. Ghosh, H.-K. Guo, K. Sinha and D. Vagie, *Collider and Gravitational Wave Complementarity in Exploring the Singlet Extension of the Standard Model*, *JHEP* **04** (2019) 052 [arXiv:1812.09333] [INSPIRE].

[42] S. Yaser Ayazi and A. Mohamadnejad, *Conformal vector dark matter and strongly first-order electroweak phase transition*, *JHEP* **03** (2019) 181 [arXiv:1901.04168] [INSPIRE].

[43] A. Mohamadnejad, *Gravitational waves from scale-invariant vector dark matter model: Probing below the neutrino-floor*, arXiv:1907.08899 [INSPIRE].

[44] A. Mazumdar and G. White, *Review of cosmic phase transitions: their significance and experimental signatures*, *Rept. Prog. Phys.* **82** (2019) 076901 [arXiv:1811.01948] [INSPIRE].

[45] E. Witten, *Cosmic Separation of Phases*, *Phys. Rev.* **D 30** (1984) 272 [INSPIRE].

[46] C.J. Hogan, *Gravitational radiation from cosmological phase transitions*, *Mon. Not. Roy. Astron. Soc.* **218** (1986) 629 [INSPIRE].

[47] L.M. Krauss, *Gravitational waves from global phase transitions*, *Phys. Lett.* **B 284** (1992) 229 [INSPIRE].

[48] A. Kosowsky, M.S. Turner and R. Watkins, *Gravitational radiation from colliding vacuum bubbles*, *Phys. Rev.* **D 45** (1992) 4514 [INSPIRE].

[49] A. Kosowsky, M.S. Turner and R. Watkins, *Gravitational waves from first order cosmological phase transitions*, *Phys. Rev. Lett.* **69** (1992) 2026 [INSPIRE].

[50] M. Kamionkowski, A. Kosowsky and M.S. Turner, *Gravitational radiation from first order phase transitions*, *Phys. Rev.* **D 49** (1994) 2837 [astro-ph/9310044] [INSPIRE].

[51] C. Lee, V. Cirigliano and M.J. Ramsey-Musolf, *Resonant relaxation in electroweak baryogenesis*, *Phys. Rev.* **D 71** (2005) 075010 [hep-ph/0412354] [INSPIRE].

[52] C. Balázs, M. Carena, A. Menon, D.E. Morrissey and C.E.M. Wagner, *The supersymmetric origin of matter*, *Phys. Rev.* **D 71** (2005) 075002 [hep-ph/0412264] [INSPIRE].

[53] S. Liebler, S. Profumo and T. Stefaniak, *Light Stop Mass Limits from Higgs Rate Measurements in the MSSM: Is MSSM Electroweak Baryogenesis Still Alive After All?*, *JHEP* **04** (2016) 143 [arXiv:1512.09172] [INSPIRE].

[54] M. Maniatis, *The Next-to-Minimal Supersymmetric extension of the Standard Model reviewed*, *Int. J. Mod. Phys.* **A 25** (2010) 3505 [arXiv:0906.0777] [INSPIRE].

[55] U. Ellwanger, C. Hugonie and A.M. Teixeira, *The Next-to-Minimal Supersymmetric Standard Model*, *Phys. Rept.* **496** (2010) 1 [arXiv:0910.1785] [INSPIRE].

[56] H.-L. Li, M. Ramsey-Musolf and S. Willocq, *Probing a scalar singlet-catalyzed electroweak phase transition with resonant di-Higgs boson production in the 4b channel*, *Phys. Rev.* **D 100** (2019) 075035 [arXiv:1906.05289] [INSPIRE].

[57] L. Bian, H.-K. Guo and J. Shu, *Gravitational Waves, baryon asymmetry of the universe and electric dipole moment in the CP-violating NMSSM*, *Chin. Phys.* **C 42** (2018) 093106 [arXiv:1704.02488] [INSPIRE].

JHEP11(2019)151

[58] S.J. Huber, T. Konstandin, T. Prokopec and M.G. Schmidt, *Electroweak Phase Transition and Baryogenesis in the NMSSM*, *Nucl. Phys.* **B 757** (2006) 172 [hep-ph/0606298] [INSPIRE].

[59] C. Balázs, A. Mazumdar, E. Pukartas and G. White, *Baryogenesis, dark matter and inflation in the Next-to-Minimal Supersymmetric Standard Model*, *JHEP* **01** (2014) 073 [arXiv:1309.5091] [INSPIRE].

[60] K. Cheung, T.-J. Hou, J.S. Lee and E. Senaha, *Singlino-driven Electroweak Baryogenesis in the Next-to-MSSM*, *Phys. Lett.* **B 710** (2012) 188 [arXiv:1201.3781] [INSPIRE].

[61] W. Huang, Z. Kang, J. Shu, P. Wu and J.M. Yang, *New insights in the electroweak phase transition in the NMSSM*, *Phys. Rev.* **D 91** (2015) 025006 [arXiv:1405.1152] [INSPIRE].

[62] S.V. Demidov, D.S. Gorbunov and D.V. Kirpichnikov, *Split NMSSM with electroweak baryogenesis*, *JHEP* **11** (2016) 148 [*Erratum ibid.* **08** (2017) 080] [arXiv:1608.01985] [INSPIRE].

[63] X.-J. Bi, L. Bian, W. Huang, J. Shu and P.-F. Yin, *Interpretation of the Galactic Center excess and electroweak phase transition in the NMSSM*, *Phys. Rev.* **D 92** (2015) 023507 [arXiv:1503.03749] [INSPIRE].

[64] M. Carena, N.R. Shah and C.E.M. Wagner, *Light Dark Matter and the Electroweak Phase Transition in the NMSSM*, *Phys. Rev.* **D 85** (2012) 036003 [arXiv:1110.4378] [INSPIRE].

[65] A. Menon, D.E. Morrissey and C.E.M. Wagner, *Electroweak baryogenesis and dark matter in the NMSSM*, *Phys. Rev.* **D 70** (2004) 035005 [hep-ph/0404184] [INSPIRE].

[66] N.F. Bell, M.J. Dolan, L.S. Friedrich, M.J. Ramsey-Musolf and R.R. Volkas, *Electroweak Baryogenesis with Vector-like Leptons and Scalar Singlets*, *JHEP* **09** (2019) 012 [arXiv:1903.11255] [INSPIRE].

[67] J. De Vries, M. Postma and J. van de Vis, *The role of leptons in electroweak baryogenesis*, *JHEP* **04** (2019) 024 [arXiv:1811.11104] [INSPIRE].

[68] C.-Y. Chen, H.-L. Li and M. Ramsey-Musolf, *CP-Violation in the Two Higgs Doublet Model: from the LHC to EDMs*, *Phys. Rev.* **D 97** (2018) 015020 [arXiv:1708.00435] [INSPIRE].

[69] H.-K. Guo, Y.-Y. Li, T. Liu, M. Ramsey-Musolf and J. Shu, *Lepton-Flavored Electroweak Baryogenesis*, *Phys. Rev.* **D 96** (2017) 115034 [arXiv:1609.09849] [INSPIRE].

[70] W. Chao and M.J. Ramsey-Musolf, *Catalysis of Electroweak Baryogenesis via Fermionic Higgs Portal Dark Matter*, arXiv:1503.00028 [INSPIRE].

[71] J.M. Cline, K. Kainulainen and D. Tucker-Smith, *Electroweak baryogenesis from a dark sector*, *Phys. Rev.* **D 95** (2017) 115006 [arXiv:1702.08909] [INSPIRE].

[72] J.M. Cline and K. Kainulainen, *Electroweak baryogenesis and dark matter from a singlet Higgs*, *JCAP* **01** (2013) 012 [arXiv:1210.4196] [INSPIRE].

[73] J.M. Cline, K. Kainulainen and M. Trott, *Electroweak Baryogenesis in Two Higgs Doublet Models and B meson anomalies*, *JHEP* **11** (2011) 089 [arXiv:1107.3559] [INSPIRE].

[74] M. Carena, Z. Liu and M. Riembau, *Probing the electroweak phase transition via enhanced di-Higgs boson production*, *Phys. Rev.* **D 97** (2018) 095032 [arXiv:1801.00794] [INSPIRE].

[75] J.M. Cline, M. Joyce and K. Kainulainen, *Supersymmetric electroweak baryogenesis in the WKB approximation*, *Phys. Lett.* **B 417** (1998) 79 [*Erratum ibid.* **B 448** (1999) 321] [hep-ph/9708393] [INSPIRE].

JHEP11(2019)151

[76] B. Grzadkowski and D. Huang, *Spontaneous CP-Violating Electroweak Baryogenesis and Dark Matter from a Complex Singlet Scalar*, *JHEP* **08** (2018) 135 [arXiv:1807.06987] [INSPIRE].

[77] S.A.R. Ellis, S. Ipek and G. White, *Electroweak Baryogenesis from Temperature-Varying Couplings*, *JHEP* **08** (2019) 002 [arXiv:1905.11994] [INSPIRE].

[78] F.P. Huang, Z. Qian and M. Zhang, *Exploring dynamical CP-violation induced baryogenesis by gravitational waves and colliders*, *Phys. Rev.* **D 98** (2018) 015014 [arXiv:1804.06813] [INSPIRE].

[79] S.A. Abel, *Destabilizing divergences in the NMSSM*, *Nucl. Phys.* **B 480** (1996) 55 [hep-ph/9609323] [INSPIRE].

[80] C. Panagiotakopoulos and K. Tamvakis, *Stabilized NMSSM without domain walls*, *Phys. Lett.* **B 446** (1999) 224 [hep-ph/9809475] [INSPIRE].

[81] C. Panagiotakopoulos and K. Tamvakis, *New minimal extension of MSSM*, *Phys. Lett.* **B 469** (1999) 145 [hep-ph/9908351] [INSPIRE].

[82] T. Elliott, S.F. King and P.L. White, *Supersymmetric Higgs bosons at the limit*, *Phys. Lett.* **B 305** (1993) 71 [hep-ph/9302202] [INSPIRE].

[83] T. Elliott, S.F. King and P.L. White, *Squark contributions to Higgs boson masses in the next-to-minimal supersymmetric standard model*, *Phys. Lett.* **B 314** (1993) 56 [hep-ph/9305282] [INSPIRE].

[84] T. Elliott, S.F. King and P.L. White, *Radiative corrections to Higgs boson masses in the next-to-minimal supersymmetric Standard Model*, *Phys. Rev.* **D 49** (1994) 2435 [hep-ph/9308309] [INSPIRE].

[85] H.H. Patel and M.J. Ramsey-Musolf, *Baryon Washout, Electroweak Phase Transition and Perturbation Theory*, *JHEP* **07** (2011) 029 [arXiv:1101.4665] [INSPIRE].

[86] J.C. Romao, *Spontaneous CP Violation in SUSY Models: A No Go Theorem*, *Phys. Lett.* **B 173** (1986) 309 [INSPIRE].

[87] P.M. Ferreira, M. Mühlleitner, R. Santos, G. Weiglein and J. Wittbrodt, *Vacuum Instabilities in the N2HDM*, *JHEP* **09** (2019) 006 [arXiv:1905.10234] [INSPIRE].

[88] N.K. Nielsen, *On the Gauge Dependence of Spontaneous Symmetry Breaking in Gauge Theories*, *Nucl. Phys.* **B 101** (1975) 173 [INSPIRE].

[89] L. Di Luzio and L. Mihaila, *On the gauge dependence of the Standard Model vacuum instability scale*, *JHEP* **06** (2014) 079 [arXiv:1404.7450] [INSPIRE].

[90] M. Laine, M. Meyer and G. Nardini, *Thermal phase transition with full 2-loop effective potential*, *Nucl. Phys.* **B 920** (2017) 565 [arXiv:1702.07479] [INSPIRE].

[91] P.B. Arnold and O. Espinosa, *The effective potential and first order phase transitions: Beyond leading-order*, *Phys. Rev.* **D 47** (1993) 3546 [*Erratum ibid.* **D 50** (1994) 6662] [hep-ph/9212235] [INSPIRE].

[92] P. Basler, M. Krause, M. Muhlleitner, J. Wittbrodt and A. Wlotzka, *Strong First Order Electroweak Phase Transition in the CP-Conserving 2HDM Revisited*, *JHEP* **02** (2017) 121 [arXiv:1612.04086] [INSPIRE].

[93] P. Basler and M. Mühlleitner, *BSMPT (Beyond the Standard Model Phase Transitions): A tool for the electroweak phase transition in extended Higgs sectors*, *Comput. Phys. Commun.* **237** (2019) 62 [arXiv:1803.02846] [INSPIRE].

JHEP11(2019)151

[94] S.R. Coleman, *The Fate of the False Vacuum. 1. Semiclassical Theory*, *Phys. Rev.* **D 15** (1977) 2929 [*Erratum ibid.* **D 16** (1977) 1248] [INSPIRE].

[95] C.G. Callan Jr. and S.R. Coleman, *The Fate of the False Vacuum. 2. First Quantum Corrections*, *Phys. Rev.* **D 16** (1977) 1762 [INSPIRE].

[96] A.D. Linde, *Fate of the False Vacuum at Finite Temperature: Theory and Applications*, *Phys. Lett.* **100B** (1981) 37 [INSPIRE].

[97] C.L. Wainwright, *CosmoTransitions: Computing Cosmological Phase Transition Temperatures and Bubble Profiles with Multiple Fields*, *Comput. Phys. Commun.* **183** (2012) 2006 [arXiv:1109.4189] [INSPIRE].

[98] L.D. McLerran, M.E. Shaposhnikov, N. Turok and M.B. Voloshin, *Why the baryon asymmetry of the universe is approximately 10**-10*, *Phys. Lett.* **B 256** (1991) 451 [INSPIRE].

[99] M. Dine, P. Huet and R.L. Singleton Jr., *Baryogenesis at the electroweak scale*, *Nucl. Phys.* **B 375** (1992) 625 [INSPIRE].

[100] P. Athron, J.-h. Park, D. Stöckinger and A. Voigt, *FlexibleSUSY—A spectrum generator generator for supersymmetric models*, *Comput. Phys. Commun.* **190** (2015) 139 [arXiv:1406.2319] [INSPIRE].

[101] P. Athron et al., *FlexibleSUSY 2.0: Extensions to investigate the phenomenology of SUSY and non-SUSY models*, *Comput. Phys. Commun.* **230** (2018) 145 [arXiv:1710.03760] [INSPIRE].

[102] B.C. Allanach, *SOFTSUSY: a program for calculating supersymmetric spectra*, *Comput. Phys. Commun.* **143** (2002) 305 [hep-ph/0104145] [INSPIRE].

[103] B.C. Allanach, P. Athron, L.C. Tunstall, A. Voigt and A.G. Williams, *Next-to-Minimal SOFTSUSY*, *Comput. Phys. Commun.* **185** (2014) 2322 [arXiv:1311.7659] [INSPIRE].

[104] F. Staub, *From Superpotential to Model Files for FeynArts and CalcHep/CompHEP*, *Comput. Phys. Commun.* **181** (2010) 1077 [arXiv:0909.2863] [INSPIRE].

[105] F. Staub, *Automatic Calculation of supersymmetric Renormalization Group Equations and Self Energies*, *Comput. Phys. Commun.* **182** (2011) 808 [arXiv:1002.0840] [INSPIRE].

[106] F. Staub, *SARAH 3.2: Dirac Gauginos, UFO output and more*, *Comput. Phys. Commun.* **184** (2013) 1792 [arXiv:1207.0906] [INSPIRE].

[107] F. Staub, *SARAH 4: A tool for (not only SUSY) model builders*, *Comput. Phys. Commun.* **185** (2014) 1773 [arXiv:1309.7223] [INSPIRE].

[108] A. Fowlie, *A fast C++ implementation of thermal functions*, *Comput. Phys. Commun.* **228** (2018) 264 [arXiv:1802.02720] [INSPIRE].

[109] F. Staub et al., *Precision tools and models to narrow in on the 750 GeV diphoton resonance*, *Eur. Phys. J.* **C 76** (2016) 516 [arXiv:1602.05581] [INSPIRE].

[110] J. Bernon and B. Dumont, *Lilith: a tool for constraining new physics from Higgs measurements*, *Eur. Phys. J.* **C 75** (2015) 440 [arXiv:1502.04138] [INSPIRE].

[111] F. Feroz and M.P. Hobson, *Multimodal nested sampling: an efficient and robust alternative to MCMC methods for astronomical data analysis*, *Mon. Not. Roy. Astron. Soc.* **384** (2008) 449 [arXiv:0704.3704] [INSPIRE].

JHEP11(2019)151

[112] F. Feroz, M.P. Hobson and M. Bridges, *MultiNest: an efficient and robust Bayesian inference tool for cosmology and particle physics*, *Mon. Not. Roy. Astron. Soc.* **398** (2009) 1601 [arXiv:0809.3437] [INSPIRE].

[113] F. Feroz, M.P. Hobson, E. Cameron and A.N. Pettitt, *Importance Nested Sampling and the MultiNest Algorithm*, arXiv:1306.2144 [INSPIRE].

[114] P. Bechtle, O. Brein, S. Heinemeyer, G. Weiglein and K.E. Williams, *HiggsBounds: Confronting Arbitrary Higgs Sectors with Exclusion Bounds from LEP and the Tevatron*, *Comput. Phys. Commun.* **181** (2010) 138 [arXiv:0811.4169] [INSPIRE].

[115] P. Bechtle, O. Brein, S. Heinemeyer, G. Weiglein and K.E. Williams, *HiggsBounds 2.0.0: Confronting Neutral and Charged Higgs Sector Predictions with Exclusion Bounds from LEP and the Tevatron*, *Comput. Phys. Commun.* **182** (2011) 2605 [arXiv:1102.1898] [INSPIRE].

[116] P. Bechtle et al., *Recent Developments in HiggsBounds and a Preview of HiggsSignals*, PoS(CHARGED 2012)024 [arXiv:1301.2345] [INSPIRE].

[117] P. Bechtle et al., HiggsBounds – 4*: Improved Tests of Extended Higgs Sectors against Exclusion Bounds from LEP, the Tevatron and the LHC*, *Eur. Phys. J.* **C 74** (2014) 2693 [arXiv:1311.0055] [INSPIRE].

[118] P. Bechtle, S. Heinemeyer, O. Stal, T. Stefaniak and G. Weiglein, *Applying Exclusion Likelihoods from LHC Searches to Extended Higgs Sectors*, *Eur. Phys. J.* **C 75** (2015) 421 [arXiv:1507.06706] [INSPIRE].

[119] J. Baglio et al., *NMSSMCALC: A Program Package for the Calculation of Loop-Corrected Higgs Boson Masses and Decay Widths in the (Complex) NMSSM*, *Comput. Phys. Commun.* **185** (2014) 3372 [arXiv:1312.4788] [INSPIRE].

[120] ATLAS collaboration, *Search for a scalar partner of the top quark in the jets plus missing transverse momentum final state at* $\sqrt{s} = 13$ *TeV with the ATLAS detector*, *JHEP* **12** (2017) 085 [arXiv:1709.04183] [INSPIRE].

[121] CMS collaboration, *Search for direct top squark pair production in events with one lepton, jets and missing transverse energy at 13 TeV*, CMS-PAS-SUS-19-009 (2019).

[122] CMS collaboration, *Search for a new scalar resonance decaying to a pair of Z bosons in proton-proton collisions at* $\sqrt{s} = 13$ *TeV*, *JHEP* **06** (2018) 127 [*Erratum ibid.* **03** (2019) 128] [arXiv:1804.01939] [INSPIRE].

[123] S. AbdusSalam, *Testing Higgs boson scenarios in the phenomenological NMSSM*, *Eur. Phys. J.* **C 79** (2019) 442 [arXiv:1710.10785] [INSPIRE].

[124] A.P. Morais, R. Pasechnik and T. Vieu, *Multi-peaked signatures of primordial gravitational waves from multi-step electroweak phase transition*, arXiv:1802.10109 [INSPIRE].

[125] J. Nelder and R. Mead, *A Simplex Method for Function Minimization*, *Comput. J.* **7** (1965) 308.

JHEP11(2019)151

Chapter 7

Outlook and conclusions

We began this work by describing the elementary particles and their interactions in the context of the SM. All experimentally observable particles are in the SM spectrum. We have also seen that astrophysical observations entail the existence in the Universe of other matter that cannot be made of SM particles. This DM constitute a strong indication of BSM physics. Motivated by this we introduced supersymmetry that offers, among other solutions to SM problems, a candidate for a DM particle. In the SUSY context, we have presented the R-parity conserving MSSM that provides the framework used for the first published work.

In the first published paper, we studied the Z/h funnel region in the MSSM. We started this work motivated by the CMS and ATLAS searches that have found different excess of data above the expected background, and by the `GAMBIT` Collaboration that has shown that these excesses can be given by the Z/h funnel region. We combined constraints from different searches using both astrophysical and collider searches. We implemented these constraints both in a simplified model and in the phenomenological MSSM. The combination of different searches results in stricter constraints that provide a better understanding of the current and future experimental bounds of the Z/h funnel region. On one hand, these new bounds add more importance to the results of ongoing experiments that, combined, will almost entirely probe the whole Z/h funnel region. On the other hand, the new bounds provide helpful insights worth to consider together with global fits performed by `GAMBIT`. In conclusion, we have shown that the Z/h funnel region of the MSSM is not an ideal interpretation of the modest excesses in recent electroweakino searches.

Secondly, going back to the SM, interactions originate from internal symmetries of the theory. With the initial $\mathrm{SU(3)_C}\otimes\mathrm{SU(2)_L}\otimes\mathrm{U(1)_Y}$ symmetry, however, fermions and gauge bosons are massless. To explain the observed

masses, we broke this symmetry using the Higgs mechanism.

After having introduced fermion masses, the transformation from the mass basis to the flavour basis was given by the CKM matrix. We saw that the CKM matrix also provides CP violation. Such CP violation is a fundamental ingredient for baryogenesis as we have shown in the Sakharov conditions.

We introduced a mechanism, electroweak baryogenesis, that employs electroweak symmetry breaking and the CP violation. Electroweak baryogenesis satisfies the Sakharov conditions and can explain the observed excess of matter over antimatter. We described the physics and the different steps that, in the early Universe, can lead to producing the observed excess of baryons in our Universe. For this mechanism, however, the CP violation provided by the SM is not enough to explain the observed excess of matter over antimatter. This is another important aspect where we need BSM physics to solve the problem.

We also studied the NMSSM that represents the SUSY framework for our second published work. We described the NMSSM superpotential and spectrum, and we introduced the SUSY breaking terms. To describe the physics of the early Universe, we added temperature corrections of the potential. The 1-loop NMSSM temperature-dependent effective potential has significant contributions from both top and stop quarks. To perform a precise calculation, we integrated out all the heavy sparticles. In this way, we reduced the NMSSM to an effective field theory. We introduced this EFT in the THDMS section.

We scanned the parameter space and studied the vacuum structure at different temperatures, following the evolution of the Universe. We have found a novel and rich phenomenology of the possible vacuum phases. For each point in the scan, we examined the FOPT, the properties of the Higgs bosons, the baryogenesis and the NMSSM parameters, together with their reciprocal relationships. This analysis allowed us to individuate and classify different phase transition scenarios. We have shown that each scenario is characterised by a specific cosmological history. Moreover, we found the regions of the parameter space that are more likely to lead to SFOPT.

This work offers different starting points for future investigations. A follow-up that we are currently developing is in the field of gravitational waves. As shown, the electroweak baryogenesis mechanism includes bubbles of a vacuum phase expanding in a different phase. Collisions among these bubbles lead to interesting gravitational signals [101–103] that can potentially be probed by future gravitational waves experiments [104, 105]. These gravitational wave signatures can thus provide hints about the cosmological history of our Universe and the baryogenesis model.

Appendix A

SARAH files

Here we present the SARAH model files we wrote to perform the scan described in the published material in sec.6.1.

A.1 THDMS.m

```
(* ::Package:: *)

Off[General::spell]

Model`Name = "THDMS";
Model`NameLaTeX ="Two Higgs Doublet Model plus Singlet";
Model`Authors = "P. Athron, G. Pozzo et al.";
Model`Date = "2017-04-28";

(*2017-04-28: Added ScalarField[[3]], S, phiS,
sigmaS, modified the lagrangian*)
(* 2014-11-06: Changed sign in Lagrangian *)
(* 2015-11-16: added conj[H1].H2 term *)


(*-------------------------------------------*)
(*   Particle Content*)
(*-------------------------------------------*)

(* Gauge Superfields *)

Gauge[[1]]={B,   U[1], hypercharge, g1,False};
Gauge[[2]]={WB, SU[2], left,        g2,True};
```

```
Gauge[[3]]={G,  SU[3], color,       g3,False};


(* Chiral Superfields *)

FermionFields[[1]] = {q, 3, {uL,dL},     1/6, 2, 3};
FermionFields[[2]] = {l, 3, {vL,eL},    -1/2, 2, 1};
FermionFields[[3]] = {d, 3, conj[dR],   1/3, 1, -3};
FermionFields[[4]] = {u, 3, conj[uR],  -2/3, 1, -3};
FermionFields[[5]] = {e, 3, conj[eR],     1, 1,  1};

ScalarFields[[1]] =  {H1, 1, {H10, H1m},-1/2, 2,  1};
ScalarFields[[2]] =  {H2, 1, {H2p, H20}, 1/2, 2,  1};
ScalarFields[[3]] =  { S, 1, Sing,         0, 1,  1};


(*-----------------------------------------------------*)
(*   DEFINITION                                        *)
(*-----------------------------------------------------*)

NameOfStates={GaugeES, EWSB};

(* ----- Before EWSB ----- *)

DEFINITION[GaugeES][Additional]= {
    {LagHC, { AddHC->True}},
    {LagNoHC,{ AddHC->False}}
};

LagNoHC = -(M112 conj[H1].H1 + M222 conj[H2].H2
            + 1/2 Lambda1 conj[H1].H1.conj[H1].H1
            + 1/2 Lambda2 conj[H2].H2.conj[H2].H2
            + Lambda3 conj[H2].H2.conj[H1].H1
            - Lambda4 (conj[H2].H1).(conj[H1].H2)
            + M332 conj[S].S
            + Lambda5 conj[S].S.conj[H1].H1
            + Lambda6 conj[S].S.conj[H2].H2
            + Lambda8 conj[S].S.conj[S].S);

LagHC = -(-Yd H1.d.q -Ye H1.e.l +Yu H2.u.q
        - M123 H1.H2.S -1/3 M5 S.S.S
        + Lambda7 conj[S].conj[S].H1.H2);

```

```
67
68  (* Gauge Sector *)
69
70  DEFINITION[EWSB][GaugeSector] =
71  {
72    {{VB,VWB[3]},{VP,VZ},ZZ},
73    {{VWB[1],VWB[2]},{VWm,conj[VWm]},ZW}
74  };
75
76
77  (* ----- VEVs ---- *)
78
79  DEFINITION[EWSB][VEVs]=
80  {   {H10, {v1, 1/Sqrt[2]},
81      {sigma1, I/Sqrt[2]},{phi1, 1/Sqrt[2]}},
82      {H20, {v2, 1/Sqrt[2]}, {sigma2, I/Sqrt[2]},
83      {phi2, 1/Sqrt[2]}},{Sing  , {vS, 1/Sqrt[2]},
84      {sigmaS, I/Sqrt[2]},{phiS, 1/Sqrt[2]}}         };
85
86  DEFINITION[EWSB][MatterSector]=
87  {   {{phi1, phi2, phiS},       {hh, ZH}},
88      {{sigma1, sigma2, sigmaS}, {Ah, ZA}},
89      {{H1m, conj[H2p]},         {Hm,ZP}},
90      {{{dL}, {conj[dR]}},      {{DL,Vd}, {DR,Ud}}},
91      {{{uL}, {conj[uR]}},      {{UL,Vu}, {UR,Uu}}},
92      {{{eL}, {conj[eR]}},      {{EL,Ve}, {ER,Ue}}}  };
93
94
95  (*-------------------------------------------------------*)
96  (* Dirac-Spinors                                         *)
97  (*-------------------------------------------------------*)
98
99  DEFINITION[EWSB][DiracSpinors]={
100  Fd ->{  DL, conj[DR]},
101  Fe ->{  EL, conj[ER]},
102  Fu ->{  UL, conj[UR]},
103  Fv ->{  vL, 0}        };
104
105 DEFINITION[EWSB][GaugeES]={
106  Fd1 ->{  FdL, 0},
107  Fd2 ->{  0, FdR},
108  Fu1 ->{  Fu1, 0},
109  Fu2 ->{  0, Fu2},
```

```
 Fe1 ->{  Fe1, 0},
 Fe2 ->{  0, Fe2}      };
```

A.2 parameters.m

```
(* ::Package:: *)

(*Added Lambda, M332, M123, M5*)


ParameterDefinitions = {

{g1,         { Description -> "Hypercharge-Coupling"}},
{g2,         { Description -> "Left-Coupling"}},
{g3,         { Description -> "Strong-Coupling"}},
{AlphaS,     {Description -> "Alpha Strong"}},
{e,          { Description -> "electric charge"}},

{Gf,         { Description -> "Fermi's constant"}},
{aEWinv,     { Description -> "inverse weak coupling
                                  constant at mZ"}},

{Yu,         { Description -> "Up-Yukawa-Coupling",
               DependenceNum ->  Sqrt[2]/v2*
                                  {{Mass[Fu,1],0,0},
                                 {0, Mass[Fu,2],0},
                                 {0, 0, Mass[Fu,3]}}}},

{Yd,         { Description -> "Down-Yukawa-Coupling",
               DependenceNum ->  Sqrt[2]/v1*
                                  {{Mass[Fd,1],0,0},
                                 {0, Mass[Fd,2],0},
                                 {0, 0, Mass[Fd,3]}}}},

{Ye,         { Description -> "Lepton-Yukawa-Coupling",
               DependenceNum ->  Sqrt[2]/v1*
                                  {{Mass[Fe,1],0,0},
                                  {0, Mass[Fe,2],0},
                                  {0, 0, Mass[Fe,3]}}}},


{Lambda1,     { LaTeX -> "\\lambda_1",
                OutputName -> Lam1,
```

```
39                 LesHouches -> {HMIX,31}}},
40
41 {Lambda2,     { LaTeX -> "\\lambda_2",
42                 OutputName -> Lam2,
43                 LesHouches -> {HMIX,32}}},
44
45 {Lambda3,     { LaTeX -> "\\lambda_3",
46                 OutputName -> Lam3,
47                 LesHouches -> {HMIX,33}}},
48
49 {Lambda4,     { LaTeX -> "\\lambda_4",
50                 OutputName -> Lam4,
51                 LesHouches -> {HMIX,34}}},
52
53 {Lambda5,     { LaTeX -> "\\lambda_5",
54                 OutputName -> Lam5,
55                 LesHouches -> {HMIX,35}}},
56
57 {Lambda6,     { LaTeX -> "\\lambda_6",
58                 OutputName -> Lam6,
59                 LesHouches -> {HMIX,36}}},
60
61 {Lambda7,     { LaTeX -> "\\lambda_7",
62                 OutputName -> Lam7,
63                 LesHouches -> {HMIX,37}}},
64
65 {Lambda8,     { LaTeX -> "\\lambda_8",
66                 OutputName -> Lam8,
67                 LesHouches -> {HMIX,38}}},
68
69 {M112,     {    LaTeX -> "m^2_1",
70                 OutputName -> M112,
71                 LesHouches -> {HMIX,20}}},
72 {M222,     {    LaTeX -> "m^2_2",
73                 OutputName -> M222,
74                 LesHouches -> {HMIX,21}}},
75
76 {M332,     {    LaTeX -> "m^2_3",
77                 OutputName -> M332,
78                 LesHouches -> {HMIX,23}}},
79
80 {M123,     {    LaTeX -> "m_{123}",
81                 OutputName -> M123,
```

```
                LesHouches -> {HMIX,24}}},

{M5,    {       LaTeX -> "m_{5}",
                OutputName -> M5,
                LesHouches -> {HMIX,25}}},

{v1,        { Description -> "Down-VEV",LaTeX -> "v_1"}},
{v2,        { Description -> "Up-VEV", LaTeX -> "v_2"}},
{v,         { Description -> "EW-VEV"}},

{\[Beta],   { Description -> "Pseudo Scalar
                              mixing angle"}},
{TanBeta,   { Description -> "Tan Beta"}},
{\[Alpha],  { Description -> "Scalar mixing angle"}},

{ZH,        { Description -> "Scalar-Mixing-Matrix",
              DependenceOptional->None }},
{ZA,        { Description->"Pseudo-Scalar-Mixing-Matrix",
              DependenceOptional->None }},
{ZP,        { Description -> "Charged-Mixing-Matrix"}},

{ThetaW,    { Description -> "Weinberg-Angle"}},

{ZZ,        {Description -> "Photon-Z Mixing Matrix"}},
{ZW,        {Description -> "W Mixing Matrix" }},


{Vu,        {Description -> "Left-Up-Mixing-Matrix"}},
{Vd,        {Description -> "Left-Down-Mixing-Matrix"}},
{Uu,        {Description -> "Right-Up-Mixing-Matrix"}},
{Ud,        {Description -> "Right-Down-Mixing-Matrix"}},
{Ve,        {Description ->"Left-Lepton-Mixing-Matrix"}},
{Ue,        {Description ->"Right-Lepton-Mixing-Matrix"}}

 };
```

A.3 particles.m

```
(* ::Package:: *)

ParticleDefinitions[GaugeES] = {
      {H0,  {    PDG -> {0},
                 Width -> 0,
```

```
6                   Mass -> Automatic,
7                   FeynArtsNr -> 1,
8                   LaTeX -> "H^0",
9                   OutputName -> "H0" }},
10
11
12      {Hp,  {     PDG -> {0},
13                  Width -> 0,
14                  Mass -> Automatic,
15                  FeynArtsNr -> 2,
16                  LaTeX -> "H^+",
17                  OutputName -> "Hp" }},
18
19
20      {VB,    { Description -> "B-Boson"}},
21      {VG,    { Description -> "Gluon"}},
22      {VWB,   { Description -> "W-Bosons"}},
23      {gB,    { Description -> "B-Boson Ghost"}},
24      {gG,    { Description -> "Gluon Ghost" }},
25      {gWB,   { Description -> "W-Boson Ghost"}}
26
27      };
28
29
30  ParticleDefinitions[EWSB] = {
31
32      {hh ,   { Description -> "Higgs"}},
33      {Ah ,   { Description -> "Pseudo-Scalar Higgs"}},
34
35      {Hm,    { Description -> "Charged Higgs"}},
36
37      {VP,    { Description -> "Photon"}},
38      {VZ,    { Description -> "Z-Boson"}},
39      {VG,    { Description -> "Gluon" }},
40      {VWm,   { Description -> "W-Boson",
41                  Goldstone -> Hm[{1}] }},
42      {gP,    { Description -> "Photon Ghost"}},
43      {gWm,   { Description -> "Negative W-Boson Ghost"}},
44      {gWmC,  { Description -> "Positive W-Boson Ghost"}},
45      {gZ,    { Description -> "Z-Boson Ghost" }},
46      {gG,    { Description -> "Gluon Ghost" }},
47
48      {Fd,    { Description -> "Down-Quarks"}},
```

```
49      {Fu,   { Description -> "Up-Quarks"}},
50      {Fe,   { Description -> "Leptons" }},
51      {Fv,   { Description -> "Neutrinos" }}
52
53        };
54
55
56
57  WeylFermionAndIndermediate = {
58
59     {H,       {   PDG -> {0},
60                   Width -> 0,
61                   Mass -> Automatic,
62                   LaTeX -> "H",
63                   OutputName -> "" }},
64
65    {H10,    {LaTeX -> "H_1^0"}},
66    {H20,    {LaTeX -> "H_2^0"}},
67    {H1m,    {LaTeX -> "H_1^-"}},
68    {H2p,    {LaTeX -> "H_2^+"}},
69    {S  ,    {LaTeX -> "S"}},
70
71    {sigma1, {LaTeX -> "\\sigma_1"}},
72    {sigma2, {LaTeX -> "\\sigma_2"}},
73    {sigmaS, {LaTeX -> "\\sigma_S"}},
74
75    {phi1,   {LaTeX -> "\\phi_1"}},
76    {phi2,   {LaTeX -> "\\phi_2"}},
77    {phiS,   {LaTeX -> "\\phi_S"}},
78
79    {dR,     {LaTeX -> "d_R" }},
80    {eR,     {LaTeX -> "e_R" }},
81    {lep,    {LaTeX -> "l" }},
82    {uR,     {LaTeX -> "u_R" }},
83    {q,      {LaTeX -> "q" }},
84    {eL,     {LaTeX -> "e_L" }},
85    {dL,     {LaTeX -> "d_L" }},
86    {uL,     {LaTeX -> "u_L" }},
87    {vL,     {LaTeX -> "\\nu_L" }},
88
89    {DR,     {LaTeX -> "D_R" }},
90    {ER,     {LaTeX -> "E_R" }},
91    {UR,     {LaTeX -> "U_R" }},
```

```
92    {EL,      {LaTeX -> "E_L" }},
93    {DL,      {LaTeX -> "D_L" }},
94    {UL,      {LaTeX -> "U_L" }}
95
96
97   };
```

A.4 SPheno.m

```
1  (* ::Package:: *)
2
3  OnlyLowEnergySPheno = True;
4
5
6  MINPAR={{1,Lambda1Input},
7          {2,Lambda2Input},
8          {3,Lambda3Input},
9          {4,Lambda4Input},
10         {5,Lambda5Input},
11         {9,M12input},
12         {10,TanBeta} };
13
14 RealParameters = {TanBeta};
15
16 ParametersToSolveTadpoles = {M112,M222};
17
18 DEFINITION[MatchingConditions]= {
19  {v1, vSM*Cos[ArcTan[TanBeta]]},
20  {v2, vSM*Sin[ArcTan[TanBeta]]},
21  {Ye, YeSM*vSM/v1},
22  {Yd, YdSM*vSM/v1},
23  {Yu, YuSM*vSM/v2},
24  {g1, g1SM},
25  {g2, g2SM},
26  {g3, g3SM}
27  };
28
29 BoundaryLowScaleInput={
30  {Lambda1, Lambda1Input},
31  {Lambda2, Lambda2Input},
32  {Lambda3, Lambda3Input},
33  {Lambda4, Lambda4Input},
34  {Lambda5, Lambda5Input},
```

```
 {M12,     M12input}
};


ListDecayParticles = {Fu,Fe,Fd,hh,Ah,Hm};

ListDecayParticles3B = {{Fu,"Fu.f90"},{Fe,"Fe.f90"},
                                      {Fd,"Fd.f90"}};


DefaultInputValues ={
  Lambda1Input -> 0.1,
  Lambda2Input -> 0.27,
  Lambda3Input -> 1.1,
  Lambda4Input ->-0.5,
  Lambda5Input -> 0.5,
  M12input     ->-5000,
  TanBeta      -> 50
};


RenConditionsDecays={
  {dCosTW, 1/2*Cos[ThetaW] * (PiVWm/(MVWm^2)
           - PiVZ/(mVZ^2)) },
  {dSinTW, -dCosTW/Tan[ThetaW]},
  {dg2, 1/2*g2*(derPiVPheavy0 + PiVPlightMZ/MVZ^2
        - (-(PiVWm/MVWm^2)+ PiVZ/MVZ^2) / Tan[ThetaW]^2
        + (2*PiVZVP*Tan[ThetaW]) / MVZ^2 )  },
  {dg1, dg2*Tan[ThetaW]+g2*dSinTW/Cos[ThetaW]
        - dCosTW*g2*Tan[ThetaW]/Cos[ThetaW]}
};
```

Bibliography

[1] P. A. R. Ade et al. "Planck 2015 results. XIV. Dark energy and modified gravity". In: *Astron. Astrophys.* 594 (2016), A14. DOI: 10.1051/0004-6361/201525814. arXiv: 1502.01590 [astro-ph.CO].

[2] T. Clifton et al. "Modified Gravity and Cosmology". In: *Phys. Rept.* 513 (2012), pp. 1–189. DOI: 10.1016/j.physrep.2012.01.001. arXiv: 1106.2476 [astro-ph.CO].

[3] A. G. Cohen, A. De Rujula, and S. L. Glashow. "A Matter - antimatter universe?" In: *Astrophys. J.* 495 (1998), pp. 539–549. DOI: 10.1086/305328. arXiv: astro-ph/9707087 [astro-ph].

[4] G. W. Bennett et al. "Final Report of the Muon E821 Anomalous Magnetic Moment Measurement at BNL". In: *Phys. Rev.* D73 (2006), p. 072003. DOI: 10.1103/PhysRevD.73.072003. arXiv: hep-ex/0602035 [hep-ex].

[5] M. Tanabashi et al. "Muon Anomalous Magnetic Moment". In: *Review of Particle Physics*. 2018. URL: http://pdg.lbl.gov/2018/reviews/rpp2018-rev-g-2-muon-anom-mag-moment.pdf.

[6] K. Hagiwara et al. "$(g-2)_\mu$ and $\alpha(M_Z^2)$ re-evaluated using new precise data". In: *J. Phys.* G38 (2011), p. 085003. DOI: 10.1088/0954-3899/38/8/085003. arXiv: 1105.3149 [hep-ph].

[7] F. Jegerlehner. "Muon g - 2 theory: The hadronic part". In: *EPJ Web Conf.* 166 (2018), p. 00022. DOI: 10.1051/epjconf/201816600022. arXiv: 1705.00263 [hep-ph].

[8] M. Davier et al. "Reevaluation of the hadronic vacuum polarisation contributions to the Standard Model predictions of the muon $g-2$ and $alpha(m_Z^2)$ using newest hadronic cross-section data". In: *Eur. Phys. J.* C77.12 (2017), p. 827. DOI: 10.1140/epjc/s10052-017-5161-6. arXiv: 1706.09436 [hep-ph].

[9] M. Tanabashi et al. "Review of Particle Physics". In: *Phys. Rev. D* 98 (Aug. 2018), p. 030001. DOI: 10.1103/PhysRevD.98.030001.

[10] M. D. Schwartz. *Quantum Field Theory and the Standard Model*. Cambridge University Press, 2014. ISBN: 978-1-107-03473-0.

[11] M. Tanabashi et al. "Quark Model". In: *Review of Particle Physics*. 2018. URL: http://pdg.lbl.gov/2018/reviews/rpp2018-rev-quark-model.pdf.

[12] M. Tanabashi et al. "Neutrino Properties". In: *Review of Particle Physics*. 2018. URL: http://pdg.lbl.gov/2018/listings/rpp2018-list-neutrino-prop.pdf.

[13] M. Tanabashi et al. "Number of Light Neutrino Types from Collider Experiments". In: *Review of Particle Physics*. 2018. URL: http://pdg.lbl.gov/2018/mobile/reviews/pdf/rpp2018-rev-light-neutrino-types-m.pdf.

[14] M. Tanabashi et al. "t' (4^{th} Generation) Quark, Searches for". In: *Review of Particle Physics*. 2018. URL: http://pdg.lbl.gov/2018/listings/rpp2018-list-t-prime-quark.pdf.

[15] M. Tanabashi et al. "b' (4^{th} Generation) Quark, Searches for". In: *Review of Particle Physics*. 2018. URL: http://pdg.lbl.gov/2018/listings/rpp2018-list-b-prime-quark.pdf.

[16] M. Tanabashi et al. "N Baryons". In: *Review of Particle Physics*. 2018. URL: http://pdg.lbl.gov/2018/tables/rpp2018-sum-baryons.pdf.

[17] A. Pich. "The Standard Model of Electroweak Interactions". In: *Proceedings, High-energy Physics. Proceedings, 18th European School (ESHEP 2010): Raseborg, Finland, June 20 - July 3, 2010*. 2012, pp. 1–50. arXiv: 1201.0537 [hep-ph].

[18] M. Tanabashi et al. "CKM Quark-Mixing Matrix". In: *Review of Particle Physics*. 2018. URL: http://pdg.lbl.gov/2018/reviews/rpp2018-rev-ckm-matrix.pdf.

[19] L. Wolfenstein. "Parametrization of the Kobayashi-Maskawa Matrix". In: *Phys. Rev. Lett.* 51 (21 Nov. 1983), pp. 1945–1947. DOI: 10.1103/PhysRevLett.51.1945. URL: https://link.aps.org/doi/10.1103/PhysRevLett.51.1945.

[20] A. J. Buras, M. E. Lautenbacher, and G. Ostermaier. "Waiting for the top quark mass, K+ —> pi+ neutrino anti-neutrino, B(s)0 - anti-B(s)0 mixing and CP asymmetries in B decays". In: *Phys. Rev.* D50 (1994), pp. 3433–3446. DOI: 10.1103/PhysRevD.50.3433. arXiv: hep-ph/9403384 [hep-ph].

[21] J. Charles et al. "CP violation and the CKM matrix: Assessing the impact of the asymmetric B factories". In: *Eur. Phys. J.* C41.1 (2005), pp. 1–131. DOI: 10.1140/epjc/s2005-02169-1. arXiv: hep-ph/0406184 [hep-ph].

[22] L. V. Silva. "CP Violation and the CKM matrix". In: *International Workshop on the CKM Unitarity Triangle (CKM2018)*. 2018. URL: https://indico.cern.ch/event/684284/contributions/2952455/attachments/1719296/2774804/Vale_Silva_3.pdf.

[23] F. Mandl and G. Shaw. *Quantum Field Theory*. 2010. ISBN: 978-0-471-49683-0.

[24] L. D. Faddeev and V. N. Popov. "Feynman diagrams for the Yang-Mills field". In: *Physics Letters B* 25.1 (July 1967), pp. 29–30. ISSN: 0370-2693. DOI: 10.1016/0370-2693(67)90067-6. URL: http://www.sciencedirect.com/science/article/pii/0370269367900676.

[25] L. H. Ryder. *Quantum Field Theory*. 1996. ISBN: 978-0521478144.

[26] M. E. Peskin and D. V. Schroeder. *An Introduction To Quantum Field Theory*. 1995. ISBN: 9780201503975.

[27] H. M. Fried and D. R. Yennie. "New Techniques in the Lamb Shift Calculation". In: *Phys. Rev.* 112 (4 Nov. 1958), pp. 1391–1404. DOI: 10.1103/PhysRev.112.1391. URL: https://link.aps.org/doi/10.1103/PhysRev.112.1391.

[28] S. P. Martin. "A Supersymmetry Primer". In: *Adv. Ser. Direct. High Energy Phys.18,1* (2016). DOI: 10.1142/9789814307505_0001. arXiv: 9709356 [hep-ph].

[29] K. A. Meissner and H. Nicolai. "Conformal Symmetry and the Standard Model". In: *Phys. Lett.* B648 (2007), pp. 312–317. DOI: 10.1016/j.physletb.2007.03.023. arXiv: hep-th/0612165 [hep-th].

[30] C. P. Burgess et al. "Failure of Perturbation Theory Near Horizons: the Rindler Example". In: *JHEP* 10 (2018), p. 122. DOI: 10.1007/JHEP10(2018)122. arXiv: 1806.11415 [hep-th].

[31] T. Banks, L. Susskind, and M. E. Peskin. "Difficulties for the Evolution of Pure States Into Mixed States". In: *Nucl. Phys.* B244 (1984), pp. 125–134. DOI: 10.1016/0550-3213(84)90184-6.

[32] S. B. Giddings. "The Black hole information paradox". In: *Particles, strings and cosmology. Proceedings, 19th Johns Hopkins Workshop and 5th PASCOS Interdisciplinary Symposium, Baltimore, USA, March 22-25, 1995*. 1995, pp. 415–428. arXiv: hep-th/9508151 [hep-th].

[33] A. D. Sakharov. "Violation of CP Invariance, c Asymmetry, and Baryon Asymmetry of the Universe". In: *Pisma Zh. Eksp. Teor. Fiz.* 5 (1967), pp. 32–35. DOI: 10.1070/PU1991v034n05ABEH002497.

[34] M. Dine et al. "Creating the baryon asymmetry at the electroweak phase transition". In: *Physics Letters B* 257.3 (1991), pp. 351–356. ISSN: 0370-2693. DOI: http://dx.doi.org/10.1016/0370-2693(91)91905-B. URL: http://www.sciencedirect.com/science/article/pii/037026939191905B.

[35] K. Rummukainen et al. "The Universal properties of the electroweak phase transition". In: *5th International Workshop on Thermal Field Theories and Their Applications Regensburg, Germany, August 10-14, 1998*. 1998. arXiv: hep-ph/9809435 [hep-ph]. URL: https://inspirehep.net/record/476476/files/arXiv:hep-ph_9809435.pdf.

[36] J. Kaspar. "Status of the Fermilab g-2 experiment". In: *Nuclear and Particle Physics Proceedings* 260 (2015). The 13th International Workshop on Tau Lepton Physics, pp. 243–246. ISSN: 2405-6014. DOI: https://doi.org/10.1016/j.nuclphysbps.2015.02.051. URL: http://www.sciencedirect.com/science/article/pii/%5C%20S2405601415001108.

[37] S. Coleman and J. Mandula. "All Possible Symmetries of the S Matrix". In: *Phys. Rev.* 159 (5 July 1967), pp. 1251–1256. DOI: 10.1103/PhysRev.159.1251. URL: https://link.aps.org/doi/10.1103/PhysRev.159.1251.

[38] R. Haag, J. T. Lopuszański, and M. Sohnius. "All possible generators of supersymmetries of the S-matrix". In: *Nuclear Physics B* 88.2 (1975), pp. 257–274. ISSN: 0550-3213. DOI: https://doi.org/10.1016/0550-3213(75)90279-5. URL: http://www.sciencedirect.com/science/article/pii/0550321375902795.

[39] M. B. Gavela et al. "Standard model CP violation and baryon asymmetry". In: *Mod. Phys. Lett.* A9 (1994), pp. 795–810. DOI: 10.1142/S0217732394000629. arXiv: hep-ph/9312215 [hep-ph].

[40] F. Quevedo, S. Krippendorf, and O. Schlotterer. "Cambridge Lectures on Supersymmetry and Extra Dimensions". In: (2010). arXiv: 1011.1491 [hep-th].

[41] L. Girardello and M. T. Grisaru. "Soft Breaking of Supersymmetry". In: *Nucl. Phys.* B194 (1982), p. 65. DOI: 10.1016/0550-3213(82)90512-0.

[42] D. J. H. Chung et al. "The Soft supersymmetry breaking Lagrangian: Theory and applications". In: *Phys. Rept.* 407 (2005), pp. 1–203. DOI: 10.1016/j.physrep.2004.08.032. arXiv: hep-ph/0312378 [hep-ph].

[43] M. Tanabashi et al. "CP violation in the quark sector". In: *Review of Particle Physics*. 2019. URL: http://pdg.lbl.gov/2019/reviews/rpp2019-rev-cp-violation.pdf.

[44] M. Tanabashi et al. "CP-violation in KS -> 3pi". In: *Review of Particle Physics*. 2019. URL: http://pdg.lbl.gov/2019/reviews/rpp2019-rev-cp-viol-k0s3pi.pdf.

[45] M. Tanabashi et al. "CP-violation in KL decays". In: *Review of Particle Physics*. 2019. URL: http://pdg.lbl.gov/2019/reviews/rpp2019-rev-cp-viol-kl-decays.pdf.

[46] M. Tanabashi et al. "Tests of conservation laws". In: *Review of Particle Physics*. 2019. URL: http://pdg.lbl.gov/2019/reviews/rpp2019-rev-conservation-laws.pdf.

[47] J. Heeck. "Interpretation of Lepton Flavor Violation". In: *Phys. Rev.* D95.1 (2017), p. 015022. DOI: 10.1103/PhysRevD.95.015022. arXiv: 1610.07623 [hep-ph].

[48] R. Barbieri and G. F. Giudice. "Upper Bounds on Supersymmetric Particle Masses". In: *Nucl. Phys.* B306 (1988), pp. 63–76. DOI: 10.1016/0550-3213(88)90171-X.

[49] P. Athron et al. "Bayesian analysis and naturalness of (Next-to-)Minimal Supersymmetric Models". In: *JHEP* 10 (2017), p. 160. DOI: 10.1007/JHEP10(2017)160. arXiv: 1709.07895 [hep-ph].

[50] H. Baer et al. "Radiative natural SUSY with a 125 GeV Higgs boson". In: *Phys. Rev. Lett.* 109 (2012), p. 161802. DOI: 10.1103/PhysRevLett.109.161802. arXiv: 1207.3343 [hep-ph].

[51] D. Bowser-Chao, D. Chang, and W.-Y. Keung. "Electron electric dipole moment from CP violation in the charged Higgs sector". In: *Phys. Rev. Lett.* 79 (1997), pp. 1988–1991. DOI: 10.1103/PhysRevLett.79.1988. arXiv: hep-ph/9703435 [hep-ph].

[52] S.-M. Zhao et al. "The one loop contributions to c(t) electric dipole moment in the CP violating BLMSSM". In: *Eur. Phys. J.* C77.2 (2017), p. 102. DOI: 10.1140/epjc/s10052-017-4627-x. arXiv: 1610.07314 [hep-ph].

[53] M. Carena et al. "The Baryogenesis Window in the MSSM". In: *Nucl. Phys.* B812 (2009), pp. 243–263. DOI: 10.1016/j.nuclphysb.2008.12.014. arXiv: 0809.3760 [hep-ph].

[54] S. Liebler, S. Profumo, and T. Stefaniak. "Light Stop Mass Limits from Higgs Rate Measurements in the MSSM: Is MSSM Electroweak Baryogenesis Still Alive After All?" In: *JHEP* 04 (2016), p. 143. DOI: 10.1007/JHEP04(2016)143. arXiv: 1512.09172 [hep-ph].

[55] F. Wang et al. "Singlet extension of the MSSM as a solution to the small cosmological scale anomalies". In: *Phys. Rev.* D90.3 (2014), p. 035028. DOI: 10.1103/PhysRevD.90.035028. arXiv: 1404.6705 [hep-ph].

[56] K. Funakubo and S. Tao. "The Higgs Sector in the Next-to-MSSM". In: *Progress of Theoretical Physics* 113.4 (Apr. 2005), pp. 821–842. ISSN: 0033-068X. DOI: 10.1143/PTP.113.821.

[57] A. G. Cohen, A. D. Rújula, and S. L. Glashow. "A Matter-Antimatter Universe?" In: *The Astrophysical Journal* 495.2 (Mar. 1998), pp. 539–549. DOI: 10.1086/305328. arXiv: astro-ph/9707087 [astro-ph].

[58] M. Tanabashi et al. "Big-Bang nucleosynthesis". In: *Review of Particle Physics*. 2018. URL: http://pdg.lbl.gov/2019/reviews/rpp2018-rev-bbang-cosmology.pdf.

[59] M. Tanabashi et al. "Big-Bang nucleosynthesis". In: *Review of Particle Physics*. 2018. URL: http://pdg.lbl.gov/2019/reviews/rpp2018-rev-bbang-nucleosynthesis.pdf.

[60] R. H. Cyburt et al. "Big Bang Nucleosynthesis: 2015". In: *Rev. Mod. Phys.* 88 (2016), p. 015004. DOI: 10.1103/RevModPhys.88.015004. arXiv: 1505.01076 [astro-ph.CO].

[61] R. H. Cyburt, B. D. Fields, and K. A. Olive. "An Update on the big bang nucleosynthesis prediction for Li-7: The problem worsens". In: *JCAP* 0811 (2008), p. 012. DOI: 10.1088/1475-7516/2008/11/012. arXiv: 0808.2818 [astro-ph].

[62] W. Hu and S. Dodelson. "Cosmic Microwave Background Anisotropies". In: *Ann. Rev. Astron. Astrophys.* 40 (2002), pp. 171–216. DOI: 10.1146/annurev.astro.40.060401.093926. arXiv: astro-ph/0110414 [astro-ph].

[63] G. Krnjaic. "Can the Baryon Asymmetry Arise From Initial Conditions?" In: *Phys. Rev.* D96.3 (2017), p. 035041. DOI: 10.1103/PhysRevD.96.035041. arXiv: 1606.05344 [hep-ph].

[64] A. D. Sakharov. "Violation of CP Invariance, c Asymmetry, and Baryon Asymmetry of the Universe". In: *Pisma Zh. Eksp. Teor. Fiz.* 5 (1967), pp. 32–35. DOI: 10.1070/PU1991v034n05ABEH002497.

[65] J. M. Cline. "Baryogenesis". In: *Les Houches Summer School - Session 86: Particle Physics and Cosmology: The Fabric of Spacetime Les Houches, France, July 31-August 25, 2006*. 2006. arXiv: hep-ph/0609145 [hep-ph].

[66] G. 't Hooft. "Symmetry Breaking through Bell-Jackiw Anomalies". In: *Phys. Rev. Lett.* 37 (1 July 1976), pp. 8–11. DOI: 10.1103/PhysRevLett.37.8.

[67] G. 't Hooft. "Computation of the quantum effects due to a four-dimensional pseudoparticle". In: *Phys. Rev. D* 14 (12 Dec. 1976), pp. 3432–3450. DOI: 10.1103/PhysRevD.14.3432.

[68] F. R. Klinkhamer and N. S. Manton. "A saddle-point solution in the Weinberg-Salam theory". In: *Phys. Rev. D* 30 (10 Nov. 1984), pp. 2212–2220. DOI: 10.1103/PhysRevD.30.2212.

[69] S. Coleman. "Fate of the false vacuum: Semiclassical theory". In: *Phys. Rev. D* 15 (10 May 1977), pp. 2929–2936. DOI: 10.1103/PhysRevD.15.2929.

[70] C. G. Callan and S. Coleman. "Fate of the false vacuum. II. First quantum corrections". In: *Phys. Rev. D* 16 (6 Sept. 1977), pp. 1762–1768. DOI: 10.1103/PhysRevD.16.1762.

[71] A. D. Linde. "Fate of the False Vacuum at Finite Temperature: Theory and Applications". In: *Phys. Lett.* 100B (1981), pp. 37–40. DOI: 10.1016/0370-2693(81)90281-1.

[72] A. F. Heckler. "The Effects of electroweak phase transition dynamics on baryogenesis and primordial nucleosynthesis". In: *Phys. Rev.* D51 (1995), pp. 405–428. DOI: 10.1103/PhysRevD.51.405. arXiv: astro-ph/9407064 [astro-ph].

[73] D. E. M orrissey and M. J. Ramsey-Musolf. "Electroweak baryogenesis". In: *New J. Phys.* 14 (2012), p. 125003. DOI: 10.1088/1367-2630/14/12/125003. arXiv: 1206.2942 [hep-ph].

[74] R. Anishetty. "Vacua for SU(2) Yang-Mills". In: *Physics Letters B* 108.4 (1982), pp. 295–298. ISSN: 0370-2693. DOI: https://doi.org/10.1016/0370-2693(82)91196-0.

[75] A. Belavin et al. "Pseudoparticle solutions of the Yang-Mills equations". In: *Physics Letters B* 59.1 (1975), pp. 85–87. ISSN: 0370-2693. DOI: https://doi.org/10.1016/0370-2693(75)90163-X.

[76] V. Kuzmin, V. Rubakov, and M. Shaposhnikov. "On anomalous electroweak baryon-number non-conservation in the early universe". In: *Physics Letters B* 155.1 (1985), pp. 36–42. ISSN: 0370-2693. DOI: https://doi.org/10.1016/0370-2693(85)91028-7.

[77] P. B. Arnold, D. Son, and L. G. Yaffe. "The Hot baryon violation rate is O (alpha-w**5 T**4)". In: *Phys. Rev.* D55 (1997), pp. 6264–6273. DOI: 10.1103/PhysRevD.55.6264. arXiv: hep-ph/9609481 [hep-ph].

[78] G. D. Moore and K. Rummukainen. "Classical sphaleron rate on fine lattices". In: *Phys. Rev.* D61 (2000), p. 105008. DOI: 10.1103/PhysRevD.61.105008. arXiv: hep-ph/9906259 [hep-ph].

[79] D. Bodeker, G. D. Moore, and K. Rummukainen. "Chern-Simons number diffusion and hard thermal loops on the lattice". In: *Phys. Rev.* D61 (2000), p. 056003. DOI: 10.1103/PhysRevD.61.056003. arXiv: hep-ph/9907545 [hep-ph].

[80] P. Arnold and L. McLerran. "Sphalerons, small fluctuations, and baryon-number violation in electroweak theory". In: *Phys. Rev. D* 36 (2 July 1987), pp. 581–595. DOI: 10.1103/PhysRevD.36.581.

[81] M. Dine, P. Huet, and R. Singleton. "Baryogenesis at the electroweak scale". In: *Nuclear Physics B* 375.3 (1992), pp. 625–648. ISSN: 0550-3213. DOI: https://doi.org/10.1016/0550-3213(92)90113-P.

[82] A. I. Bochkarev, S. V. Kuzmin, and M. E. Shaposhnikov. "Model dependence of the cosmological upper bound on the Higgs-boson mass". In: *Phys. Rev. D* 43 (2 Jan. 1991), pp. 369–374. DOI: 10.1103/PhysRevD.43.369.

[83] A. Ahriche. "What is the criterion for a strong first order electroweak phase transition in singlet models?" In: *Phys. Rev.* D75 (2007), p. 083522. DOI: 10.1103/PhysRevD.75.083522. arXiv: hep-ph/0701192 [hep-ph].

[84] P. B. Arnold and O. Espinosa. "The Effective potential and first order phase transitions: Beyond leading-order". In: *Phys. Rev.* D47 (1993). [Erratum: Phys. Rev.D50,6662(1994)], p. 3546. DOI: 10.1103/physrevd.50.6662.2,10.1103/PhysRevD.47.3546. arXiv: hep-ph/9212235 [hep-ph].

[85] M. Dine et al. "Towards the theory of the electroweak phase transition". In: *Phys. Rev. D* 46 (2 July 1992), pp. 550–571. DOI: 10.1103/PhysRevD.46.550.

[86] M. Tanabashi et al. "Supersymmetric Particle Searches". In: *Review of Particle Physics*. 2019. URL: http://pdg.lbl.gov/2019/listings/rpp2019-list-supersymmetric-part-searches.pdf.

[87] H. H. Patel and M. J. Ramsey-Musolf. "Baryon Washout, Electroweak Phase Transition, and Perturbation Theory". In: *JHEP* 07 (2011), p. 029. DOI: 10.1007/JHEP07(2011)029. arXiv: 1101.4665 [hep-ph].

[88] A. Das. *Finite Temperature Field Theory*. World Scientific, 1997, p. 416. ISBN: 978-981-02-2856-9. URL: http://inspirehep.net/record/457892.

[89] J. I. Kapusta and P. Landshoff. "Finite-temperature field theory". In: *Journal of Physics G: Nuclear and Particle Physics* 15.3 (1989), p. 267. DOI: 10.1088/0954-3899/15/3/005.

[90] K. Freese. "Status of Dark Matter in the Universe". In: *Int. J. Mod. Phys.* 1.06 (2017), pp. 325–355. DOI: 10.1142/S0218271817300129. arXiv: 1701.01840 [astro-ph.CO].

[91] S. W. Allen, A. E. Evrard, and A. B. Mantz. "Cosmological Parameters from Observations of Galaxy Clusters". In: *ARAandA* 49.1 (Sept. 2011), pp. 409–470. DOI: 10.1146/annurev-astro-081710-102514. arXiv: 1103.4829 [astro-ph.CO].

[92] D. Clowe et al. "A direct empirical proof of the existence of dark matter". In: *Astrophys. J.* 648 (2006), pp. L109–L113. DOI: 10.1086/508162. arXiv: astro-ph/0608407 [astro-ph].

[93] V. Springel et al. "Simulating the joint evolution of quasars, galaxies and their large-scale distribution". In: *Nature* 435 (2005), pp. 629–636. DOI: 10.1038/nature03597. arXiv: astro-ph/0504097 [astro-ph].

[94] S. M. Faber and R. E. Jackson. "Velocity dispersions and mass-to-light ratios for elliptical galaxies." In: *Astrophysical Journal* 204 (Mar. 1976), pp. 668–683. DOI: 10.1086/154215.

[95] A. Refregier. "Weak Gravitational Lensing by Large-Scale Structure". In: *ARAandA* 41 (Jan. 2003), pp. 645–668. DOI: 10.1146/annurev.astro.41.111302.102207. arXiv: astro-ph/0307212 [astro-ph].

[96] P. A. R. Ade et al. "Planck 2015 results. XIII. Cosmological parameters". In: *Astron. Astrophys.* 594 (2016), A13. DOI: 10.1051/0004-6361/201525830. arXiv: 1502.01589 [astro-ph.CO].

[97] W. J. Percival et al. "Measuring the Baryon Acoustic Oscillation scale using the SDSS and 2dFGRS". In: *Mon. Not. Roy. Astron. Soc.* 381 (2007), pp. 1053–1066. DOI: 10.1111/j.1365-2966.2007.12268.x. arXiv: 0705.3323 [astro-ph].

[98] J. A. Peacock et al. "A Measurement of the cosmological mass density from clustering in the 2dF Galaxy Redshift Survey". In: *Nature* 410 (2001), pp. 169–173. DOI: 10.1038/35065528. arXiv: astro-ph/0103143 [astro-ph].

[99] K. Garrett and G. Duda. "Dark Matter: A Primer". In: *Adv. Astron.* 2011 (2011), p. 968283. DOI: 10.1155/2011/968283. arXiv: 1006.2483 [hep-ph].

[100] G. Bertone, D. Hooper, and J. Silk. "Particle dark matter: Evidence, candidates and constraints". In: *Phys. Rept.* 405 (2005), pp. 279–390. DOI: 10.1016/j.physrep.2004.08.031. arXiv: hep-ph/0404175 [hep-ph].

[101] J. Ellis, M. Lewicki, and J. M. No. "On the Maximal Strength of a First-Order Electroweak Phase Transition and its Gravitational Wave Signal". In: (2018). [JCAP1904,003(2019)]. DOI: 10.1088/1475-7516/2019/04/003. arXiv: 1809.08242 [hep-ph].

[102] A. Addazi, A. Marcianò, and R. Pasechnik. "Probing Trans-electroweak First Order Phase Transitions from Gravitational Waves". In: *MDPI Physics* 1.1 (2019), pp. 92–102. DOI: 10.3390/physics1010010. arXiv: 1811.09074 [hep-ph].

[103] A. Ahriche et al. "Gravitational Waves from Phase Transitions in Models with Charged Singlets". In: *Phys. Lett.* B789 (2019), pp. 119–126. DOI: 10.1016/j.physletb.2018.12.013. arXiv: 1809.09883 [hep-ph].

[104] F. P. Huang et al. "Hearing the echoes of electroweak baryogenesis with gravitational wave detectors". In: *Phys. Rev.* D94.4 (2016), p. 041702. DOI: 10.1103/PhysRevD.94.041702. arXiv: 1601.01640 [hep-ph].

[105] M. Kamionkowski, A. Kosowsky, and M. S. Turner. "Gravitational radiation from first order phase transitions". In: *Phys. Rev.* D49 (1994), pp. 2837–2851. DOI: 10.1103/PhysRevD.49.2837. arXiv: astro-ph/9310044 [astro-ph].